AN ABSTRACT OF THE THESIS OF

William S. White for the degree of Master of Science in Civil Engineering presented on April 30, 2013.

Title: Adjacent Structure Response Sensitivity to Seismic Events using the Direct Differentiation Method

Abstract approved: ____

H. Benjamin Mason

The response of adjacent structural systems to earthquake motions is investigated using the finite element framework OpenSees. Results of sensitivity analyses demonstrate that structural response quantities can increase in either or both of the adjacent structures for specific configurations. The structural models used include steel moment-resisting frames and rigid shear walls. The soil that underlies both buildings is modeled with a "structure-soil-structure spring" that connects the structural models. Due to the variety of building heights in urban environments, all combinations of four-, eight-, and twenty-story buildings are analyzed. Six shallow crustal earthquake motions are selected to model the dynamic responses of structural models. Sensitivity analyses are carried out using the direct differentiation method (DDM) with respect to parameters associated with the structure-foundation-soil systems, including floor mass, story stiffness, and soil stiffness. The DDM allows for computation of the time history of response sensitivity with respect to each parameter, in addition to the deterministic, or mean, time history response computed as part of an ordinary, non-linear, dynamic analysis. The response time histories can then be used to make a first-order approximation of the change in building response with respect to prescribed changes in a given parameter. The results of these analyses demonstrate that the effects of structure-soil-structure interaction are generally negligible for the steel, moment-

resisting frame structure pairs investigated. The rigid shear walls demonstrated effects of structure-soil-structure interaction, particularly in the smaller wall mimicking the motion of the larger wall. Further research is needed in this area, particularly in refining the soil model to more fully reflect the response of realistic soil.

Adjacent Structure Response Sensitivity to Seismic Events using the Direct Differentiation Method

by

William S. White

A THESIS

submitted to

Oregon State University

in partial fulfillment of
the requirements for the
degree of

Master of Science

Presented April 30, 2013
Commencement June 2013

Master of Science thesis of William S. White presented on April 30, 2013.

APPROVED:

Major Professor, representing Civil Engineering

Head of the School of Civil and Construction Engineering

Dean of the Graduate School

I understand that my thesis will become part of the permanent collection of Oregon State University libraries. My signature below authorizes release of my thesis to any reader upon request.

William S. White, Author

ACKNOWLEDGEMENTS

First, I would like to thank my advisor, Dr. Ben Mason and my unofficial co-advisor, Dr. Michael Scott. The understanding and guidance of Dr. Mason were pivotal throughout my work on this project. Though my name appears on this document, it was through the vision and capacities of Dr. Mason that the concept of this work truly progressed. Dr. Scott was equally pivotal to this project, truly making it function on the ground level. Without his ability to construct brilliantly efficient code, I would have spent many more hours toiling away to no avail. Dr. Scott forgets more about writing code on any given day than I will ever know, and I am very grateful that his efforts were applied to this project. I'm also grateful to Dr. Matt Evans and Dr. Dave Myrold, who graciously agreed to be on my committee. I am also grateful to Dr. Nathan Gibson in the Department of Mathematics. His expertise in LaTeX was invaluable in making this final document a reality. I'd also like to thank all of the support staff in Civil and Construction Engineering. Their support was invaluable, though their job is often thankless.

I am also grateful to my parents, who have supported me and tried to teach me everything they know throughout my life. This effort is, ultimately, one of the fruits of their labors. There are many primary and secondary school teachers who inspired me, but above the rest, I'd like to thank my middle school shop teach, Mr. Moore, whose first name I'm not sure I ever knew. He inspired me to study civil engineering over a decade ago, and I've never looked back.

Finally, I cannot conclude these remarks without acknowledging the Lord my God; who I believe watches over me daily. His sustaining power and influence have magnified my abilities beyond that which I was otherwise able. During the process of this work, He has, countless times, brought things to my remembrance and inspired me with words when I had none. Though this work and its author are fallible, I want the reader to recognize the hand of the Eternal God in its completion. I am now, more than ever, eternally indebted to Him.

TABLE OF CONTENTS

TABLE OF CONTENTS (Continued)

LIST OF FIGURES

LIST OF FIGURES (Continued)

LIST OF FIGURES (Continued)

LIST OF FIGURES (Continued)

LIST OF TABLES

LIST OF APPENDIX FIGURES

LIST OF APPENDIX FIGURES (Continued)

LIST OF APPENDIX FIGURES (Continued)

LIST OF APPENDIX FIGURES (Continued)

LIST OF APPENDIX FIGURES (Continued)

LIST OF APPENDIX FIGURES (Continued)

LIST OF APPENDIX FIGURES (Continued)

LIST OF APPENDIX FIGURES (Continued)

LIST OF APPENDIX FIGURES (Continued)

LIST OF APPENDIX FIGURES (Continued)

LIST OF APPENDIX FIGURES (Continued)

LIST OF APPENDIX FIGURES (Continued)

Adjacent Structure Response Sensitivity to Seismic Events using the Direct Differentiation Method

Chapter 1 Introduction

During an earthquake, it is possible for large buildings to interact through the soil that underlies them. This interaction is commonly referred to a structure-soil-structure interaction (SSSI) or cross-coupling of adjacent structures (see Menglin et al., 2011 for a recent SSSI literature review). Previous researchers have shown, by using theoretical arguments, that SSSI effects can be important for the case of two adjacent, infinitely-long, rigid shear walls (e.g., Luco and Contesse, 1973; Wong and Trifunac, 1975). In these cases, it was determined that the response of a smaller shear wall could be affected by the motion of an adjacent larger wall. Additionally, these researchers found that adjacent structures with natural frequency similar to the predominant frequency of the input motion could exhibit SSSI effects.

In urban areas, steel, moment-resisting frame structures are common; therefore, there is a need to understand the effects of SSSI on these structures as well. Recent experimental research has focused on this topic (e.g., Mason et al., 2013; Trombetta et al., 2013) with scaled centrifuge tests of moment-resisting frame structures subject to earthquake motions. Though multiple experiments have been performed, SSSI effects in urban environments is not yet fully understood. The numerical modeling presented herein seeks to bring further understanding of this topic.

It is important to note that structural design codes often omit SSSI effects from consideration, which could be detrimental to the stability and safety of existing and future buildings. Accordingly, there is a need to understand how SSSI affects realistic buildings in urban areas. Herein, the seismic response of adjacent steel, moment-resisting frame structures is simulated for realistic earthquake motions using the open source software framework OpenSees (McKenna et al., 2000). Three different building models are constructed to represent 4-story, 8-story, and 20-story buildings and placed adjacent to one another to form six systems of adjacent structures. The sensitivity of structural response-time history is tracked with respect to changes in structural mass, structural stiffness, and soil stiffness efficiently using the direct differentiation method (Kleiber et al., 1997).

This study is intended to be a preliminary work using a simple soil model. Relatively little work has been done in the field of numerical modeling of the response of adjacent moment-resisting frame structures with nonlinear members to earthquake motions. More research will be required based on the findings presented herein. This study does not consider the damaging effects caused by pounding of adjacent buildings.

The study presented herein includes a review of the current literature on the topics of SSI and SSSI in the literature review chapter. This is followed by a discussion of the structural models used, the analyses performed, and the ground motions applied in chapter 2. Finally, the results are presented and conclusions are drawn in chapters 3 and 4, respectively. An appendix is included, which contains a sample of the response time histories for the moment-resisting frame structures.

Chapter 2 Literature Review

The characterization of adjacent structures subject to seismic loading is a complex process that requires a thorough understanding of both soil and structural systems. The response of such structures is not solely dependent on the characteristics of either structure or soil, but on how the components in the system interact. As such, soil-structure (SSI) and structure-soil-structure interaction (SSSI) have been and continue to be the topic of various research projects (e.g. Veletsos and Meek, 1974; Lee and Wesley, 1973; Stewart et al., 1999a; Stewart et al., 1999b). This chapter provides a review of the applicable literature on the interaction of soil-structure systems consisting of both single and multiple structures.

This review is divided into four separate sections: soil-structure interaction, soil springs and impedance functions, experimental SSI research, and sensitivity analyses. The first section gives an overview of the analytical models that have been used to simulate SSI and the implications to engineering design. The soil springs and impedance functions section provides a description of the calibration of soil elements used in soil-structure interaction analyses. The experimental SSI research section summarizes previous studies, which investigated SSI in realistic systems. Finally, the sensitivity analysis section gives an overview of structural optimization in general and describes the direct differentiation method.

2.1 Soil-Structure Interaction

2.1.1 Overview

In seismic structural analysis, models are often assumed to have rigid bases, which constrain the bottom of the lowest set of columns to neither translate nor rotate. However, this model does not necessarily reflect reality. Structures are usually constructed with a shallow or deep foundation overlaying non-rigid soil or rock. Because the soil-foundation system that underlies the structure is not perfectly rigid, the structure may be able to translate and/or rotate in a seismic event. It is often assumed that a rigid base will predict higher values of stress in structural members, thus making the rigid-base assumption conservative (ASCE 7-10, 2010). However, the presence of flexibility in the soil-foundation system fundamentally changes the problem of structural analysis in a way that is difficult to predict a priori.

Early SSI work was performed by Housner and his colleagues (Merritt and Housner, 1954 and Housner, 1957). These studies found that the response of buildings on a flexible soil medium can deviate significantly from the fixed-base response. In the early to mid-1970s, there were multiple theoretical studies performed to analyze the effects of SSI. Jennings and Bielak (1973) studied two-dimensional, multiple degree of freedom oscillators atop a homogeneous, linear elastic halfspace. Lee and Wesley (1973) modeled multiple nuclear reactor and turbine buildings as oscillators atop a linear elastic halfspace. Researchers have also investigated how site effects and the position of a structure atop the soil can change apparent SSI effects (e.g. Duke et al., 1970 and Scanlan, 1976). Additionally, several applicable references were produced by Veletsos and his colleagues (e.g. Veletsos and Verbic, 1973 and Veletsos and Meek, 1974). The work of Veletsos and Meek (1974) provides a good summary of the work of the early to mid-1970s. The remainder of this subsection is referenced to the work by Veletsos and Meek (1974), though many of the methods and results are similar to those found by other authors.

Veletsos and Meek (1974) modeled soil-structure interaction for a single-degree of freedom structure atop a homogeneous, linearly elastic halfspace. The two-dimensional structural model of height h, shown in Figure 2.1, was given values of mass (m), story stiffness (k), and viscous damping (c). The rigid, circular foundation of the structure was also given mass (m_0) and was assumed to have negligible thickness. This structural model is a simple, yet realistic, representation of a one-story building or a multi-story building which is vibrating only in its first fundamental frequency. The structural system shown in 2.1 was set atop a foundation-halfspace system, shown in Figure 2.2, which allowed horizontal translation and rotation. The soil elements were given stiffness and damping values for both the translational and rotational modes based on the shear modulus and Poisson's ratio of the soil and the radius of the foundation.

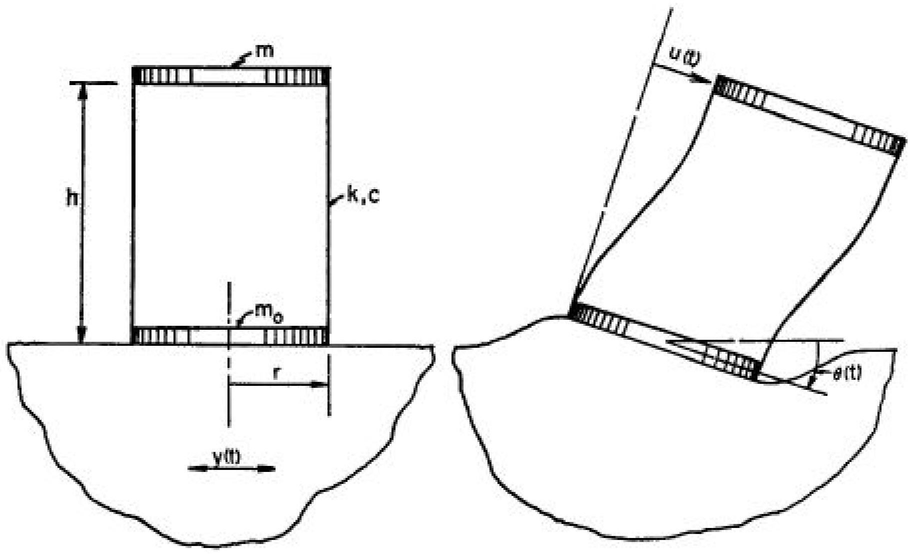

Figure 2.1: Single degree of freedom model employed by Veletsos and Meek (1974)

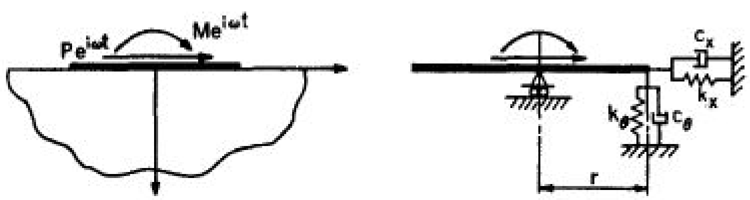

Figure 2.2: Halfspace-foundation system used by Veletsos and Meek (1974)

The soil-foundation-structure system shown in 2.2 was subject to three varieties of excitation: harmonic, pulse-like, and recorded earthquake displacement-time series. All three of these excitation types were modeled as free-field ground displacements, which are assumed to be the lateral motion of the foundation-soil interface in a seismic event. The results of all excitation types show that the nature of structural vibration is changed when a flexible base is introduced and that the results can be detrimental in certain cases. Figure 2.3, shows a set of response spectra for a structural model in which the height is five times the foundation radius subject to the harmonic excitation. In this particular case, as the flexibility of the soil-foundation system is increased, both the resonant period and the peak response are increased, resulting in the upward-right movement in the peak of the spectra.

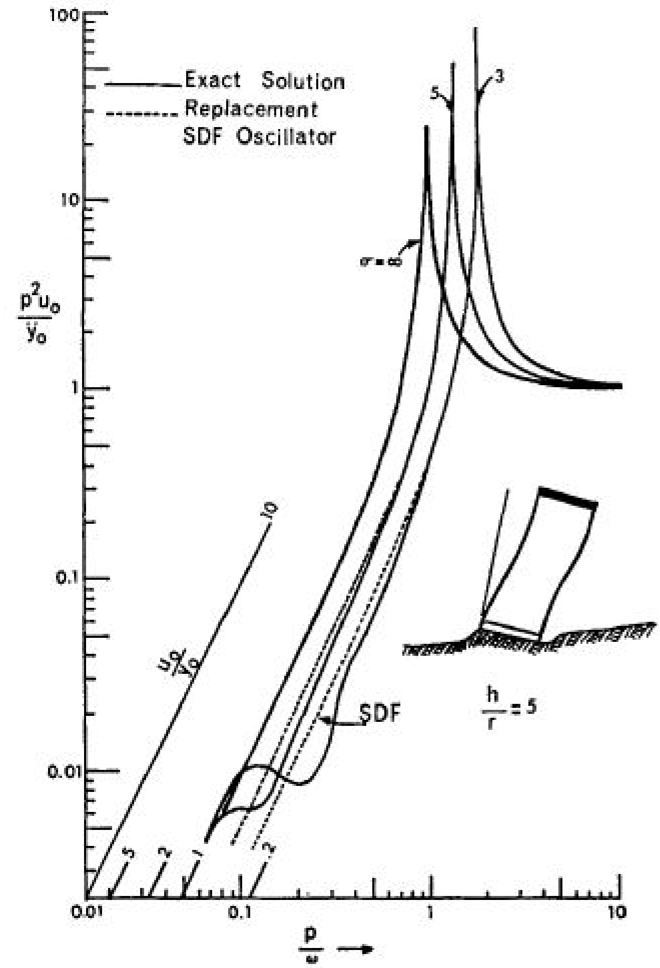

Figure 2.3: Response spectra of flexible-base structure subject to harmonic excitation. (Veletsos and Meek 1974)

In general, Veletsos and Meek (1974) found that soil-structure interaction largely depends on the stiffness of the structure with respect to the stiffness of the foundation, the ratio of superstructure height to the equivalent radius of the foundation, and the natural frequency of the structure in question compared to the design spectrum. Veletsos and Meek (1974) found that for structures with any combination of relatively flexible foundations, low height-to-radius ratios, or natural frequencies drastically different from the frequency content of expected earthquakes, soil-structure interaction effects are unlikely to be detrimental. However, for structures that do not meet these criteria, it is possible that soil-structure interaction may be significant. Additionally, the principal effects of soil-structure interaction are to reduce a system's natural frequency and to change its effective damping, which may result in either increased or decreased structural deformations. Finally, Veletsos and Meek (1974) gave several recommendations for structural design, based on the parameters described above.

Stewart et al. (1999a,b) summarized the accepted analytical methods for soil-structure interaction and corroborated these methods with empirical findings. The analytical methods portion of the work included many of the findings of Veletsos and Meek (1974), as well as additional insights that had been made in the intervening years (e.g. Apsel and Luco, 1987; Dobry and Gazetas, 1986; Riggs and Waas, 1985).

Stewart et al. (1999a,b) explains that there are two mechanisms of interaction that take place between structure, foundation, and soil. The first mechanism is inertial interaction, which is more commonly considered in practice and often has more significant effects (Kramer and Stewart, 2004). Inertial interaction is often modeled with a series of springs and dashpots that resist motion. This interaction occurs when the inertia of a structure induces base shear and moment, which causes deviations in the foundation motion compared to that of the free-field motion.

Additionally, kinematic interaction is associated with the deviation from the free-field motion of rigid foundations as a result of ground motion incoherence, wave inclination, or embedment. Kinematic interaction is generally caused by either the wave passage effect or the ground motion incoherence effect (Kim and Stewart, 2003). The former condition occurs when incident waves impinge on the foundation at an angle relative to the vertical axis. The latter condition occurs when incident cannot be discerned as a single, coherent motion. Kinematic interaction is typically taken into account using a transfer function applied to the ground motion. Veletsos and Prasad (1989) and Veletsos et al. (1997) developed a model of this type of interaction that considers both the spatial variation of the ground motion and the variation of soil-foundation contact (Kramer and Stewart, 2004). Kim and Stewart (2003) further quantified kinematic interaction by comparing free-field ground motions to those recorded at the foundation level for 29 strong earthquake motion recordings.

The model that Stewart et al. (1999a,b) used is similar to that used by Veletsos and Meek (1974). In addition, several modifications and correction factors are presented to account for non-uniform soil profiles, embedment of foundations, and foundation shape/flexibility. In general, these factors have relatively little impact on the analysis, but may require special modification for extreme cases.

The empirical findings Stewart et al. (1999a,b) showed that the effects of kinematic interaction in buildings are often negligible. For anaylses of inertial interaction, the predicted and empirical values of period elongation and damping were similar, though these values at some sites varied greatly. The factor that has the greatest effect on period elongation and damping is the ratio of the structure stiffness to the soil stiffness. A taller structure with a longer natural period constructed atop soft soil will be more vulnerable to detrimental SSI effects than a shorter structure constructed atop stiffer soil. In particular, both Veletsos and Meek (1974) and Stewart et al. (1999a) cite the dimensionless parameter

$$\sigma = \frac{V_s T}{h} \tag{2.1}$$

where V_s is the shear wave velocity of the soil, T is the fixed-base period of the structure, and h is the effective height of the structure. A lower value of aspect ratio and a high value of σ are preferred to prevent deleterious effects of SSI.

In general, a prescriptive, assumed response spectrum, or design spectrum, is used for the structural design of buildings. Prescriptive design spectra are meant to be inherently conservative and take into account many factors, particularly the factors that will be most detrimental to the designed structures (Mylonakis and Gazetas, 2000). Resembling the shape of many response spectra, design spectra usually possess a prescribed shape.

Mylonakis and Gazetas (2000) state that the decaying hyperbolic curve, typically used for the high period range of many design spectra, may not be suitable in soft soils due to site effects. This period elongation can have detrimental effects on structures with elongated natural periods due to the effects of soil-structure interaction. Figure 2.4 shows a typical, smooth-curved design spectrum with four response spectra from actual seismic events. Although the design spectrum appears to be sufficient in the low and middle period range, the actual spectral responses of three of the motions increased in the high period range.

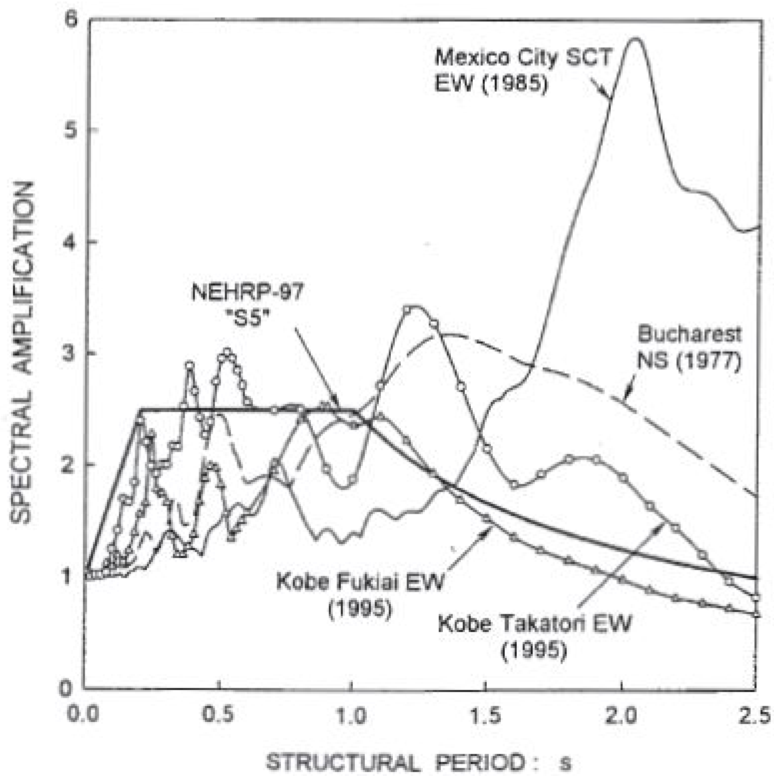

Figure 2.4: Typical design spectrum plotted with four response spectra of buildings on soft soil. (Mylonakis and Gazetas 2000)

This phenomenon may largely be due to the period elongation associated with soil-structure interaction. For tall, relatively slender structures sitting atop soft soils, the response at longer periods may be higher than what is generally anticipated by design spectra.

Thus, soil-structure interaction is often significant for the design of buildings on soft soil. This finding corroborates what was theoretically postulated by previous researchers: that buildings with high aspect ratios and low values of σ are more subject to effects of SSI.

2.1.2 Structure-Soil-Structure Interaction

In addition to the simple case of a single structure interacting with its underlying soil, it is also possible for adjacent structures to interact with one another through the underlying soil. This phenomenon, called structure-soil-structure interaction (SSSI), holds particularly meaningful consequences for buildings in urban environments, where relatively tall, heavy buildings are constructed in close proximity to one another. During a large earthquake, the responses of adjacent buildings may interact in a way that could be detrimental to some or all of the adjacent buildings.

The model used to study this concept has typically been a two-dimensional anti-plane cross section of two adjacent, infinitely-long shear walls with rigid, half-cylindrical foundations, pictured as Figure 2.5. This foundation model is assumed to promote transfer of in-plane rocking motions between the walls through the soil model. The soil is represented by an elastic, homogeneous, and isotropic halfspace, to which the foundations are perfectly bonded. In the work by Luco and Contesse (1973), the model is subject to vertically-incident horizontal shear (SH) waves with harmonic time dependence.

Some of the results of this research are shown herein. In each case, the response is presented as the absolute value of wall displacement (Δ_i) normalized by double the initial SH wave amplitude (w_0). These values are plotted against the frequency parameter $k * r$, where k is the circular frequency (ω) of the motion divided by the shear wave velocity (V_s) of the halfspace. The multiplication of k by r creates a dimensionless parameter, which represents the vibrational frequency of the system. These figures essentially plot normalized response of the structure against increasing natural frequency of the system. Figure 2.6 shows the response of two identical, rigid shear walls for three different values of

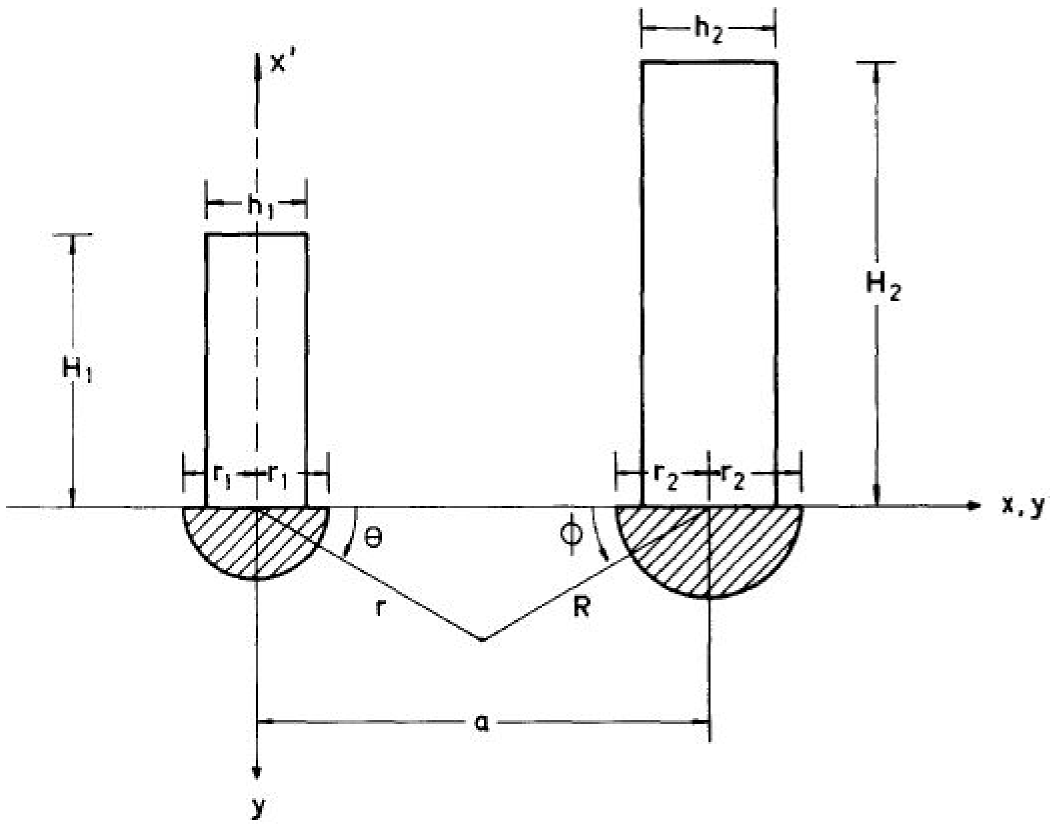

Figure 2.5: Model of adjacent, infinitely-long shear walls on elastic halfspace often used for SSSI analyses.(Luco and Contesse 1973)

the wall spacing (a) normalized by the foundation radius (r). Similarly, Figure 2.7 shows the response of two rigid shear walls where wall 2 has twice the geometrical dimensions of wall 1. In addition, the authors provided plots for the responses of flexible shear walls. These are similar to those shown below except displaying multiple modal responses.

In Figure 2.6, divergence of the response curves can be observed with changing distance, suggesting that there exists some interaction between the adjacent shear walls at both distances $a/r_1 = 10$ and $a/r_1 = 4$ that differs from the single-structure case, $a/r_1 = \infty$. Similar results are observed in Figure 2.7 for two different sized shear walls.

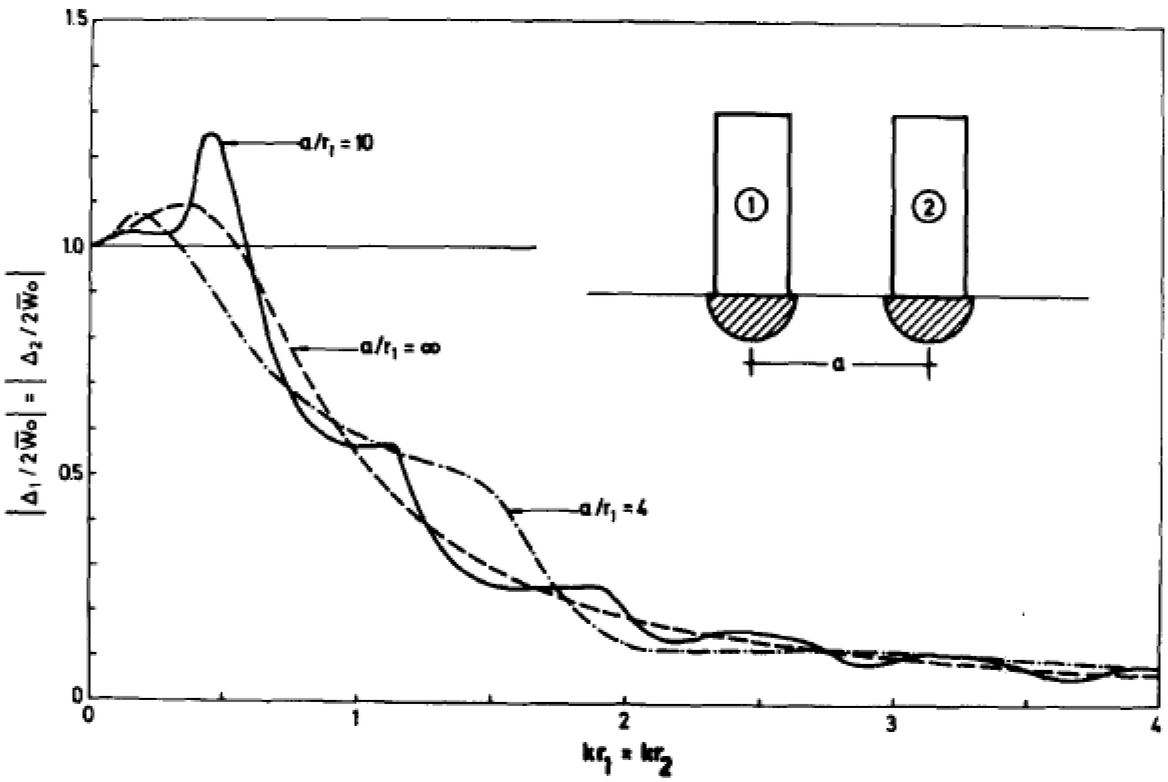

Figure 2.6: Normalized responses of identical shear walls at various values of spacing. The parameter $\Delta_i/2w_0$ is the wall displacement normalized to initial ground displacement and kr_i is analygous to the natural frequency of the structural system. (Luco and Contesse 1973)

Based on these results, Luco and Contesse (1973) concluded that SSSI effects can be significant for low frequencies (i.e. 3 to 14 Hz), which are generally those of most interest to

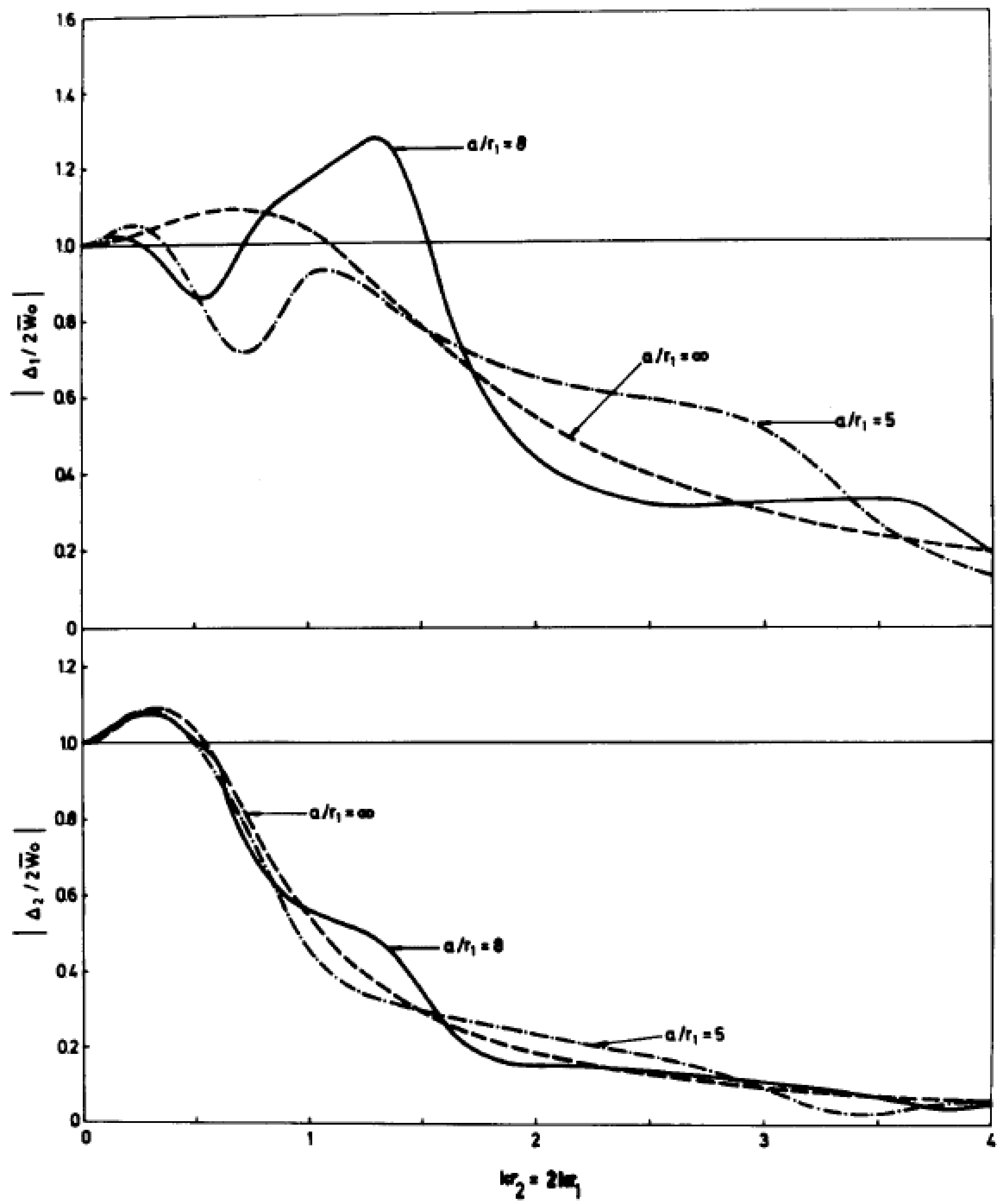

Figure 2.7: Normalized responses of two differenct rigid shear walls for various values of spacing. The parameter $\Delta_i/2w_0$ is the wall displacement normalized to initial ground displacement and kr_i is analygous to the natural frequency of the structural system. (Luco and Contesse 1973)

engineering practice. Also, the interaction effects are most significant for a small shear wall adjacent to a larger one. In that case, the motion of the smaller structure can be significantly different from the corresponding results ignoring the adjacent larger shear wall.

The work of Wong and Trifunac (1975) is similar to the work of Luco and Contesse (1973). The primary difference between the two is that this work uses a set of many shear walls instead of limiting the analysis to two walls. Additionally, Wong and Trifunac (1975) analyze, in more detail, the direction of the incident SH wave. The results were similar, though several key additions to the knowledge base were made. The authors found that if a small structure was in front of a larger structure (i.e. between the large structure and the wave), that the motion of the foundation could experience a large change in the frequency of vibration. This is primarily due to the standing wave pattern created by the larger structure. In the case of a smaller structure behind a larger one, the wave was shown to be scattered by the larger structure, causing the smaller structure to move with the larger one. For a small structure between two or more structures, the scattered wave energy from the adjacent structures may interfere constructively, causing large-amplitude vibration in the smaller structure. In general, it is found that the observed motion at the base of a structure may be very different from the free-field ground motion because of SSSI effects.

Multiple studies have been conducted on soil-structure interaction using the finite element method with a variety of elements and boundary elements. In the case of SSSI, the use of the finite element method has been somewhat more limited. Lysmer (1975) carried out a two-dimensional analysis of nuclear containment structures in the presence of two adjacent structures. This study concluded that SSSI can be significant, particularly when massive structures are embedded deeply in the soil.

A study by Lin et al. (1987) investigated the effects of alignment (i.e. the spatial placement of the adjacent foundations, with respect to one another), mode of vibration, and foundation embedment on SSSI. The model used is shown in Figure 2.8 and consists of a pair of square foundations atop a discretized disc of near-field soil and horizontally-layered far-field soil. The motions used for these analyses include a discrete representation of the motion in the near field and semi-discrete modes of vibration along with particular solutions in the far field. The first author describes the analysis method in detail in an earlier research report (Lin, 1984).

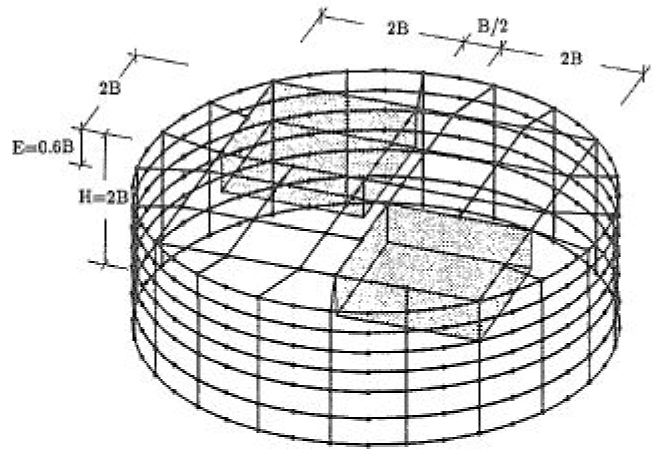

Figure 2.8: Model for discretization of the near-field soil overlaid with square foundations. (Lin et. al. 1987)

The Lin et al. (1987) study found that the influence of an adjacent foundation, though smaller in magnitude than the primary inertial motion, can be comparable to that of the inertial motion. The coupling of adjacent foundation motions is particularly pronounced when the mode of vibration is similar between the two foundations. Translational motions, whether vertical or horizontal, will tend to couple other translational motions, while rotational motions, rocking and torsion, will tend to couple other rotational motions. Though some interaction between translation and rotational motions was observed, it was generally less significant than interactions between similar vibration modes. When foundations are aligned along their diagonals, as they are in Figure 2.8, the interaction is less pronounced. Additionally, the embedment of foundations can affect the coupling of foundation motions significantly. Increased foundation embedment was universally found to increase the amplitude of motion due to SSSI effects. This effect was observed most significantly in the rocking mode of vibration induced by lateral motion.

2.2 Soil Springs and Impedance Functions

In structural analyses that include soil-structure interaction, a formulation has to be made to properly model the soil. Soil elements are often treated, and calibrated, as simple springs. To calibrate these soil elements properly, characterizations, called impedance functions, must be made of the stiffness and effective damping of the foundation-soil system. Because a soil-foundation system will react differently to different types of motion, it is often necessary to define multiple impedance functions for a single structure. In general, impedance functions are defined for horizontal, vertical, rocking, and torsional modes of vibration.

Much of the knowledge of researchers is gathered into a reasonably comprehensive set of formulas and normalized charts useful to calculate impedance functions of shallow foundations in Gazetas (1991). Foundations can be of any shape, as the function is based on a circumscribed rectangle, seen in Figure 2.9, and can be either sitting on the surface or embedded. The formulations were taken from models using a homogenous halfspace, and are thus limited in the scope of soil conditions that they can accurately model. Additionally, impedance functions are inherently frequency-dependent and sensitive to changes in Poisson's ratio. For the ranges of natural frequency and Poisson's ratio usually encountered in civil structures, the formulas and charts included are a reasonable estimation of the actual impedance of the soil-foundation system (Gazetas, 1991).

Gazetas (1991) gives a pair of tables that contain the algebraic formulas for calculating both stiffness and damping for each of five different modes. Stiffness is calculated using a baseline static stiffness multiplied by a dynamic stiffness coefficient that may increase or decrease the final value of stiffness. Each of the functions for stiffness depends on the shear modulus and Poisson's ratio of the soil and the dimensions of the circumscribed rectangle. Damping is generally based on the density and shear wave velocity of the soil, as well as the dimensions of the circumscribed rectangle. The specific impedance functions selected is discussed further in chapter 3.

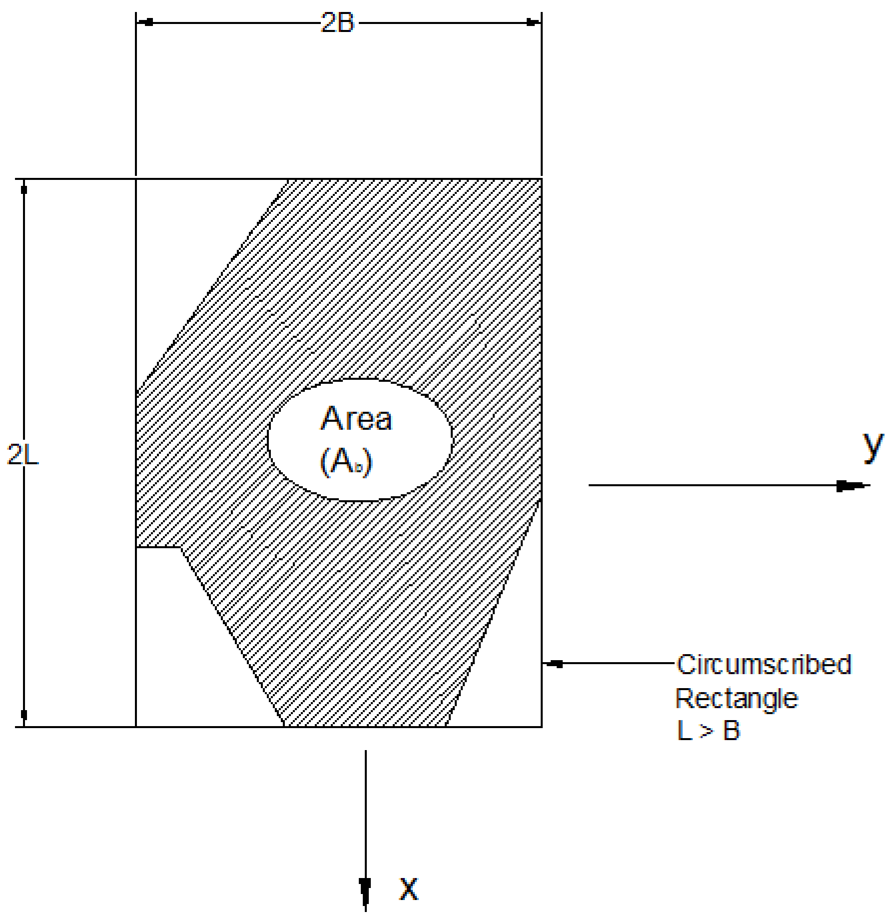

Figure 2.9: Circumscribed rectangle used for impedance function calculations (after Gazetas 1991)

In addition to defining the impedance of individual soil-foundation systems, the stiffness and damping of the soil which underlies multiple foundations has also been characterized. Qian and Beskos (1995) use the boundary element method to analyze the response of adjacent foundations to harmonic excitations. This method uses the dynamic Green's function to discretize the surface of the halfspace and to characterize the soil-foundation interface. The model used is a three-dimensional, rigid, massless, surface foundation bonded to a homogeneous, isotropic, linearly elastic halfspace.

Mulliken and Karabalis (1998) present a discrete model for predicting the stiffness and damping for a foundation-soil-foundation system. The model consists of multiple, adjacent, rigid foundations sitting atop a homogeneous, isotropic, and linearly elastic halfspace. The foundation geometry and notation used is shown in Figure 2.10 and the spring and dashpot model is shown in Figure 2.11. The analyses were performed using a modified version of the Wilson-theta method that takes into consideration the time-lagging effects of wave propagation (Mulliken and Karabalis, 1998).

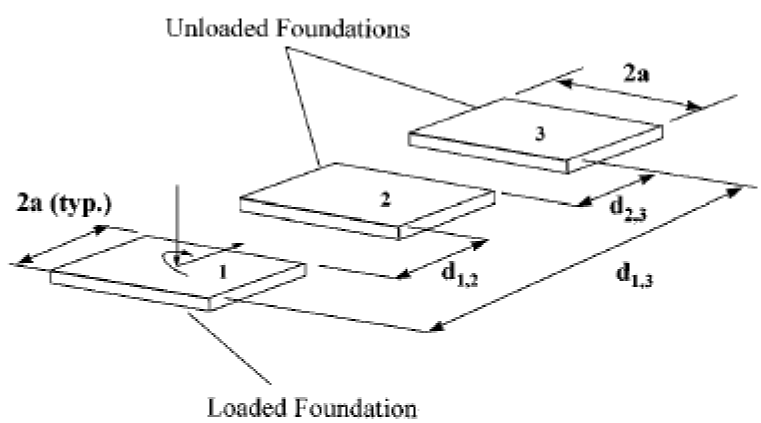

Figure 2.10: Foundation system geometry and notation employed by Mulliken and Karabalis (1998)

The formulas presented for the computation of coupling coefficients for foundation-soil-foundation interaction are based largely on the work of Wolf (1985), who presents expressions for stiffness of square surface foundations for each of four modes of vibration.

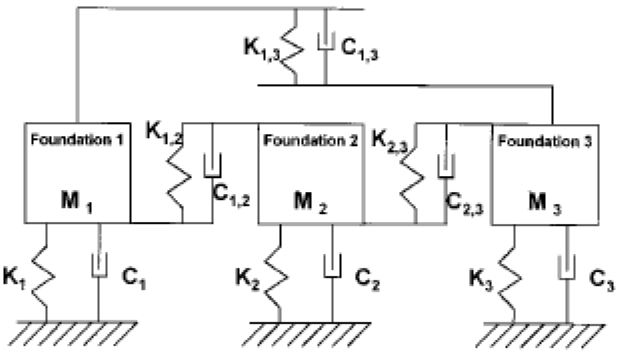

Figure 2.11: Spring and dashpot model used by Mulliken and Karabalis (1998)

Table 2.1: Mulliken and Karabalis (1998) Table III - Coupling Coefficients for Structure-Soil-Structure Interaction, expressed in terms of shear modulus (G), Poisson's ratio (ν), foundation half-width (a), and shear wave velocity (V_s).

	Vertical motion	Horizontal motion	Rocking motion	Torsional motion
Stiffness	$\Gamma_3 \times \frac{Ga}{(1-\nu)}$	$\Gamma_1 \times \frac{Ga}{(2-\nu)}$	$\Gamma_{\phi 2} \times \frac{Ga^3}{(1-\nu)}$	$\Gamma_{\phi 3} \times Ga^3$
Damping	$\Psi_3 \times \frac{Ga^2}{V_S(1-\nu)}$	$\Psi_1 \times \frac{Ga^2}{V_S(2-\nu)}$	$\Psi_{\phi 2} \times \frac{Ga^4}{V_S(1-\nu)}$	$\Psi_{\phi 3} \times \frac{Ga^4}{V_S}$

These equations for stiffness are presented in terms of the shear modulus (G), Poisson's ratio (ν) of the soil and half the foundation width (a). The expressions for damping also incorporated the shear wave velocity of the soil. Instead of multiplying these expressions by numerical constants, as Wolf (1985) suggested, Mulliken and Karabalis (1998) suggest multiplying by dimensionless empirical functions of the distance ratio (d/a) to find the coupling coefficient between foundations. These empirical functions are also presented for each of four different modes of vibration. The tables of impedance for adjacent foundations and interaction coefficients, as presented by Mulliken and Karabalis (1998), are presented below as Tables 2.1 and 2.2, respectively.

Table 2.2: Mulliken and Karabalis (1998) Table IV - Explicit Expressions of Coupling Functions for Structure-Soil-Structure Interaction, expressed in terms of spacing between foundations (d) and foundation half-width (a)

	Vertical motion	Horizontal motion	Rocking motion	Torsional motion
Stiffness, Γ	$1{\cdot}614 \times 10^{-0{\cdot}16257(d/a)}$	$3{\cdot}7561 \times 10^{-0{\cdot}18995(d/a)}$	$-(0{\cdot}04234 - 0{\cdot}2396 \times \mathrm{LOG}_{10}(d/a))$	$0{\cdot}05931$
Damping, Ψ	$8{\cdot}504$	$13{\cdot}2875$	$7{\cdot}3823 - 6{\cdot}775 \times \mathrm{LOG}_{10}(d/a)$	$4{\cdot}4429 – 2{\cdot}9125 \times \mathrm{LOG}_{10}(d/a)$

The coupling functions presented by Mulliken and Karabalis (1998) are applied to both two- and three-foundation systems. These models are subject to impulse forces or moments and the calculated response is compared to solutions found using the boundary element method, the finite element method, and a Green's function solution. The solutions found using the presented methods and those using the more mathematically complex methods were found to be similar. Figure 2.12 shows the horizontal displacement response of two adjacent foundations ($d/a = 1.0$) calculated using both the method presented and the boundary element method. The squares and triangles represent motions of the loaded and unloaded foundations, respectively, and the smooth curves represent those calculated by the boundary element method. The axes used for this figure are: Displ. (xE-10) ft on the ordinate and Time (x0.00001821 sec) on the abscissa. The atypical axes used indicate that the motion of the adjacent foundations is both high frequency and low amplitude. No additional information is given on the accuracy or precision of the models used at lower frequencies and/or higher amplitudes.

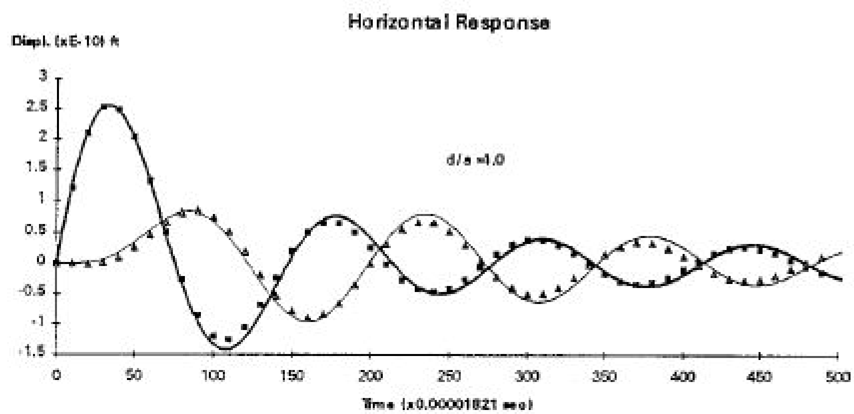

Figure 2.12: Horizontal displacement of adjacent foundations with $d/a = 1.0$ calculated using both the methods presented in Mulliken and Karabalis (1998) and the BEM. [The axes used are Time (x0.00001821 sec) on the ordinate and Displ. (xE-10) ft on the abscissa.]

2.3 Experimental SSI Research

Experiments and field tests have been planned and carried out to model both SSI and SSSI. The experiments modeling a single structure have, largely, shown that structural response is affected by SSI and that current models for predicting response with SSI are reasonably accurate. Despite the presence of non-linear behavior in the experimental soil, the linear-elastic models were adequate to reasonably approximate structural response.

Recent studies by Mason et al. (2013) and Trombetta et al. (2013) were conducted with scaled moment-resisting frame structures subject to earthquake motions in a centrifuge. These studies modeled adjacent steel structures both with and without basements using a variety of spacings and earthquake motions. It was found that kinematic interaction can have a significant effect on structural response, particularly for adjacent buildings. Additionally, these studies concluded that the response of steel structures is complex and that the circumstances under which SSSI could occur are not easily discerned. The steel structures tested exhibited few effects of SSSI. The greatest SSSI effects were observed when a large structure with a basement was placed adjacent to a smaller structure with no basement. This scenario created a fixed ground condition in which the foundations of both structures vibrate in harmony atop a relatively fixed mass of soil.

Additionally, several experiments have been performed on SSI effects. de Barros and Luco (1995) used a one-quarter scale Hualien containment model to test the effects of SSI and the validity of methods for determining impedance functions. For the applicable tests, a 16-meter tall cylindrical, reinforced concrete structure with a base diameter slightly less than 11 m was founded approximately 5 m beneath the ground surface. The structure was founded on a 3-meter thick circular slab that had the same diameter as the base of the superstructure. The soil in place at the test site consisted mostly of sands and gravels that were subjected to a variety of geotechnical and geophysical tests to determine their physical and mechanical properties. In particular, the shear wave velocities of the soil were carefully measured using a variety of applicable techniques, such as down-hole logging, cross-hole measurement, and down-hole measurement. The model was subject to harmonic forced vibrations that ranged from 2 to 25 Hz in frequency in both the horizontal and vertical directions. The vibration was scaled to have a force amplitude equal to approximately one tf (9806 N).

The experiment provided reasonable estimates of soil-foundation impedance functions for frequencies between about 5 and 14 Hz. The data acquired from tests outside of that frequency range were not of sufficient quality to make reliable characterizations of the soil impedance. de Barros and Luco (1995) found that estimates of impedance theoretically-derived from a linear, homogeneous, isotropic halfspace tend to slightly overestimate the values of stiffness and underestimate values of damping. Nevertheless, this theoretically-derived method for calculating soil-structure interaction response account for most observed phenomena.

A small-scale shake table test was also performed by Pitilakis et al. (2008) and was purposely designed to confirm the numerical substructure technique of simulating SSI, providing ideal conditions for SSI to be observed. A laminar box of about 550 by 1190 by 814 mm was constructed on the shake table at the University of Bristol. A dry, Hostun S28 sand was placed in this container with a single degree of freedom oscillator placed atop the sand. The final length scale used in the experiment was approximately 1:30 and the applied motion was scaled as necessary. The motion selected was the N-S component of the motion from the Friuli, Italy earthquake, San Rocco station, because of its wide frequency bandwidth.

In general, the experiment showed that the numerical model agreed with the scaled structural response to the tested ground motion. As seen in Figure 2.13, the recorded response of the scale model was similar to that of the numerical SSI model in both the time and frequency domains. Within the range of frequencies applicable to engineering analysis, response of the soil was properly captured by the numerical model that incorporated SSI effects.

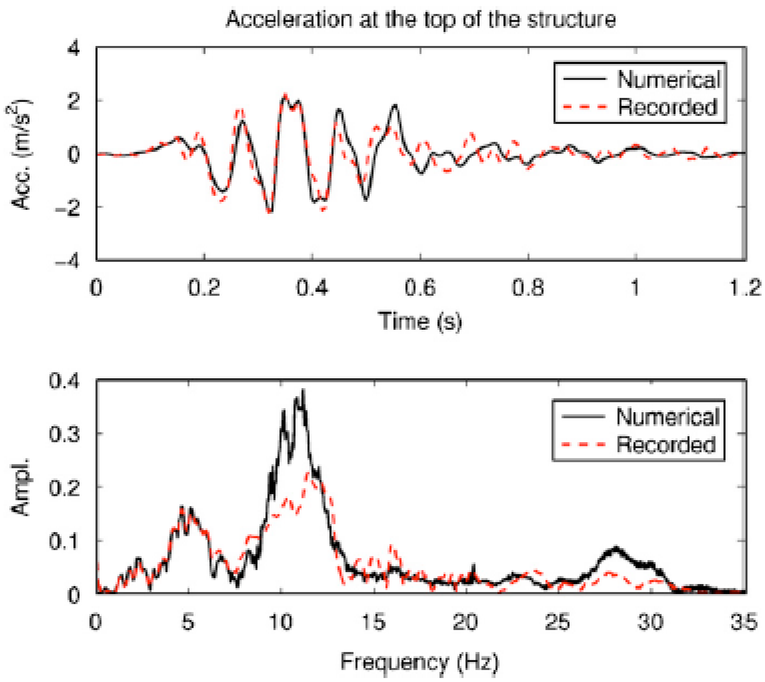

Figure 2.13: Recorded and numerical response of oscillator on dry sand. (Pitilakis et al. 2008)

Nakagawa et al. (1998) studied the effect of SSSI on a nuclear power plant in Japan. Nuclear power plants are often constructed with the reactor building in close proximity to the turbine building. Additionally, some plants are constructed with multiple reactors in close proximity to one another. Because of the detrimental consequences of failure for these structures, characterization of SSSI and other structural response phenomena is critical.

A full-scale forced vibration test was performed on the Hamaoka Unit 4 reinforced concrete reactor building and adjacent turbine building in Japan. A pair of exciters was placed on the reactor building and harmonic forces were applied in the N-S, E-W, and vertical directions at a variety of frequencies. Servo-type velocity sensors were placed on both the reactor and turbine buildings and displacements were found from the velocity data.

Additionally, a lattice model was adopted to assess the accuracy of analytical SSI analyses. The lattice model included lumped masses connected by bending-shear elements that represent the main shear walls of the buildings. The soil is modeled with a lattice model consisting of four lumped-mass soil columns with viscous boundaries connected by shear and axial springs. The physical and mechanical properties of the soil columns were calibrated to the properties of the soil at the Hamaoka site using in-situ and laboratory testing. A similar harmonic motion to that used on the actual building was applied in the N-S direction of the analytical model.

The results of both the experimental and analytical tests show signs of SSI effects of the reactor building and the underlying soil. Slight fluctuations are seen in the analytical model when the foundations of both the reactor and turbine buildings are caused to rotate out of phase, as shown in Figure 2.14. This result suggests that SSSI effects are observed in both the analytical model and the observed forced vibration tests; however the SSSI effects are small compared to the total response.

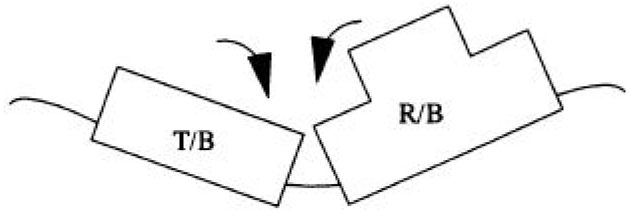

Figure 2.14: Interaction between the reactor building and turbine building in an out-of-phase rotational mode. (Nakagawa et. al. 1998)

2.4 Direct Differentiation Method

Optimization has been a topic of relevance in many engineering disciplines. The goal of optimization is to create effective and efficient designs. In structural engineering, optimization is often used to ensure that systems are of approximately equal strength in order to resist loads as efficiently and economically as possible. More specifically, sensitivity analyses are concerned with the relationship between system parameters and output response. Most often, the gradient, or rate of change, of the response with respect to system parameters is calculated to characterize this relationship.

Sensitivity analyses are generally divided into three different commonly accepted methods: (1) the finite difference method, (2) the direct differentiation method (DDM), and (3) the adjoint system method (ASM; Kleiber et al., 1997). The finite difference method is an approximate method that generally gives an accurate first-order approximation of sensitivity. However, it is not particularly efficient, especially for approximations of higher order than first, and requires a relatively precise selection of the change in the design parameter to produce an accurate sensitivity value. The direct differentiation or adjoint system methods are more frequently used (Kleiber et al., 1997). These can be used for either discretized or continuum systems and each can use a semi-analytical approximation method or a fully-analytical exact method. The direct differentiation method involves a simple differentiation of the system equation. The primary advantage of this method is its simplicity in concept and in calculation. Using the DDM, the stiffness matrix remains constant, requiring only back-substitution of the pseudo-load. The DDM is largely unaffected by the number of problem constraints. However, it is more significantly affected by the number of design variables and load cases. For a problem with relatively few design variables and load cases, the DDM is often the best option for sensitivity analysis (Kleiber et al., 1997).

The adjoint system method is conceptually similar to the DDM. The ASM involves introducing an adjoint variable vector and inverting the stiffness matrix before differentiating the equation and solving for sensitivity. In contrast to the DDM, the ASM is generally preferred for problems that have relatively many design variables and load cases with few constraints (Kleiber et al., 1997).

Chapter 3 Methodology

3.1 Analyses

3.1.1 Overview

All analyses in conjunction with this research were performed using the Open System for Earthquake Engineering Simulation (OpenSees, McKenna et al., 2000) finite element framework. This framework is capable of a wide variety of solution algorithms using both linear and non-linear analyses. Structural models of adjacent buildings and shear walls connected by a structure-soil-structure spring were created and subjected to recorded acceleration time series of earthquake motions. Five quantities were chosen to characterize the structural response: roof displacement, roof acceleration, first-story axial column force, and interstory drift in the first- and second-story columns. These parameters represent a typical set of variables tracked by earthquake engineers to characterize building response at both the top and bottom of the structure. All final mathematical processing was performed using MATLAB.

OpenSees is used in a variety of structural and geotechnical engineering applications (McKenna et al., 2000). For these analyses, the equation of motion was solved at each time step in a ground acceleration time history, $\ddot{u}_g(t)$, given by

$$\mathbf{m}\ddot{\mathbf{u}} + \mathbf{c}\dot{\mathbf{u}} + \mathbf{p}_r(\mathbf{u}, \dot{\mathbf{u}}) = -\mathbf{m}\boldsymbol{\iota}\ddot{u}_g(t) \tag{3.1}$$

where $\mathbf{m}$ is the mass matrix, $\mathbf{c}$ is the damping matrix, and $\mathbf{p}_r$ is the static resisting force vector. The ground acceleration, $\ddot{u}_g(t)$, provides external forces on the right-hand side of Equation 3.1 via the mass matrix and the influence vector, $\boldsymbol{\iota}$. The results give a mean response time history for each structure in a system.

Structural member properties, applied loads, and nodal spacing can also be identified in OpenSees to perform response sensitivity analyses with the DDM. The combination of the finite element framework with the appropriate software patterns for identifying parameters allows for computation of dynamic response sensitivity of nonlinear systems (Scott and Haukaas, 2008). The sensitivity of the nodal displacements with respect to a given model parameter, θ, is found by differentiating Equation 3.1 to find

$$\mathbf{k}_T \frac{\partial \mathbf{u}}{\partial \theta} = -\frac{\partial \mathbf{m}}{\partial \theta}(\ddot{\mathbf{u}} + \boldsymbol{\iota}\ddot{u}_g(t)) - \frac{\partial \mathbf{c}}{\partial \theta}\dot{\mathbf{u}} - \left.\frac{\partial \mathbf{p}_r}{\partial \theta}\right|_{\mathbf{u},\dot{\mathbf{u}}} \tag{3.2}$$

where $\mathbf{m}$ is the mass matrix, $\mathbf{c}$ is the damping matrix, $\mathbf{p}_r$ is the static resisting force vector, $\mathbf{u}$ is the nodal displacement, and $\mathbf{k}_T$ is the effective stiffness matrix. On the right-hand side of the equation, $\partial\mathbf{m}/\partial\theta$ and $\partial\mathbf{c}/\partial\theta$ are the derivatives of the mass and damping matrices, respectively, with respect to the specified model parameter, while $\left.\frac{\partial \mathbf{p}_r}{\partial \theta}\right|_{\mathbf{u},\dot{\mathbf{u}}}$ is the conditional derivative of the static resisting vector, which represents the forces that must be applied to the structure to keep the nodes fixed from motion under variations in the model parameter, θ. The values of the gradients calculated from this equation can be multiplied by the magnitude of the parameter change ($\Delta\theta$), then added to and subtracted from the initial response time history to find the response range for variance in a given parameter.

$$u(t) = u_o(t) \pm \frac{\partial u(t)}{\partial \theta}\Delta\theta \tag{3.3}$$

Table 3.1: Earthquake Motions Selected for Analysis

Earthquake	Station	PGA (g)	PGV (cm/s)	$D_{5\text{-}95}$ (s)
Northridge-01	Sylmar - Converter Station	0.59	130	13.5
Loma Prieta	Hollister - South & Pine	0.27	56.6	20.1
Chi-Chi, Taiwan	CHY034	0.29	28.7	30.0
Imperial Valley-06	Brawley Airport	0.16	36.1	15.2
Chi-Chi, Taiwan	CHY008	0.12	23.3	23.3
Loma Prieta	Salinas - John & Work	0.10	13.6	19.3

For the analyses performed, the model parameters selected for variance were building story mass, story stiffness, and structure-soil-structure spring stiffness. Each of these parameters was assumed to vary by plus or minus 10 percent. A variation of 10 percent was chosen for this study because it represents a realistic change that could occur in engineering practice and is significant enough to induce visible changes in response.

3.1.2 Earthquake Motions

Acceleration time series were taken from a gournd motion database prepared for the Pacific Earthquake Engineering Research Center (PEER) Transportation Systems Research Program (Baker et al., 2011). The selected time series were taken from set 1a of this database, which contains earthquake motions of approximately magnitude 7 at soil sites with an epicentral distance of 10 km. From this suite, six motions were selected based on intensity using peak ground acceleration (PGA). These motions were chosen in order to obtain a variety of both ground acceleration values and geographical locations. Two motions were selected from the Loma Prieta, 1989 earthquake in northern California and the 1999 Chi Chi, Taiwan earthquake. Additionally, two motions were selected from southern California earthquakes: the 1994 Northridge and 1979 Imperial Valley earthquakes. Table 3.1 contains the six selected ground motions including earthquake, station, and intensity parameters.

Table 3.2: Parameters for Proof of Concept Model

Parameter	Value	Metric
Story Height	10 ft	3.0 m
Bay Width	12 ft	3.7 m
Floor Mass	100 kip	455 kN
Modulus of Elasticity	30000 ksi	207 GPa
2nd Moment of Area	1400 in^4	580x10^6 mm^4
Cross-sectional Area	20 in^2	13000 mm^2

3.2 Proof of Concept

A proof of concept test was performed by analyzing a model of a two-story building adjacent to a one-story building, as can be seen in Figure 3.1. Throughout this research, the building that was taller and/or heavier was referred to as the Primary structure, and the shorter and/or lighter building was referred to as the Secondary structure. This nomenclature is guided by previous research (e.g. Luco and Contesse, 1973; Wong and Trifunac, 1975), which generally suggests that cases in which a large structure is immediately adjacent to a smaller one are more sensitive to SSSI. Adjustments in design parameters used to measure sensitivity were made to the Primary structure. The structural elements of these buildings were modeled with rectangular cross sections and linear-elastic material. The model parameters used for this analysis are found in Table 3.2.

The structural members used in this analysis are analogous to members of a square cross section made of a material with the same elastic modulus as steel, but which does not yield, regardless of stress. Each of the members were modeled as force-based beam-columns (Neuenhofer and Filippou, 1998). Though beam-columns with the capacity for non-linear analysis were used to model the structural members, the specified elastic sections forced a linear analysis of the structure for this model. The selection of elements with capacity for material nonlinearity made the transition to a fully nonlinear analysis simpler. As seen in Figure 3.1, both the Primary and Secondary structures had completely fixed bases on the outer side, while the inner sides of both structures were free to translate laterally. The adjacent structures were connected to each other by the structure-soil-structure spring, shown in Figure 3.1.

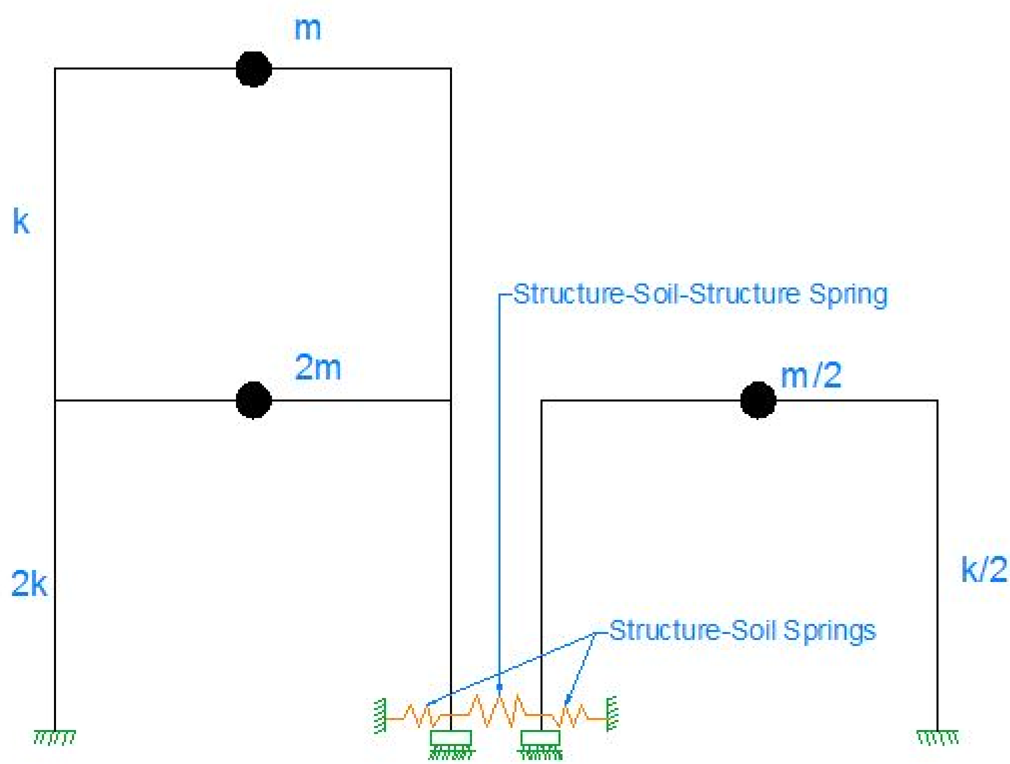

Figure 3.1: Proof of concept model.

To model the soil, a material was created with stiffness equal to 10 percent of the story stiffness of the Primary structure and assigned to both the structure-soil springs and the structure-soil-structure spring. For sensitivity analysis, the second moment of area of the columns was varied as the structural stiffness parameter in addition to the floor mass and structure-soil-structure-soil spring stiffness. This model was subjected to an acceleration-time series recorded during the 1979 Tabas, Iran earthquake, Tabas station, NNE component and the response time histories are shown below as Figures 3.2 through 3.4. The dashed lines in each of these figures represent the mean displacement response, while the solid lines represent the mean plus or minus the difference in response due to the 10 percent change in the specified model parameter, as calculated with Equation 3.3.

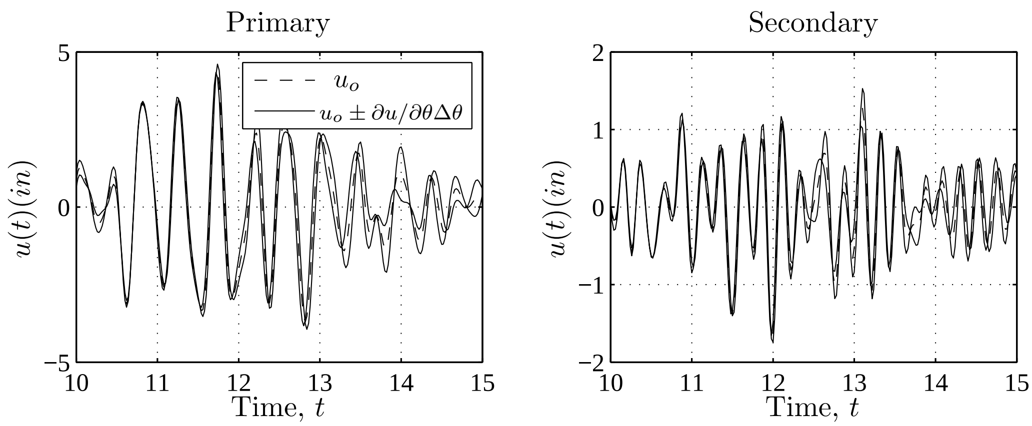

Figure 3.2: Sensitivity of Primary (left) and Secondary (right) structures roof displacement response with respect to changes in the stiffness of the Primary structure. (Note differing vertical scales.)

These results exhibited sufficient divergence in structural response to all three model parameters to continue on to additional structural models. The divergence of the response curves of the Secondary structure to changes in either stiffness or mass of the Primary structure are particularly noteworthy. Without the influence of SSSI effects, the response of the Secondary structure would not change with changes of design parameters in the Primary structure. Figures 3.2 through 3.4 illustrate that some SSSI effects are seen using the proof of concept model.

3.3 Structural Models

3.3.1 Trial Moment Frame Structures

The structural models used, at all design iterations, are intended to be largely scientific, with building models that are not unilaterally realistic in order to discern structure-soil-structure

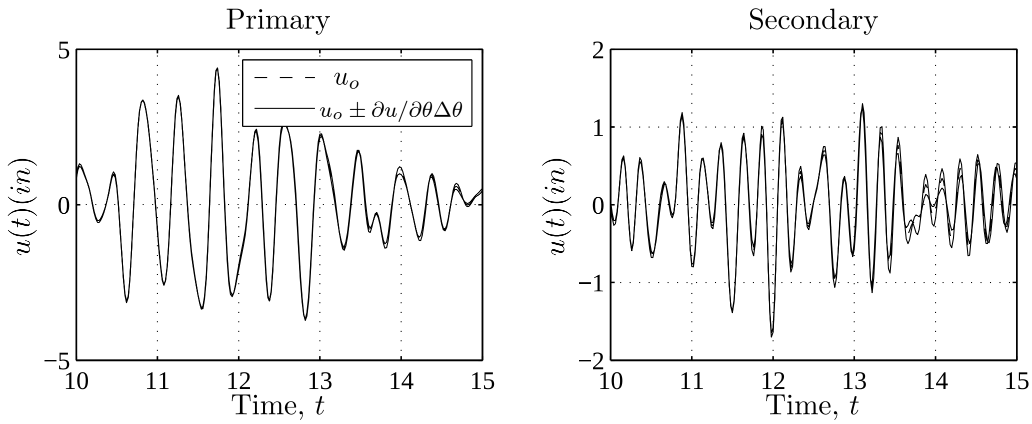

Figure 3.3: Sensitivity of Primary (left) and Secondary (right) structures roof displacement response with respect to changes in the mass of the Primary structure. (Note differing vertical scales.)

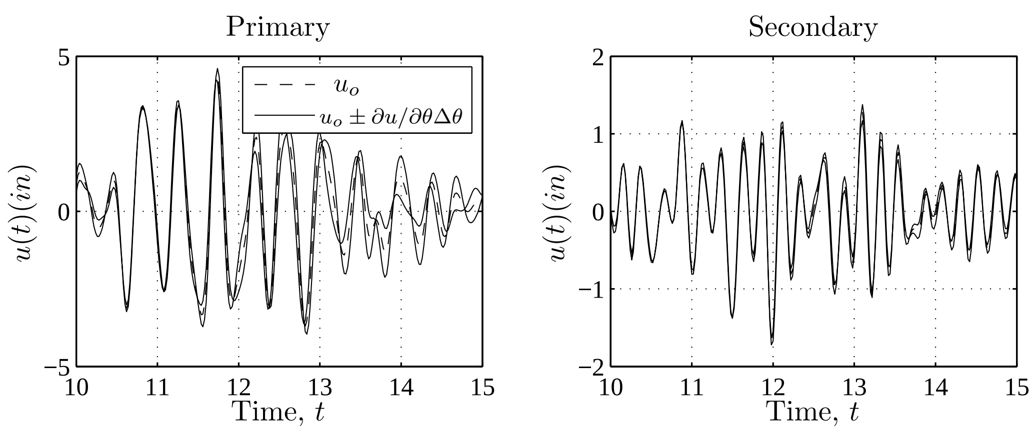

Figure 3.4: Sensitivity of Primary (left) and Secondary (right) structures roof displacement response with respect to changes in the stiffness of the structure-soil-structure spring. (Note differing vertical scales.)

interaction. The initial models used for moment-resisting frame structures were based on the proof of concept model. Rectangular elastic sections were replaced by wide-flange sections and the number of stories was increased to four or eight. The 20-story structure was not considered at this phase of development, but was considered for the final building models. A system of a 4-story building adjacent to another 4-story building (4x4) and a system of an 8-story building adjacent to a 4-story building (8x4) were tested. A preliminary design of W12x79 columns with W21x111 beams were used in the 4-story building and W14x82 columns with the same beams were used in the 8-story buildings. All steel sections were assumed to have a Modulus of Elasticity of 30,000 ksi (207 GPa). Building models of 10-ft (3.0-m) story height and 12-ft (3.7-m) base width were constructed for both the 4x4 and 8x4 building models were designed. A floor mass of 40 kips (178 kN) was divided in half and placed at the nodes at either side of structure for each floor. For both the trial and final moment-resisting frame structures, foundations were considered to be massless, which simplifies the analysis of the results. Rayleigh damping was used to model the material damping of the structures, given by

$$\mathbf{c} = a_0\mathbf{m} + a_1\mathbf{k} \tag{3.4}$$

where $\mathbf{c}$ is the Rayleigh damping matrix, $\mathbf{m}$ is the mass matrix, and $\mathbf{k}$ is the stiffness matrix. To calculate the mass-proportional (a_0) and stiffness-proportional (a_1) damping coefficients, the first and third natural frequencies were used for the 4-story system and the second and sixth natural frequencies were used for the 8-story system. Eventually, the fourth and twelfth natural frequencies were used to calculate the damping coefficients of the 20-story system. For the 8- and 20-story structure, the damping estimated at the first and second modes of vibration was relatively high. However, when the model was analyzed with a lower value of damping at these modes, the response only changed slightly in amplitude and did not affect sensitivity analyses. The motion of the models used herein is likely dominated by the first natural mode of vibration, making the selected Rayleigh damping coefficients somewhat unrealistic. In future work, it is advised that the first mode of vibration be used to calculate the damping coefficients used for Rayleigh damping. The mass-proportional and stiffness-proportional damping coefficients are given by

$$a_0 = \zeta \frac{2\omega_i \omega_j}{\omega_i + \omega_j} \tag{3.5}$$

and

$$a_1 = \zeta \frac{2}{\omega_i + \omega_j} \tag{3.6}$$

where ω_i is the natural circular frequency of the lower selected mode, ω_j is the natural circular frequency of the higher mode, and ζ is the baseline damping value, set to 4 percent. In the first iteration of the analyses, the structures were initially fixed at the outer ends and allowed to translate laterally at the inner end, where the structure-soil-structure spring was placed. Figure 3.5 shows an example of this model for the 4-story by 4-story system. Using this model, it was found that buildings with the same number of floors and identical floor masses vibrated in harmony, resulting in zero sensitivity to the structure-soil-structure spring stiffness. For analysis of these systems, the Secondary structure was assigned a mass equal to three-quarters that of the Primary structure.

After further consideration, this model was thought to be too restrictive and not particularly reflective of reality, where a structure is not necessarily constrained against lateral motion at one of its foundations. The only restraint against lateral motion is applied by the rigidity of the foundation and the underlying soil. As a result, the lateral constraint was removed from the far end of the Secondary structure and soil springs were placed at each of the column bases to better reflect the actual response of structures founded on a flexible soil medium. The outer end of the Primary structure remained restrained in order to properly model the response of each structure. Without this restraint, the models continued in unrealistic free-vibration. The improved structure-soil interface model is depicted for the 8-story by 4-story system in Figure 3.6. Additionally, the section properties of the

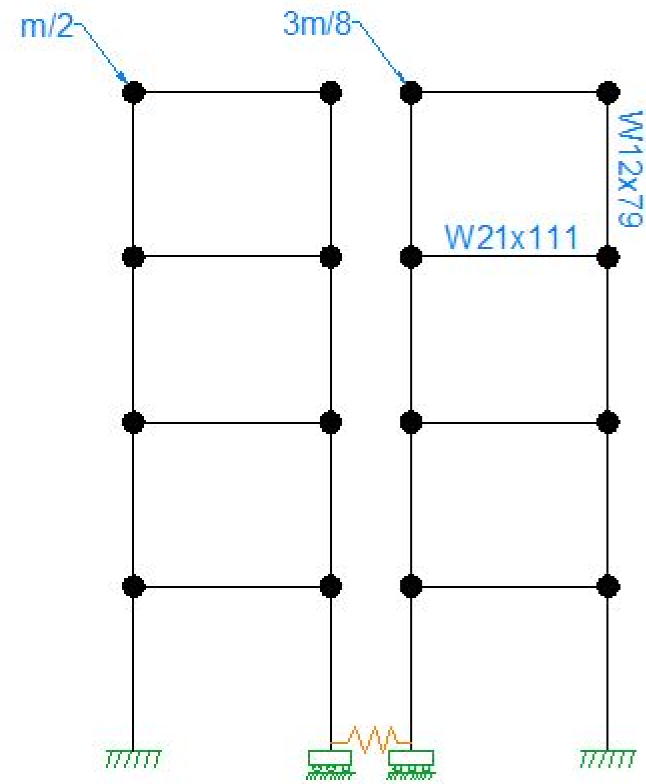

Figure 3.5: Four-by-Four system with lateral constraint on far end of Secondary structure. Each floor mass (m) is divided in half and placed at either end of the floor.

Table 3.3: Section Properties of Structural Members Modeled in 4-story Buildings

Parameter	Value	Metric	Value	Metric
Shape	W12x79		W21x111	
Depth	12.4 in	315 mm	21.5 in	546 mm
Flange Width	12.1 in	307 mm	12.3 in	312 mm
Flange Thickness	0.735 in	18.7 mm	0.875 in	22.2 mm
Web Thickness	0.470 in	11.9 mm	0.550 in	14.0 mm
Cross-sectional Area	23.2 in^2	15000 mm^2	32.7 in^2	21000 mm^2

Table 3.4: Section Properties of Structural Members Modeled in 8-story Buildings

Parameter	Value	Metric	Value	Metric
Shape	W14x82		W21x111	
Depth	14.3 in	363 mm	21.5 in	546 mm
Flange Width	10.1 in	257 mm	12.3 in	312 mm
Flange Thickness	0.855 in	21.7 mm	0.875 in	22.2 mm
Web Thickness	0.510 in	13.0 mm	0.550 in	14.0 mm
Cross-sectional Area	24.0 in^2	15000 mm^2	32.7 in^2	21000 mm^2

structural members appear below in Tables 3.3 and 3.4 for the 4-story and 8-story buildings, respectively.

Because of the change from rectangular to wide-flange sections, the second moment of area was no longer user-defined, and thus, could not be varied directly. However, a new parameter, the depth of the columns, was user-defined and was varied to modify building stiffness. It should be noted that lateral stiffness does not vary linearly with column depth. For rectangular sections, the second moment of area, which dictates stiffness, increases with the cube of depth, making the change in stiffness more significant than in the proof of concept model.

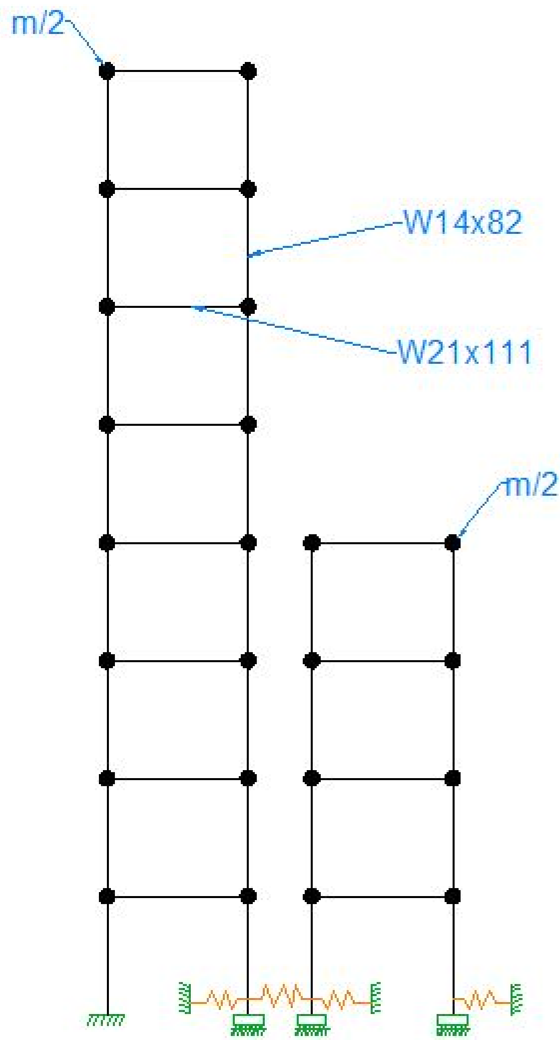

Figure 3.6: Eight-by-four system with column bases restrained by structure-soil springs.

Table 3.5: Material Properties of Steel Used in All Final Models

Property	US Cust. (ksi)	Metric (MPa)
Elastic Modulus	30000	206800
Yield Stress	50	345
Hardening	2432	16770

3.3.2 Final Moment Frame Structures

The moment-resisting frame structures used in the final analysis are similar to those used in the second iteration of the trial structures. After some test analyses of the previous iterations, a nonlinear constitutive model was applied to the structures. The material used in these analyses is similar A992 steel with modulus of elasticity of 30,000 ksi (206,800 MPa), yield stress of 50 ksi (345 MPa), and kinematic hardening modulus of 2432 ksi (16770 MPa).

The introduction of nonlinear analysis required modification of the building design. With a finite yield stress, both of the buildings failed in their original configuration. The redesign of the column sections was guided by the work of Mathur (2011), who used three different sets of 3-, 9-, and 20-story buildings representing typical structures constructed in Boston, Los Angeles, and Seattle. The overall building design of Mathur (2011) used a realistic building design with multiple bays and variable sections along the height of the structure. The more scientific models presented herein apply similar column section selection with only a single bay and identical section along the height of the structure. The final buildings used in the analysis included W12x190, W14x257, and W14x370 columns in the 4-, 8-, and 20-story buildings, respectively, as well as W21x111 beams in every structure. Figure 3.7 shows the 8-story by 4-story system after the modifications to the design, similar to Figure 3.6, which showed the buildings before modifications. Table 3.5 shows the material properties used in the modified structures. Tables 3.6 through 3.8 show the section properties of the columns used for each of the 4-, 8-, and 20-story buildings, respectively, while Table 3.9 shows the section properties of the beams used in all buildings.

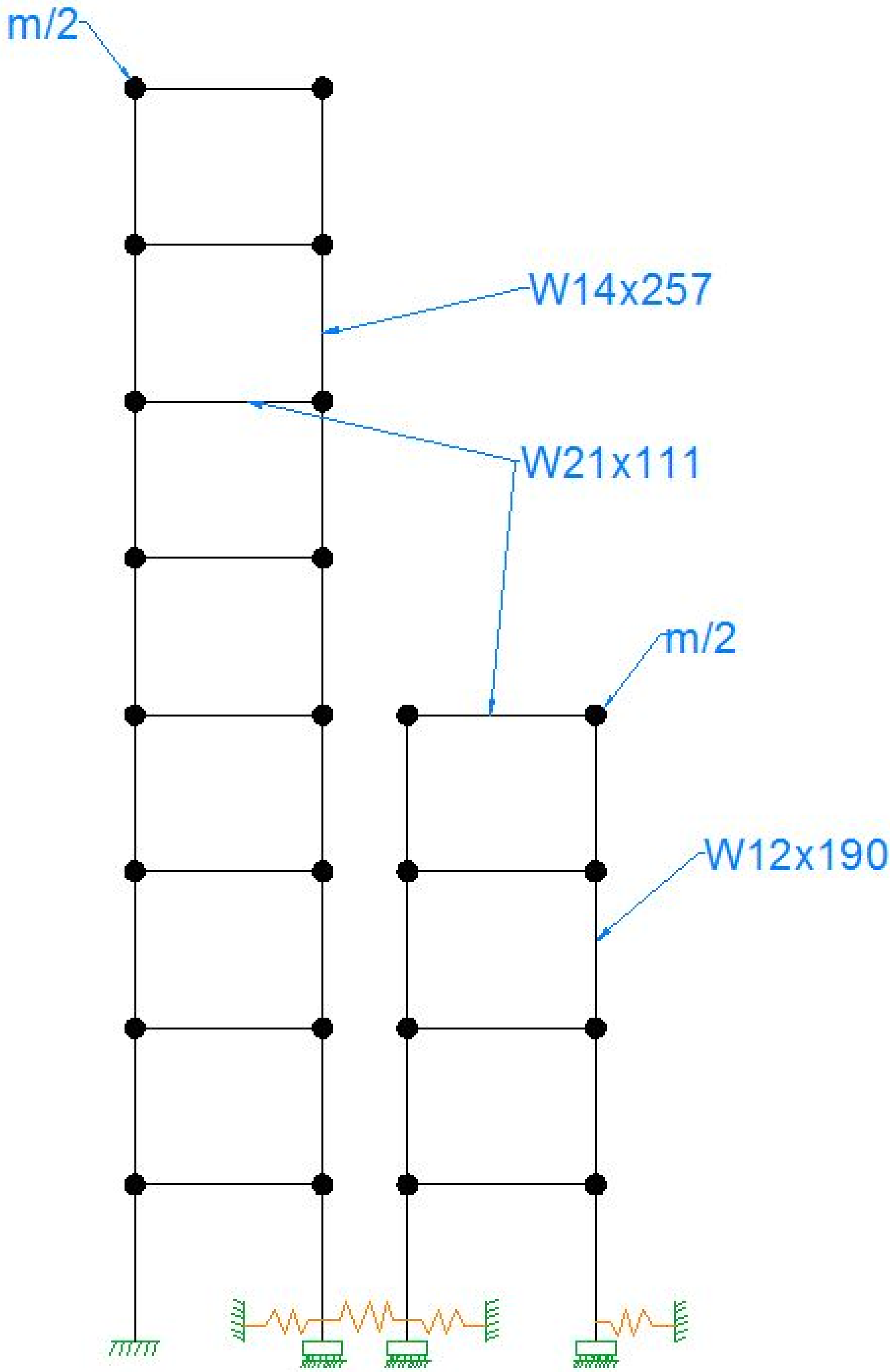

Figure 3.7: 8-story by 4-story building system with modified building design.

Table 3.6: Section Properties of Columns Used in Final 4-story Building Models

Parameter	US Cust.	Metric
Shape	W12x190	W12x190
Depth	14.4 in	366 mm
Flange Width	12.7 in	323 mm
Flange Thickness	1.74 in	44.2 mm
Web Thickness	1.06 in	26.9 mm
Cross-sectional Area	55.8 in^2	36000 mm^2

Table 3.7: Section Properties of Columns Used in Final 8-story Building Models

Parameter	US Cust.	Metric
Shape	W14x257	W14x257
Depth	16.4 in	417 mm
Flange Width	16.0 in	406 mm
Flange Thickness	1.89 in	48.0 mm
Web Thickness	1.18 in	30.0 mm
Cross-sectional Area	75.6 in^2	49000 mm^2

Table 3.8: Section Properties of Columns Used in Final 20-story Building Models

Parameter	US Cust.	Metric
Shape	W14x370	W14x370
Depth	17.9 in	455 mm
Flange Width	16.5 in	419 mm
Flange Thickness	2.66 in	67.6 mm
Web Thickness	1.66 in	42.2 mm
Cross-sectional Area	109 in^2	70000 mm^2

Table 3.9: Section Properties of Beams Used in All Final Building Models

Parameter	US Cust.	Metric
Shape	W21x111	W21x111
Depth	21.5 in	546 mm
Flange Width	12.3 in	312 mm
Flange Thickness	0.875 in	22.2 mm
Web Thickness	0.550 in	14.0 mm
Cross-sectional Area	32.7 in^2	21000 m^2

For reference, each building was also considered as a single structure similar to the primary structure used in this model, and shown in Figure 3.8. The first natural period of each of these structures, as calculated using OpenSees, is given in Table 3.10. The independent structures were modeled without any influence of soil. For this model, the structure independent of both soil and adjacent structures is considered the baseline.

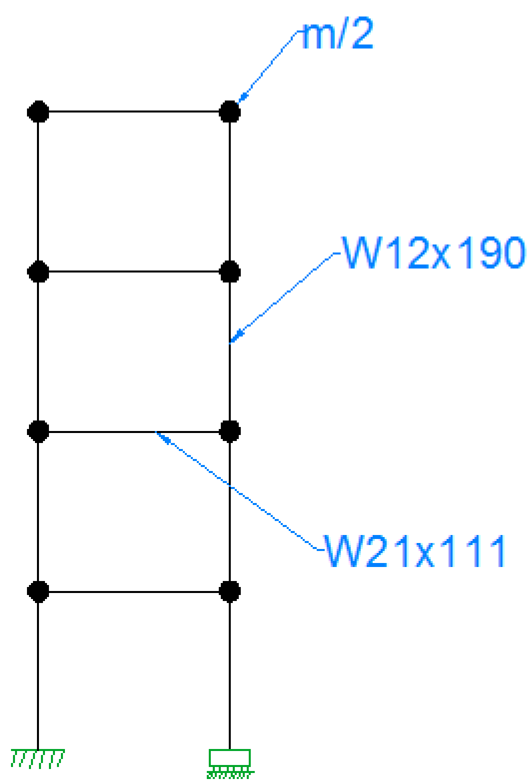

Figure 3.8: Example of 4-story structural system analyzed independent of adjacent structures.

Table 3.10: First Natural Period of Each Independent Structure

Structure	Period, T_n (s)
4-story	0.37
8-story	0.67
20-story	2.15

3.3.3 Shear Wall Structures

In addition to the moment-resisting frame structures, adjacent shear wall structures were selected based on the theoretical work by Luco and Contesse (1973) and Wong and Trifunac (1975). The researchers investigated two infinitely-long, rigid shear walls, which interact through the underlying soil. A similar model was produced in OpenSees with two adjacent, very stiff beam-column elements that were restrained with zero-length element springs to only rotate in plane. The OpenSees model did not include foundations at the base of the walls, however, a foundation width was required in order to compute the stiffness of the structure-soil and structure-soil-structure springs. Both walls were assumed to be 10 feet (3.0 meters) tall with the mass placed on the top. The Primary wall was assumed to be 2 feet (0.61 meters) wide with a weight of 100 kips (445 kN). The Secondary wall was assumed to have half the geometric dimensions of the Primary wall. A depiction of these shear wall models is show as Figure 3.9, below, and the model parameters are shown in Table 3.11.

The shear wall beam column elements were constrained with zero-length elements with rotational stiffness in plane as well as a similar zero-length element with a unique rotational stiffness acting as a structure-soil-structure spring. For the purpose of this analysis, the beam column elements were intended to produce negligible structural deformation, with all displacements coming as a result of the deformation of the underlying soil springs.

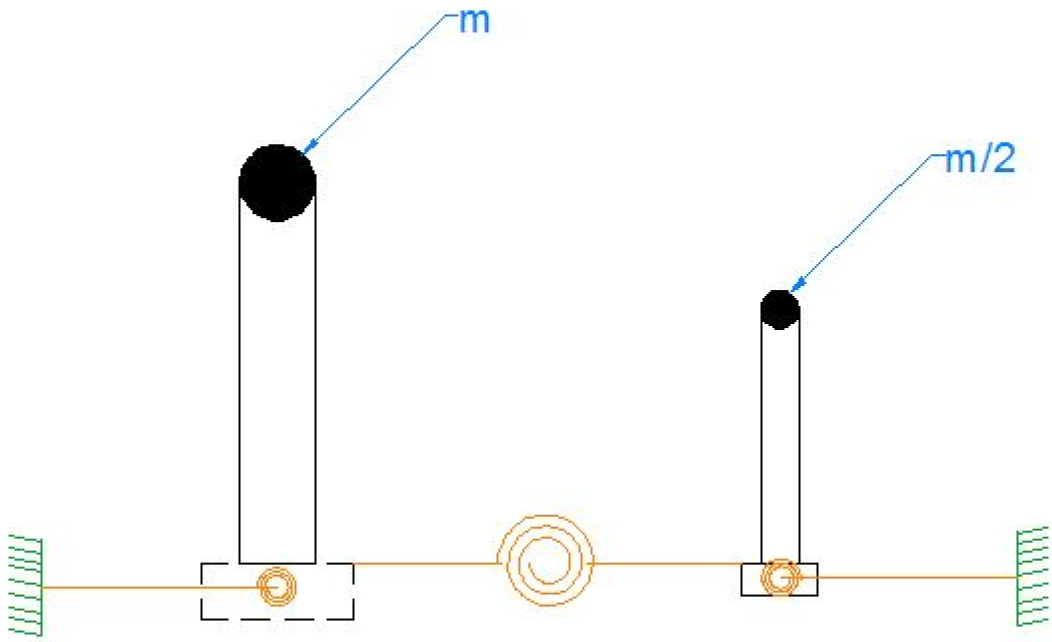

Figure 3.9: Adjacent, infinitely-long shear wall structures.

Table 3.11: Model Parameters for Shear Wall Structures

Parameter	Primary	Metric	Secondary	Metric
Height	15 ft	4.6 m	7.5 ft	2.3 m
Width	2 ft	0.61 m	1 ft	0.30 m
Mass	9 kip	44 kN	4.5 kip	22 kN
Foundation Width	4 ft	1.2 m	2 ft	0.61 m
Foundation Spacing	8 ft	2.4 m		

3.4 Soil Spring Models

Two different soil spring models are defined. Each foundation, aside from the left foundation of the Primary structure, which is fixed, has a soil spring attached to model the interaction between that foundation and the underlying soil. This is referred to as the soil-structure spring. Additionally, a structure-soil-structure spring with lateral stiffness is used to connect the Primary and Secondary structures. Both of these spring models are highly simplified, with only a single value of lateral stiffness assigned to each spring. For this preliminary work, single-mode springs with lateral stiffness only were assumed.

3.4.1 Soil-Structure Spring

The soil-structure springs used in all models were calibrated using the charts and tables published by Gazetas (1991). This model requires knowledge of the foundation geometry, as well as the shear modulus (G) and Poisson's Ratio (ν) of the soil. Square surface foundations of eight-foot width were selected to be modeled atop either dense sand or soft clay. Values of shear modulus were selected from (Budhu, 2011) and are given in Table 3.12. Because earthquake loading is often too rapid to allow for drainage of soil, the theorectical maximum of Poisson's Ratio (0.5) was selected as is reflected in Table 3.12. These values were applied to compute the soil spring stiffness, given by

$$K_y = \frac{2GL}{2-\nu}\left(2 + 2.5\chi^{0.85}\right) \tag{3.7}$$

where L is half the foundation width. This equation is taken from Gazetas (1991) for the static stiffness in the horizontal (lateral) mode of vibration. For a square foundation, the dimensionless parameter χ reduces to one, simplifying the Equation 3.7 to:

$$K_y = \frac{9GL}{2-\nu} \tag{3.8}$$

Table 3.12: Selected Soil Parameters and Calculated Stiffness for Soil-Structure Spring

	Shear Modulus			Calc. Stiffness	
	(ksi)	(MPa)	Poisson's Ratio	(kip/in)	(kN/m)
Sand	5	34.5	0.5	1300	227500
Clay	0.5	3.45	0.5	150	26250

In addition to the static stiffness, a dynamic coefficient is applied, which can either increase or decrease the stiffness of the system. In this work, the dynamic stiffness multiplier was assumed to be one. The final calculated values of stiffness used for the analyses are reported in Table 3.12.

3.4.2 Structure-Soil-Structure Spring

The structure-soil-structure spring was calibrated using the stiffness equations suggested by Mulliken and Karabalis (1998), which are identical to those suggested by Wolf (1985) for soil-structure impedance, except that they are multiplied by different coefficients, which are functions of the foundation spacing. Mulliken and Karabalis (1998) suggest that lateral stiffness of adjacent foundations is given by

$$K = \Gamma \frac{Ga}{2 - \nu} \tag{3.9}$$

where a is the half foundation width, for lateral stiffness of the foundation-soil-foundation system. Further Mulliken and Karabalis (1998) give

$$\Gamma = 3.7651 * 10^{[-0.18995(d/a)]} \tag{3.10}$$

as the function to calculate the coupling coefficient, where d is the distance between foundations. For this work, the foundations were taken to be as closely spaced as possible ($d/a = 0$), reducing the interaction coefficient to $\Gamma = 3.7651$. The stiffness values used

Table 3.13: Selected Soil Parameters and Calculated Stiffness for Structure-Soil-Structure Spring

	Shear Modulus			Calc. Stiffness	
	(ksi)	(MPa)	Poisson's Ratio	(kip/in)	(kN/m)
Sand	5	34.5	0.5	540	94500
Clay	0.5	3.45	0.5	56	9800

for the structure-soil-structure spring are found in Table 3.13. Though the Mulliken and Karabalis (1998) model was based on values of $d/a = 0.25$, the coefficient associated with the structure-soil-structure spring for $d/a = 0$ (3.7651) was assumed to be a reasonable approximation, particularly in comparison to the analogous coefficient for the soil-structure springs.

Additionally, it is noteworthy that the effects of direct contact of the structures, at the foundation level or the superstructure level were not considered in these analysis. Though pounding is an important consideration for the analysis and design of adjacent structures, it is not considered as part of the scope of this research.

Chapter 4 Results

The output parameters from the steel moment-resisting frame structures considered as a part of this research include lateral roof displacement, lateral roof acceleration, axial force in the first-story columns, and the interstory drift ratios of the first and second stories. Interstory drift ratio is defined as

$$IDR = \frac{\Delta_{i+1} - \Delta_i}{H} \tag{4.1}$$

where Δ_i is the lateral displacement of floor i, Δ_{i+1} is the lateral displacement of the floor immediately above floor i, and H is the story height. These five parameters give a general sense of a buildings response to each strong earthquake motion both at the top of the building (i.e. roof displacement and acceleration) and at the bottom (column force and IDR). The parameters were tracked throughout each analysis as well as the gradient of response with respect to column depth (stiffness), floor mass, and structure-soil-structure spring stiffness.

Seven of the analyses that were run failed to converge. The numerical analysis was modified in several ways, including modifying tolerance, increasing the maximum number of iterations, and changing solution algorithm, but all seven analyses still failed to converge despite these modifications. The only change that ameliorated convergence failure was an increase in structural section properties. Table 4.1 shows the system, ground motion, and soil type of each instance in which the analysis failed to converge. For each of the analyses that failed to converge, the structure-soil-structure spring, which transmits motions between the buildings, was removed and the analysis was rerun. In two cases, denoted by an asterisk (*) in Table 4.1, the analysis did not fail to converge when the structure-soil-structure spring

Table 4.1: Analyses that Failed to Converge

System	Soil	Earthquake	Station
*8 by 4	Clay	Chi-Chi, Taiwan	CHY034
8 by 4	Sand	Northridge-01	Sylmar - Converter Station
8 by 8	Clay	Northridge-01	Sylmar - Converter Station
8 by 8	Sand	Northridge-01	Sylmar - Converter Station
20 by 8	Sand	Northridge-01	Sylmar - Converter Station
*20 by 20	Clay	Northridge-01	Sylmar - Converter Station
20 by 20	Sand	Northridge-01	Sylmar - Converter Station

was removed. Future research with a more robust soil model may shed more light on these particular circumstances.

Additionally, the structures that were considered independent of adjacent buildings were analyzed and the lateral roof displacement time history is shown in Figure 4.1. One factor that is worth noting is the response of the 8-story buildings to the higher-intensity earthquake motions. Of the seven analyses that failed to converge, five of them were of systems that contained 8-story buildings. Additionally, in the case of the 20 by 8 system founded on soft clay, subject to the Chi Chi earthquake, Chiayi station 034 (CHY034) motion, the response of the 8-story building was greater than that of the 20-story building. Figure 4.2 shows the column force response time histories of both the Primary and Secondary structures for the CHY034 earthquake motion. Note that the vertical scale of the plot for the 8-story Secondary structure is greater that of the 20-story Primary structure. The larger response observed in the 8-story building is likely due to the proximity of the natural frequency of the 8-story building to the predominant frequency content of the applied earthquake motions. Table 4.2 shows the mean period and predominant period of each motion used in these analyses. Recall that the first natural period of the 8-story structure is $T = 0.67s$, which is the closest of any of the moment-resisting frame structures to the predominant periods of the earthquake motions.

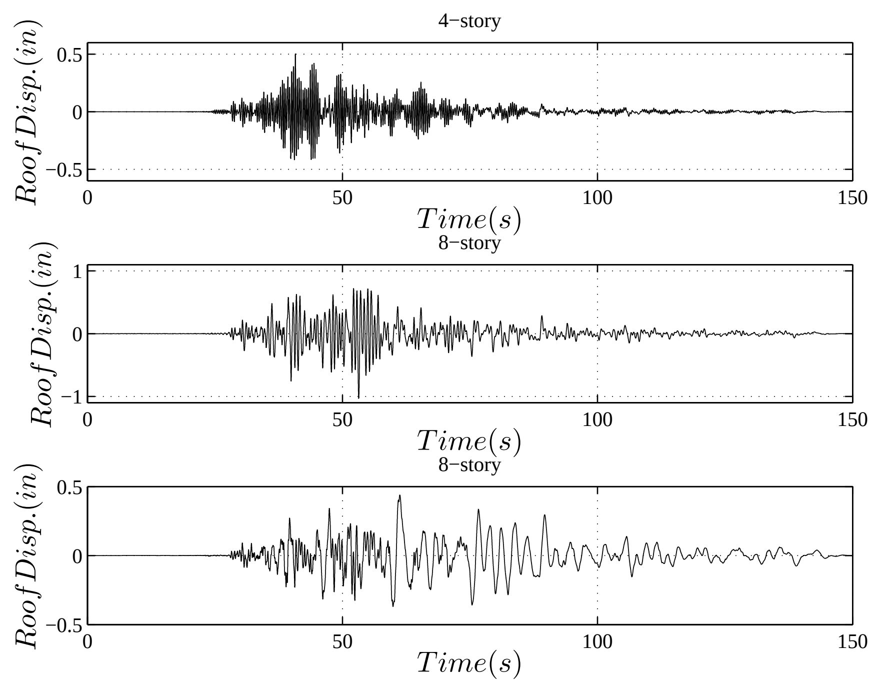

Figure 4.1: Roof displacement response time history of each structure considered independent of any adjacent structure.

Table 4.2: Average and Predominant Period for each Earthquake Motion

Earthquake	Station	T_{AVG} (s)	T_P (s)
Northridge-01	Sylmar - Converter Station	1.12	1.07
Loma Prieta	Hollister - South & Pine	1.04	1.66
Chi-Chi, Taiwan	CHY034	0.91	0.83
Imperial Valley-06	Brawley Airport	1.37	2.14
Chi-Chi, Taiwan	CHY008	1.45	0.98
Loma Prieta	Salinas - John & Work	0.88	1.71

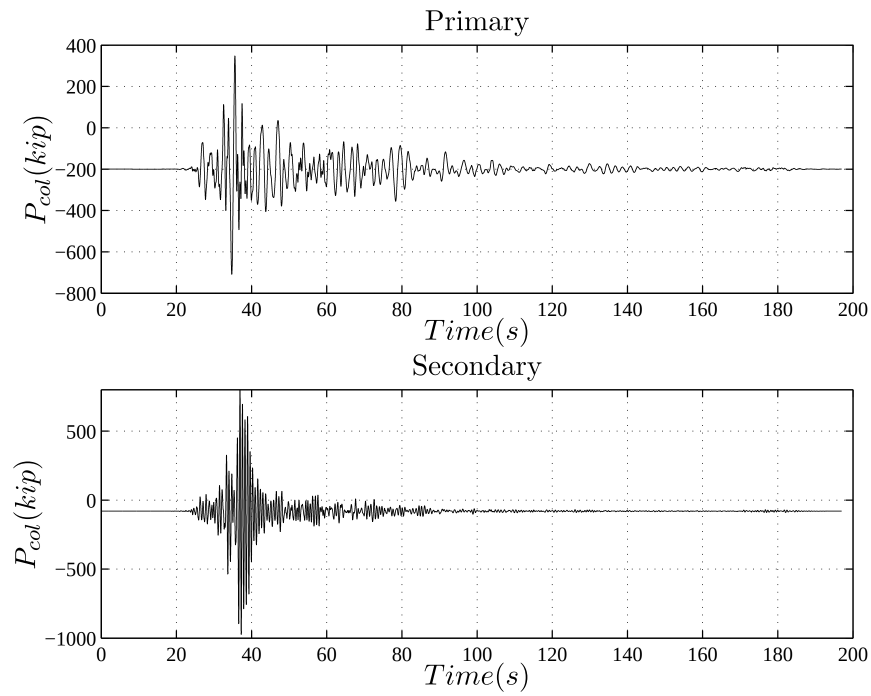

Figure 4.2: Mean column force response time history of the 20 by 8 system structures founded on soft clay subject to the 1999 Chi Chi earthquake, Chiayi station 034. Note differing vertical scales.

For each case presented herein, the results from the motion of the Chi Chi 1999 earthquake, Chiayi station 008 (CHY008) will be shown. These results are typical of all analyses performed. Additional results plots are presented in the appendix.

4.1 Sensitivity to Bulding Stiffness

Of the analyses performed, the output parameters observed in the 4-story by 4-story system contained some of the most discernible sensitivity to column depth. The results of the 4 by 4 system on dense sand subject to the 1999 Chi Chi CHY008 motion are presented below in their entirety. Figures 4.3 through 4.7 present the mean response time histories of the Primary and Secondary structures for each of the five output parameters.

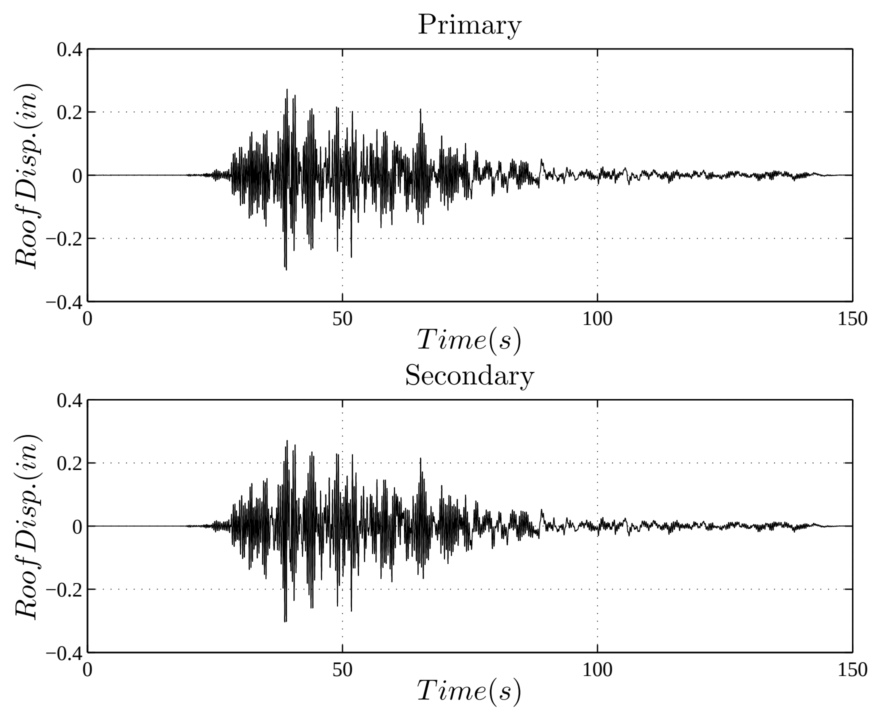

Figure 4.3: Mean roof displacement response time history of the 4 by 4 system structures founded on dense sand subject to the 1999 Chi Chi earthquake, Chiayi station 008.

In addition to these mean response time histories, each analysis was considered with a 10 percent change in column depth of the Primary structure, while the Secondary structure was

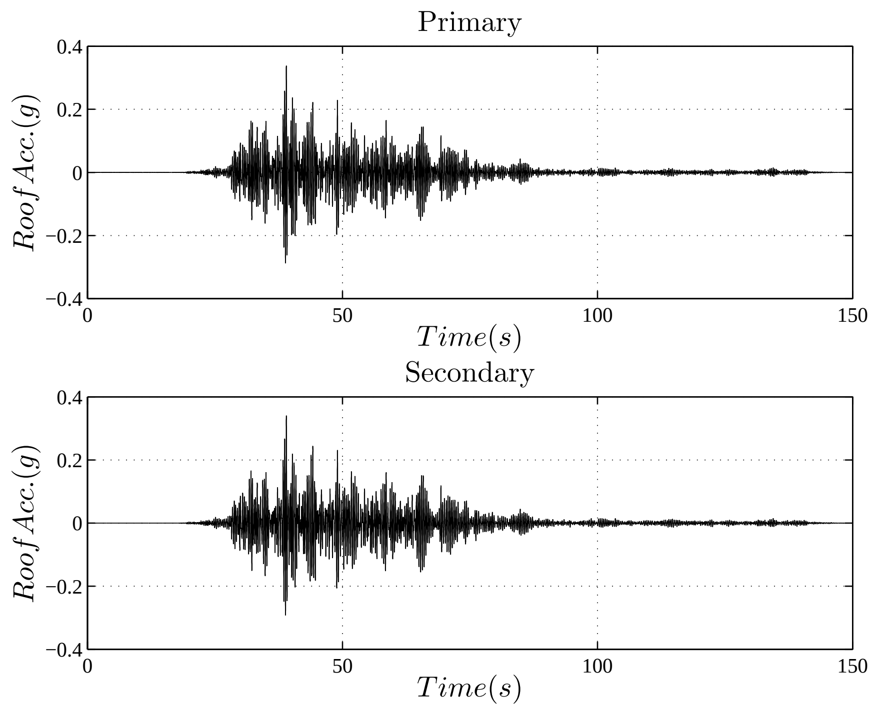

Figure 4.4: Mean roof acceleration response time history of the 4 by 4 system structures founded on dense sand subject to the 1999 Chi Chi earthquake, Chiayi station 008.

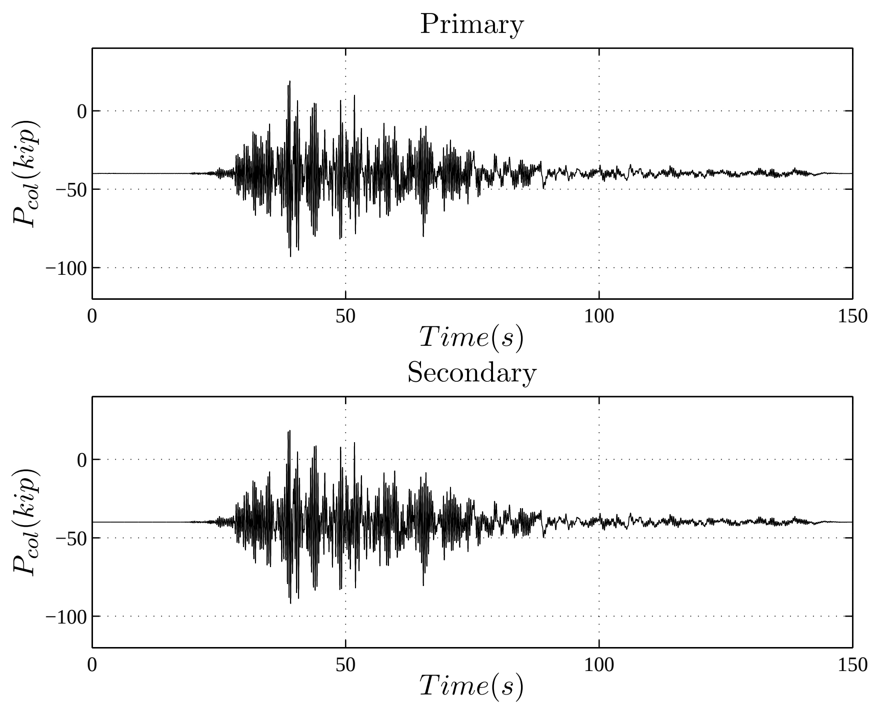

Figure 4.5: Mean column force response time history of the 4 by 4 system structures founded on dense sand subject to the 1999 Chi Chi earthquake, Chiayi station 008.

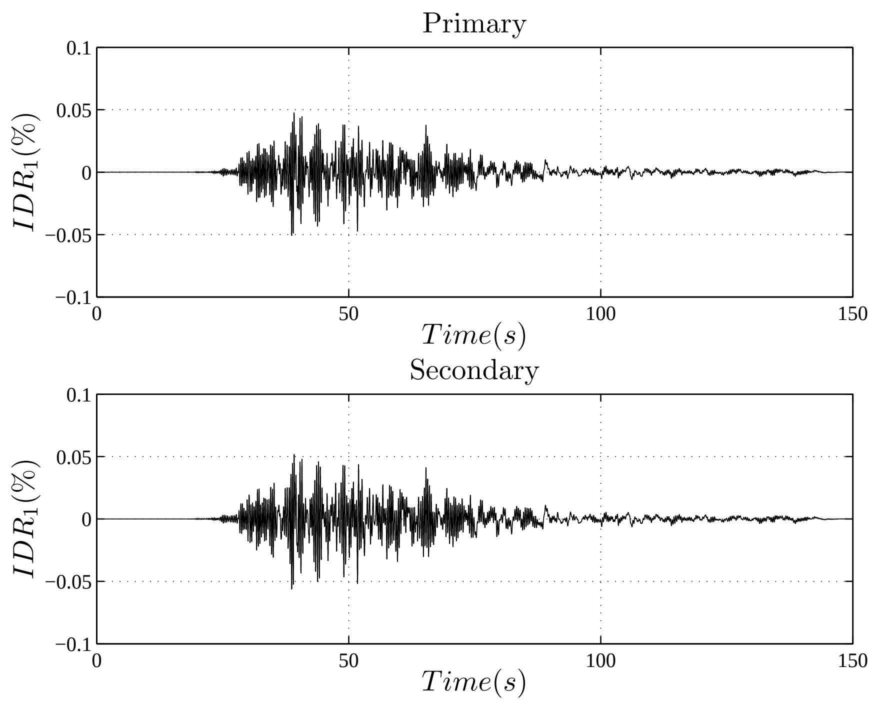

Figure 4.6: Mean first-story IDR response time history of the 4 by 4 system structures founded on dense sand subject to the 1999 Chi Chi earthquake, Chiayi station 008.

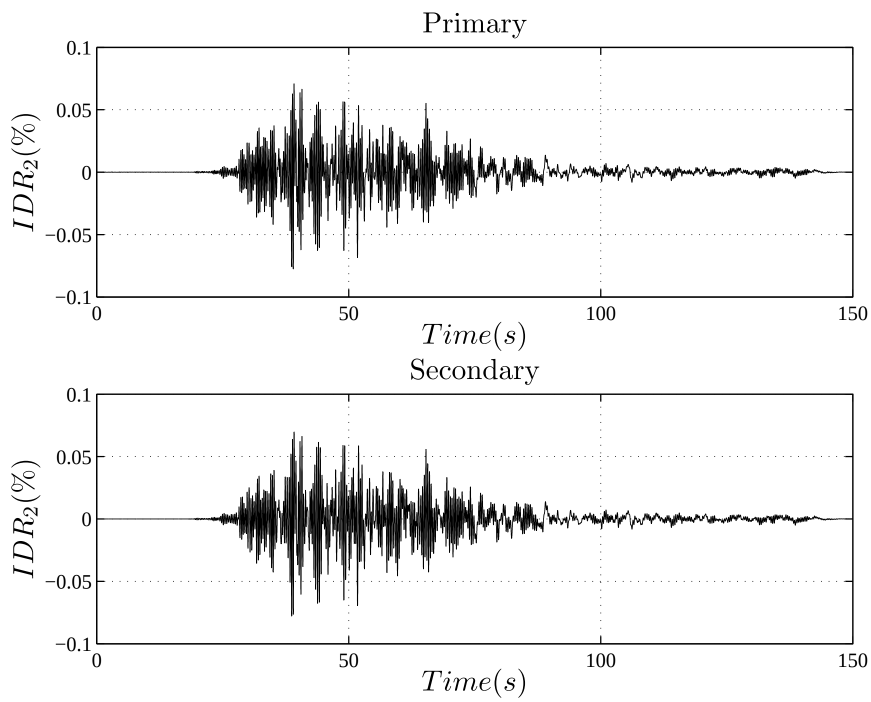

Figure 4.7: Mean second-story IDR response time history of the 4 by 4 system structures founded on dense sand subject to the 1999 Chi Chi earthquake, Chiayi station 008.

left unchanged. For each output parameter, all three response time histories are plotted on the same axes. Because of the information density of these plots, it is difficult to discern the effects of the change in response while viewing the entire time history. A 10-second window was, therefore, selected to view the response time histories. For the Chi Chi CHY008 motion, the window of 35 to 45 seconds was selected. The mean response time history is shown in each figure as a dashed line, while each of the time histories with a 10 percent change in column depth applied is shown as a solid line.

Each of Figures 4.8 through 4.12 present the time history of the five selected output parameters with and without the change in column depth applied. As can be seen in all five figures, the response of the Primary structure changes significantly, while that of the Secondary structure remains almost unchanged. The change in the responses of the Primary structure is expected, inasmuch as the lateral stiffness of this structure is being directly changed. Changes in the response of the Secondary structure would not be expected unless the effects of SSSI are present. Thus, the changes in the response of the Secondary structure suggest that some SSSI effects have occurred in these analyses. However, these effects are minimal in these structural models subject to this earthquake motion.

Resultant time series are also similar when the buildings in the system are founded on the soft clay soil. Figure 4.13 shows that the mean roof displacement response time history exhibits similar motions, but with greater amplitude. The difference in the magnitude of the Primary and Secondary structures is due to the restrained left column of the primary structure. Figure 4.13 presents the roof displacement time histories that consider sensitivity to column depth. Similarly to the buildings founded on sand, the response of the Primary structure changes significantly, while that of the Secondary structure changes little.

For the other building systems, any changes in response were too small to be accurately discerned. Figure 4.15 shows the second-story IDR responses, including changes due to column depth modification, of the 8 by 8 system founded on soft clay. Though some change in the Secondary structure response can be discerned by a divergence of the three curves plotted atop one another, these changes can reasonably be considered entirely negligible.

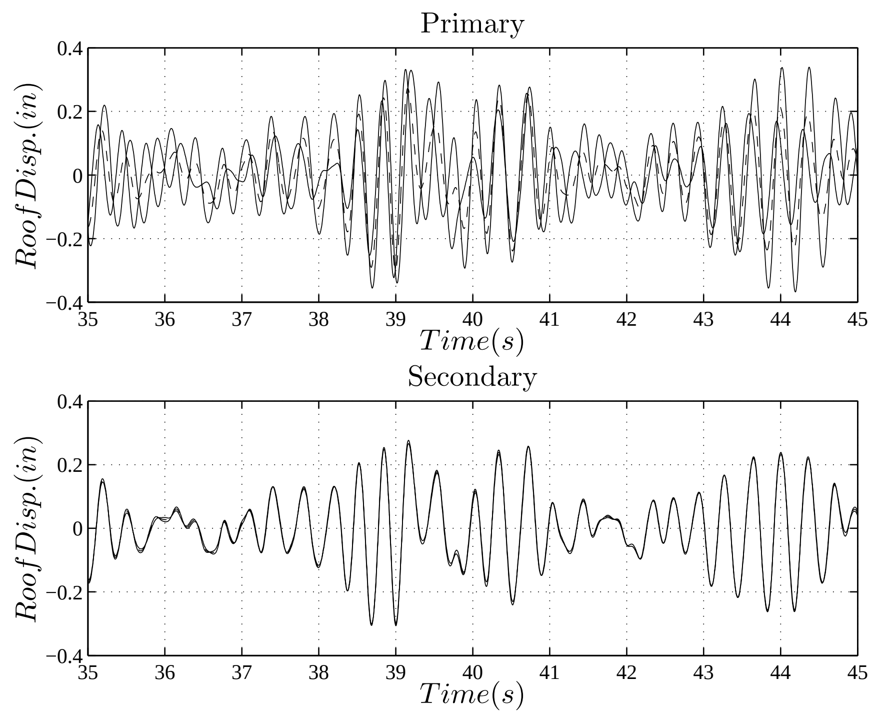

Figure 4.8: Mean roof displacement time history plotted with time histories which include 10 percent changes in column depth. The mean time history appears as a dashed line, and the two time histories that include sensitivity analysis appear as solid lines.

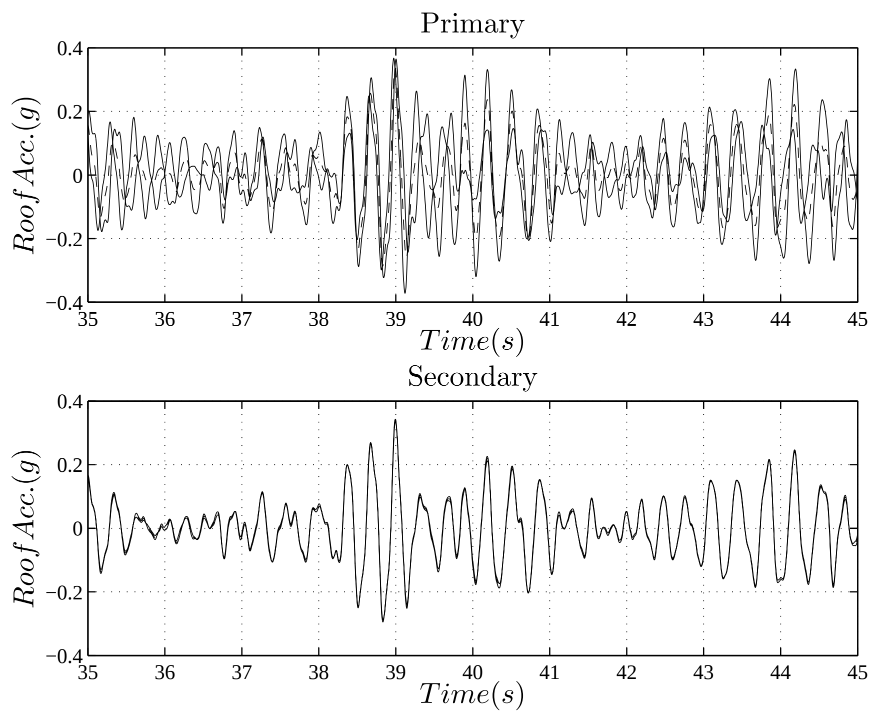

Figure 4.9: Mean roof acceleration time history plotted with time histories which include 10 percent changes in column depth. The mean time history appears as a dashed line, and the two time histories that include sensitivity analysis appear as solid lines.

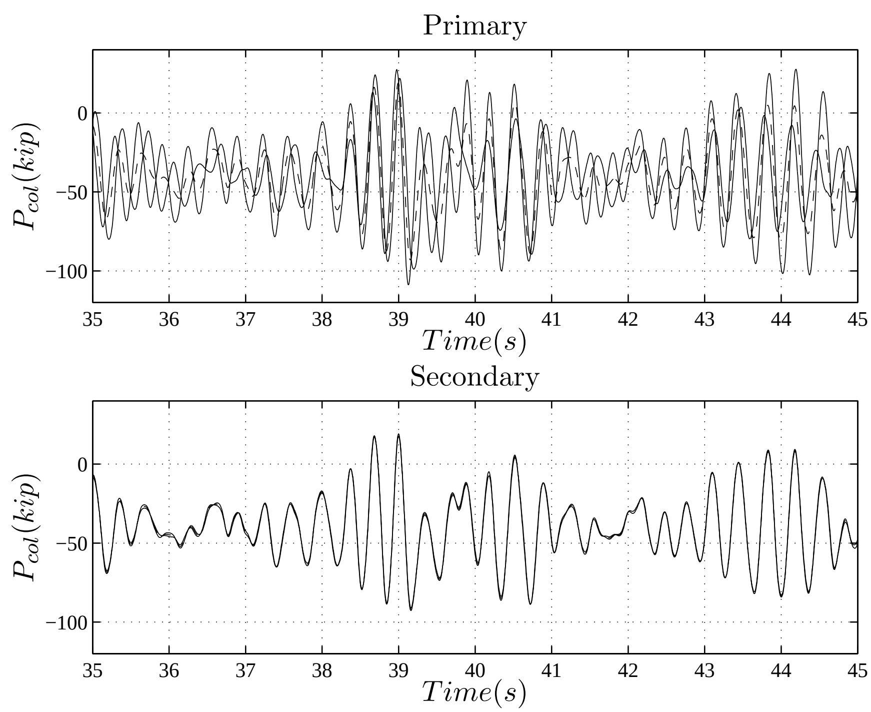

Figure 4.10: Mean column force time history plotted with time histories which include 10 percent changes in column depth. The mean time history appears as a dashed line, and the two time histories that include sensitivity analysis appear as solid lines.

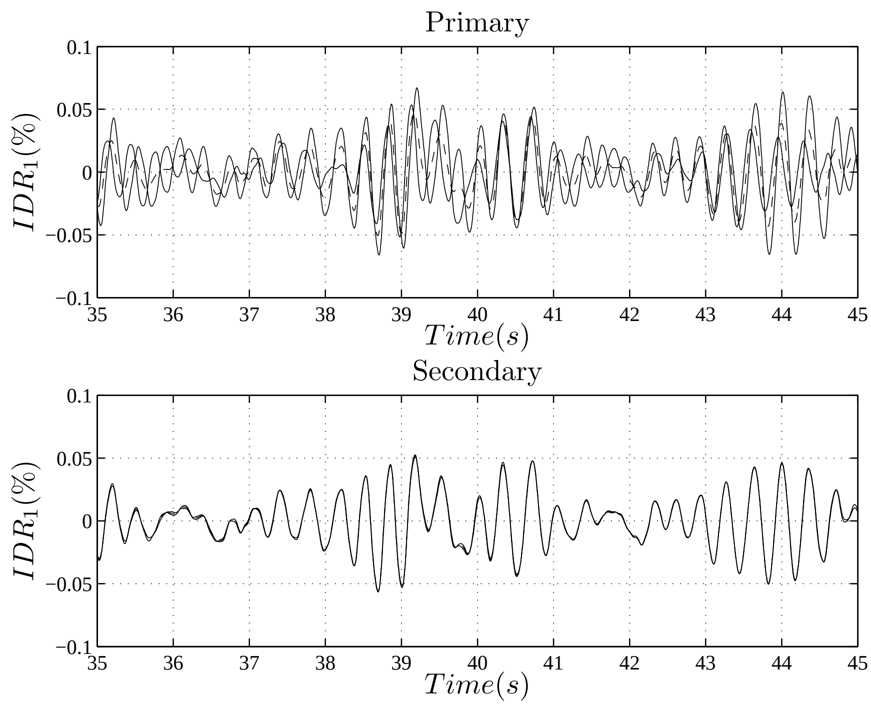

Figure 4.11: Mean first-story IDR time history plotted with time histories which include 10 percent changes in column depth. The mean time history appears as a dashed line, and the two time histories that include sensitivity analysis appear as solid lines.

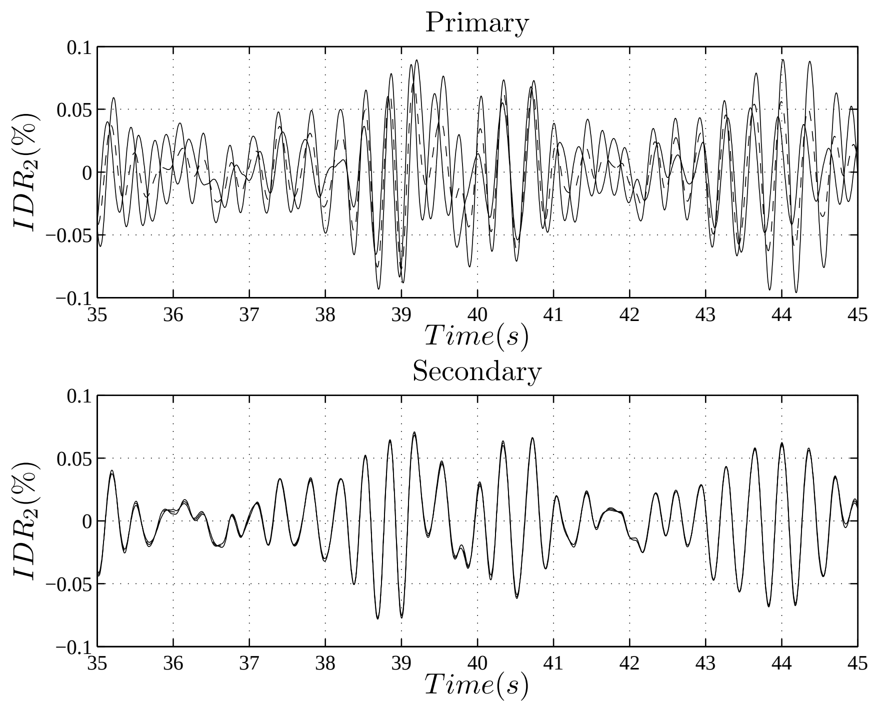

Figure 4.12: Mean second-story IDR time history plotted with time histories which include 10 percent changes in column depth. The mean time history appears as a dashed line, and the two time histories that include sensitivity analysis appear as solid lines.

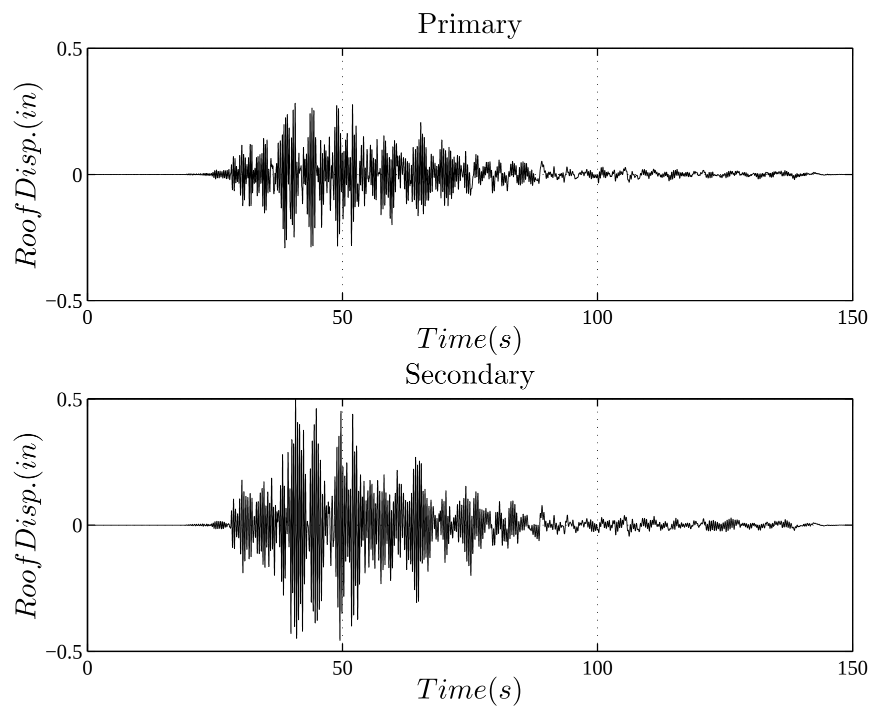

Figure 4.13: Mean roof displacement response time history of the 4 by 4 system structures founded on soft clay subject to the 1999 Chi Chi earthquake, Chiayi station 008.

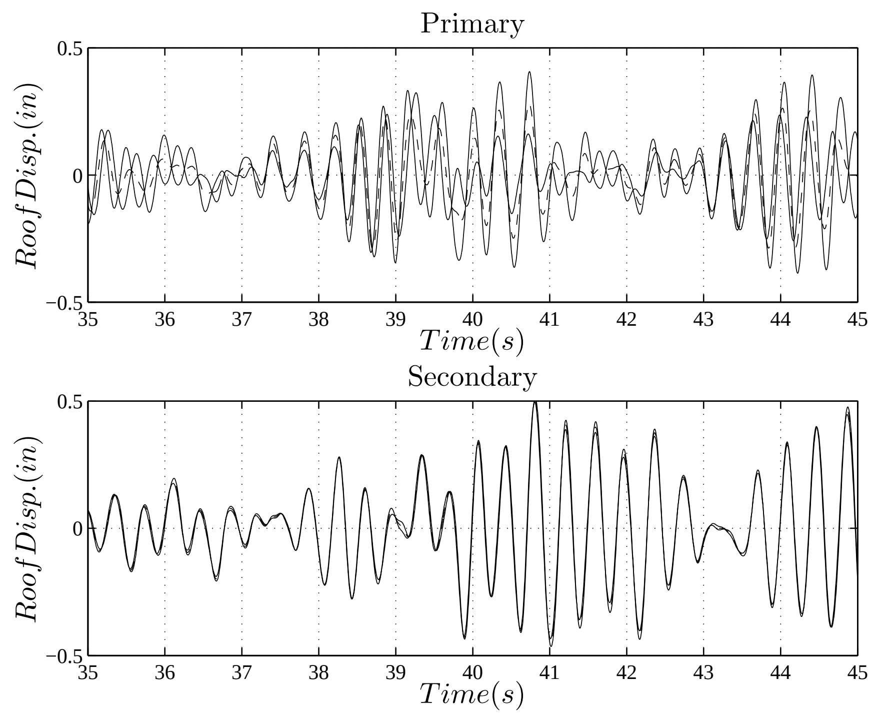

Figure 4.14: Mean roof displacement time history plotted with time histories which include 10 percent changes in column depth. The mean time history appears as a dashed line, and the two time histories that include sensitivity analysis appear as solid lines.

The divergence of the curves can be discerned by either the appearance of three distinct curves, or by a curve that appears slightly thicker in places because of only slight divergence of the curves. Similar results were found in all other structural systems for all other response output parameters.

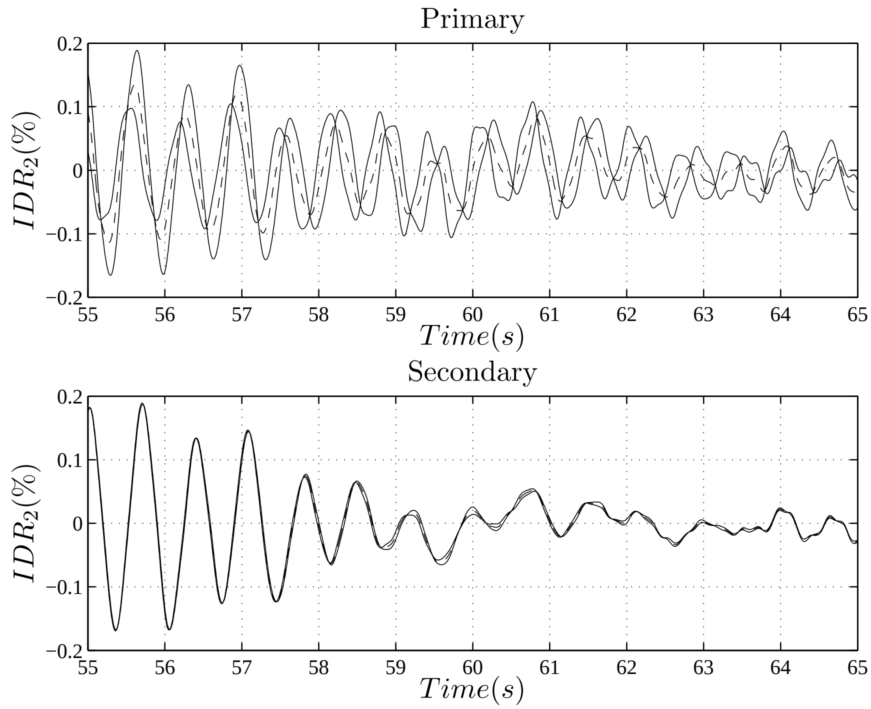

Figure 4.15: Second-story IDR responses of the 8 by 8 system founded on soft clay, including changes for sensitivity analysis. The mean time history appears as a dashed line, and the two time histories that include sensitivity analysis appear as solid lines.

Another observation from these analyses is that there is a difference in responses of symmetrical systems (i.e. 4 by 4, 8 by 8, and 20 by 20) caused by the difference in the boundary conditions between the Primary and Secondary structures. The differences in response of the symmetrical system is most observable in the 20 by 20 system, where the magnitude of response and influence of higher modes is greatest. The output parameter time series taken at the bottom of each structure (i.e. column force and IDR) tend to be similar, as shown in Figure 4.16, which displays the column force response for the 20 by 20 system founded on dense sand. However, the effects of the differing boundary conditions becomes more evident in the response time series recorded in the higher stories. Figure 4.17 shows the roof displacement response of the same system.

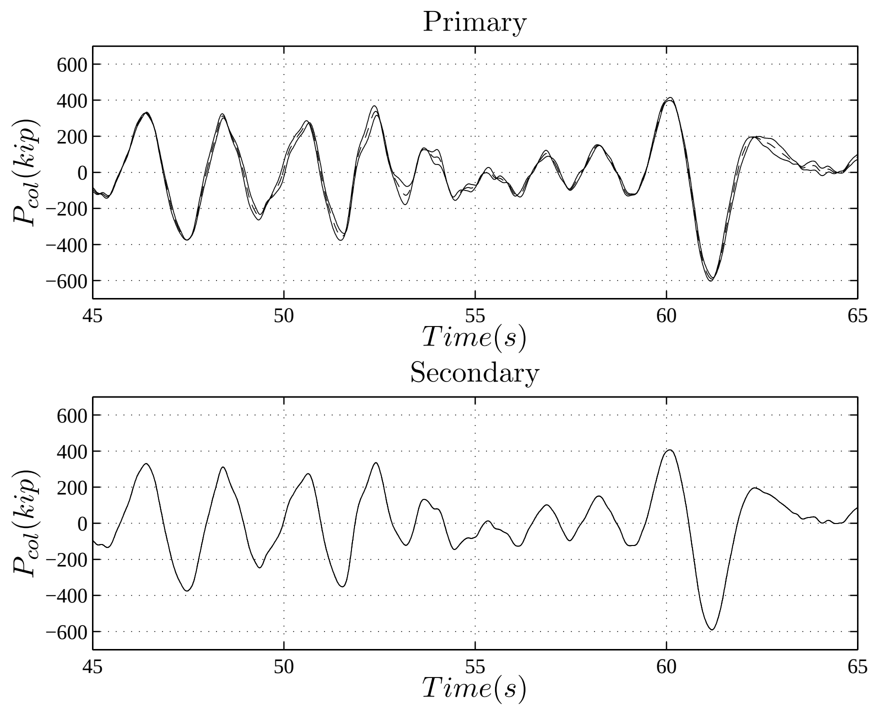

Figure 4.16: Mean column force time history plotted with time histories which include 10 percent changes in column depth. The mean time history appears as a dashed line, and the two time histories that include sensitivity analysis appear as solid lines.

In these analyses, P-Δ effects were not considered to be significant. Though there is a set of vertical loads on each structure and lateral deflection of the structure, the effects would not be great enough to induce significant additional overturning moment. These P-Δ effects would affect the 20-story structure more than either of the others, because it is significantly taller, with identical width. For this structure, the maximum displacement experienced for any earthquake motion was on the order of 1.5 ft in a 200-ft tall structure. This degree of deflection is likely not enough to induce significant P-Δ effects, even if all mass was lumped at the top of the structure. However, the mass is distributed at each floor, making P-Δ effects even less significant.

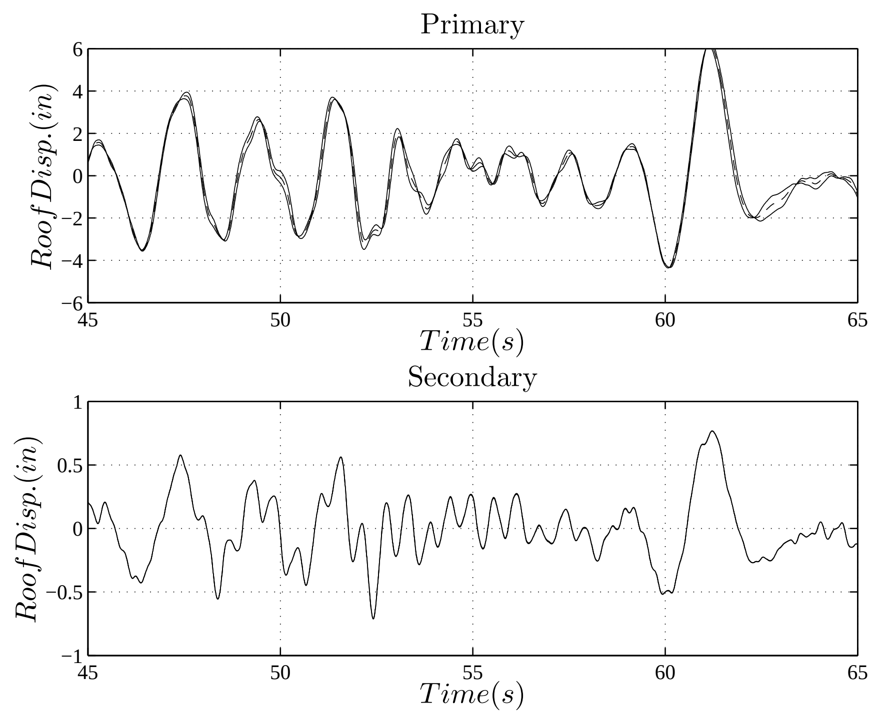

Figure 4.17: Roof displacement responses of the 20 by 20 system founded on dense sand, including changes for sensitivity analysis. The mean time history appears as a dashed line, and the two time histories that include sensitivity analysis appear as solid lines. Note differing vertical scales.

4.2 Sensitivity to Building Floor Mass

The sensitivity of output parameters to changes in building mass is similar to that for changes in structural stiffness. This result is expected, inasmuch as stiffness and mass are the two fundamental parameters which determine the natural frequency of a structure. For a fixed-base single degree of freedom structure, the fundamental natural frequency is given by

$$f = 2\pi\sqrt{\frac{k}{m}} \tag{4.2}$$

where k is the lateral stiffness of the structure and m is the mass thereof. Though the structures analyzed as part of this research have multiple degrees of freedom, the principle that natural frequency is proportional to stiffness and inversely proportional to mass remains valid (Chopra, 2012). To make this calculation for a multiple degree of freedom system, the mass and stiffness matrices, which account for each degree of freedom, would be constructed and reduced in order to find the natural frequency for each mode of structural vibration.

Figures 4.18 through 4.22 illustrate the responses of each of the five considered output parameters for both the Primary and Secondary structures in the 4 by 4 system founded on dense sand. These plots are similar to those given as Figures 4.8 through 4.12 in the previous section, except that they consider sensitivity to floor mass instead of column depth (also, recall that the full response time histories are given as Figures 4.3 through 4.7 of the previous section.) The plots shown in Figures 4.18 through 4.22 exhibit similar changes in response with respect to change in floor mass as was seen with change in stiffness. As expected, the Primary structure exhibited a significant change in response, and the Secondary structure showed only a few small changes in response.

Additionally, the other structural systems also showed little sensitivity to changes in floor mass. Some divergence of the curves occurred at certain points, as shown in Figure 4.23, which shows the second-story IDR response of the 8 by 8 system on dense sand.

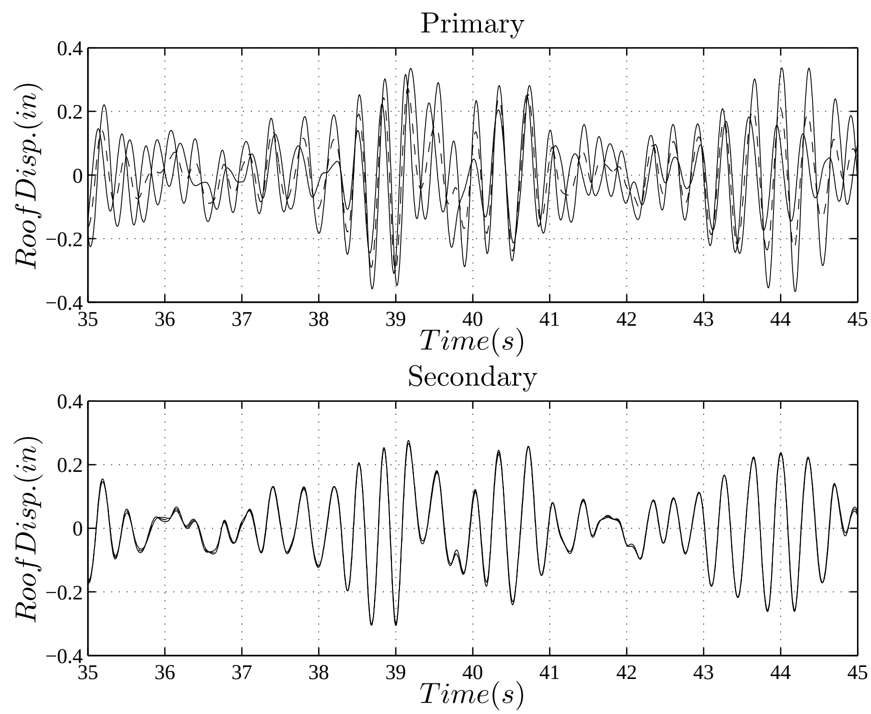

Figure 4.18: Roof displacement responses of the 4 by 4 system founded on dense sand, including changes for sensitivity analysis. The mean time history appears as a dashed line, and the two time histories that include sensitivity analysis appear as solid lines.

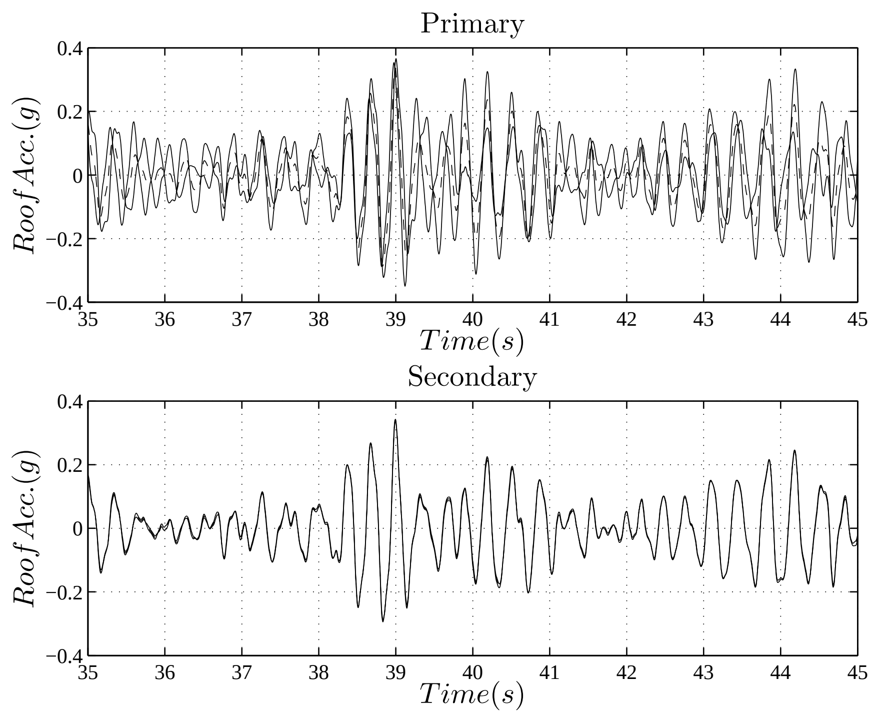

Figure 4.19: Roof acceleration responses of the 4 by 4 system founded on dense sand, including changes for sensitivity analysis. The mean time history appears as a dashed line, and the two time histories that include sensitivity analysis appear as solid lines.

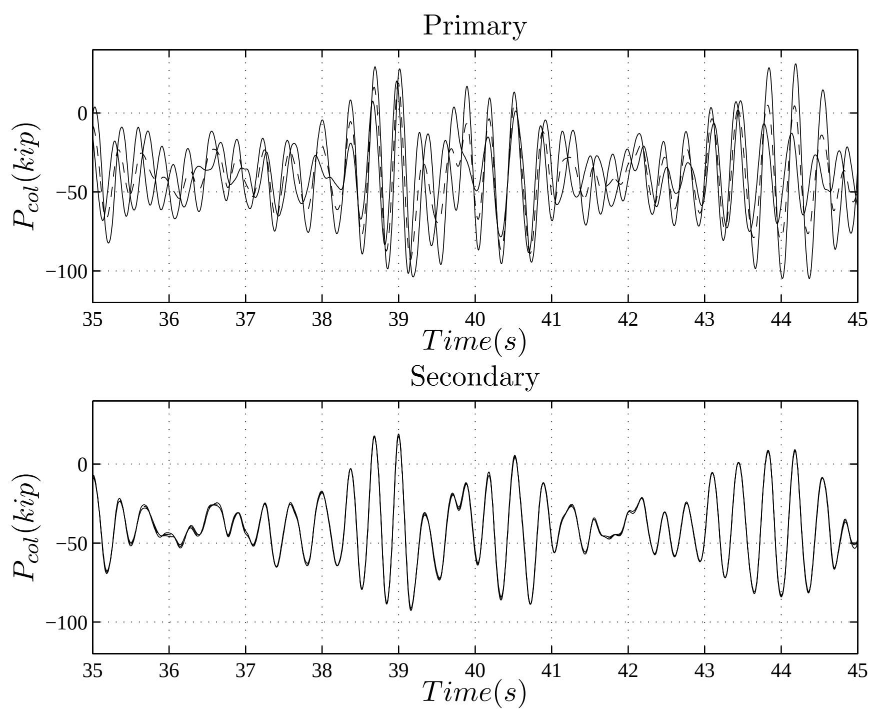

Figure 4.20: Column force responses of the 4 by 4 system founded on dense sand, including changes for sensitivity analysis. The mean time history appears as a dashed line, and the two time histories that include sensitivity analysis appear as solid lines.

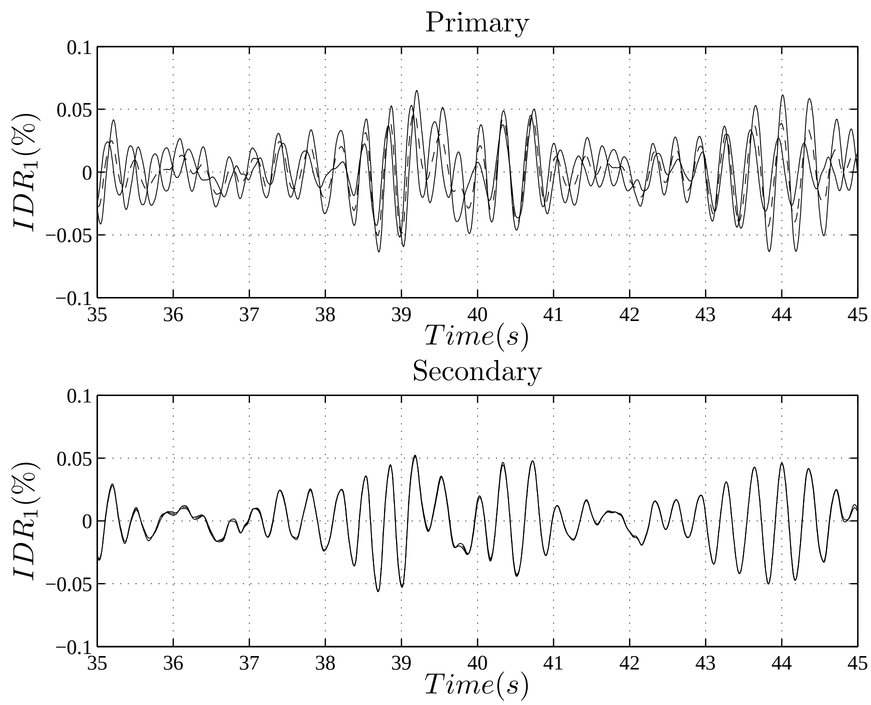

Figure 4.21: First-story IDR responses of the 4 by 4 system founded on dense sand, including changes for sensitivity analysis. The mean time history appears as a dashed line, and the two time histories that include sensitivity analysis appear as solid lines.

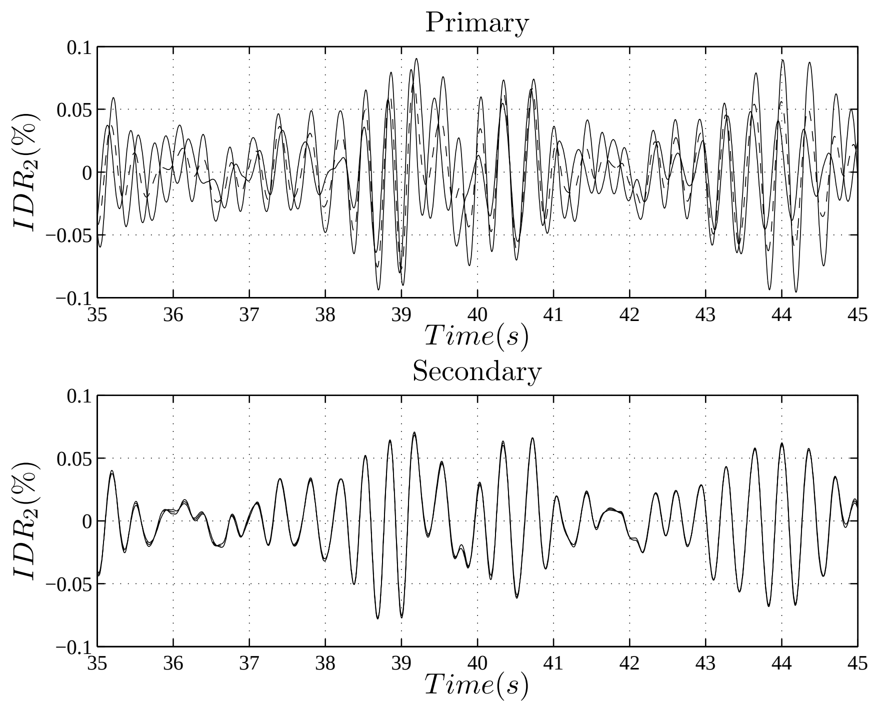

Figure 4.22: Second-story IDR responses of the 4 by 4 system founded on dense sand, including changes for sensitivity analysis. The mean time history appears as a dashed line, and the two time histories that include sensitivity analysis appear as solid lines.

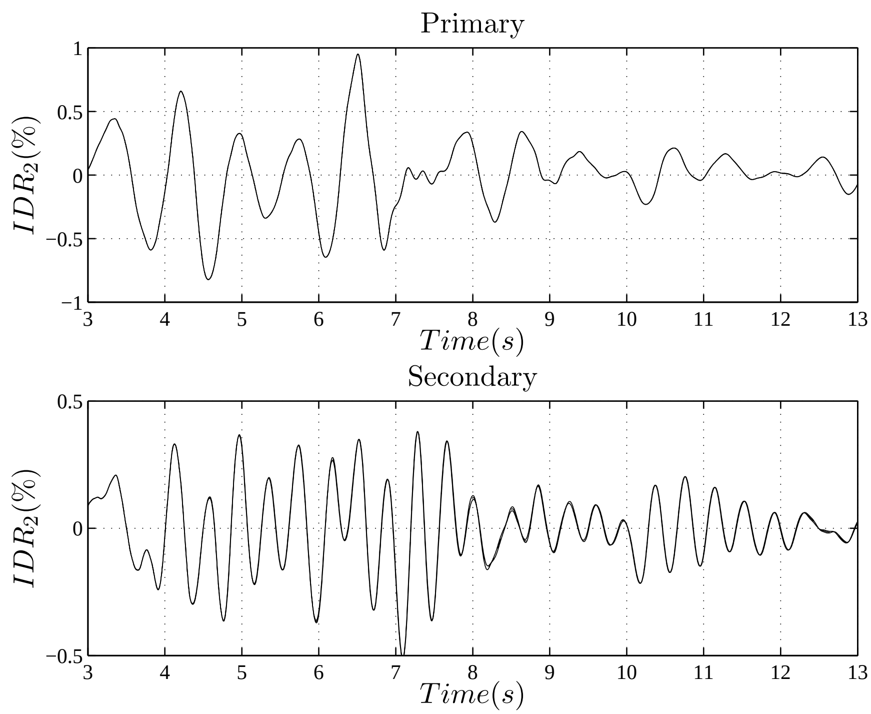

Figure 4.23: Second-story IDR responses of the 8 by 8 system founded on dense sand, including changes for sensitivity analysis. The mean time history appears as a dashed line, and the two time histories that include sensitivity analysis appear as solid lines.

4.3 Structure-Soil-Structure Spring Stiffness Sensitivity

In the majority of steel moment-resisting frame structures, changes in the stiffness of the structure-soil-structure spring induced almost no changes in the response of either the Primary or the Secondary structure. In most of the associated sensitivity plots, there is no discernible difference in the three response curves plotted atop one another. The output files from the numerical analyses were examined to ensure that the response values were not precisely identical among each of the three plotted curves. Upon examination, the output files were found to contain distinct values for each of the three responses, but each was in a narrow range.

Similar to the previous two sections, Figures 4.24 through 4.28 represent the responses of both the Primary and Secondary structures in each of the five output parameters, including sensitivity analyses. The mean responses over the entire earthquake motion for each output parameter are given as Figures 4.3 through 4.12.

Some of the analyses exhibited slight, but discernible sensitivity to changes in structure-soil-structure spring stiffness. These changes were not any higher than those exhibited in the analyses of building stiffness and floor mass, and can be reasonably deemed negligible. An example of this sensitivity can be observed in the second-story interstory drift ratio response for the 8 by 4 system founded on soft clay, subject to the 1994 Northridge, California earthquake, Sylmar Converter Station motion (note the different motion). As seen in Figure 4.29, some divergence of the Secondary structure curve can be discerned, but has little effect on the overall response of the system.

4.4 Infinitely-long Shear Wall Models

The modified models of infinitely-long, rigid shear walls were also tested for each earthquake motions and soil type considered. Figure 4.30 shows the mean lateral displacement response of the top of both Primary and Secondary structures, subject to the CHY008 motion, founded on dense sand. Figure 4.31 shows the mean lateral displacement curve, as well

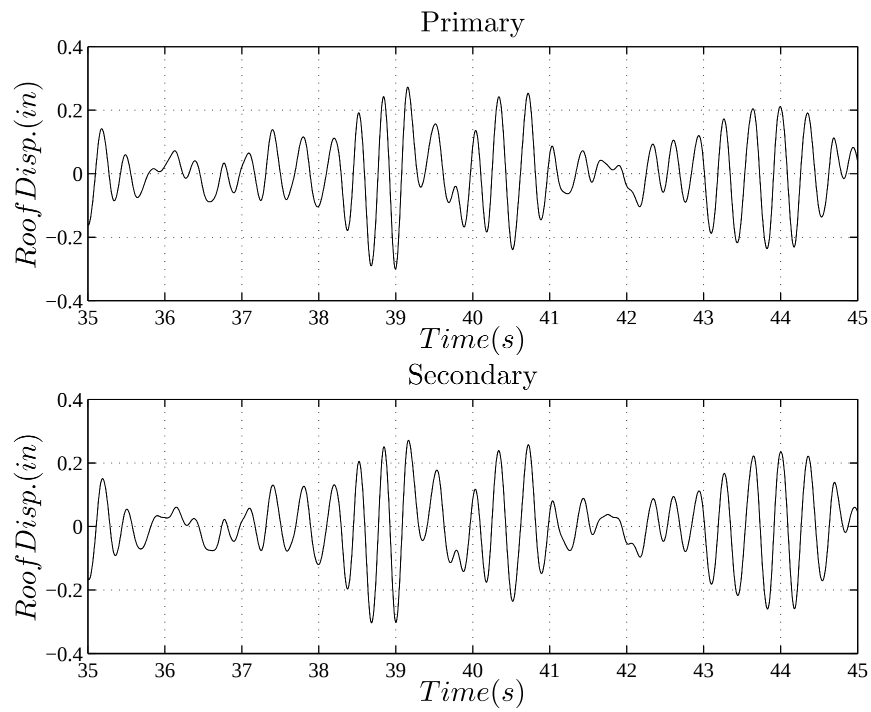

Figure 4.24: Roof displacement responses of the 4 by 4 system founded on dense sand, including changes for sensitivity to structure-soil-structure spring stiffness. The mean time history appears as a dashed line, and the two time histories that include sensitivity analysis appear as solid lines.

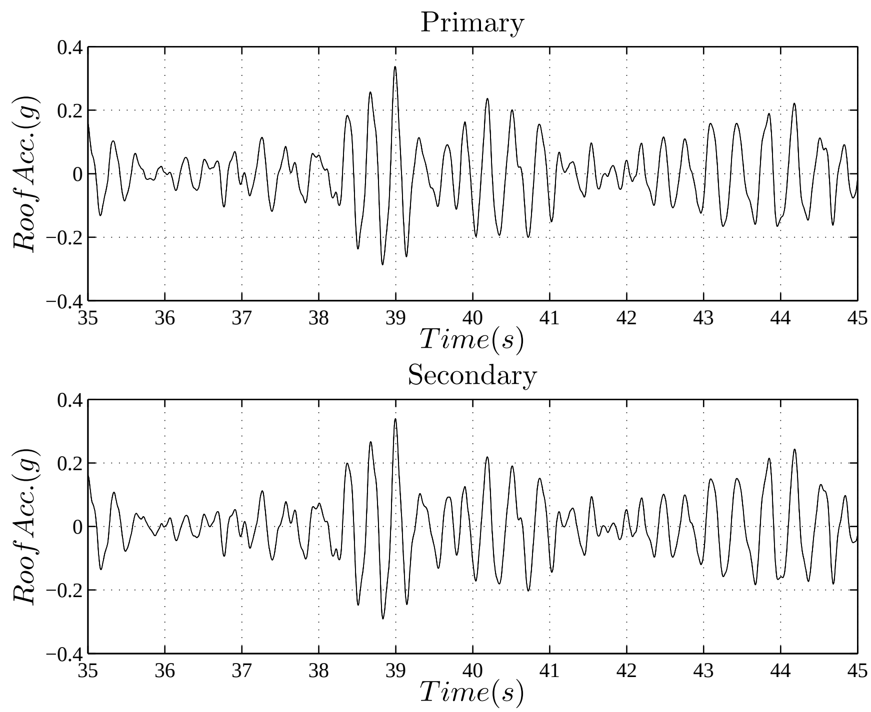

Figure 4.25: Roof acceleration responses of the 4 by 4 system founded on dense sand, including changes for sensitivity to structure-soil-structure spring stiffness. The mean time history appears as a dashed line, and the two time histories that include sensitivity analysis appear as solid lines.

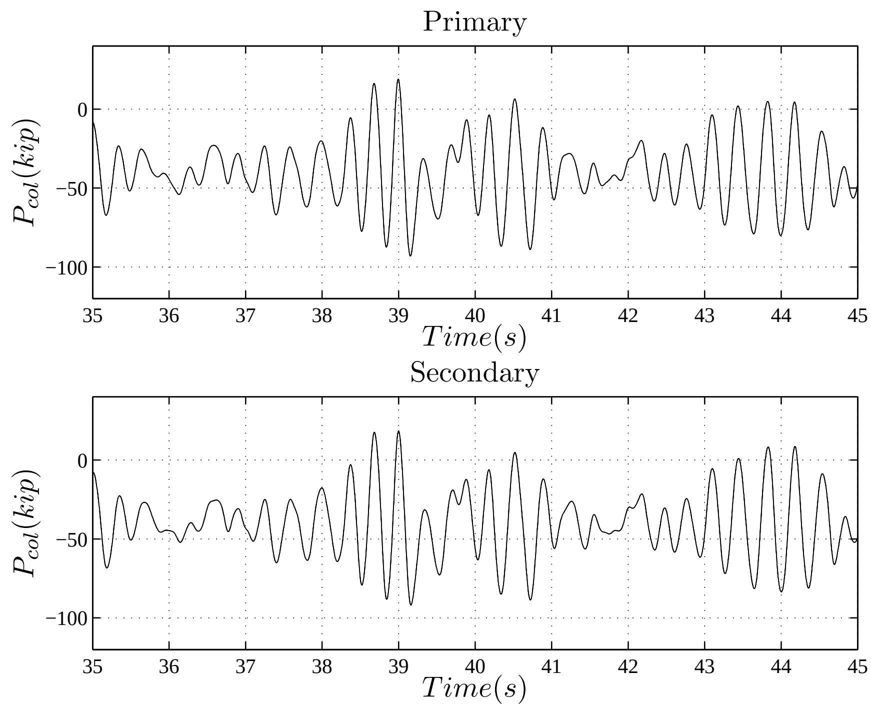

Figure 4.26: Column force responses of the 4 by 4 system founded on dense sand, including changes for sensitivity to structure-soil-structure spring stiffness. The mean time history appears as a dashed line, and the two time histories that include sensitivity analysis appear as solid lines.

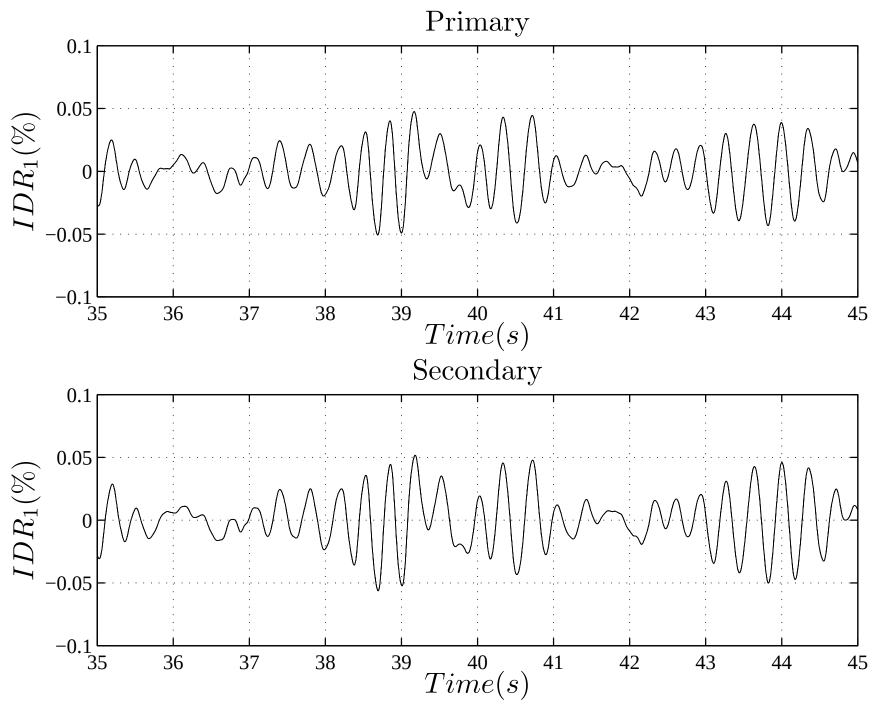

Figure 4.27: First-story IDR responses of the 4 by 4 system founded on dense sand, including changes for sensitivity to structure-soil-structure spring stiffness. The mean time history appears as a dashed line, and the two time histories that include sensitivity analysis appear as solid lines.

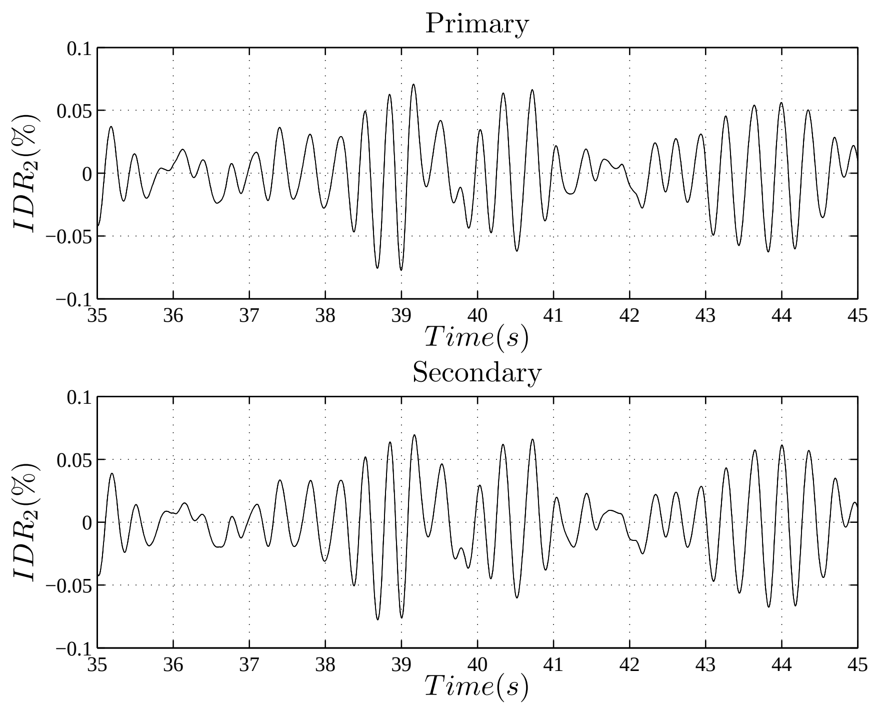

Figure 4.28: Second-story IDR responses of the 4 by 4 system founded on dense sand, including changes for sensitivity to structure-soil-structure spring stiffness. The mean time history appears as a dashed line, and the two time histories that include sensitivity analysis appear as solid lines.

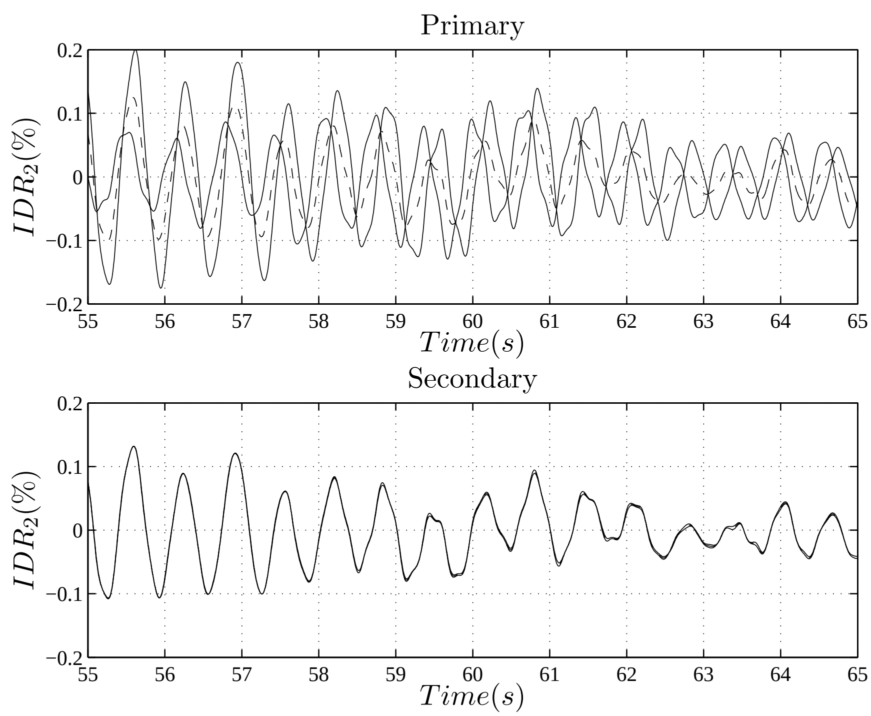

Figure 4.29: Second-story IDR responses of the 8 by 4 system founded on soft clay, subject to the Northridge Sylmar Converter Station motion, including changes for sensitivity to structure-soil-structure spring stiffness. The mean time history appears as a dashed line, and the two time histories that include sensitivity analysis appear as solid lines. Note differing vertical scales.

as the curves considering sensitivity to wall mass for the same earthquake motion and soil type. These results exhibit an almost entirely in-phase relationship between the Primary and Secondary structure. This in-phase relationship is maintained when sensitivity analyses are performed and changes to the design parameters are made. This finding agrees with the findings of Luco and Contesse (1973) and Wong and Trifunac (1975). These researchers found that the response of a smaller wall could be significantly affected by the motion of an adjacent, larger wall. However, the motion of one wall did not entirely dominate the other. The almost complete harmony of the Primary and Secondary wall motions found in this study is unexpected and likely does not reflect the realistic response of structures atop soil.

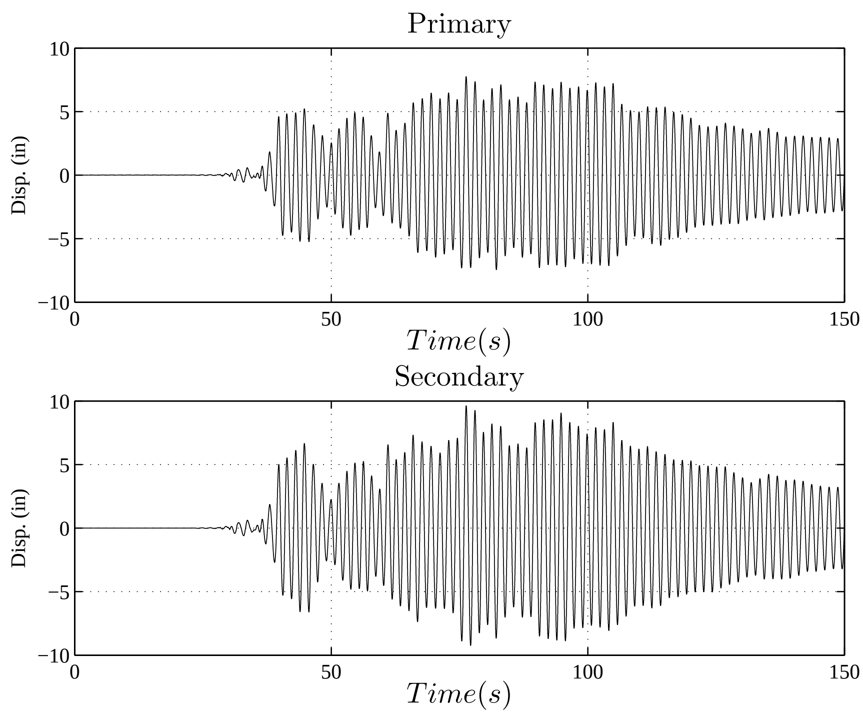

Figure 4.30: Mean lateral displacement time history of Primary and Secondary shear walls, founded on dense sand and subject to the 1999 Chi Chi CHY008 motion.

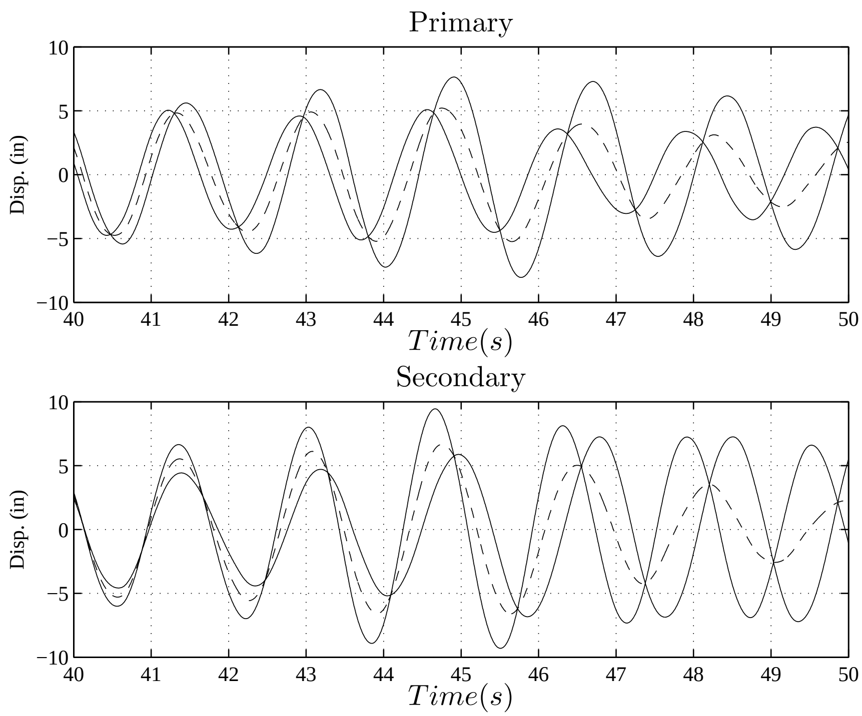

Figure 4.31: Lateral displacement response time history of Primary and Secondary shear walls founded on dense sand, including changes for sensitivity analysis. The mean time history appears as a dashed line, and the two time histories that include sensitivity analysis appear as solid lines.

Chapter 5 Conclusions

5.1 Direct Differentiation Method

The direct differentiation method (DDM) was used within the OpenSees framework for sensitivity analyses, to track changes in structural response with respect to changes in design parameters. The DDM was found to be an efficient and effective method of analyzing adjacent structures and the soil that underlies them. For a single ground motion, changes in structural and soil response could be estimated using a first-order approximation in which the derivative of the mean response is multiplied by the magnitude of a parameter change. The efficiency of the DDM lies in using the same, factored stiffness matrix to solve for the mean response and the sensitivity of response to each parameter, where other sensitivity analysis methods would require modification to the factored stiffness matrix. This is more efficient than the traditional method of senstivity analysis, in which parameters are modified and the analysis is rerun. The DDM allows the effect of parameter changes on the response of adjacent structures and underlying soil to be assessed for several ground motions in approximately the same amount of time it would take to analyze the system repeatedly for a single ground motion with perturbed parameter values.

The OpenSees framework allows for several output parameters and design parameters to be selected for sensitivity analyses. Within the DDM analysis, design and soil parameters can be changed in the Primary structure, while left unchanged in the Secondary structure. Observing changes in the response of the Secondary structure when no changes were made to its design parameters allows analysts to discern SSSI effects. For each output parameter, the selected design parameter can be increased and/or decreased by a specified proportion and the model re-analyzed to discern changes in response.

Changes in response can be observed by divergence of response curves considering parametric sensitivity from the mean curves. These results can be observed, particularly, as the mean response of the structure is plotted on the same axes as the responses with design parameters changed. In this configuration, analysts can see the change in response of each structure as a visual difference between the curves, allowing for relatively simple discernment of SSSI effects.

5.2 Implications of Structure-Soil-Structure Interaction

The results shown imply that the effects of structure-soil-structure interaction are minimal on the types of steel moment-resisting frame structures examined. Although there is some divergence in the response of the Secondary structure when the design parameters of the Primary structure are modified, the divergence is largely observed to be negligible. Had structure-soil-structure interaction effects been more significant, the response of the Secondary structure would have changed more significantly when changes were made to the Primary structure.

The results of earlier researchers, such as Luco and Contesse (1973) and Wong and Trifunac (1975) showed that SSSI effects could be significant for very specific scenarios. For instance, the results shown in Luco and Contesse (1973) and Wong and Trifunac (1975) were based on the model of adjacent, infinitely-long shear walls subject to SH waves. The infinitely-long shear wall model varies in two significant ways from the moment-resisting frame structures examined. First, the moment-resisting frames used herein are inherently more flexible than the shear walls. This flexibility tends to induce higher modes of vibration, which changes the vibrational characteristics and the energy dissipation associated therewith. The second difference between the two models is that the infinitely-long shear walls model employed by Luco and Contesse (1973) and Wong and Trifunac (1975) uses a more complex soil model, which considers the complex rocking mode of vibration. The soil in the moment-resisting frame model only considers the translational mode of vibration.

The difference in results between these two models could be as a result of either of these two model differences or could be a combination of these differences with other, smaller factors.

The tests of the infinitely-long shear walls model that were run as a part of this study largely corroborated the findings of previous researchers. However, the results presented herein are preliminary, because the full details of the previous researchers models could not be fully elucidated. Unlike the results of Luco and Contesse (1973) and Wong and Trifunac (1975), the tested shear walls vibrate almost entirely in phase with one another. This result suggests that the model of the infinitely-long shear walls used may not be sufficiently robust to accurately model the behavior of the soil during vibration.

The results of these numerical models corroborates those found by Mason et al. (2013) and Trombetta et al. (2013) in which scaled moment-resisting frames were subject to earthquake motions within a centrifuge. These studies concluded that the effects of structure-soil-structure interaction are present in adjacent moment-resisting frame structures, but are relatively small. Both the results of Mason et al. (2013) and Trombetta et al. (2013) and those presented herein are likely functions of a complex system of interaction between adjacent moment-resisting frame structures. The response of each individual structure to loading from an earthquake is a complex event, particularly when the effects of soil-structure-interaction and higher modes of vibration are relevant. This complexity makes the interaction of adjacent buildings through the soil mass that underlies them unlikely in most realistic scenarios. It is unlikely that the complex response of any two adjacent buildings would synchronize in a way that would produce structure-soil-structure interaction effects.

5.3 Limitations and Future Work

A limitation of this work, that should be further investigated, is the soil model. A set of single springs that have an assigned value of stiffness and no damping provides a reasonable approximation of soil response, but is not a precise, robust soil model. Furthermore, each of the systems analyzed herein only consider one degree of freedom: the lateral translational mode for the moment-resisting frame structures and the rotational mode for the rigid shear walls. In realistic scenarios, a structure will vibrate in both vertical and horizontal translational modes and the rotational mode simultaneously.

A more thorough model would also consider the effects of shear modulus reduction and plastic soil damping (see Seed and Idriss, 1970). When soil is subject to hysteretic motion, it usually exhibits changes in both stiffness and damping as functions of shear strain. The effect is usually a decrease in soil stiffness and an increase in damping. However, the natures of modulus reduction and soil damping vary widely with soil type and specific characterization of the soil is required to understand its behavior. How the application of these principles to this model would affect the results is unclear. Reduced stiffness would likely result in greater response and both the presence of damping and its increase as a function of hysteretic motion would likely reduced the magnitude of response. Further research is needed to elucidate the effects of modulus reduction and soil damping on the effects of SSSI.

Additionally, a realistic, finite structural system can vibrate in six different modes: the vertical mode, two horizontal modes, two rocking modes, and the torsional mode. A more robust model would take into consideration more, if not all of these modes. For the two-dimensional problems that were considered herein, the number of possible modes is reduced to three: vertical, horizontal, and rocking. Further research could realistically consider all three of the applicable modes of vibration for the two-dimensional case.

In addition to the soil model, the structural models analyzed are not altogether realistic. In particular, each structure was modeled with a single bay and identical column shapes along the height of the structure. While a single bay may be a realistic model for the 4-story structure, 8- and 20-story buildings would likely have multiple bays. Additionally, while design engineers will sometimes use a single section up the entire height of the structure, they will often consider specifying smaller sections for higher story. The effects of having multiple bays and variable sections within a structure would make the model more realistic. It is unclear how a change in the number of bays would affect the results of these analyses. Additional bays would be further removed from the adjacent structure, which would tend to make the effects of multiple bays less significant. However, additional bays would also increase the stiffness of the structure, likely increasing the effects of SSSI.

A more robust model could consider a series of compression-only springs with assigned values of stiffness and damping and as well as more realistic moment-resisting frame structures. This type of soil model would be particularly valuable for these moment-resisting frame structures, in which the motion is largely translational. For the infinitely-long shear wall structures, it is likely that a finite element mesh would be needed to accurately model the soil behavior. Complex stress states associated with rocking motion and the transmission of motion through the soil mass and not easily modeled through springs. The use of the direct method (e.g., Kramer and Stewart, 2004) for analyzing soil-structure interaction effects — that is, modeling an entire soil-foundation-structure system, with proper constitutive models for all materials — is a research topic that deserves much more attention.

Bibliography

R.J. Apsel and J.E. Luco. Impedance functions for foundations embedded in a layered medium. *Earthquake Engineering & Structural Dynamics*, 15(2):213–231, 1987.

ASCE 7-10. *Minimum Design Loads of Buildings and Other Structures*. American Society of Civil Engineers, Reston, VA, 2010.

J.W. Baker, T. Lin, S.K. Shahi, and N. Jayaram. New ground motion selection procedures for the PEER transportation research program. Technical report, PEER, 2011.

M. Budhu. *Soil Mechanics and Foundations*. John Wiley and Sons, 4 edition, 2011.

A. K. Chopra. *Dynamics of Structures*. Prentice-Hall, Upper Saddle River, NJ, 4 edition, 2012.

F.C.P. de Barros and J.E. Luco. Identification of foundation impedance functions and soil properties from vibration tests of the hualien containment model. *Soil Dynamics and Earthquake Engineering*, 14:229–248, 1995.

R. Dobry and G. Gazetas. Dynamic response of arbitrarily shaped foundations. *Journal of Geotechnical Engineering*, pages 109–135, 1986.

C. M. Duke, J. E. Luco, A. R. Carriveau, P. J. Hradilek, R. Lastrico, and D. Ostrom. Strong earthquake motion and site conditions: Hollywood. *Bulletin of the Seismological Society of America*, 60(4):1271–1289, 1970.

George Gazetas. Formulas and charts for impedances of surface and embedded foundations. *Journal of Geotechnical Engineering*, 117(9):1363–1381, 1991.

G. W. Housner. Interaction of building and ground during and earthquake. *Bulletin of the Seismological Society of America*, 47(3):179–186, 1957.

Paul C. Jennings and Jacobo Bielak. Dynamics of building-soil interaction. *Bulletin of the Seismological Society of America*, 63(1):9–48, 1973.

Seunghyun Kim and Jonathan P. Stewart. Kinematic soil-structure interaction from strong motion recordings. *Journal of Geotechnical and Geoenvironmental Engineering*, 129(4): 323–335, 2003.

M. Kleiber, H. Antunez, T. D. Hien, and P. Kowalczyk. *Parameter Sensitivity in Nonlinear Mechanics*. John Wiley & Sons, 1997.

Steven L. Kramer and Jonathan P. Stewart. Geotechnical aspects of seismic hazards. In Yousef B. Bozorgnia and V. V. B. Bertero, editors, *Earthquake Engineering: from Engineering Seismology to Performance Based Engineering*. CRC Press, Boca Raton, FL, 2004.

T. H. Lee and D. A. Wesley. Soil-structure interaction of nuclear reactor structures considering through-soil coupling between adjacent structures. *Nuclear Engineering and Design*, 24(3):374–387, 1973.

H.-T. Lin. A hybrid method for problems of dynamics of foundations. In The University of Texas at Austin Department of Civil Engineering, editor, *Geotechnical Engineering Research Report GR84-16*, 1984.

H.-T. Lin, J.M. Roesset, and J.L. Tassoulas. Dynamic interaction between adjacent foundations. *Earthquake Engineering & Structural Dynamics*, 25:323–343, 1987.

J. Enrique Luco and Luis Contesse. Dynamic structure-soil-structure interaction. *Bulletin of the Seismological Society of America*, 63(4):1289–1303, 1973.

J. Lysmer. Efficient finite element analysis fo seismic soil-structure interaction. In Earthquake Engineering Research Center, editor, *in Report: EERC-75-34*, Berkeley, CA, 1975.

H. B. Mason, N. W. Trombetta, Z. Chen, J. D. Bray, T. C. Hutchinson, and B. L. Kutter. Seismic soil-foundation-structure interaction observed in geotechnical centrifuge experiments. *Soil Dynamics and Earthquake Engineering*, 2013.

Kapil Mathur. Effects of residual stresses and initial imperfections on earthquake response of steel moment frames. Master's thesis, University of Illinois at Urbana-Champaign, 2011.

F. McKenna, G. L. Fenves, and M. H. Scott. *Open System for Earthquake Engineering Simulation*. University of California, Berkeley, CA, 2000. http://opensees.berkeley.edu.

L. Menglin, C. Huaifeng, C. Xi, and Z. Yongmei. Structure-soil-structure interaction: Literature review. *Soil Dynamics and Earthquake Engineering*, 31:1724–1731, 2011.

R. G. Merritt and G. W. Housner. Effect of foundation compliance on earthquake stresses in multistory buildings. *Bulletin of the Seismological Society of America*, 44(4):551–569, 1954.

Jeffrey S. Mulliken and Dimitris L. Karabalis. Discrete model for dynamic through-the-soil coupling of 3-D foundations and structures. *Earthquake Engineering & Structural Dynamics*, 27(7):687–710, 1998.

George Mylonakis and George Gazetas. Seismic soil-structure interaction: Beneficial or detrimental? *Journal of Earthquake Engineering*, 4(3):277–301, 2000.

S. Nakagawa, M. Kuno, Y. Naito, T. Nozawa, T. Momma, J. Mizuno, T. Tsukamoto, S. Motohashi, and M. Niwa. Forced vibration tests and simulation analyses of a nuclear reactor building. *Nulcear Engineering and Design*, pages 145–156, 1998.

A. Neuenhofer and F. C. Filippou. Geometrically nonlinear flexibility-based frame finite element. *Journal of Structural Engineering*, 124(6):704–711, June 1998.

Dimitirs Pitilakis, Matt Dietz, David Muir Wood, Didier Clouteau, and Arezou Modaressi. Numerical simulation of dynamic soil-structure interaction in shaking table testing. *Soil Dynamics and Earthquake Engineering*, 28:453–467, 2008.

J. Qian and D. E. Beskos. Dynamic interaction between 3-D rigid surface foundations and comparison with the ATC-3 provisions. *Earthquake Engineering & Structural Dynamics*, 24(3):419–437, 1995.

H.R. Riggs and G. Waas. Influence of foundation flexibility on soil-structure interaction. *Earthquake Engineering & Structural Dynamics*, 13(5):597–615, 1985.

R.H. Scanlan. Seismic wave effects on soil-structure interaction. *Earthquake Engineering & Structural Dynamics*, 4:379–388, 1976.

M. H. Scott and T. Haukaas. Software framework for parameter updating and finite-element response sensitivity analysis. *Journal of Computing in Civil Engineering*, 22(5):281–291, 2008.

H.B. Seed and I.M. Idriss. Moduli and damping factors for dynamic response analyses. In Earthquake Engineering Research Center, editor, *in Report: EERC-70-10*, Berkeley, CA, 1970.

Jonathan P. Stewart, Gregory L. Fenves, and Raymond B. Seed. Seismic soil-structure interaction in buildings. I: Analytical methods. *Journal of Geotechnical and Geoenvironmental Engineering*, 125(1):26–37, 1999a.

Jonathan P. Stewart, Raymond B. Seed, and Gregory L. Fenves. Seismic soil-structure interaction in buildings. II: Empirical findings. *Journal of Geotechnical and Geoenvironmental Engineering*, 125(1):38–48, 1999b.

N.W. Trombetta, H.B. Mason, Z. Chen, T.C. Hutchinson, J.D. Bray, and B.L. Kutter. Nonlinear dynamic foundation and frame structure response observed in geotechnical centrifuge experiments. *Soil Dynamics & Earthquake Engineering*, 50:117–133, 2013.

A. S. Veletsos and B. Verbic. Vibration of viscoelastic foundations. *Earthquake Engineering & Structural Dynamics*, 2(1):87–102, 1973.

A. S. Veletsos, A. M. Prasad, and W. H. Wu. Transfer functions for rigid rectangular foundations. *Earthquake Engineering & Structural Dynamics*, 26(1):5–17, 1997.

Anestis S. Veletsos and Jethro W. Meek. Dynamic behaviour of building-foundation systems. *Earthquake Engineering & Structural Dynamics*, 3(2):121–138, 1974.

Anestis S. Veletsos and Anumolu M. Prasad. Seismic interaction of structures and soils: stochastic approach. *Journal of Structural Engineering*, 115(4):935–956, 1989.

J. P. Wolf. *Dynamic Soil-Structure Interaction*. Prentice Hall, Inc., Upper Saddle River, NJ, 1985.

H. L. Wong and M. D. Trifunac. Two-dimensional, antiplane, building-soil-building interaction for two or more buildings and for incident planet SH waves. *Bulletin of the Seismological Society of America*, 65(6):1863–1885, 1975.

APPENDIX

APPENDIX Response Time Series of the 4-story by 4-story System

This appendix contains time series for each of the five output parameters for the 4 by 4 building system. Though the other listed systems were tested, they have been excluded for the purpose of saving space. Each of these time histories have been reviewed extensively and the results do not differ in any significant way from those of the 4 by 4 system. Recall that each of the mean time histories are presented for the entire earthquake duration, while those time histories that incorporate sensitivity analysis show a 10-second interval of the motion, specific to the earthquake motion used. In each of the plots shown below that include sensitivity analysis, the mean time series is shown as a dashed line, while the time series that include sensitivity analysis are shown as solid lines.

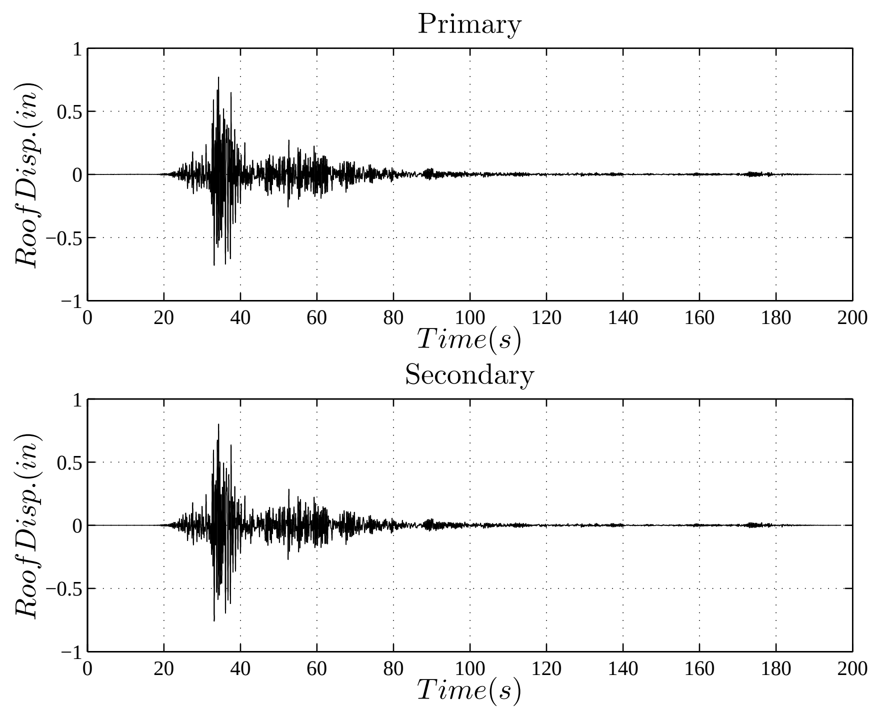

Figure 1: Mean roof displacement response, Chi Chi CHY034 motion, founded on dense sand.

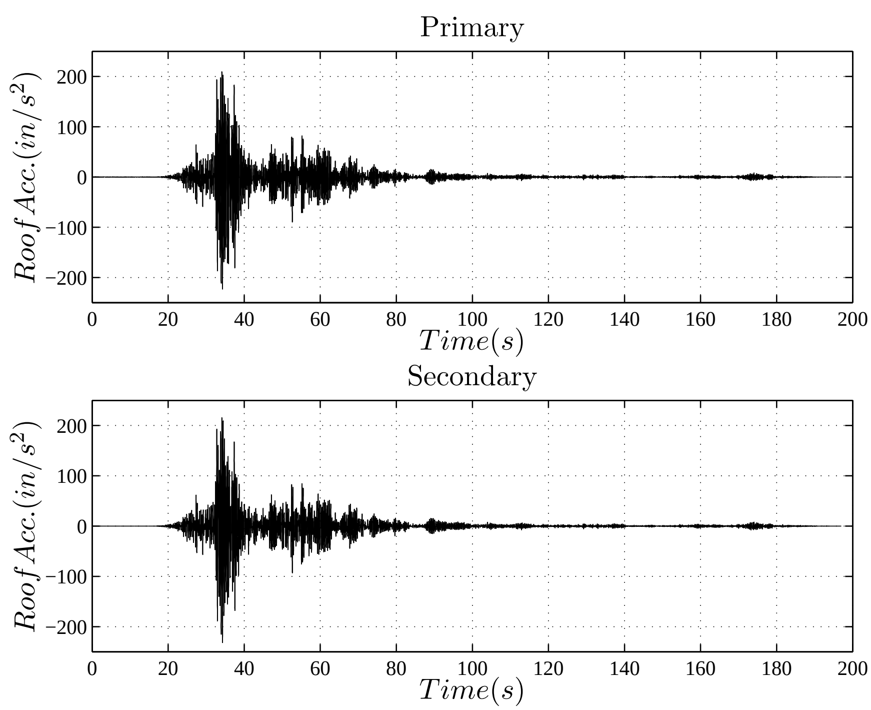

Figure 2: Mean roof acceleration response, Chi Chi CHY034 motion, founded on dense sand.

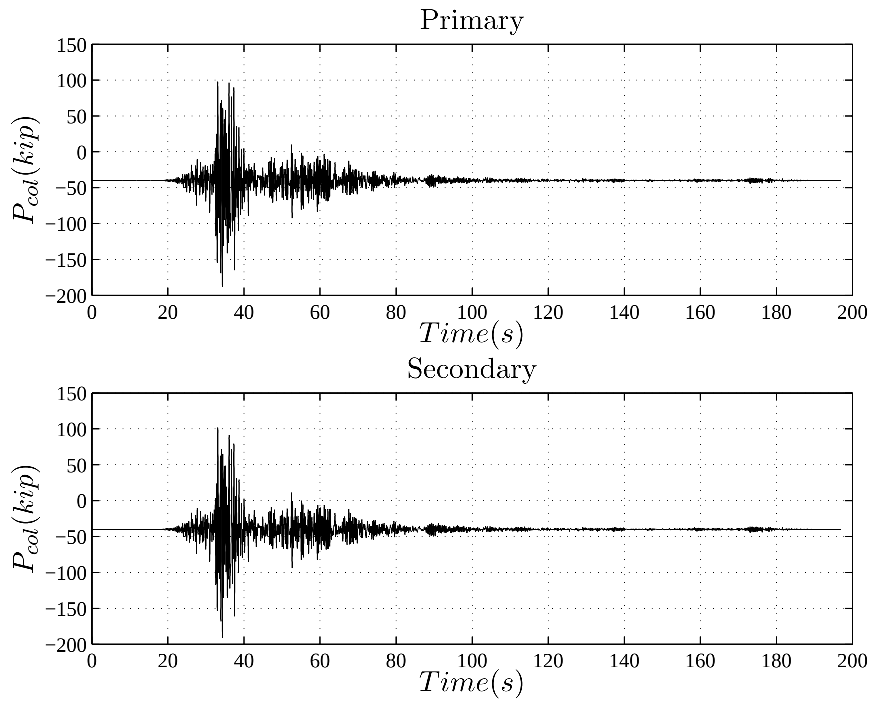

Figure 3: Mean column response, Chi Chi CHY034 motion, founded on dense sand.

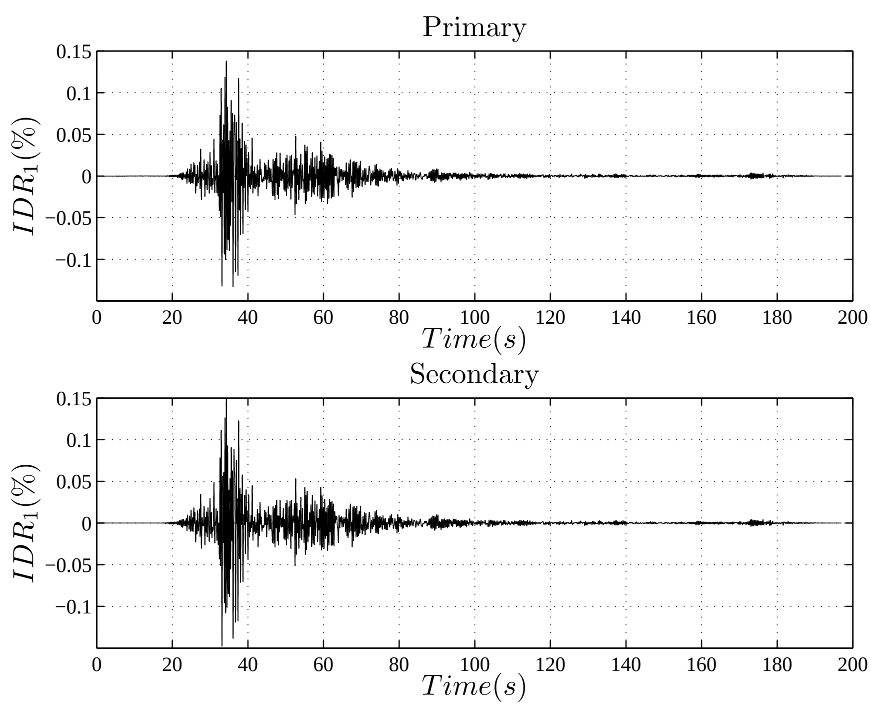

Figure 4: Mean first-story IDR response, Chi Chi CHY034 motion, founded on dense sand.

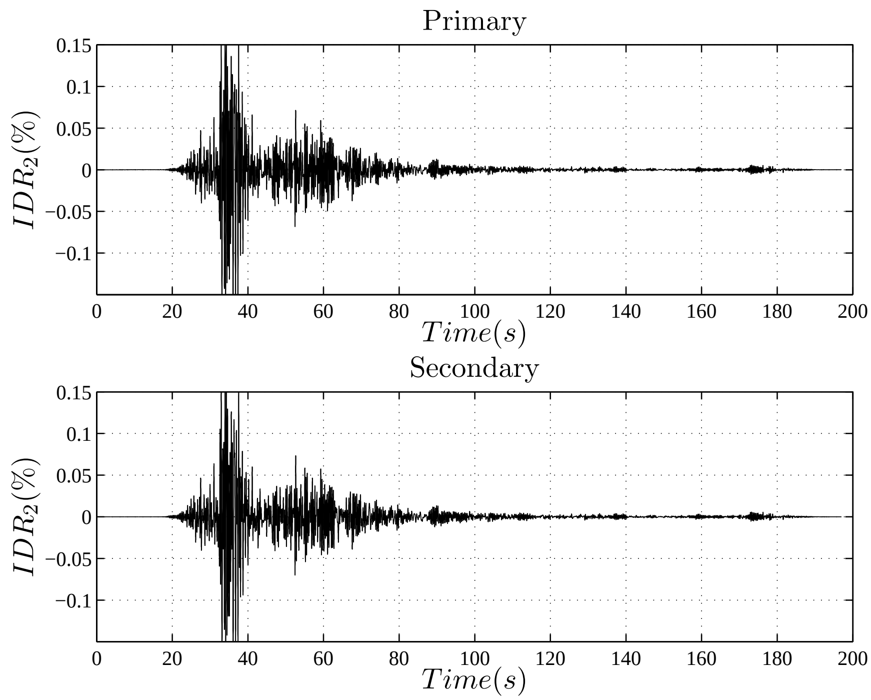

Figure 5: Mean roof displacement response, Chi Chi CHY034 motion, founded on dense sand.

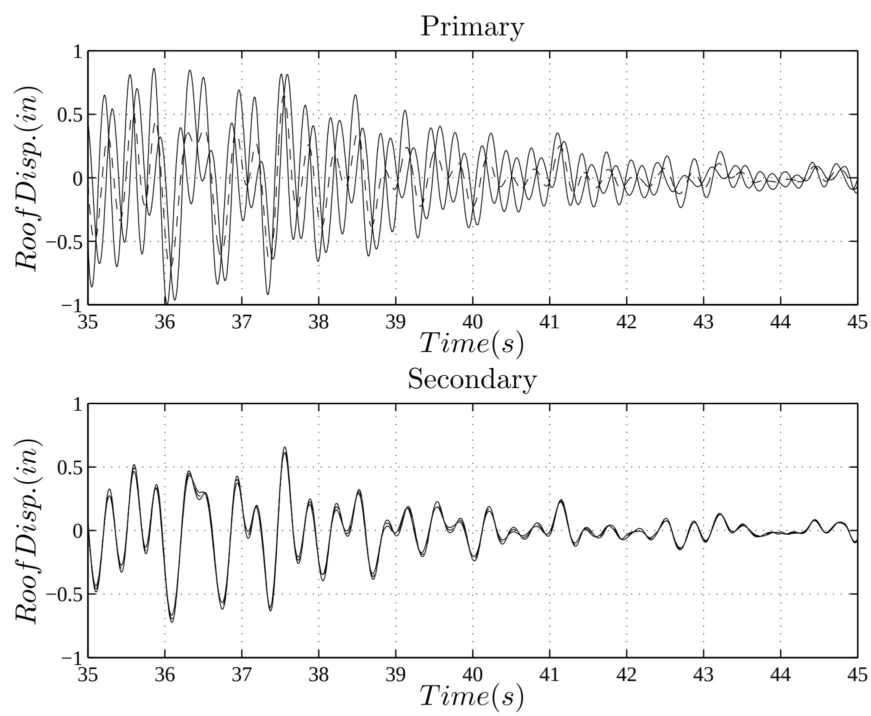

Figure 6: Roof displacement response with sensitivity to building stiffness, Chi Chi CHY034 motion, founded on dense sand.

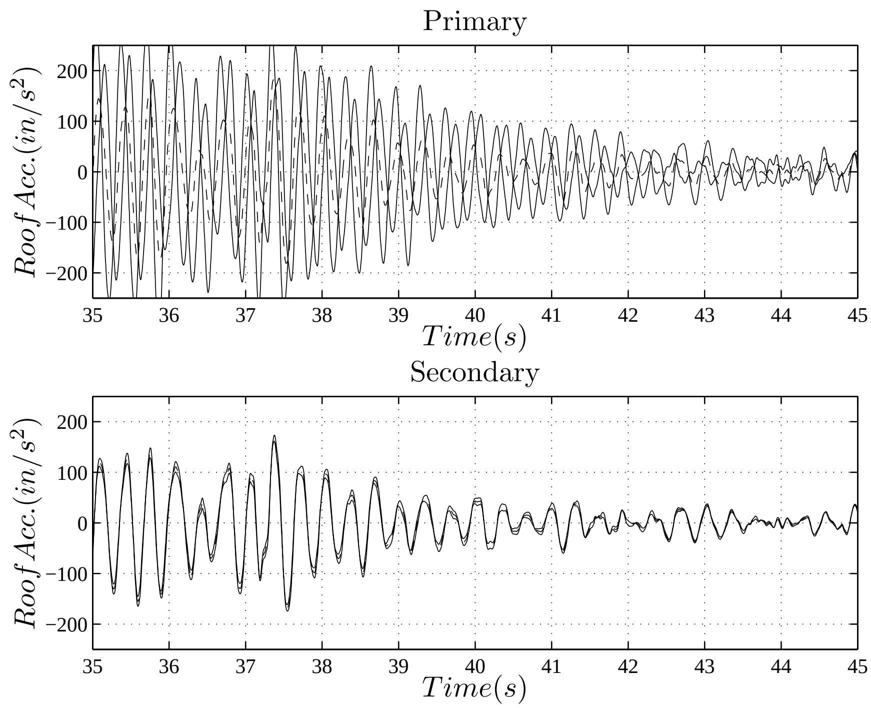

Figure 7: Roof acceleration response with sensitivity to building stiffness, Chi Chi CHY034 motion, founded on dense sand.

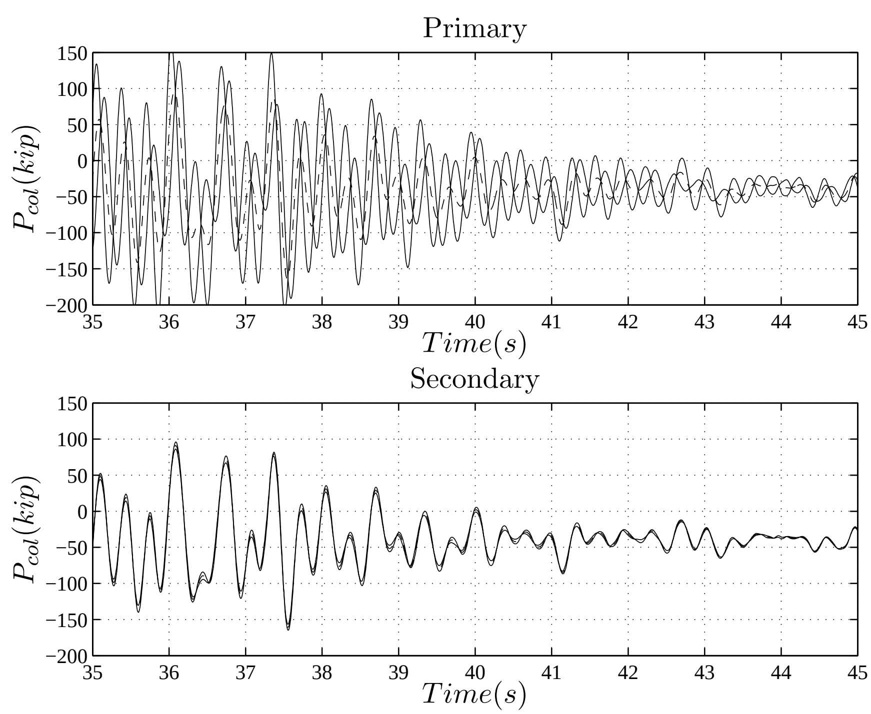

Figure 8: Column force response with sensitivity to building stiffness, Chi Chi CHY034 motion, founded on dense sand.

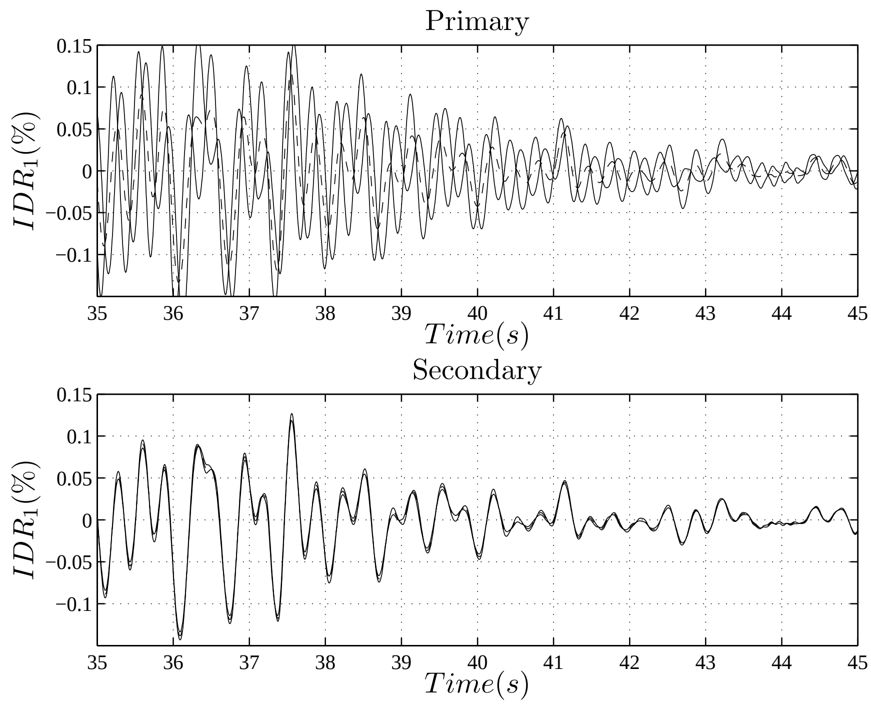

Figure 9: First-story IDR response with sensitivity to building stiffness, Chi Chi CHY034 motion, founded on dense sand.

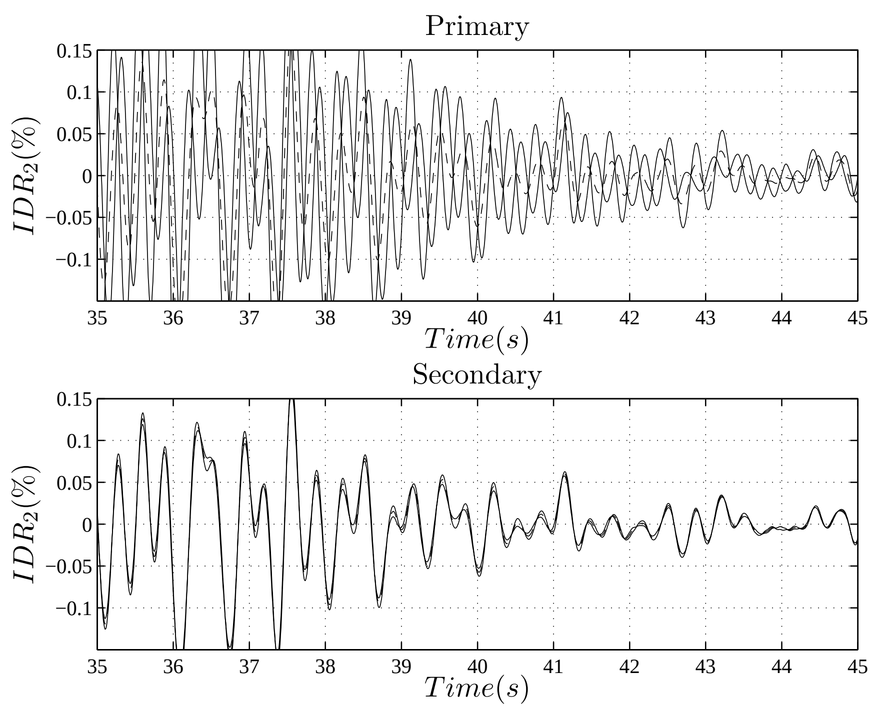

Figure 10: Second-story IDR response with sensitivity to building stiffness, Chi Chi CHY034 motion, founded on dense sand.

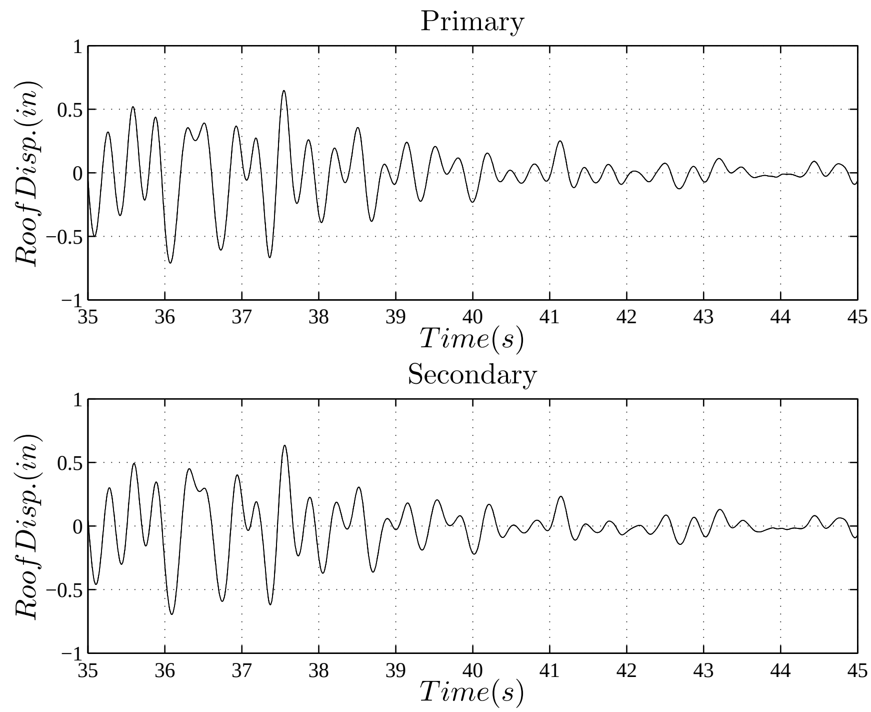

Figure 11: Roof displacement response with sensitivity to soil spring stiffness, Chi Chi CHY034 motion, founded on dense sand.

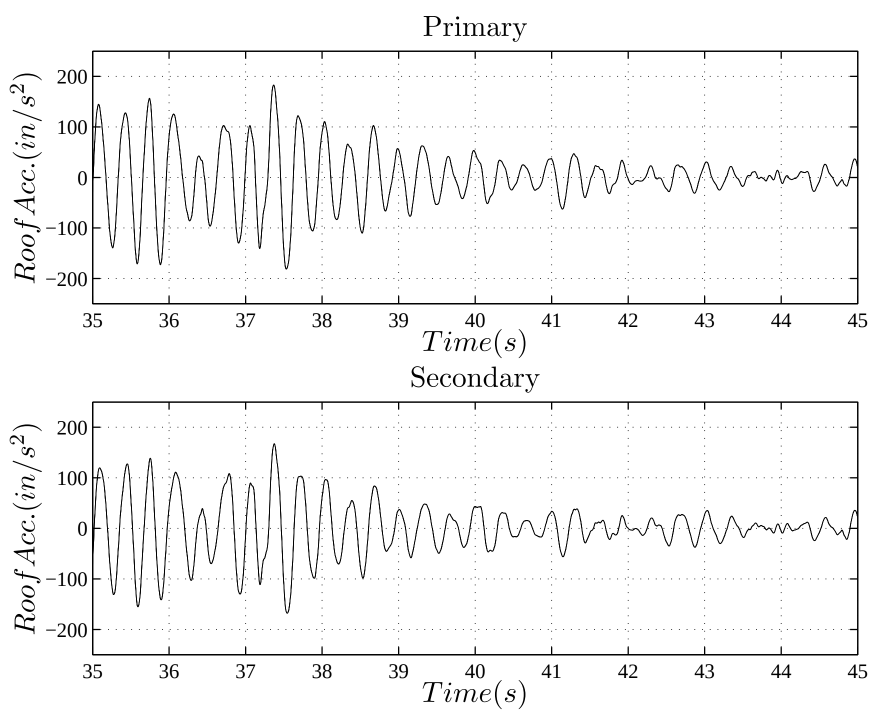

Figure 12: Roof acceleration response with sensitivity to soil spring stiffness, Chi Chi CHY034 motion, founded on dense sand.

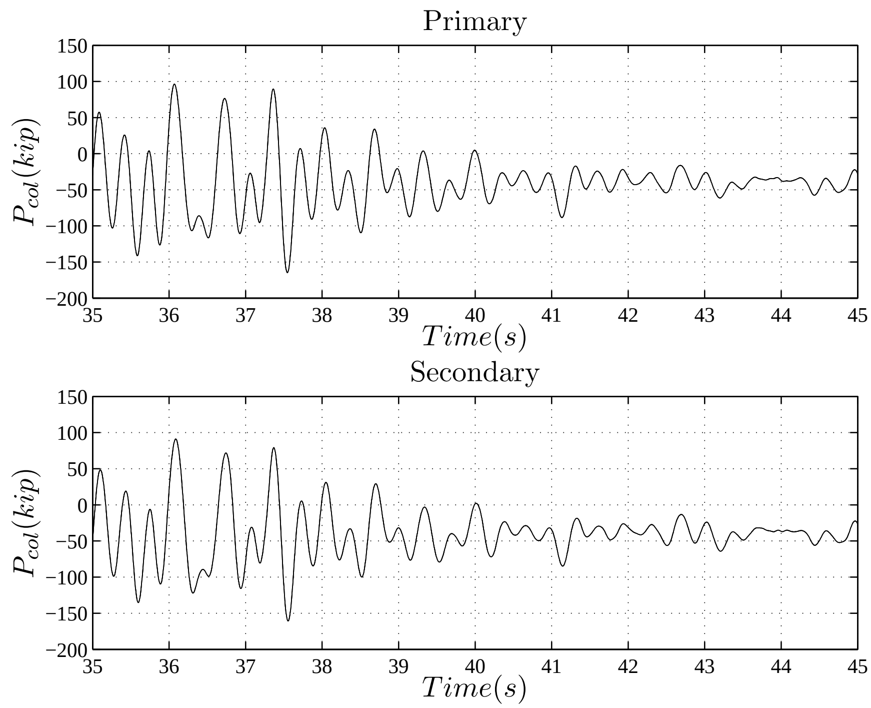

Figure 13: Column force response with sensitivity to soil spring stiffness, Chi Chi CHY034 motion, founded on dense sand.

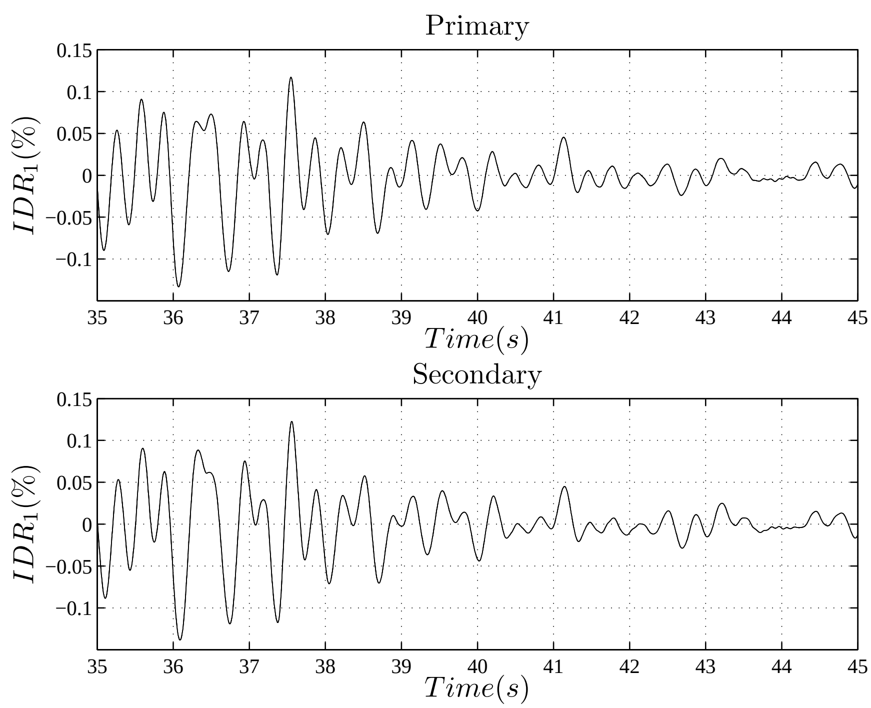

Figure 14: First-story IDR response with sensitivity to soil spring stiffness, Chi Chi CHY034 motion, founded on dense sand.

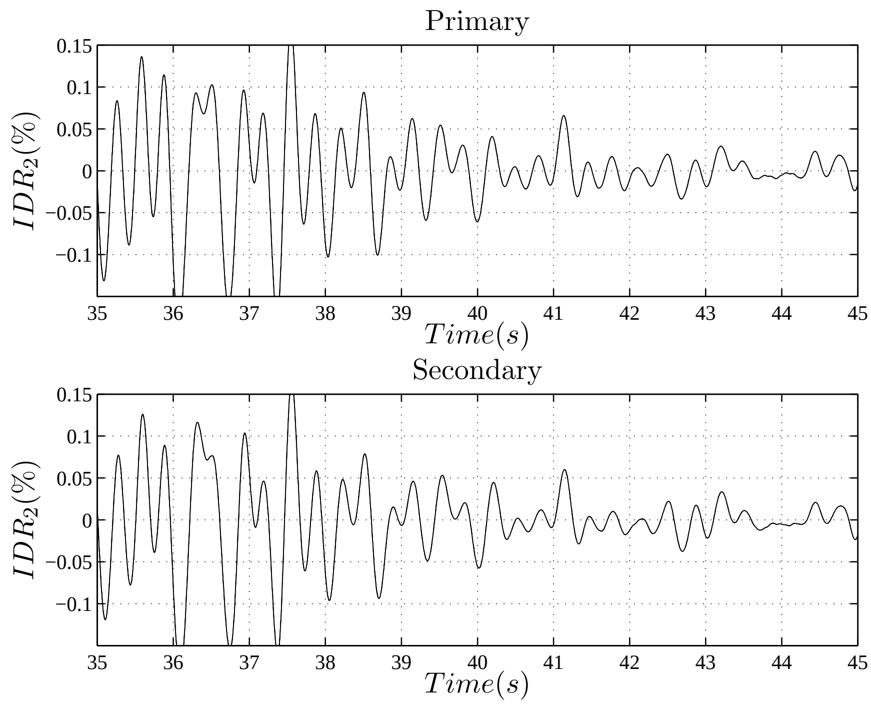

Figure 15: Second-story IDR response with sensitivity to soil spring stiffness, Chi Chi CHY034 motion, founded on dense sand.

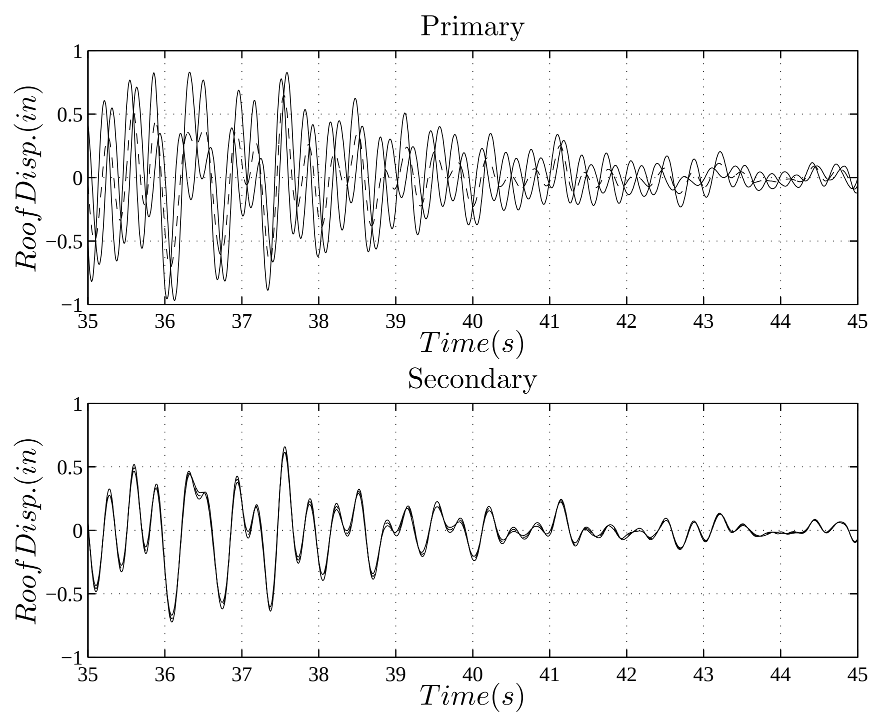

Figure 16: Roof displacement response with sensitivity to floor mass, Chi Chi CHY034 motion, founded on dense sand.

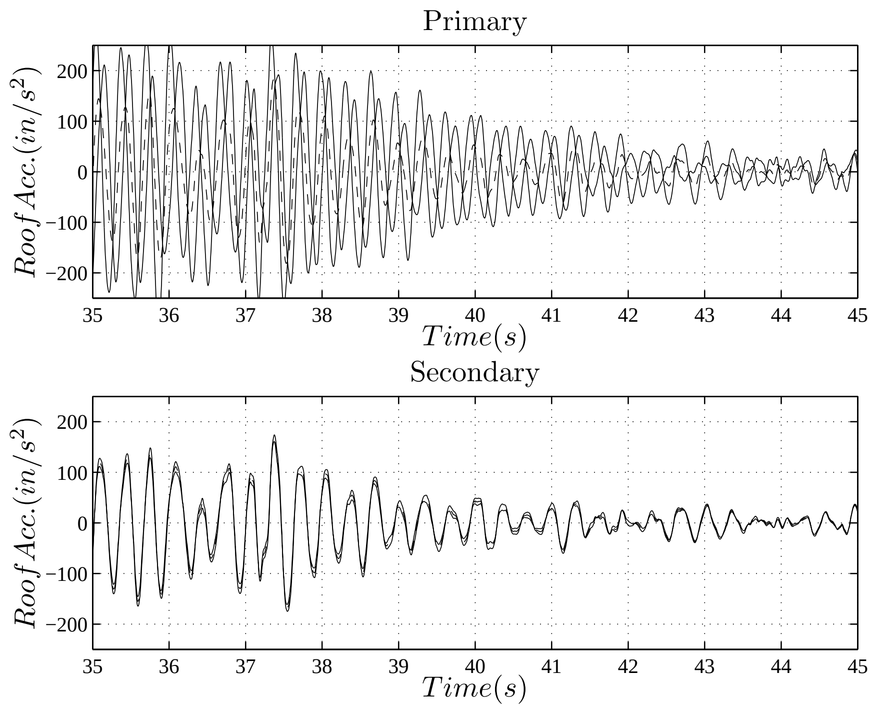

Figure 17: Roof acceleration response with sensitivity to floor mass, Chi Chi CHY034 motion, founded on dense sand.

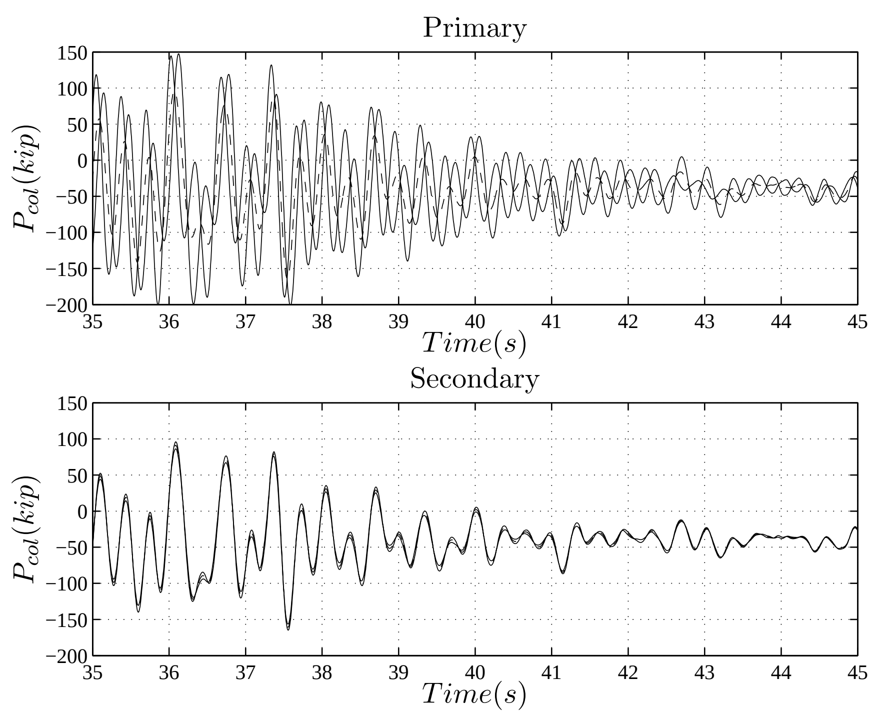

Figure 18: Column Force response with sensitivity to floor mass, Chi Chi CHY034 motion, founded on dense sand.

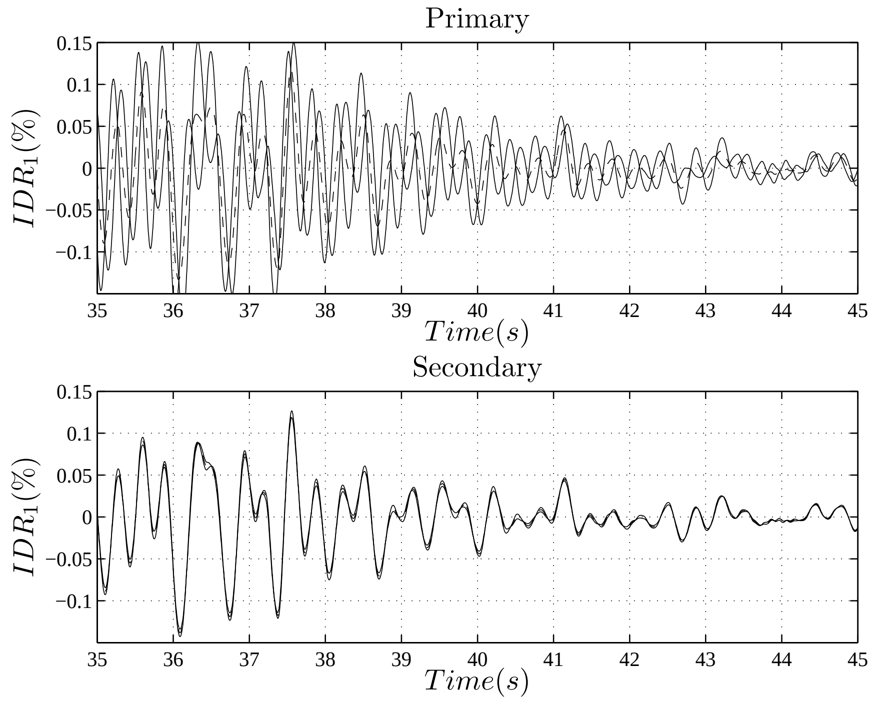

Figure 19: First-story IDR response with sensitivity to floor mass, Chi Chi CHY034 motion, founded on dense sand.

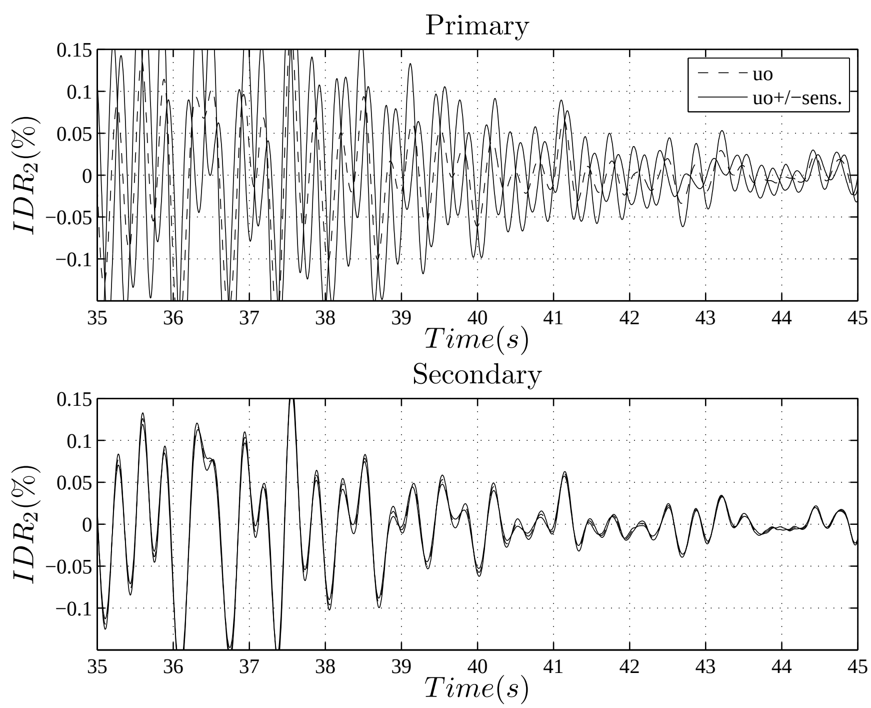

Figure 20: Second-story IDR response with sensitivity to floor mass, Chi Chi CHY034 motion, founded on dense sand.

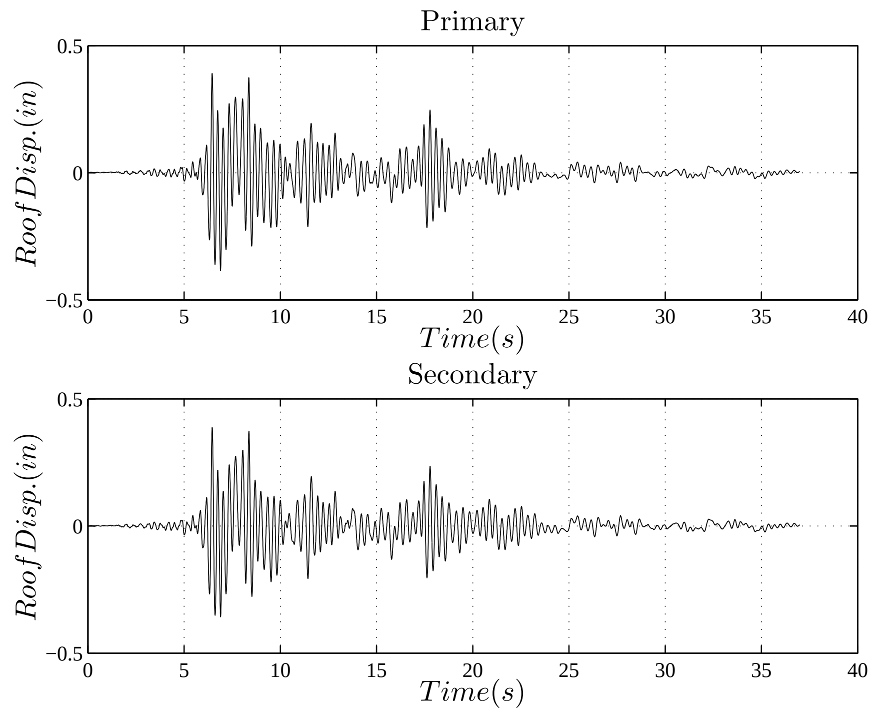

Figure 21: Mean roof displacement response, 1979 Imperial Valley - Brawley Airport motion, founded on dense sand.

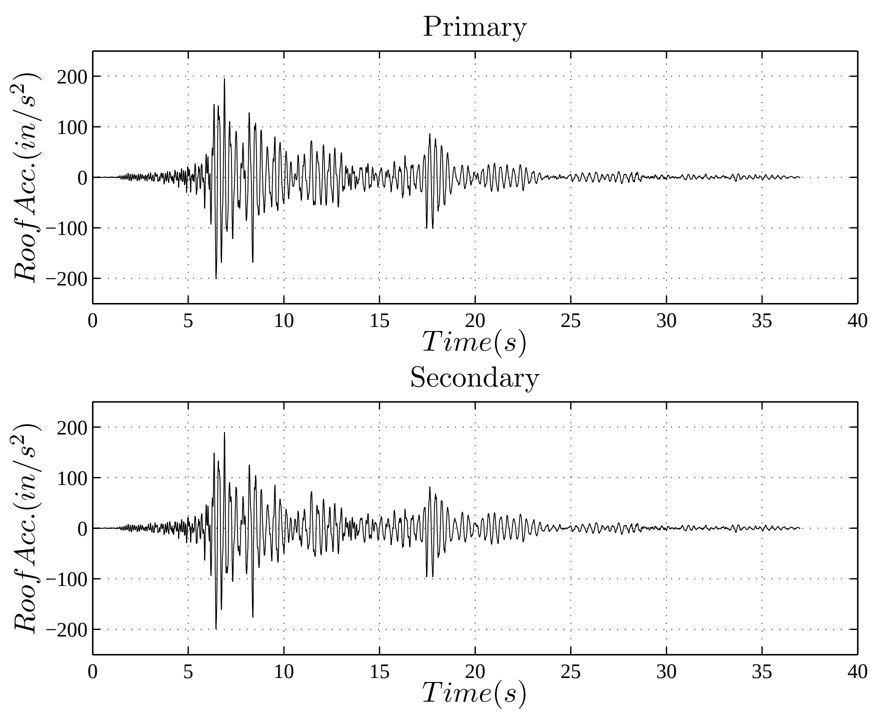

Figure 22: Mean roof acceleration response, 1979 Imperial Valley - Brawley Airport motion, founded on dense sand.

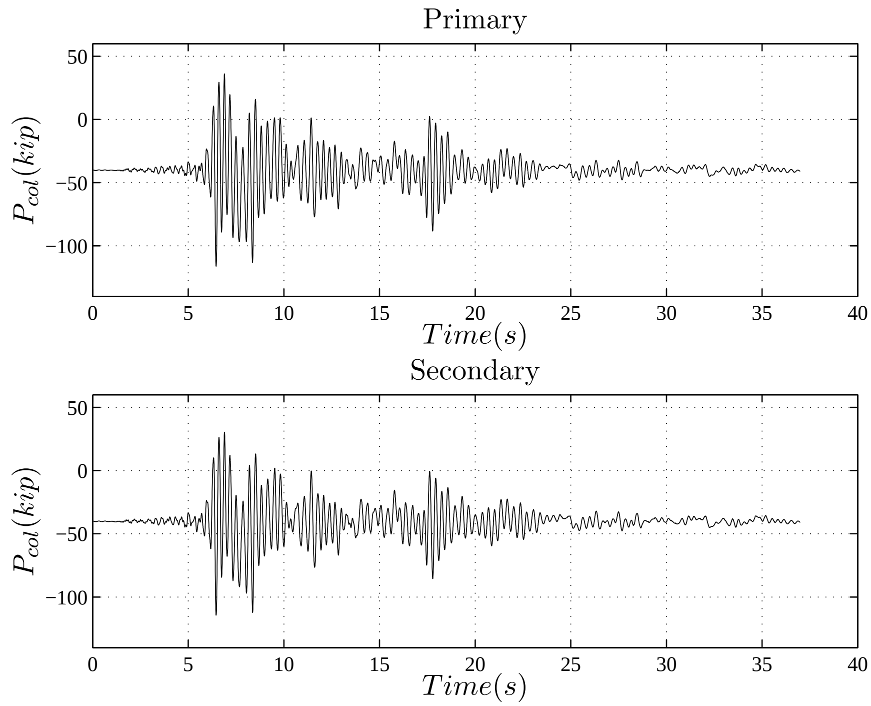

Figure 23: Mean column response, 1979 Imperial Valley - Brawley Airport motion, founded on dense sand.

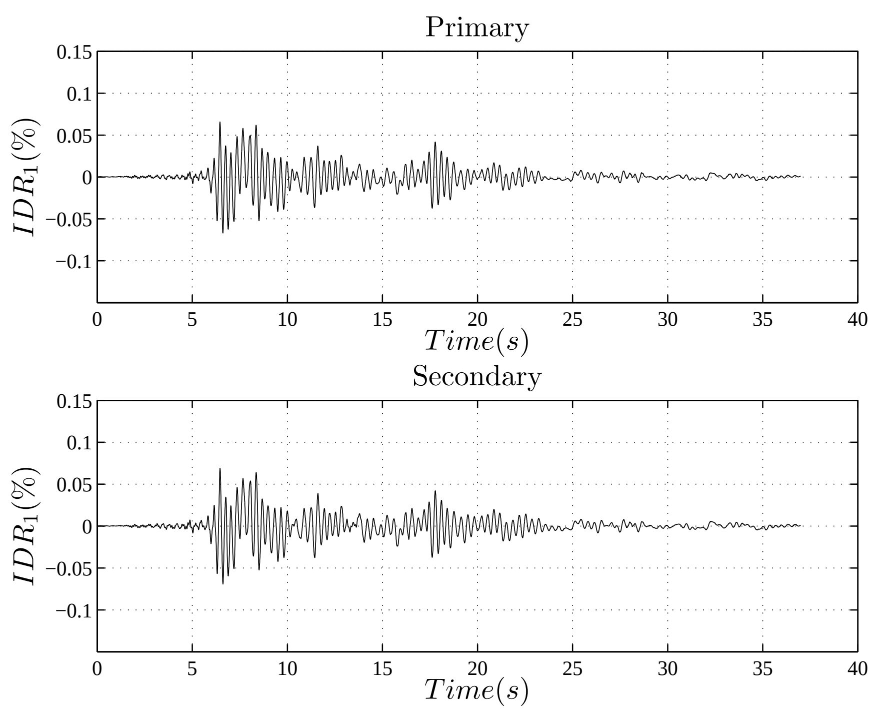

Figure 24: Mean first-story IDR response, 1979 Imperial Valley - Brawley Airport motion, founded on dense sand.

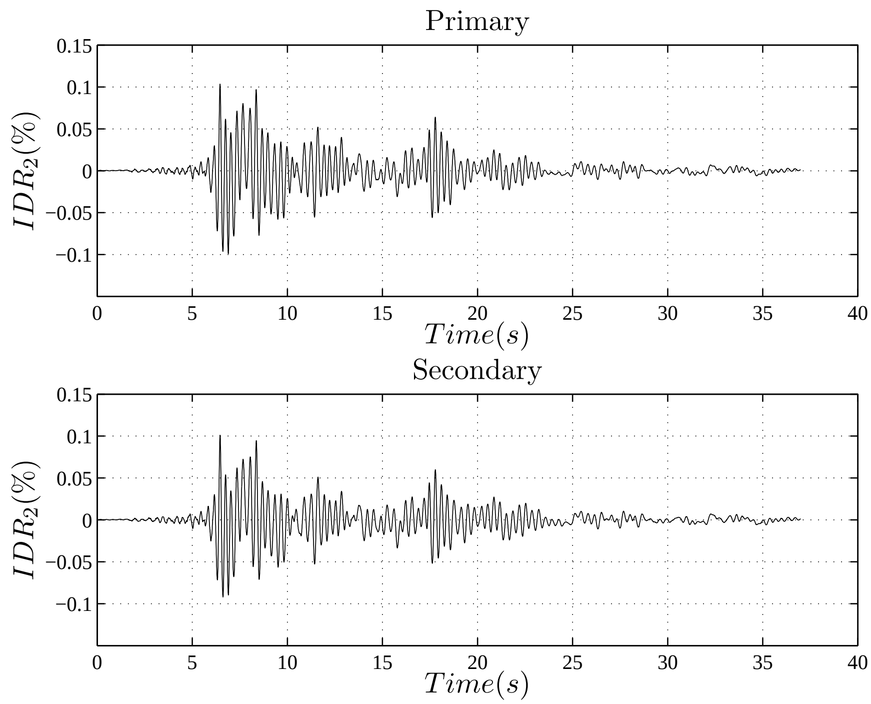

Figure 25: Mean roof displacement response, 1979 Imperial Valley - Brawley Airport motion, founded on dense sand.

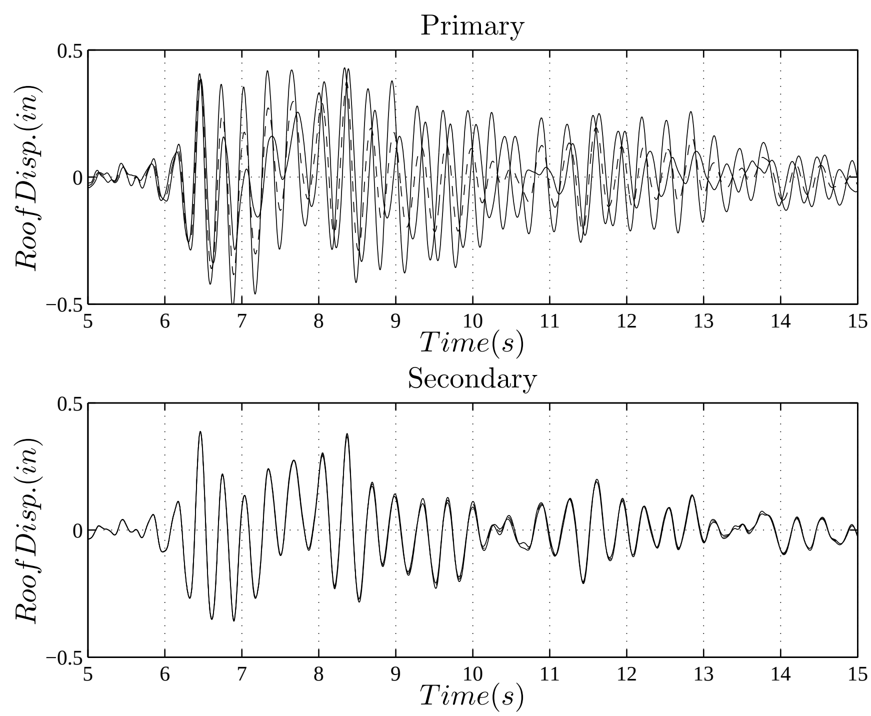

Figure 26: Roof displacement response with sensitivity to building stiffness, 1979 Imperial Valley - Brawley Airport motion, founded on dense sand.

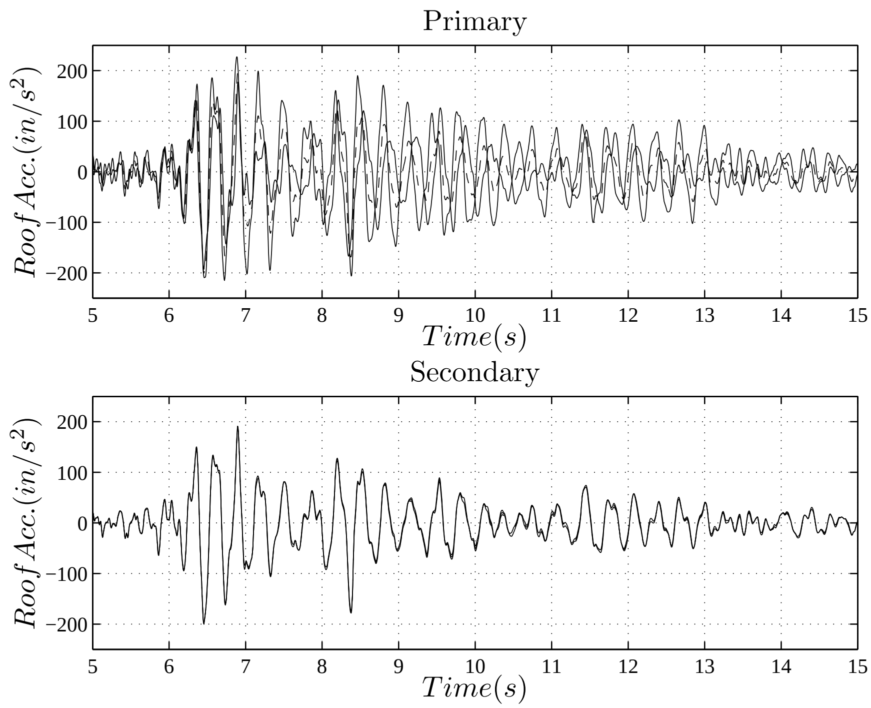

Figure 27: Roof acceleration response with sensitivity to building stiffness, 1979 Imperial Valley - Brawley Airport motion, founded on dense sand.

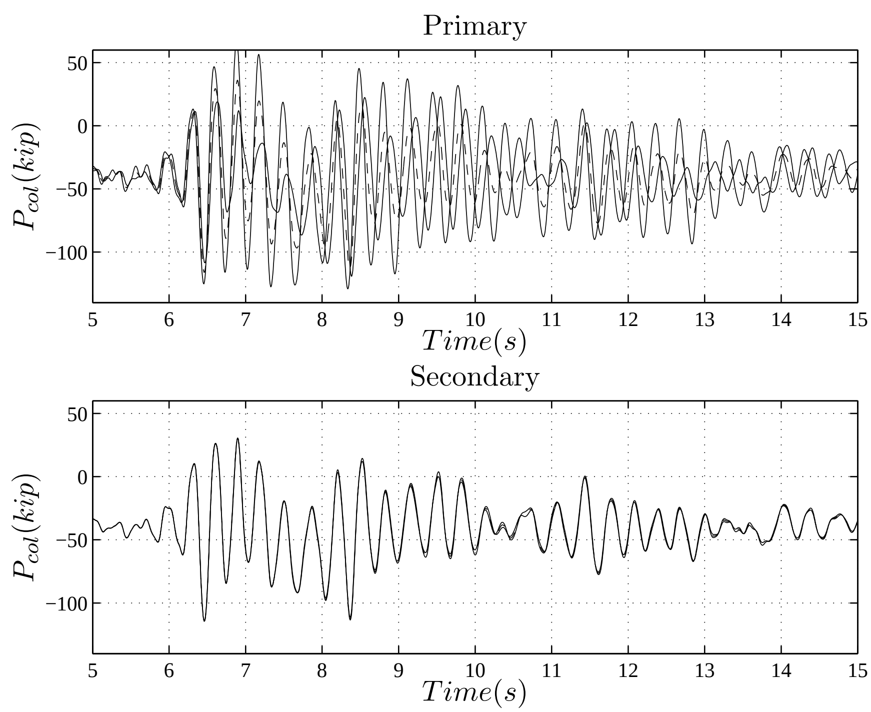

Figure 28: Column force response with sensitivity to building stiffness, 1979 Imperial Valley - Brawley Airport motion, founded on dense sand.

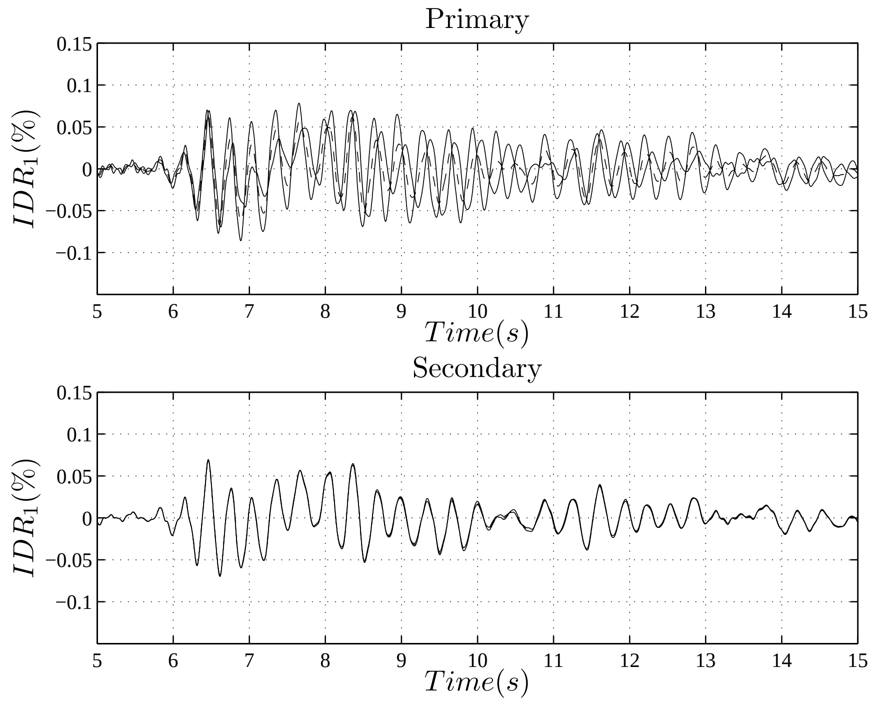

Figure 29: First-story IDR response with sensitivity to building stiffness,1979 Imperial Valley - Brawley Airport motion, founded on dense sand.

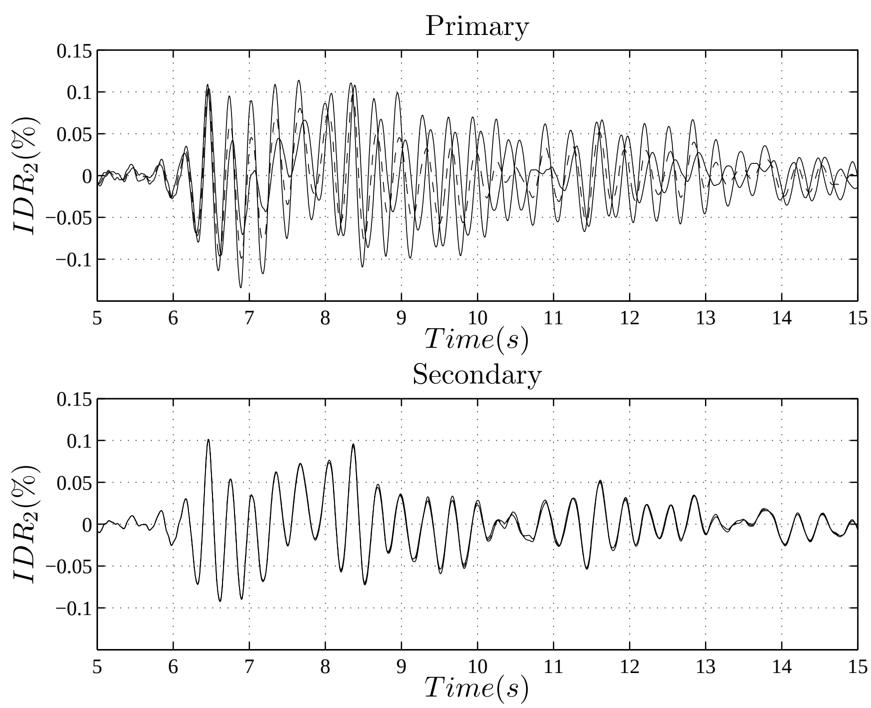

Figure 30: Second-story IDR response with sensitivity to building stiffness, 1979 Imperial Valley - Brawley Airport motion, founded on dense sand.

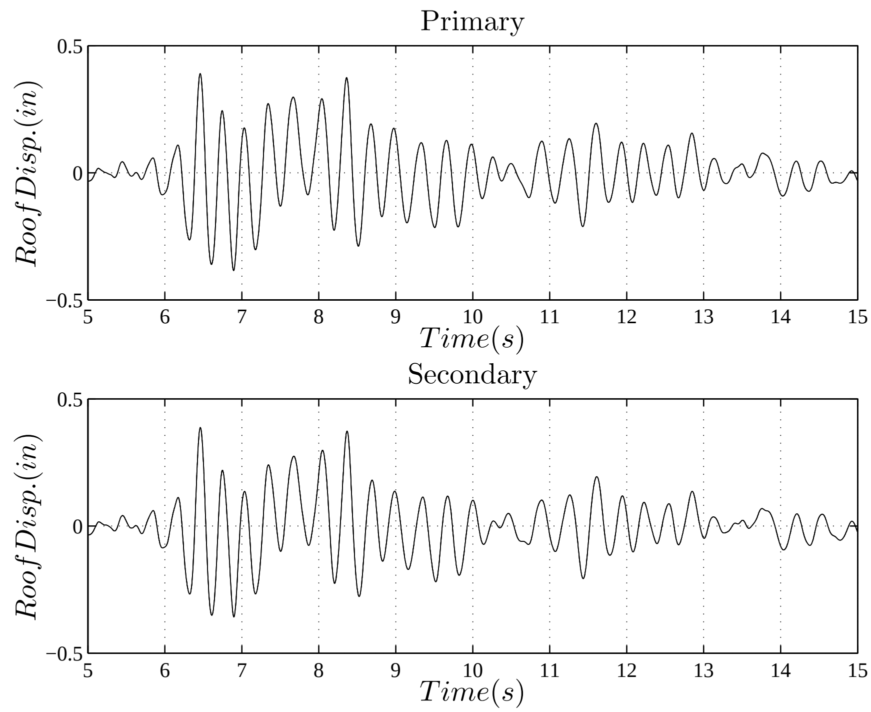

Figure 31: Roof displacement response with sensitivity to soil spring stiffness, 1979 Imperial Valley - Brawley Airport motion, founded on dense sand.

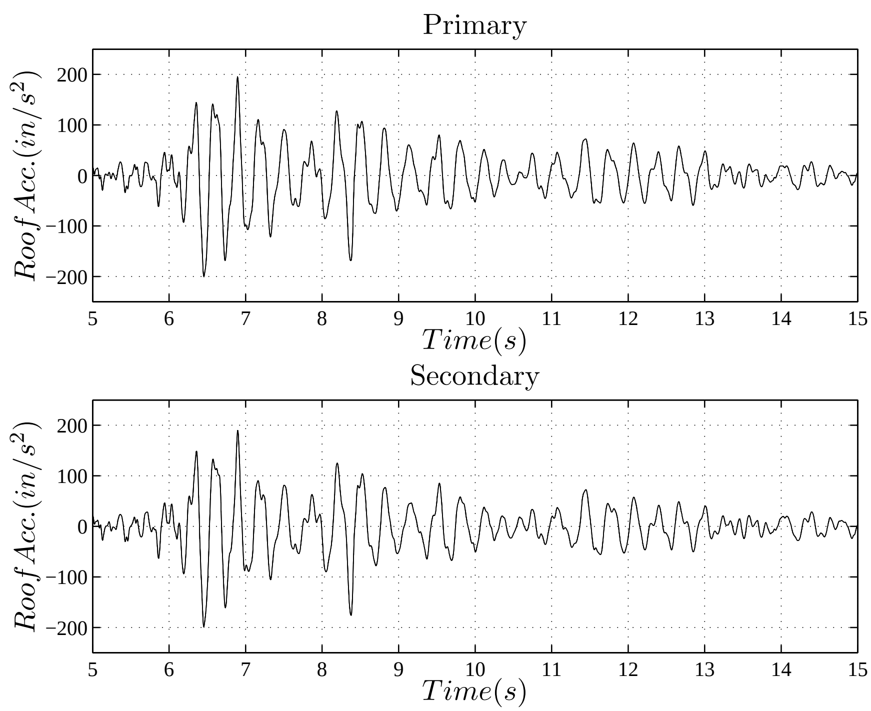

Figure 32: Roof acceleration response with sensitivity to soil spring stiffness, 1979 Imperial Valley - Brawley Airport motion, founded on dense sand.

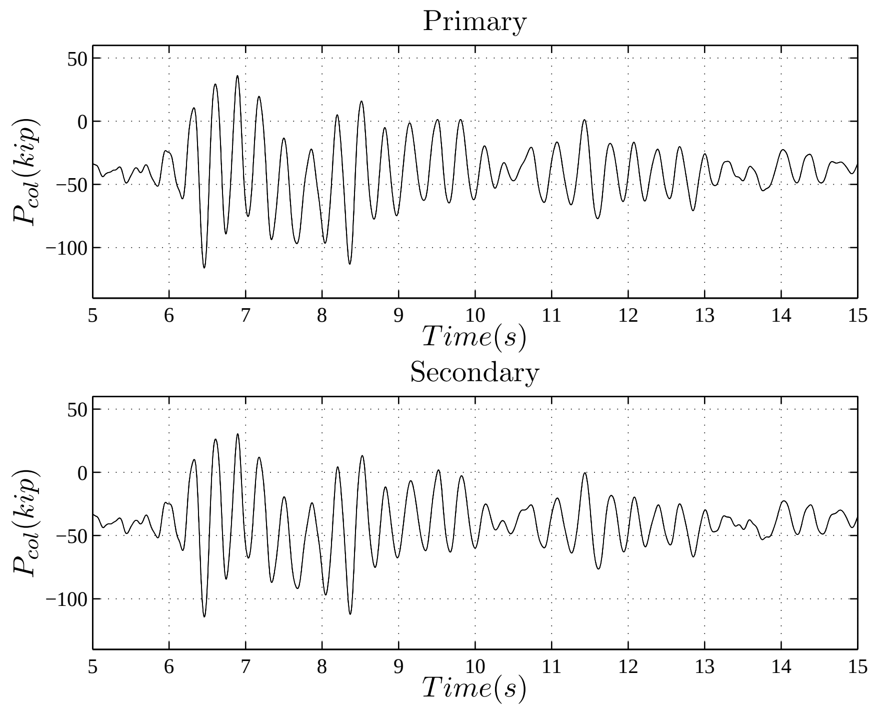

Figure 33: Column force response with sensitivity to soil spring stiffness, 1979 Imperial Valley - Brawley Airport motion, founded on dense sand.

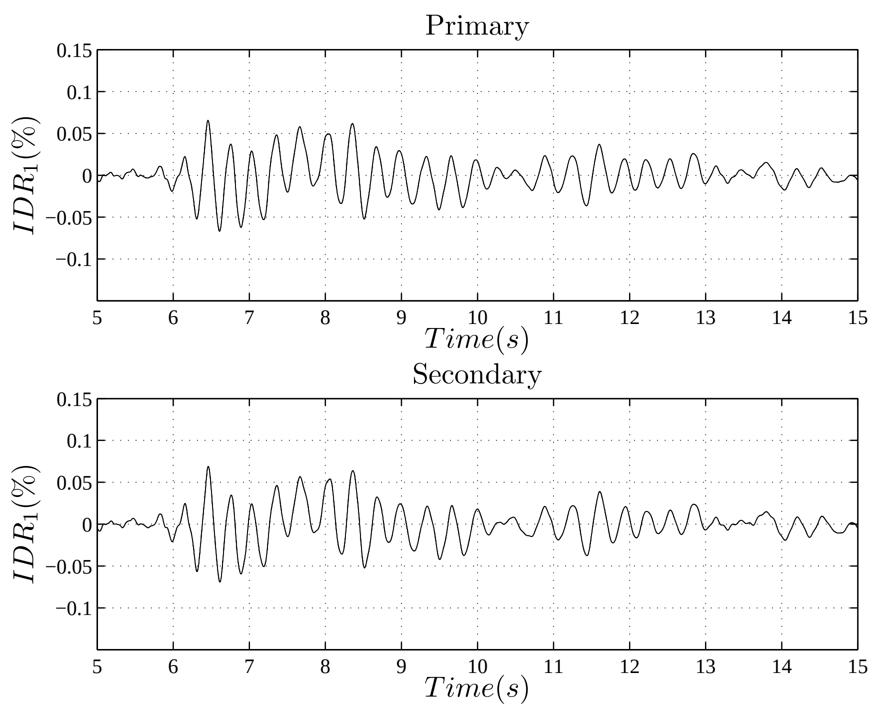

Figure 34: First-story IDR response with sensitivity to soil spring stiffness, 1979 Imperial Valley - Brawley Airport motion, founded on dense sand.

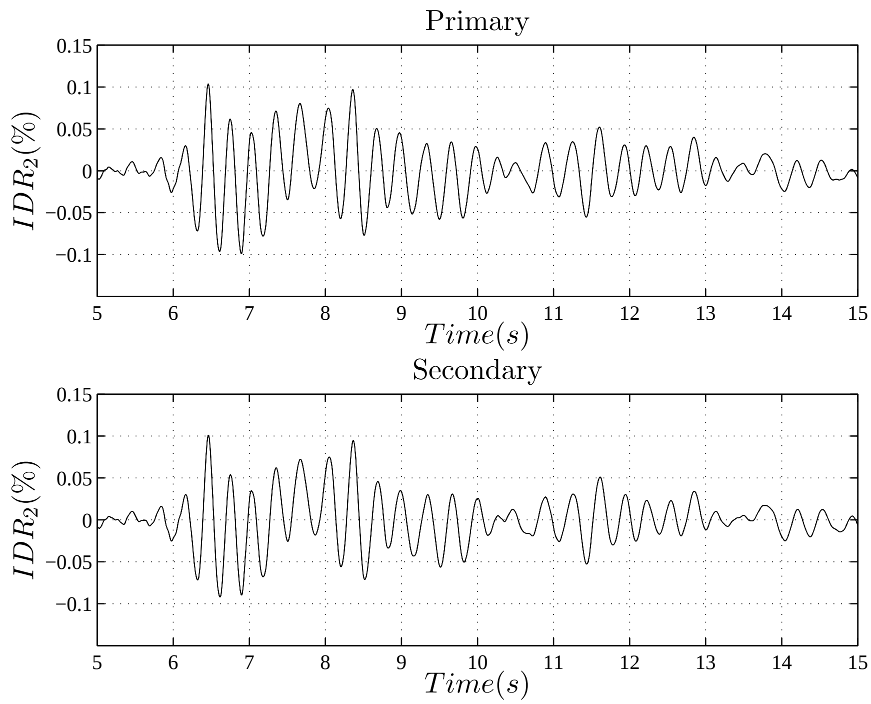

Figure 35: Second-story IDR response with sensitivity to soil spring stiffness, 1979 Imperial Valley - Brawley Airport motion, founded on dense sand.

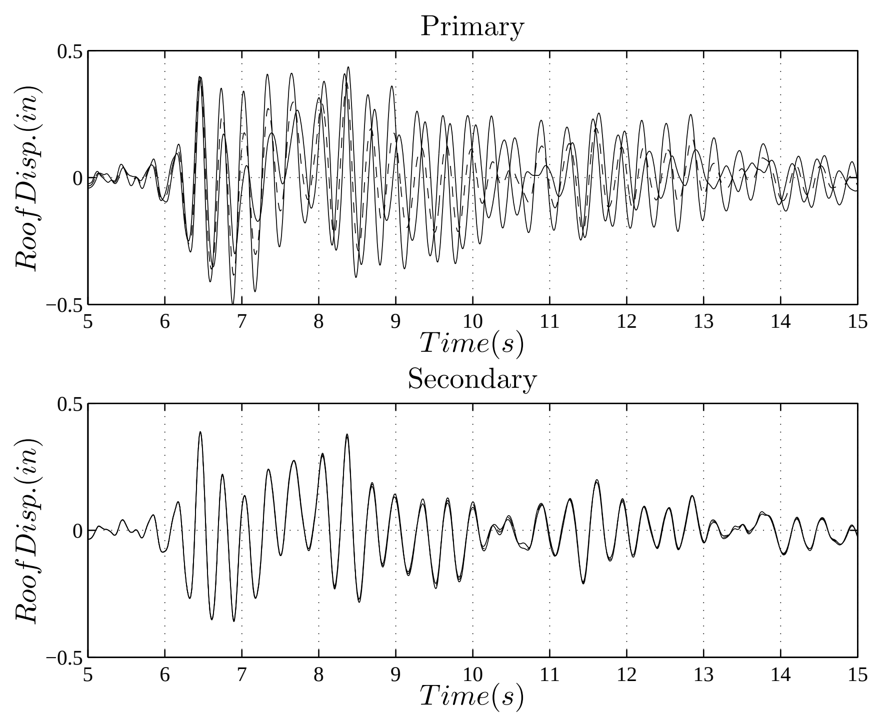

Figure 36: Roof displacement response with sensitivity to floor mass, 1979 Imperial Valley - Brawley Airport motion, founded on dense sand.

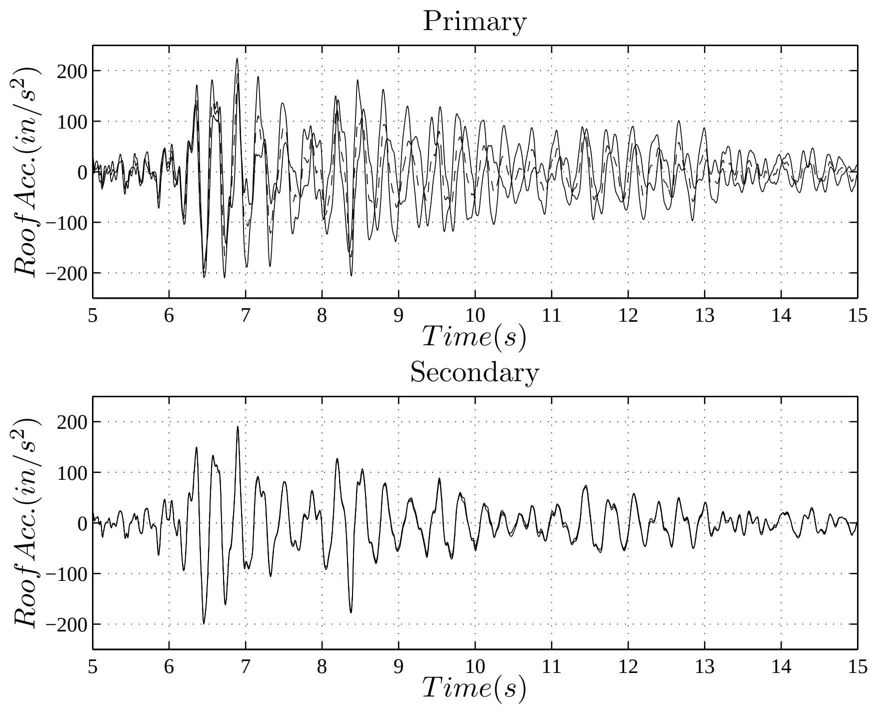

Figure 37: Roof acceleration response with sensitivity to floor mass, 1979 Imperial Valley - Brawley Airport motion, founded on dense sand.

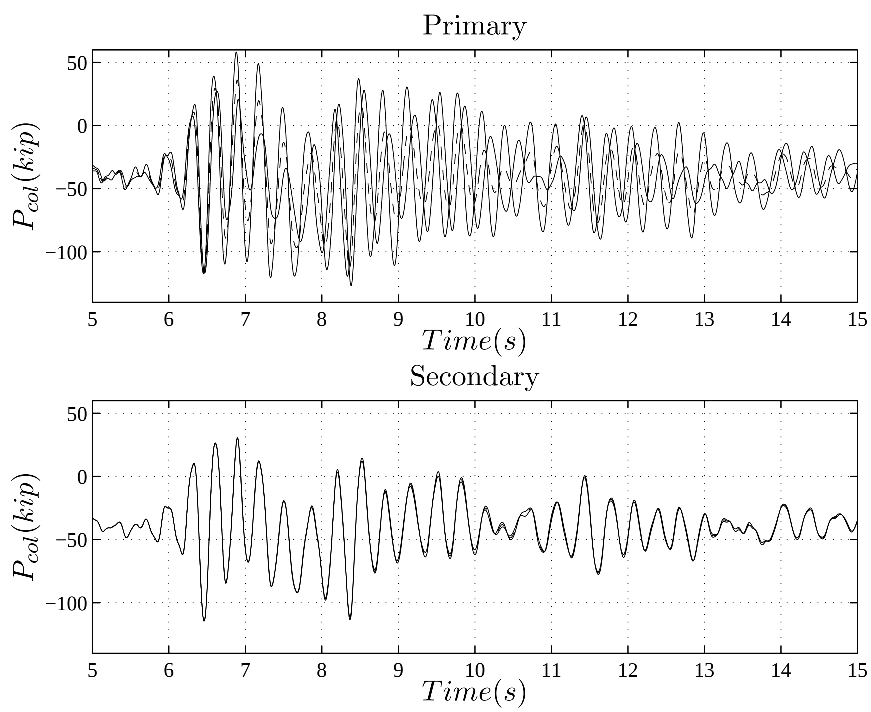

Figure 38: Column Force response with sensitivity to floor mass, 1979 Imperial Valley - Brawley Airport motion, founded on dense sand.

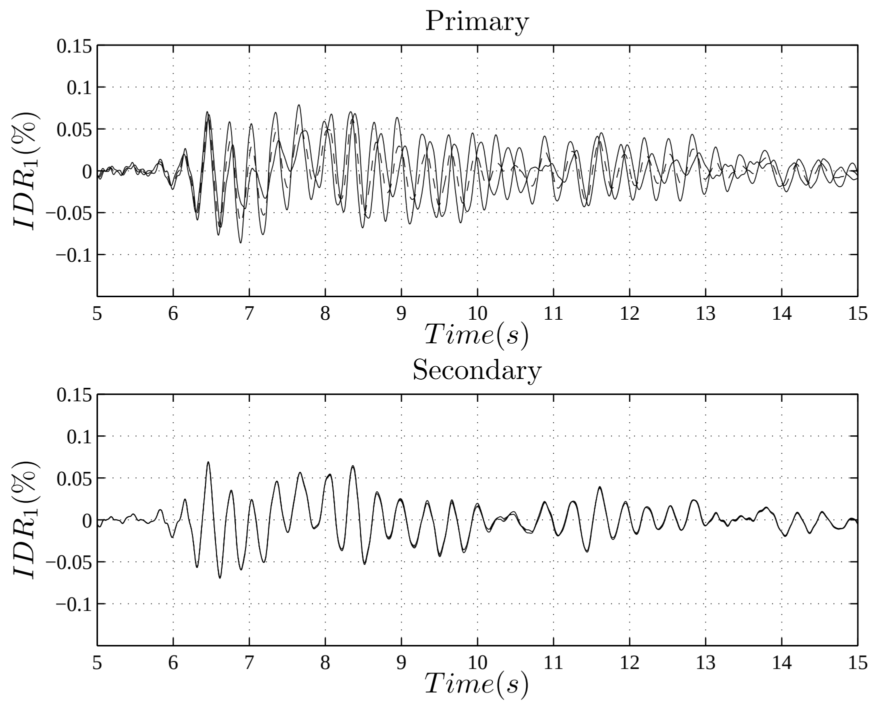

Figure 39: First-story IDR response with sensitivity to floor mass, 1979 Imperial Valley - Brawley Airport motion, founded on dense sand.

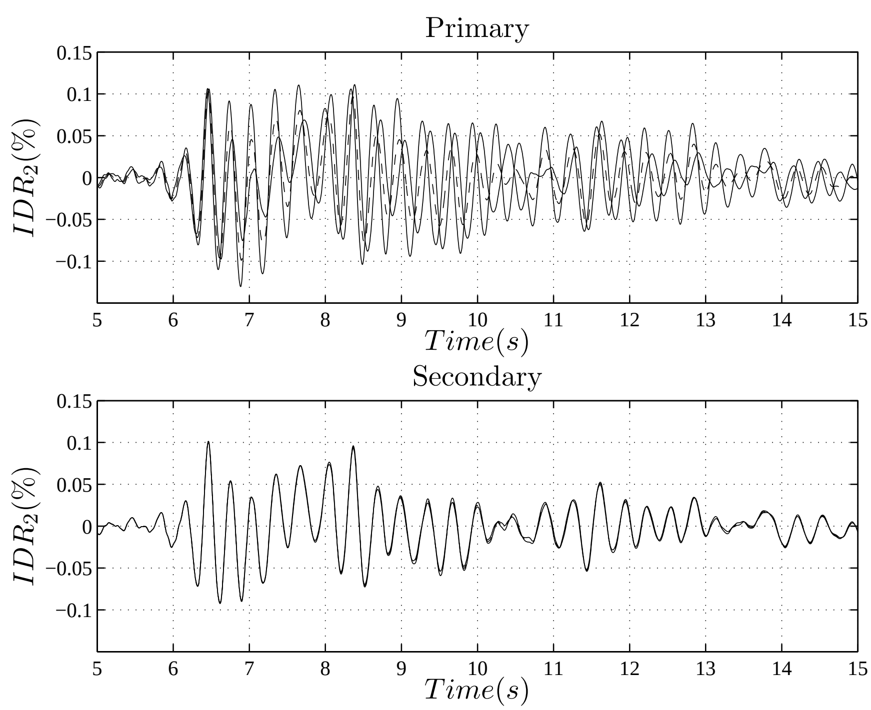

Figure 40: Second-story IDR response with sensitivity to floor mass, 1979 Imperial Valley - Brawley Airport motion, founded on dense sand.

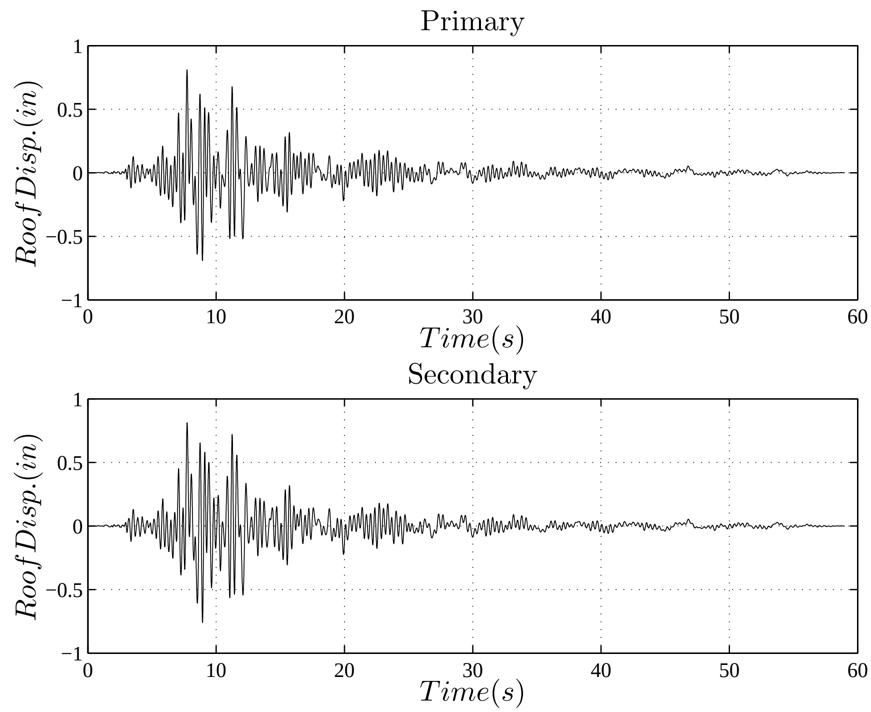

Figure 41: Mean roof displacement response, Loma Prieta Hollister - South & Pine motion, founded on dense sand.

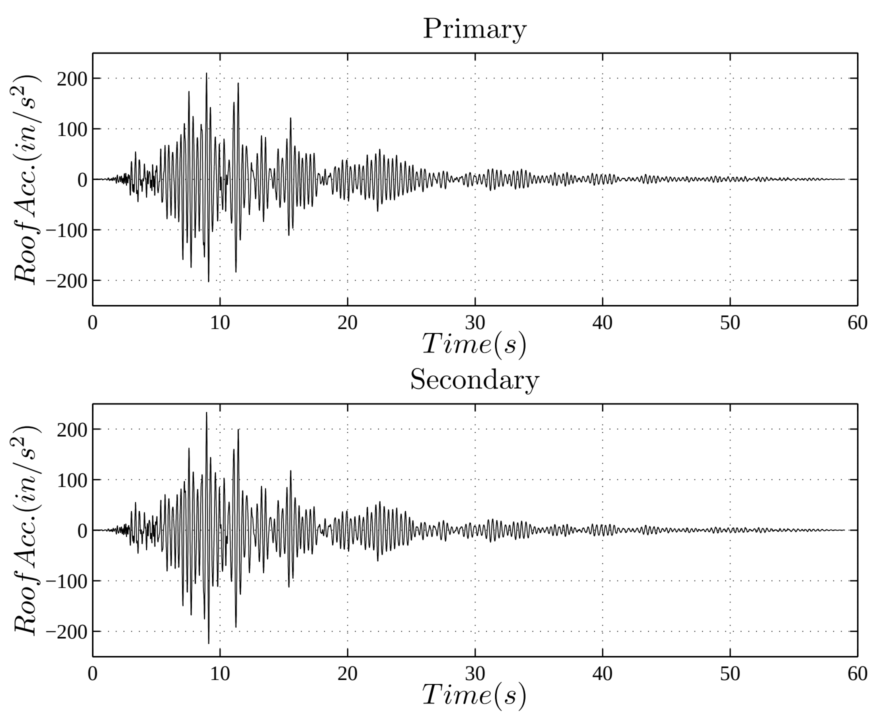

Figure 42: Mean roof acceleration response, Loma Prieta Hollister - South & Pine motion, founded on dense sand.

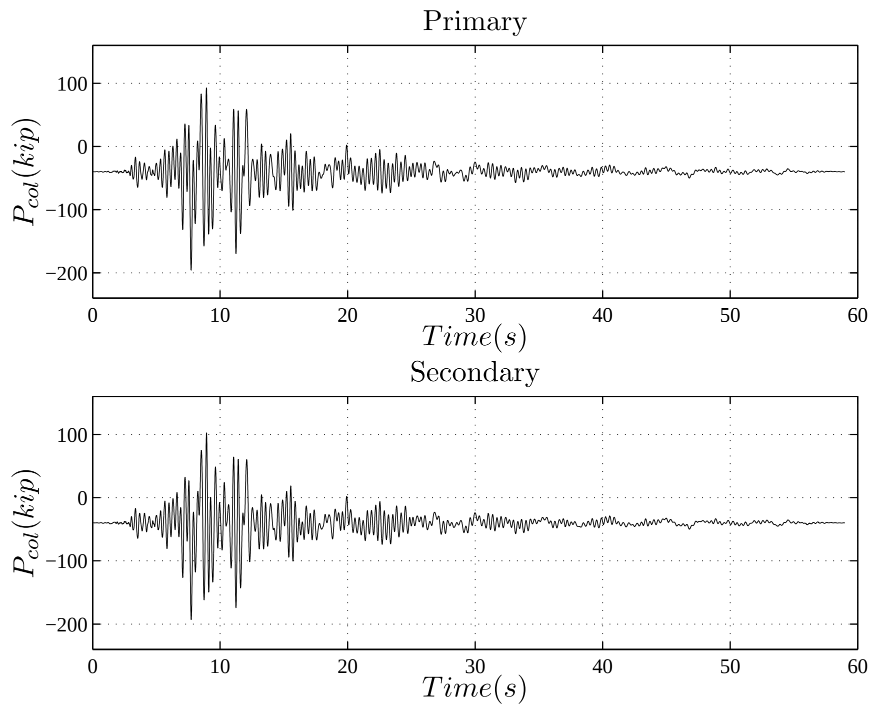

Figure 43: Mean column response, Loma Prieta Hollister - South & Pine motion, founded on dense sand.

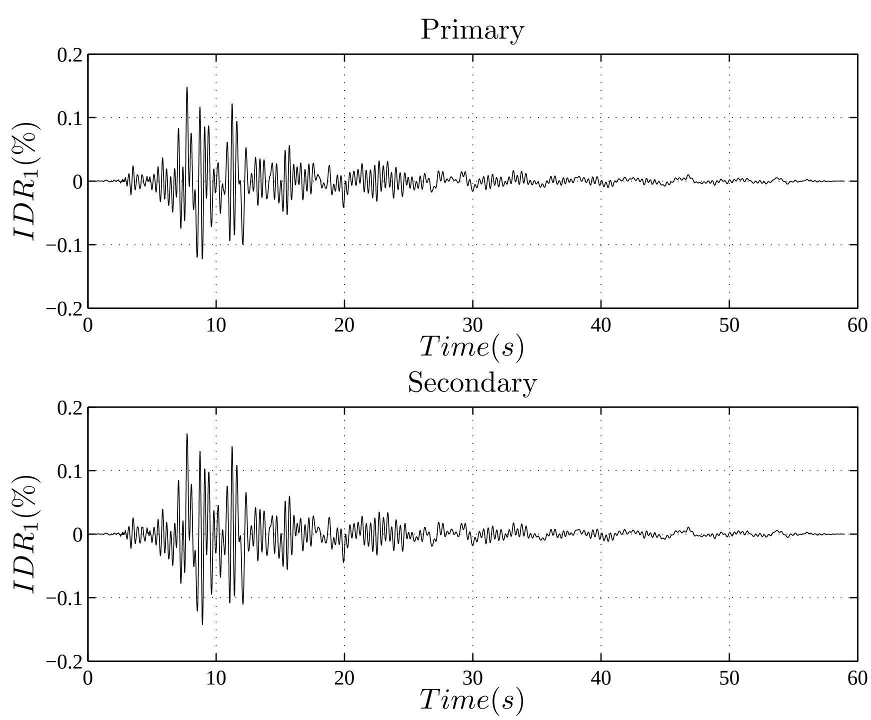

Figure 44: Mean first-story IDR response, Loma Prieta Hollister - South & Pine motion, founded on dense sand.

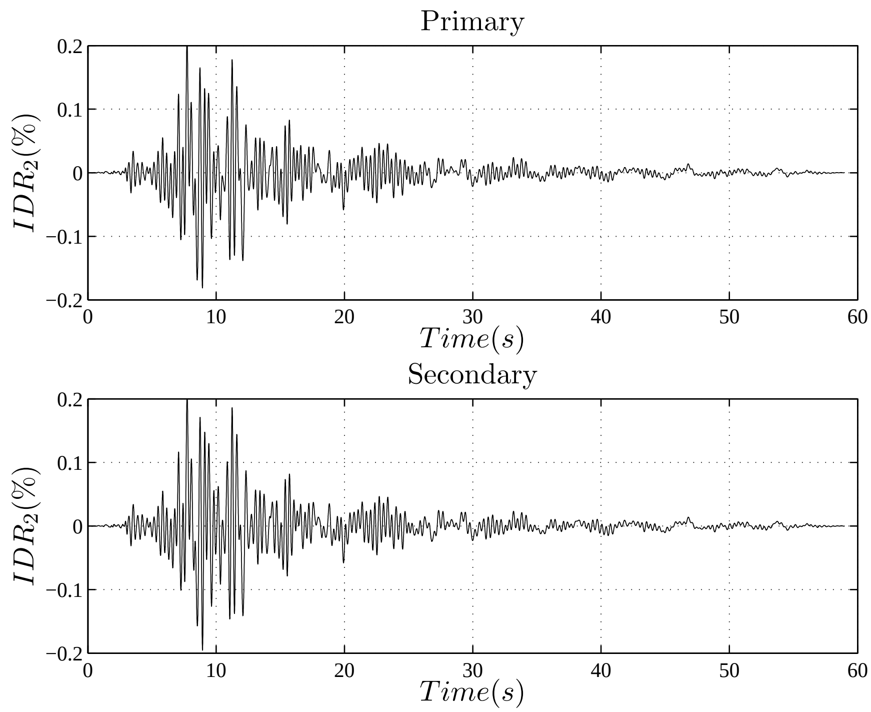

Figure 45: Mean second-story IDR response, Loma Prieta Hollister - South & Pine motion, founded on dense sand.

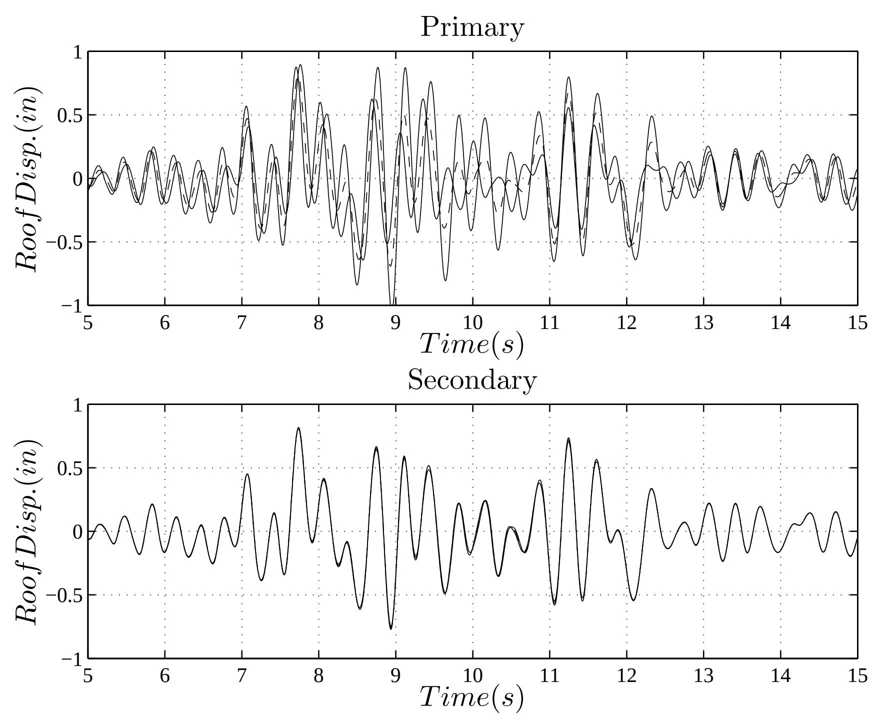

Figure 46: Roof displacement response with sensitivity to building stiffness, Loma Prieta Hollister - South & Pine motion, founded on dense sand.

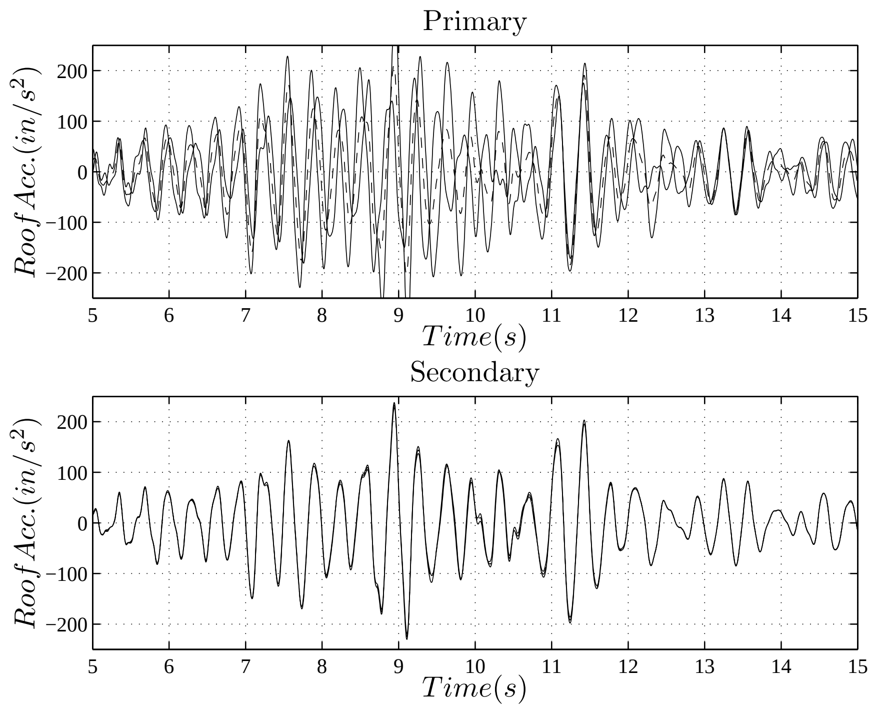

Figure 47: Roof acceleration response with sensitivity to building stiffness, Loma Prieta Hollister - South & Pine motion, founded on dense sand.

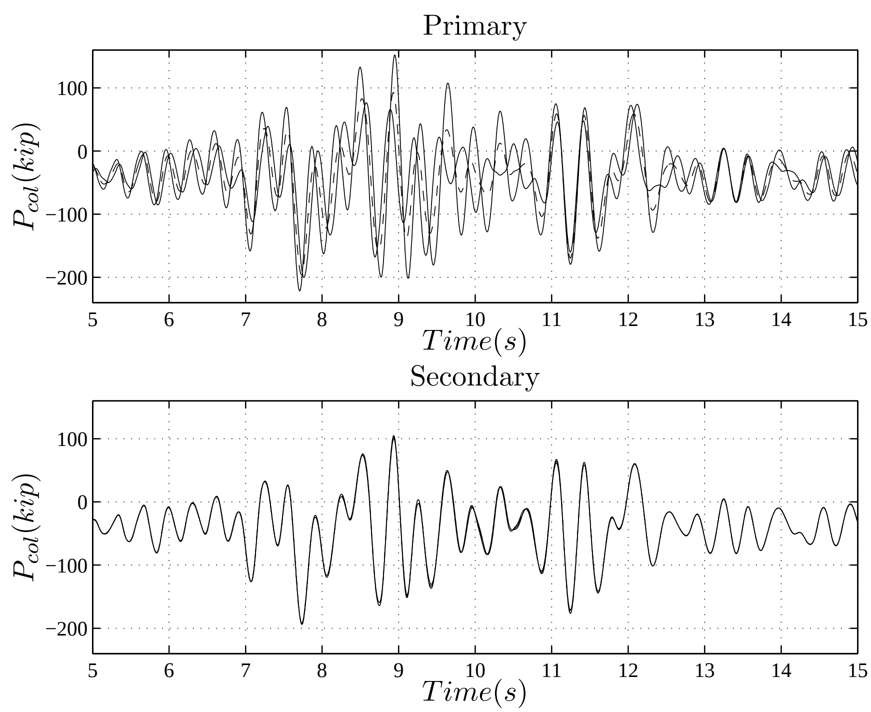

Figure 48: Column force response with sensitivity to building stiffness, Loma Prieta Hollister - South & Pine motion, founded on dense sand.

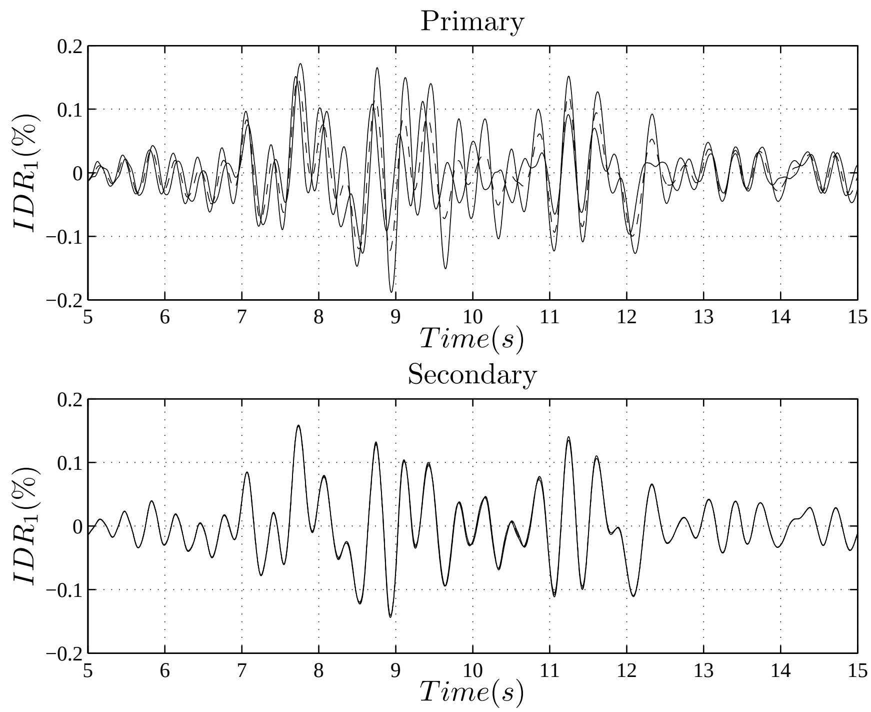

Figure 49: First-story IDR response with sensitivity to building stiffness, Loma Prieta Hollister - South & Pine motion, founded on dense sand.

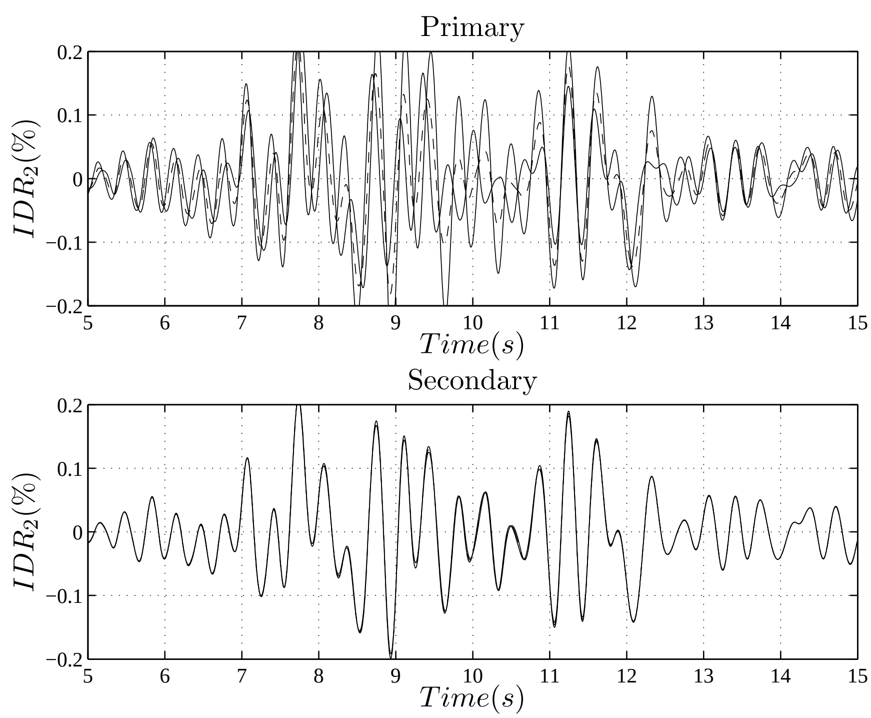

Figure 50: Second-story IDR response with sensitivity to building stiffness, Loma Prieta Hollister - South & Pine motion, founded on dense sand.

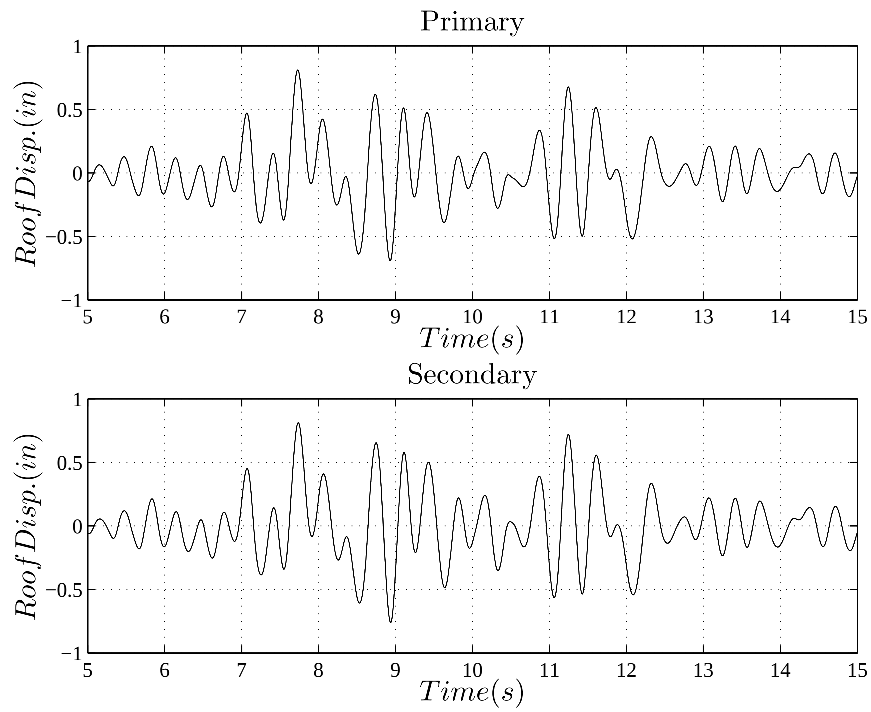

Figure 51: Roof displacement response with sensitivity to soil spring stiffness, Loma Prieta Hollister - South & Pine motion, founded on dense sand.

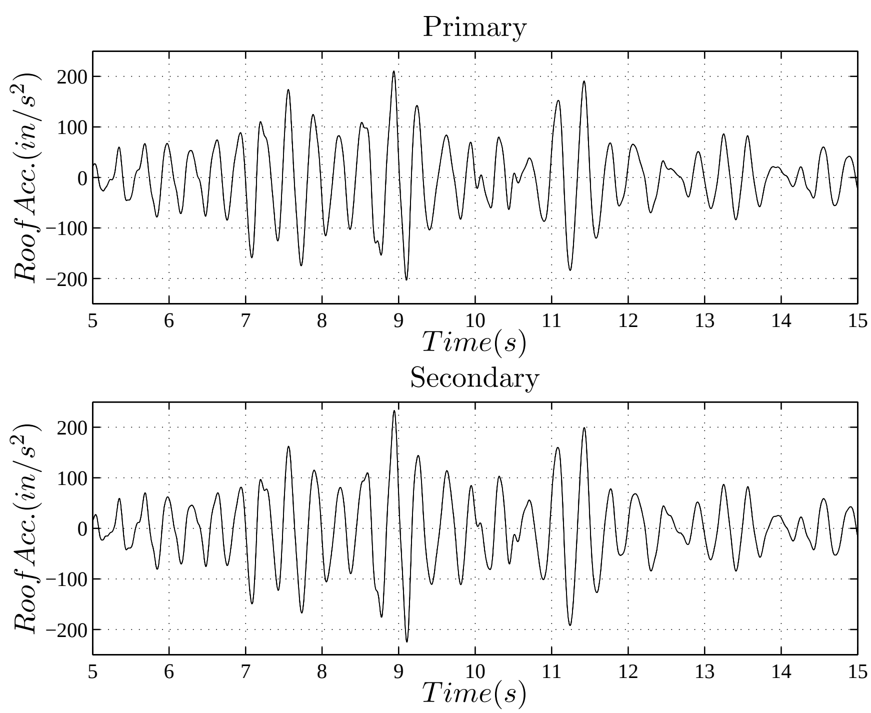

Figure 52: Roof acceleration response with sensitivity to soil spring stiffness, Loma Prieta Hollister - South & Pine motion, founded on dense sand.

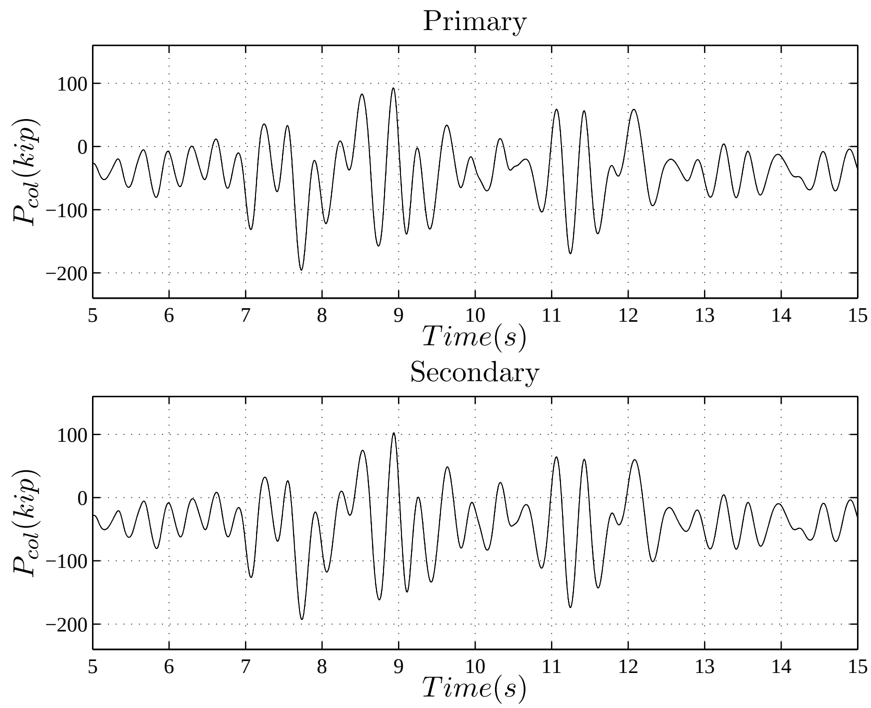

Figure 53: Column force response with sensitivity to soil spring stiffness, Loma Prieta Hollister - South & Pine motion, founded on dense sand.

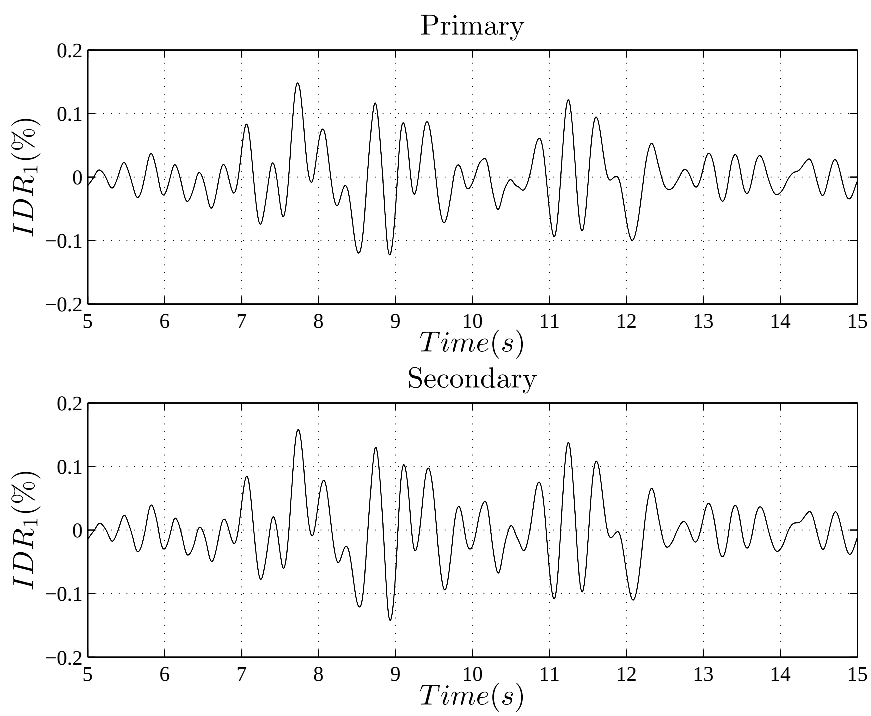

Figure 54: First-story IDR response with sensitivity to soil spring stiffness, Loma Prieta Hollister - South & Pine motion, founded on dense sand.

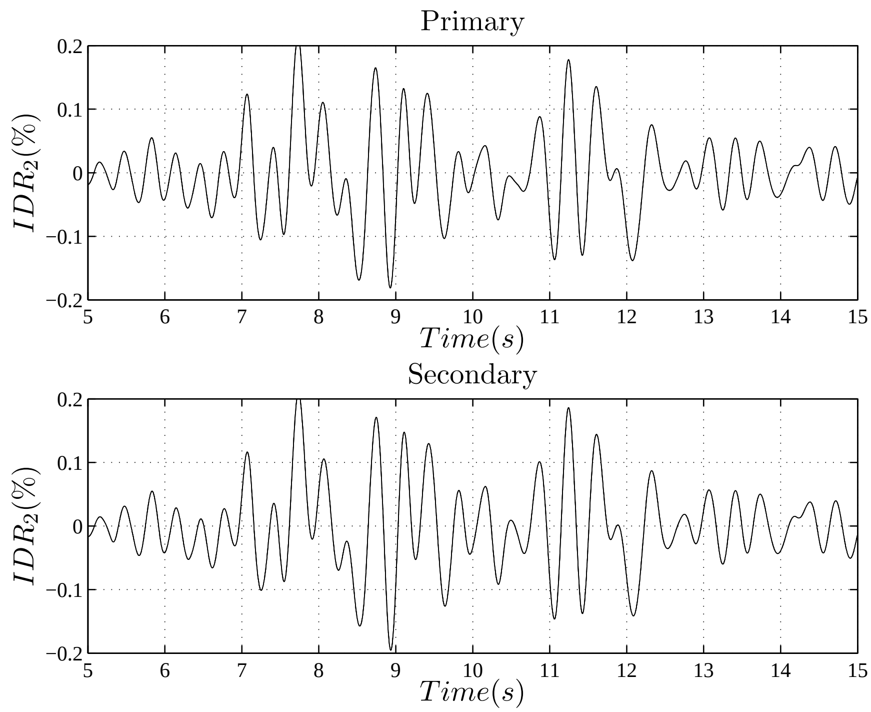

Figure 55: Second-story IDR response with sensitivity to soil spring stiffness, Loma Prieta Hollister - South & Pine motion, founded on dense sand.

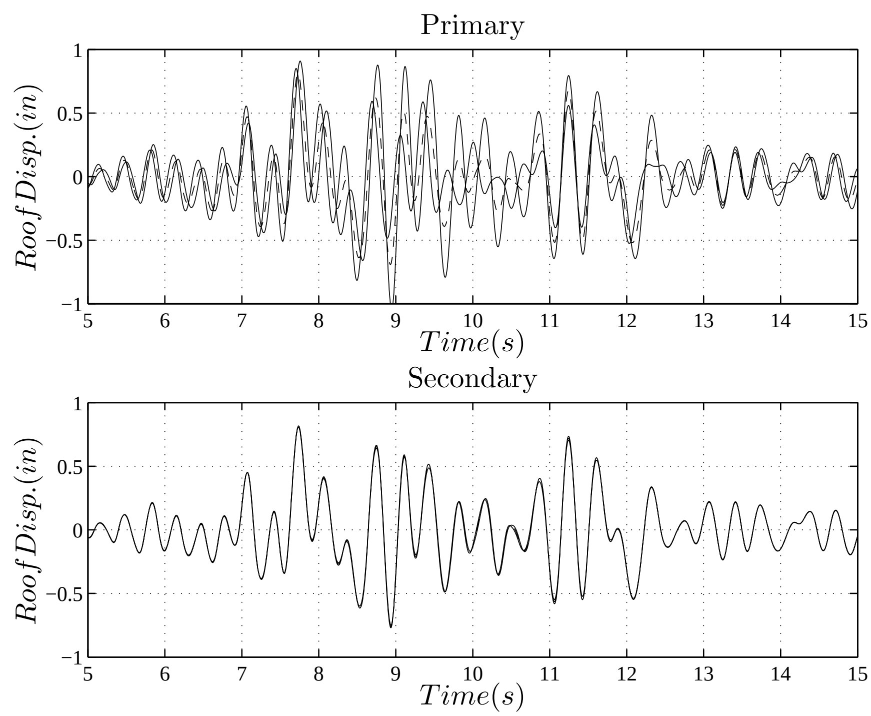

Figure 56: Roof displacement response with sensitivity to floor mass, Loma Prieta Hollister - South & Pine motion, founded on dense sand.

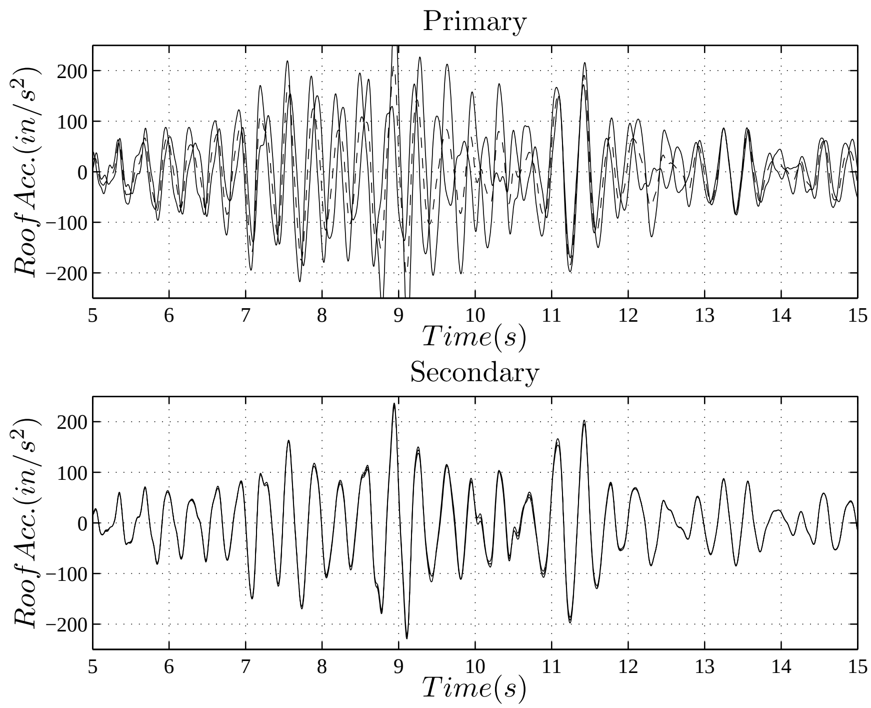

Figure 57: Roof acceleration response with sensitivity to floor mass, Loma Prieta Hollister - South & Pine motion, founded on dense sand.

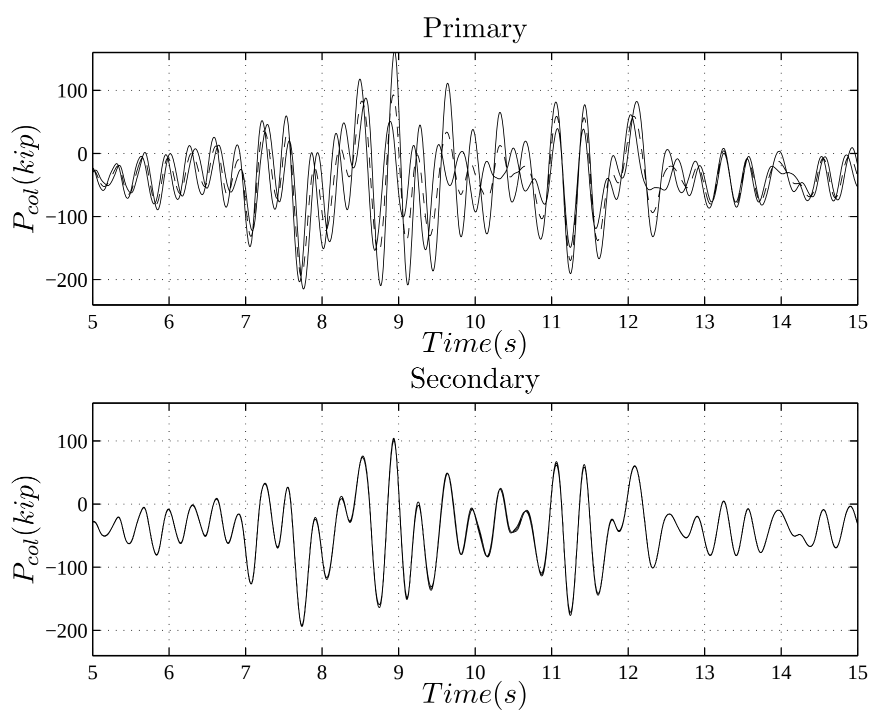

Figure 58: Column Force response with sensitivity to floor mass, Loma Prieta Hollister - South & Pine motion, founded on dense sand.

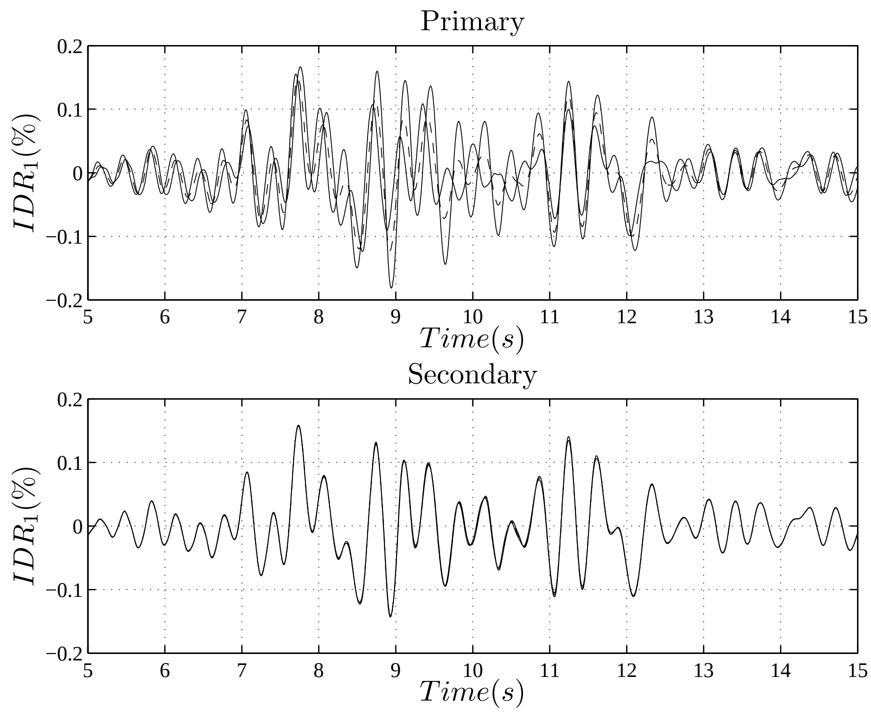

Figure 59: First-story IDR response with sensitivity to floor mass, Loma Prieta Hollister - South & Pine motion, founded on dense sand.

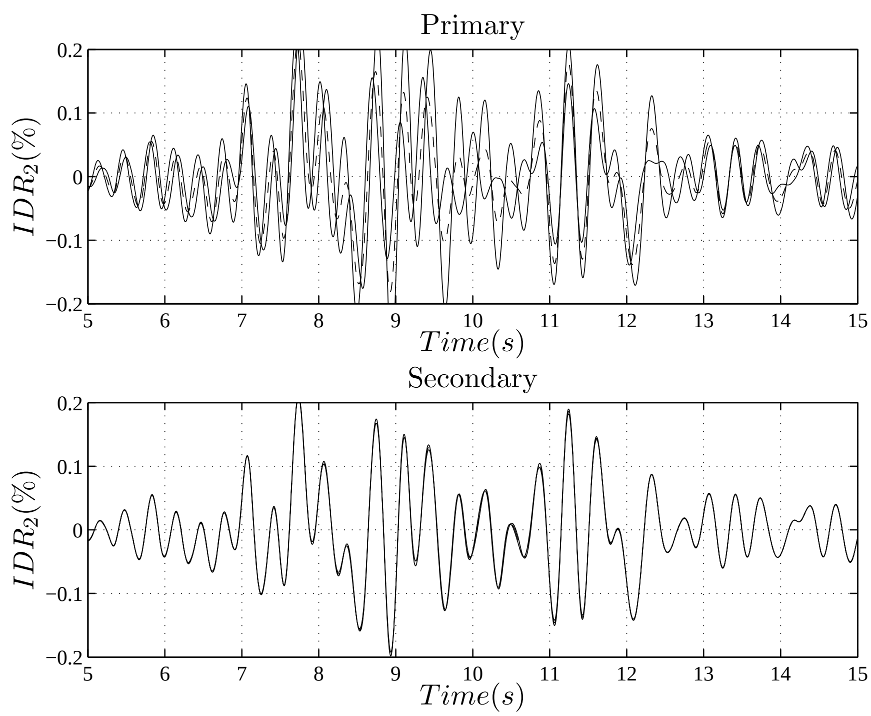

Figure 60: Second-story IDR response with sensitivity to floor mass, Loma Prieta Hollister - South & Pine motion, founded on dense sand.

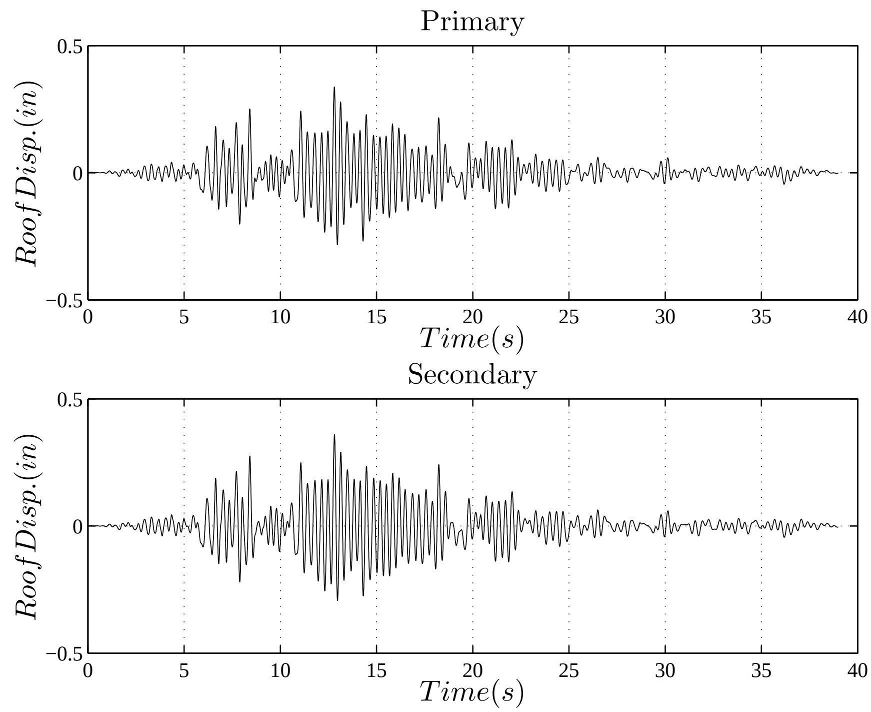

Figure 61: Mean roof displacement response, Loma Prieta Salinas - John & Work motion, founded on dense sand.

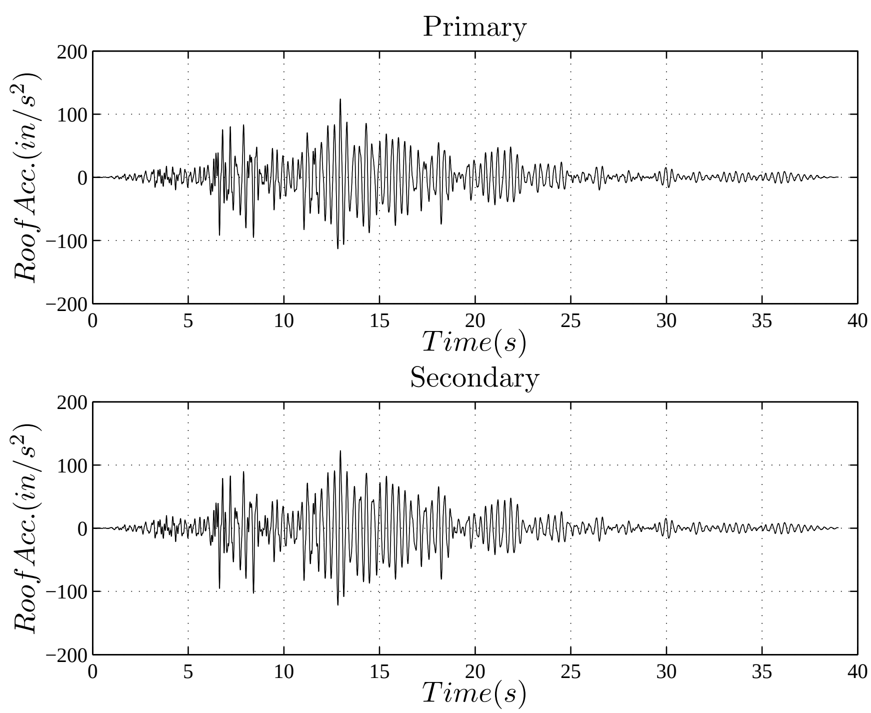

Figure 62: Mean roof acceleration response, Loma Prieta Salinas - John & Work motion, founded on dense sand.

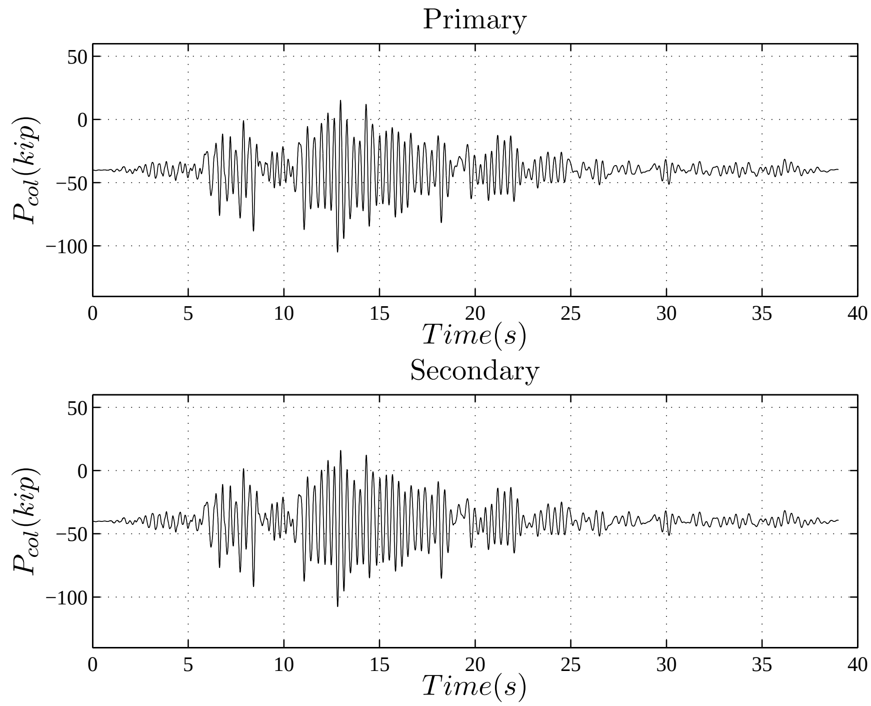

Figure 63: Mean column response, Loma Prieta Salinas - John & Work motion, founded on dense sand.

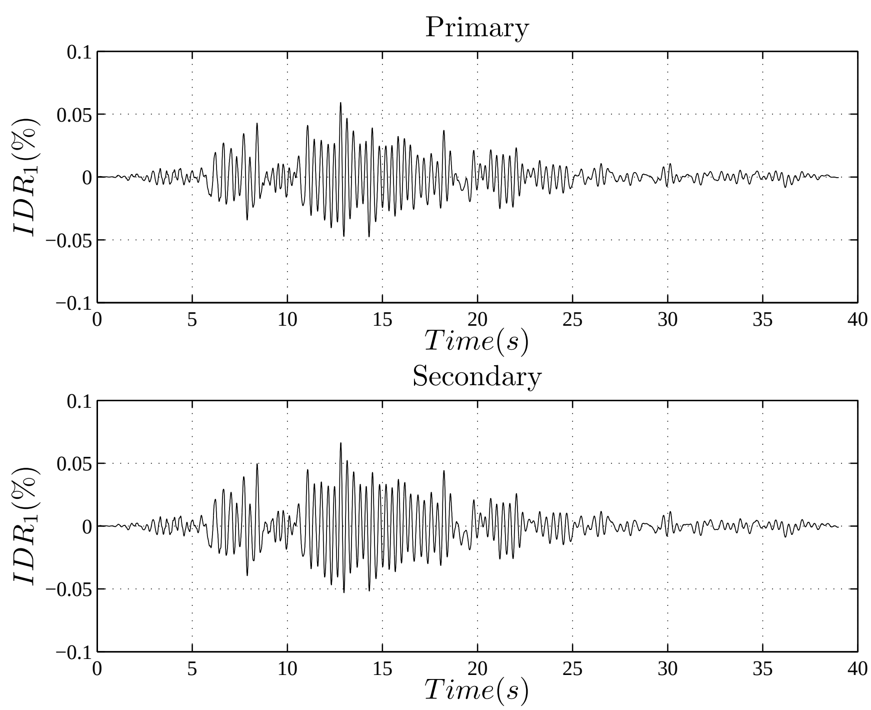

Figure 64: Mean first-story IDR response, Loma Prieta Salinas - John & Work motion, founded on dense sand.

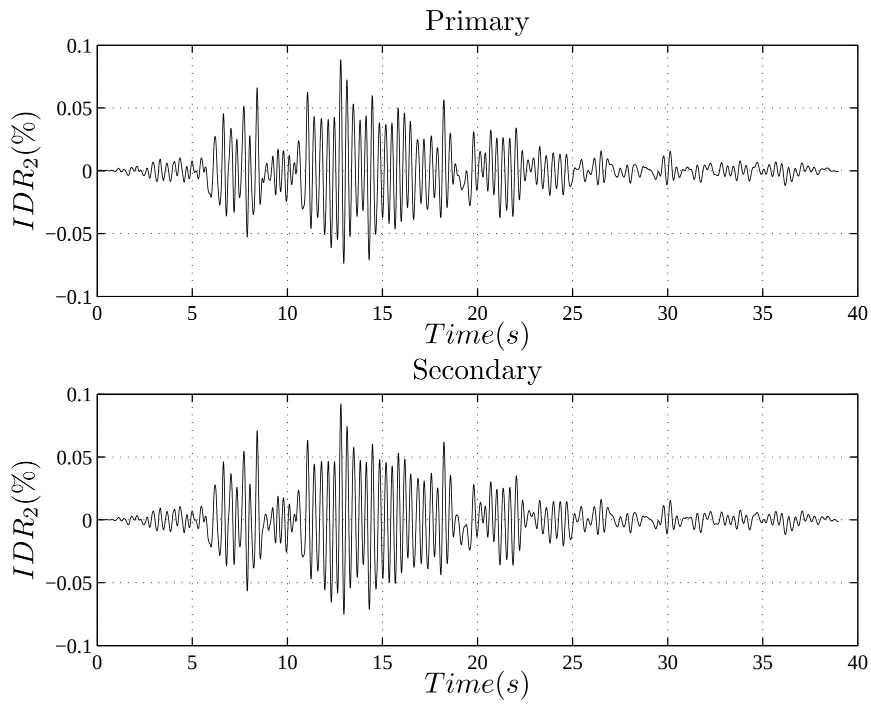

Figure 65: Mean roof displacement response, Loma Prieta Salinas - John & Work motion, founded on dense sand.

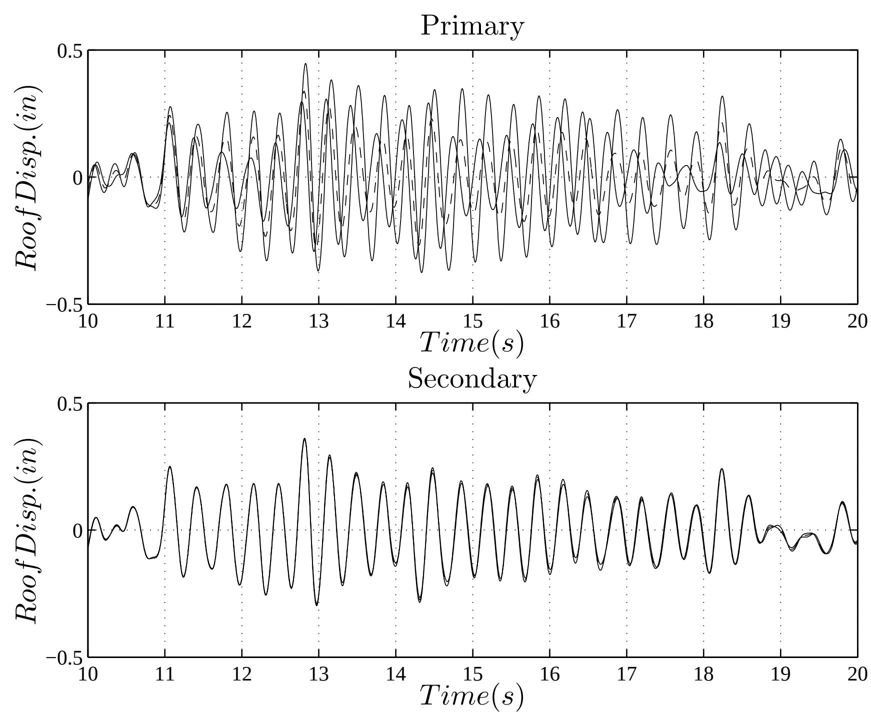

Figure 66: Roof displacement response with sensitivity to building stiffness, Loma Prieta Salinas - John & Work motion, founded on dense sand.

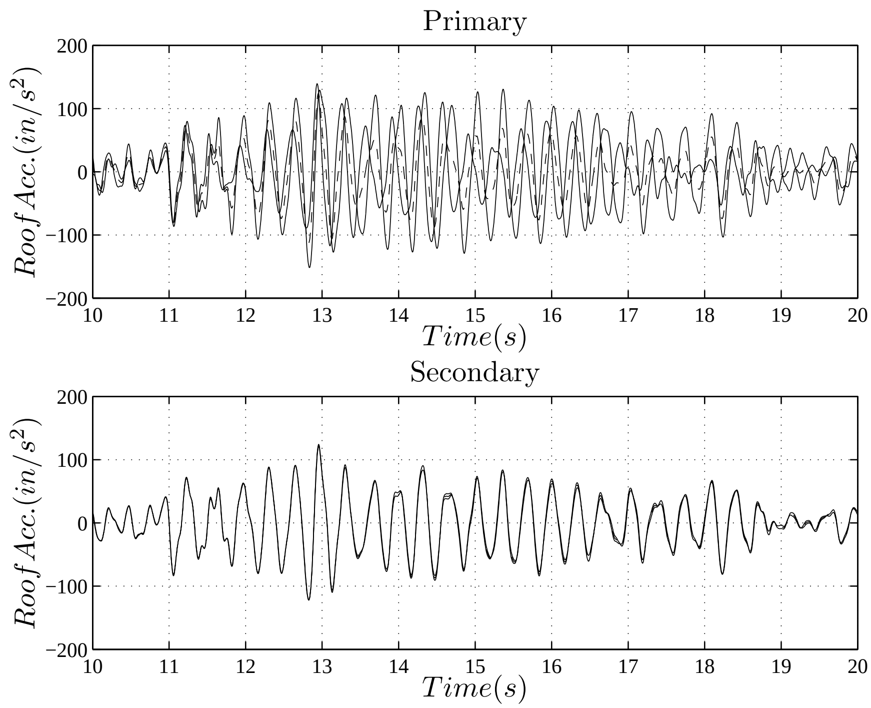

Figure 67: Roof acceleration response with sensitivity to building stiffness, Loma Prieta Salinas - John & Work motion, founded on dense sand.

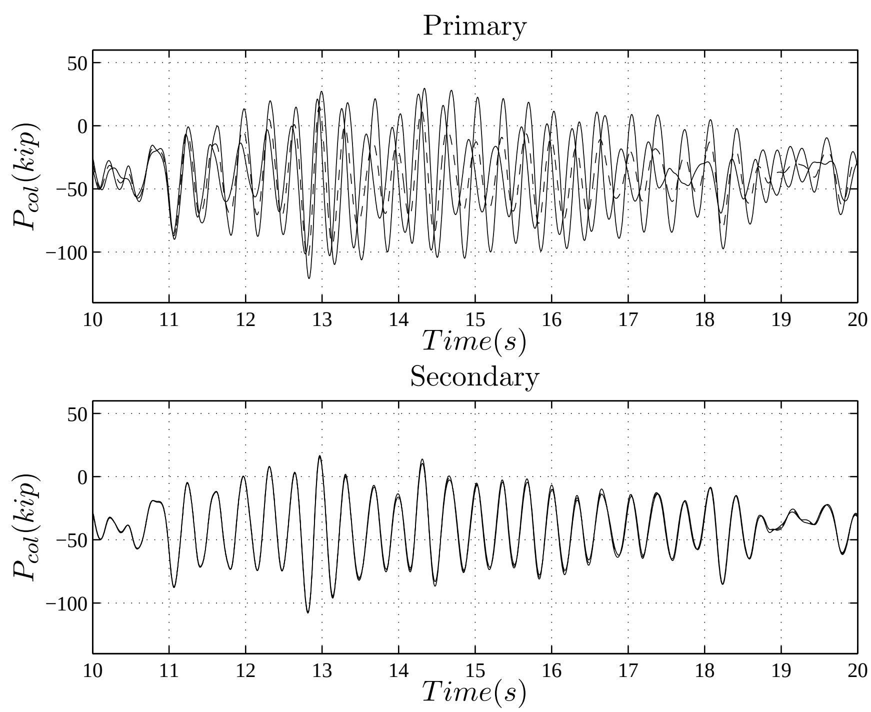

Figure 68: Column force response with sensitivity to building stiffness, Loma Prieta Salinas - John & Work motion, founded on dense sand.

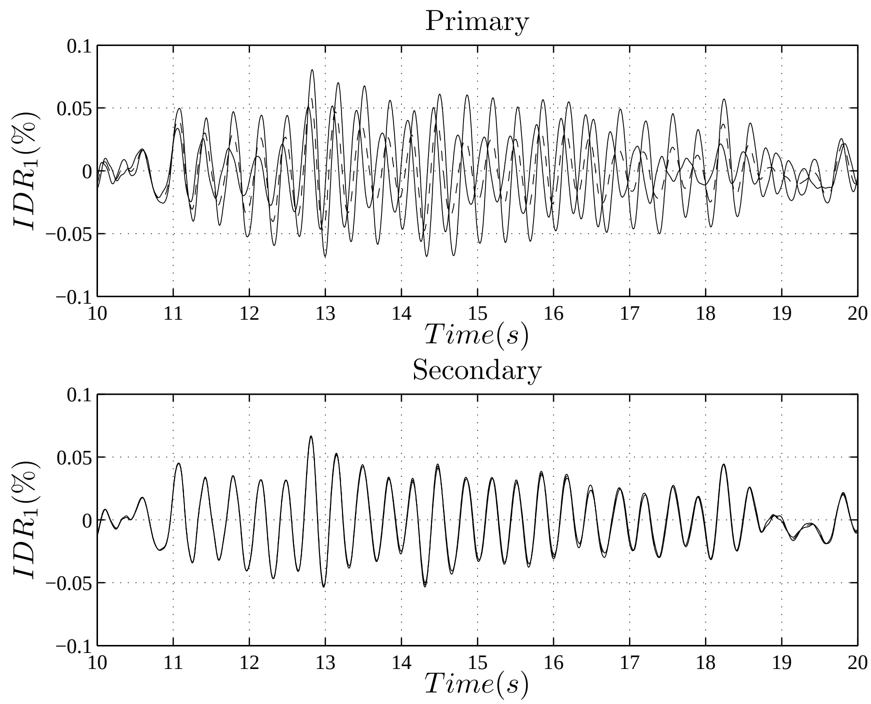

Figure 69: First-story IDR response with sensitivity to building stiffness, Loma Prieta Salinas - John & Work motion, founded on dense sand.

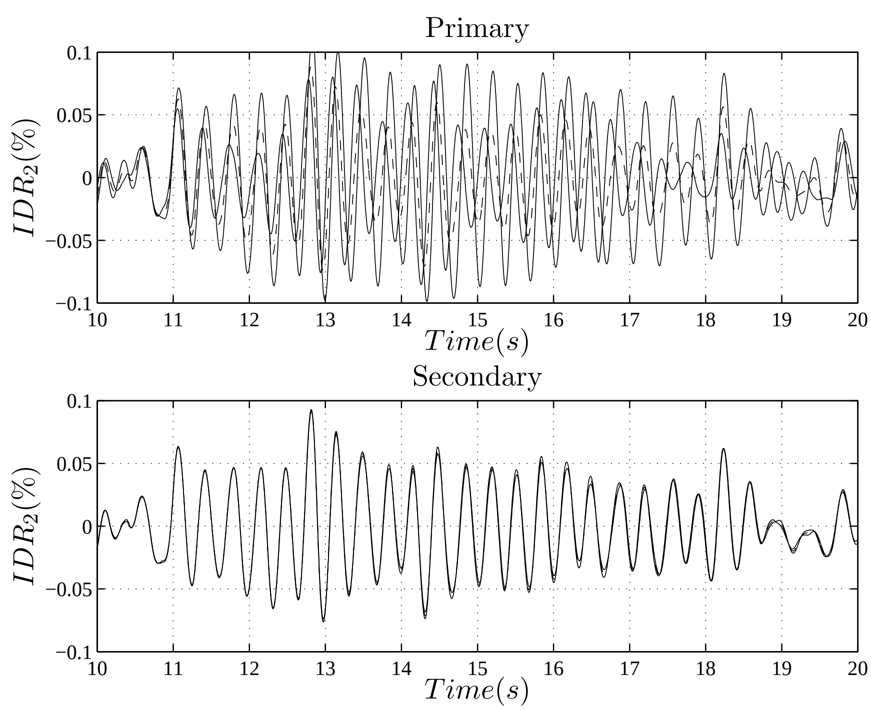

Figure 70: Second-story IDR response with sensitivity to building stiffness, Loma Prieta Salinas - John & Work motion, founded on dense sand.

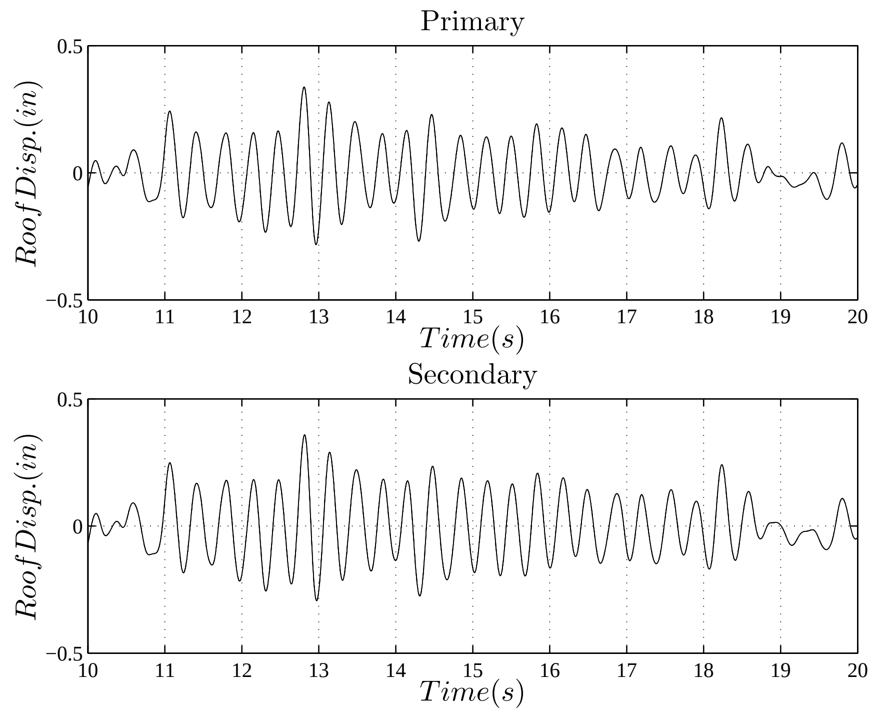

Figure 71: Roof displacement response with sensitivity to soil spring stiffness, Loma Prieta Salinas - John & Work motion, founded on dense sand.

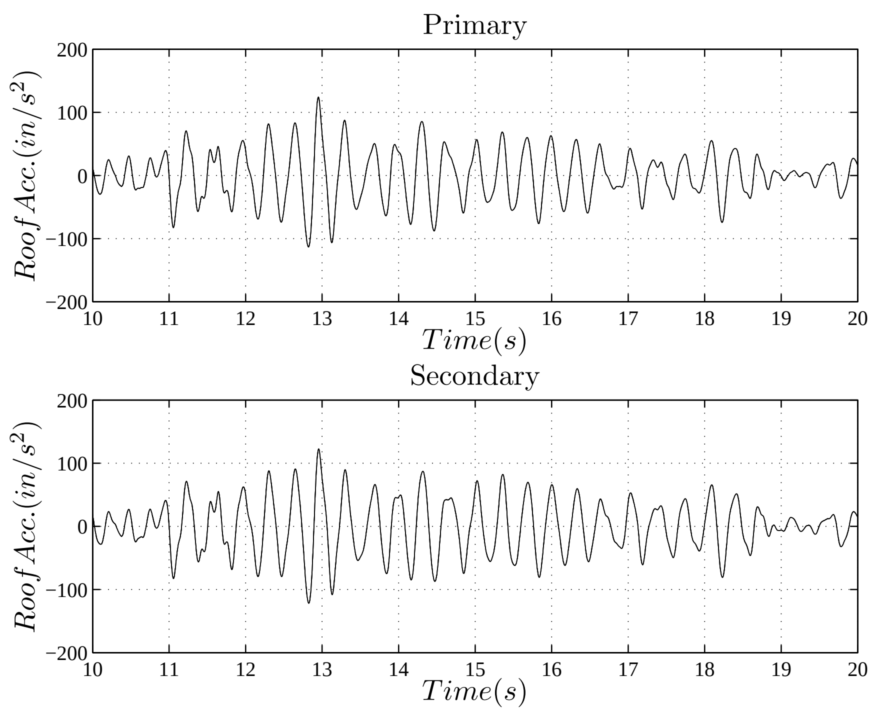

Figure 72: Roof acceleration response with sensitivity to soil spring stiffness, Loma Prieta Salinas - John & Work motion, founded on dense sand.

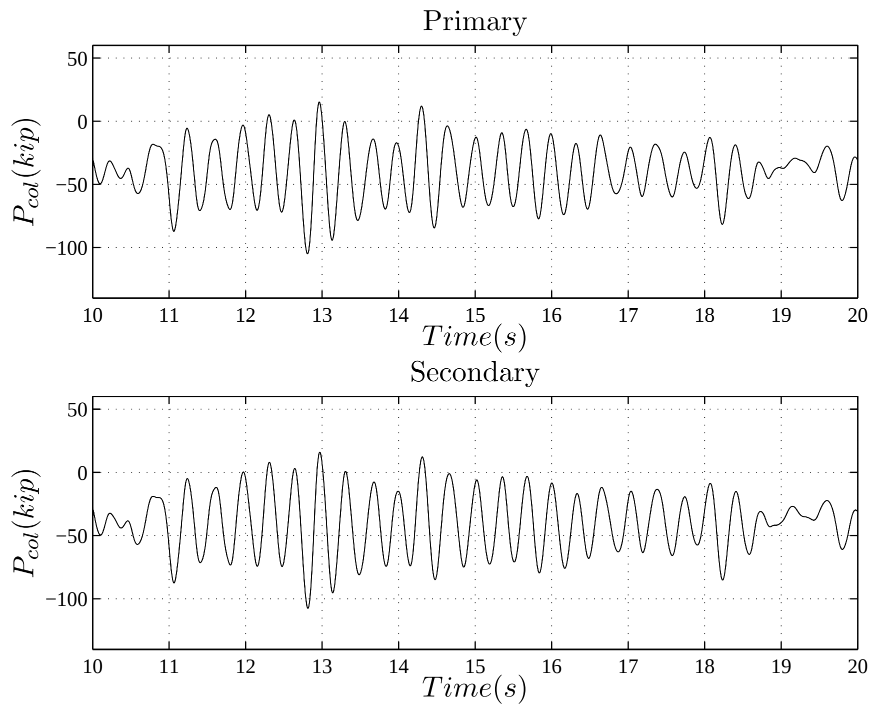

Figure 73: Column force response with sensitivity to soil spring stiffness, Loma Prieta Salinas - John & Work motion, founded on dense sand.

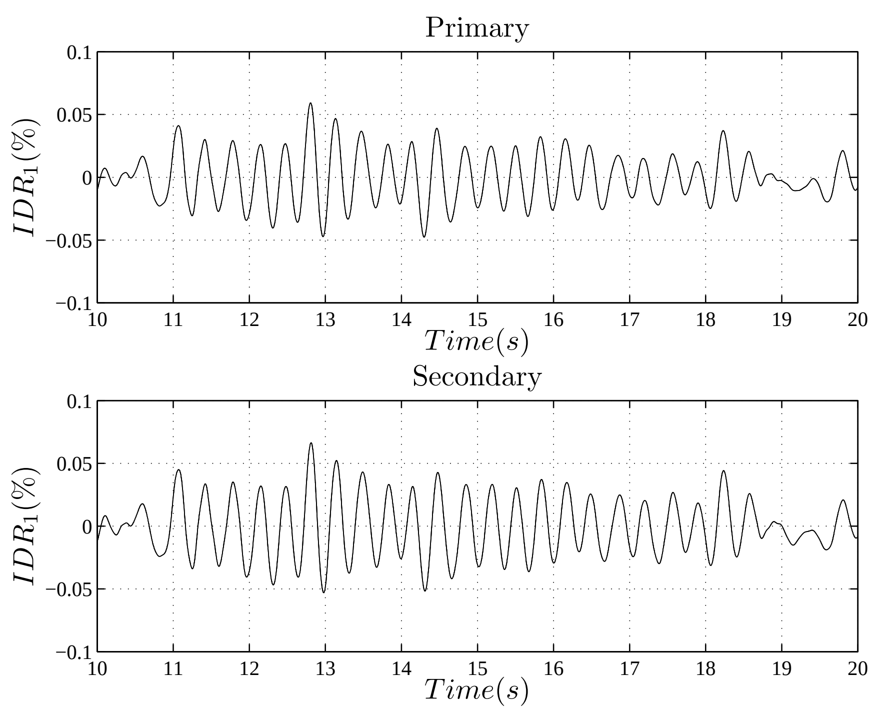

Figure 74: First-story IDR response with sensitivity to soil spring stiffness, Loma Prieta Salinas - John & Work motion, founded on dense sand.

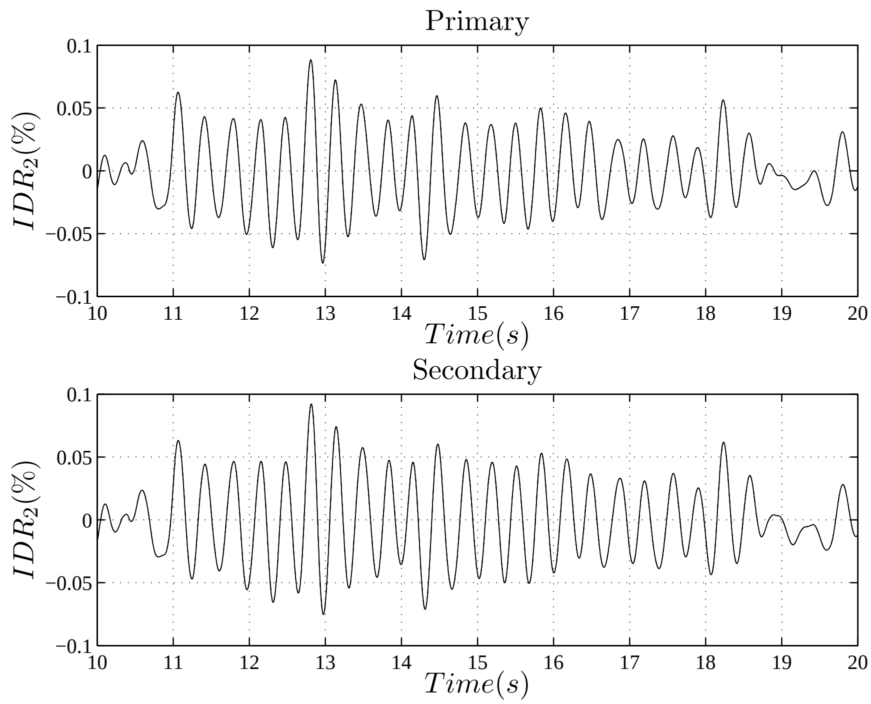

Figure 75: Second-story IDR response with sensitivity to soil spring stiffness, Loma Prieta Salinas - John & Work motion, founded on dense sand.

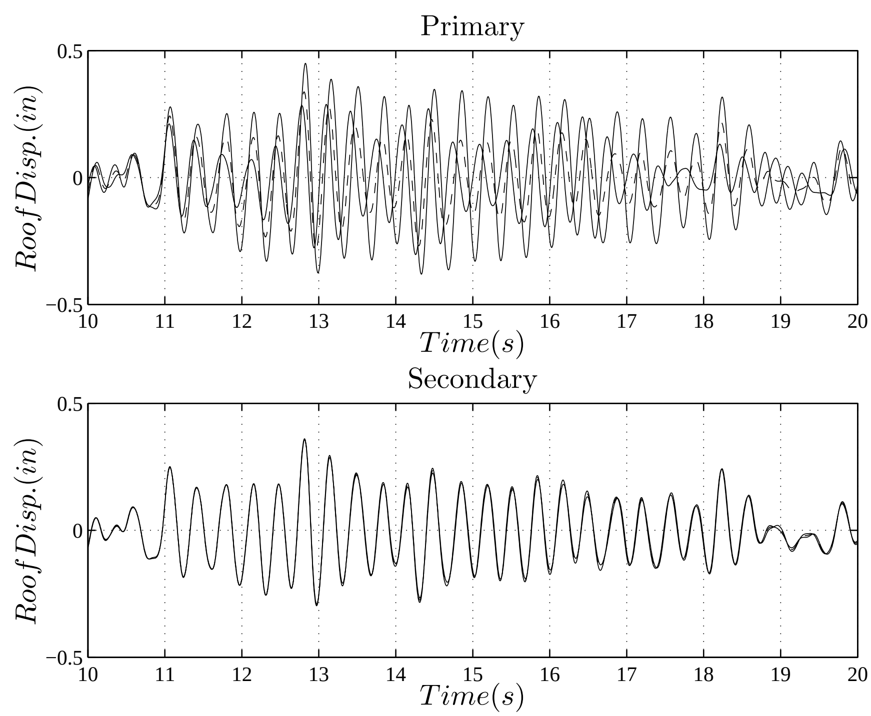

Figure 76: Roof displacement response with sensitivity to floor mass, Loma Prieta Salinas - John & Work motion, founded on dense sand.

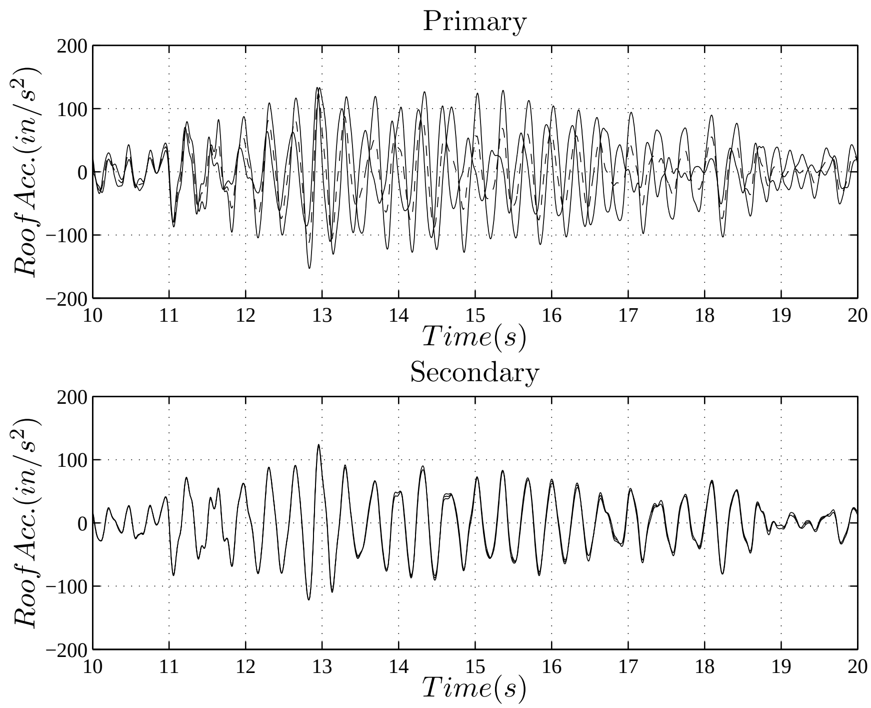

Figure 77: Roof acceleration response with sensitivity to floor mass, Loma Prieta Salinas - John & Work motion, founded on dense sand.

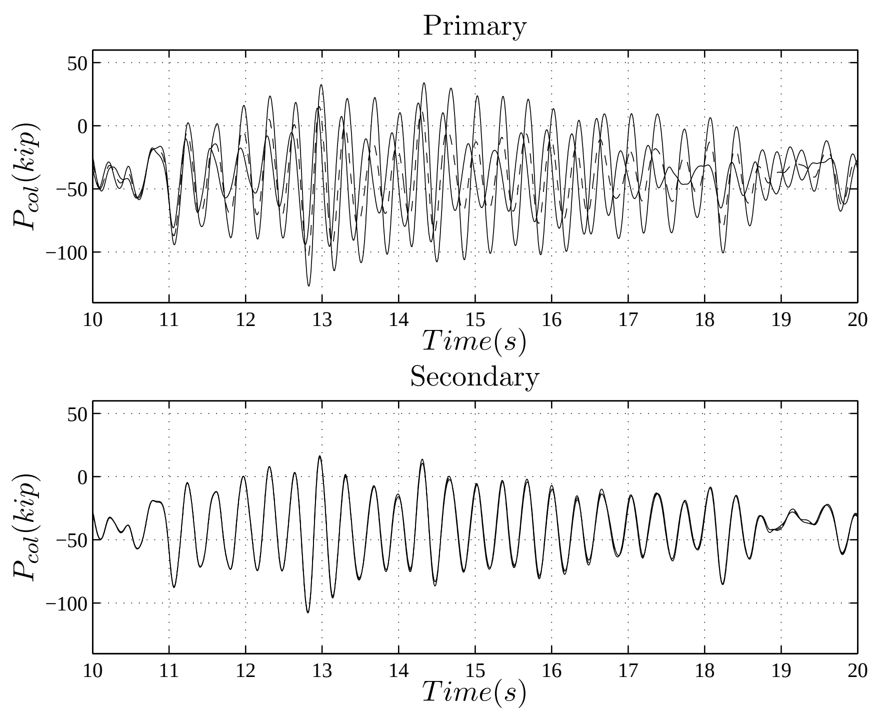

Figure 78: Column Force response with sensitivity to floor mass, Loma Prieta Salinas - John & Work motion, founded on dense sand.

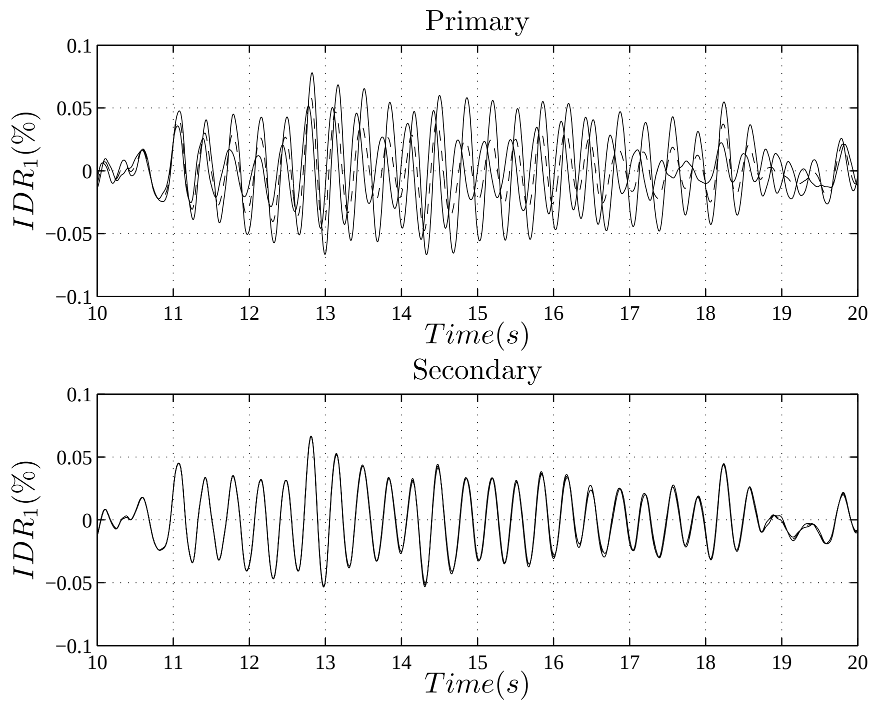

Figure 79: First-story IDR response with sensitivity to floor mass, Loma Prieta Salinas - John & Work motion, founded on dense sand.

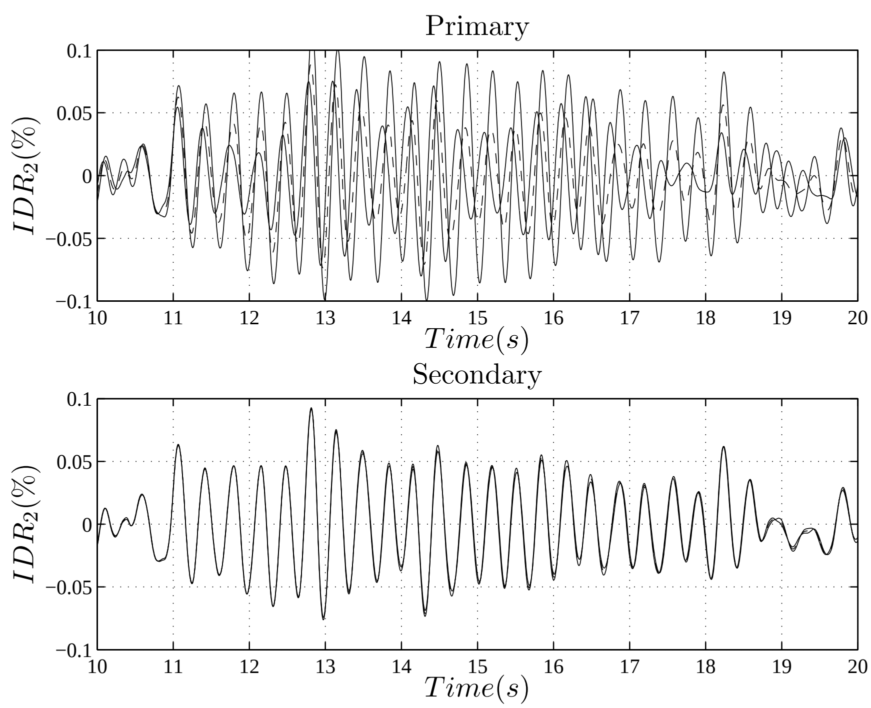

Figure 80: Second-story IDR response with sensitivity to floor mass, Loma Prieta Salinas - John & Work motion, founded on dense sand.

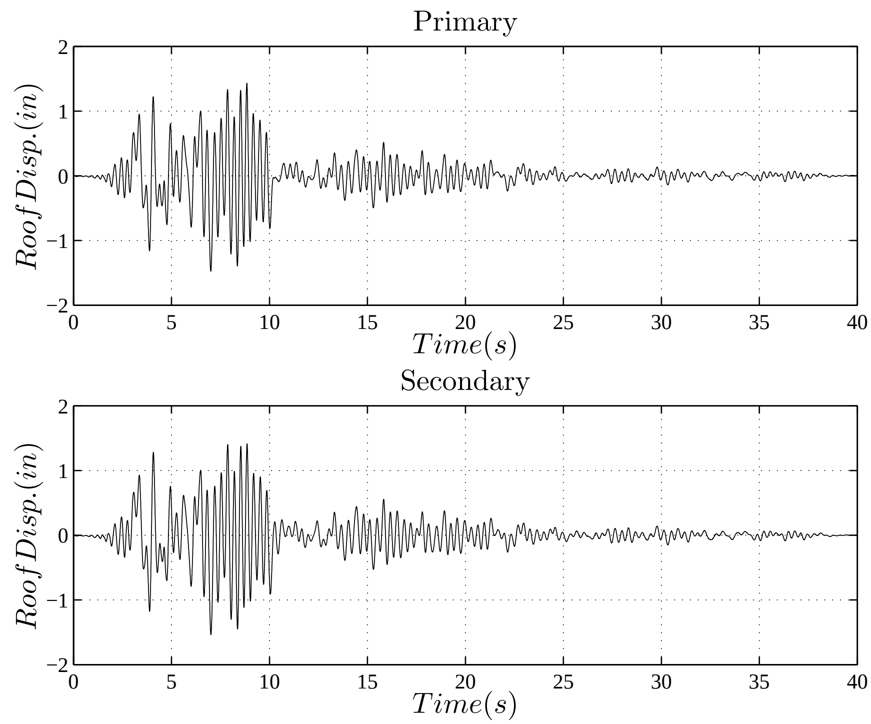

Figure 81: Mean roof displacement response, Northridge - Sylmar Converter Station motion, founded on dense sand.

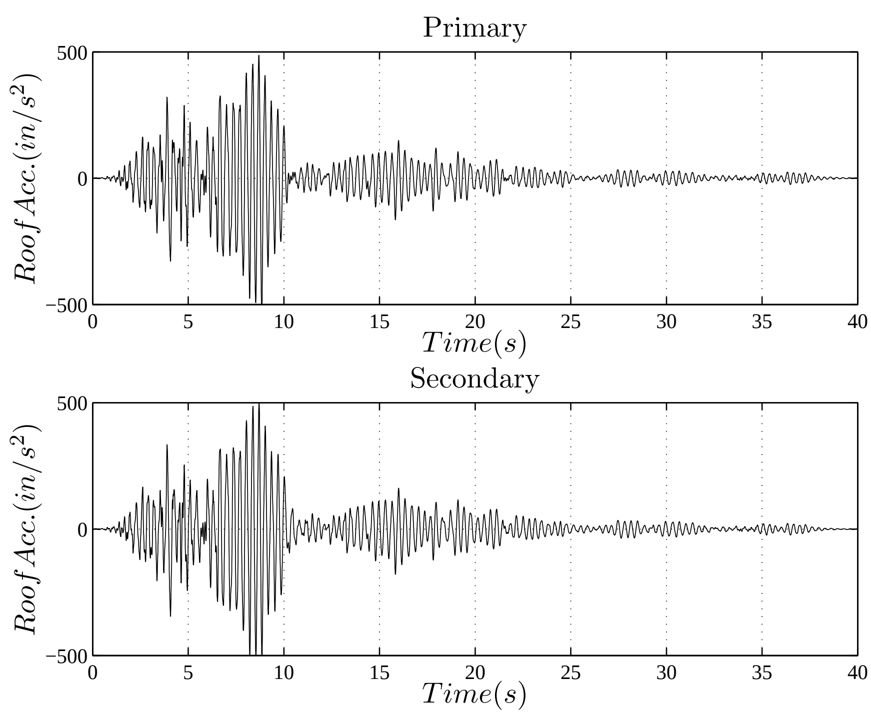

Figure 82: Mean roof acceleration response, Northridge - Sylmar Converter Station motion, founded on dense sand.

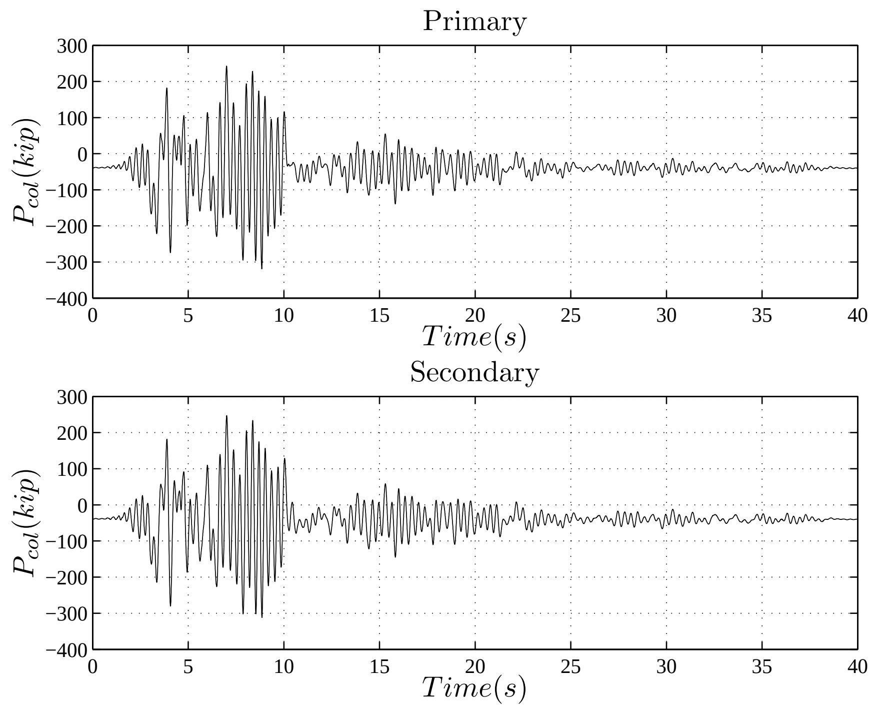

Figure 83: Mean column response, Northridge - Sylmar Converter Station motion, founded on dense sand.

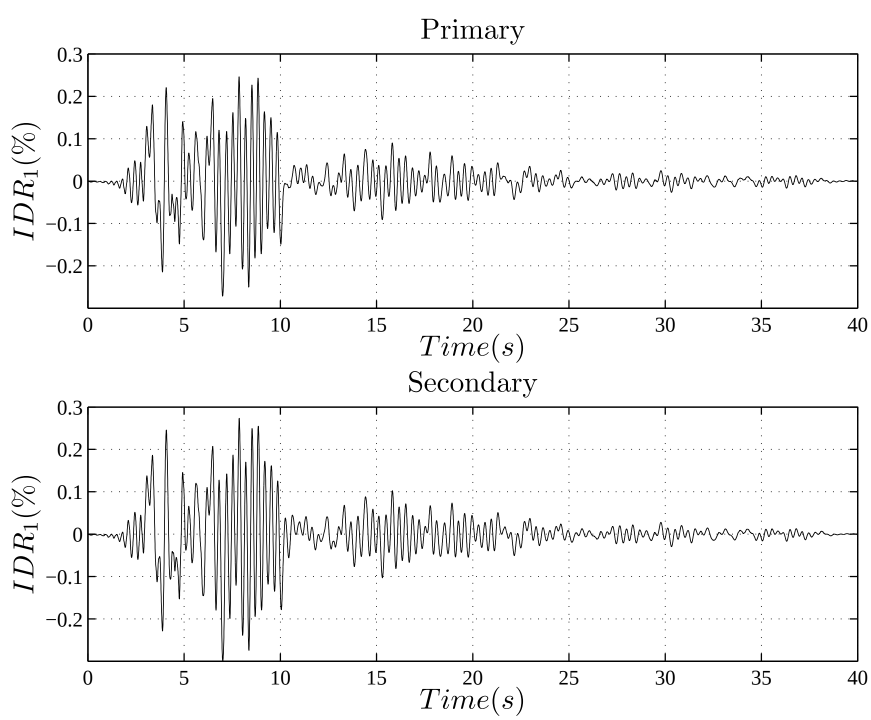

Figure 84: Mean first-story IDR response, Northridge - Sylmar Converter Station motion, founded on dense sand.

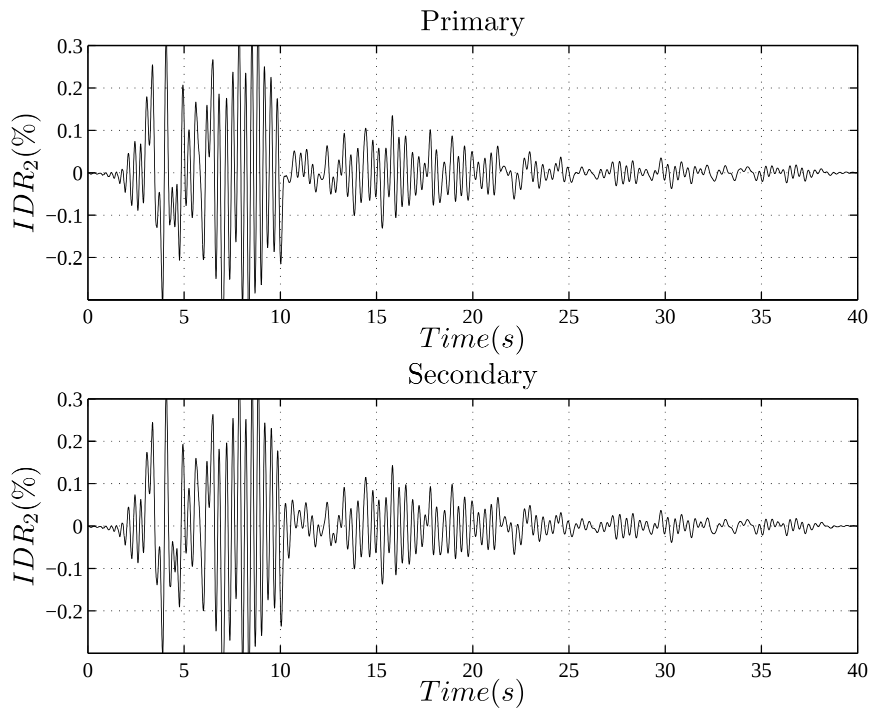

Figure 85: Mean roof displacement response, Northridge - Sylmar Converter Station motion, founded on dense sand.

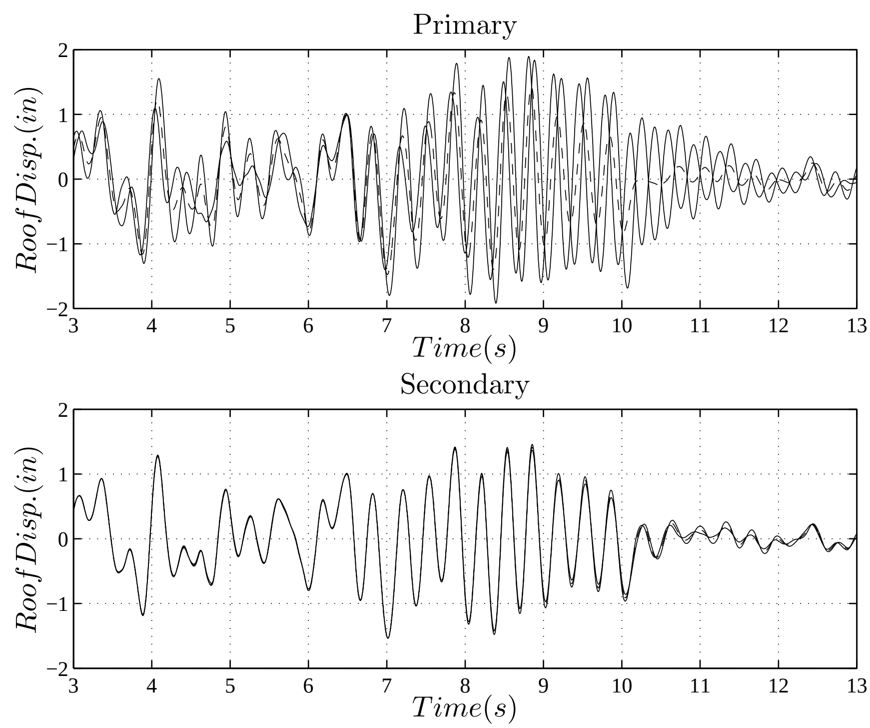

Figure 86: Roof displacement response with sensitivity to building stiffness, Northridge - Sylmar Converter Station motion, founded on dense sand.

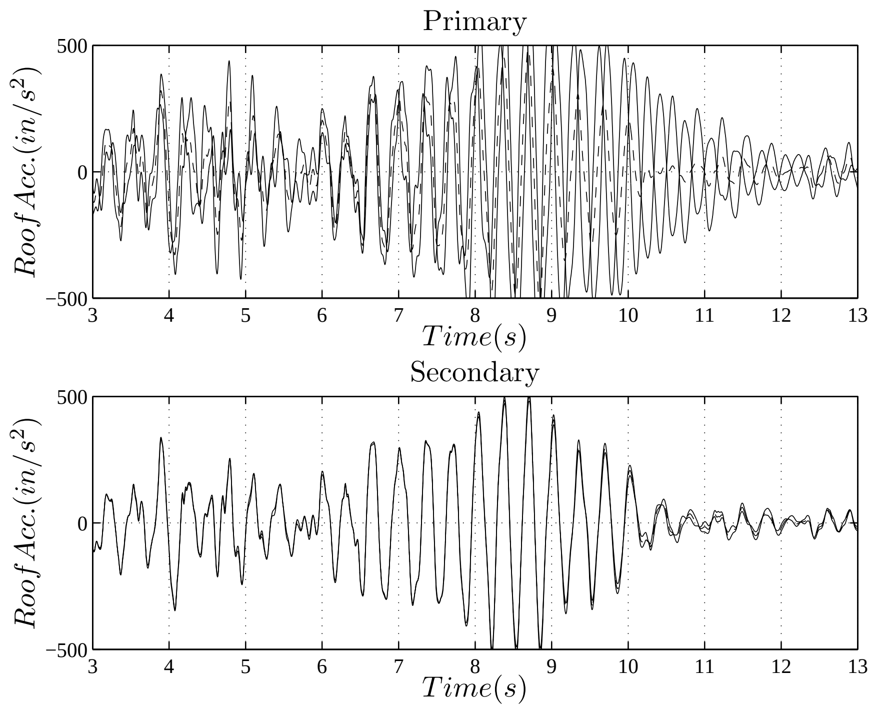

Figure 87: Roof acceleration response with sensitivity to building stiffness, Northridge - Sylmar Converter Station motion, founded on dense sand.

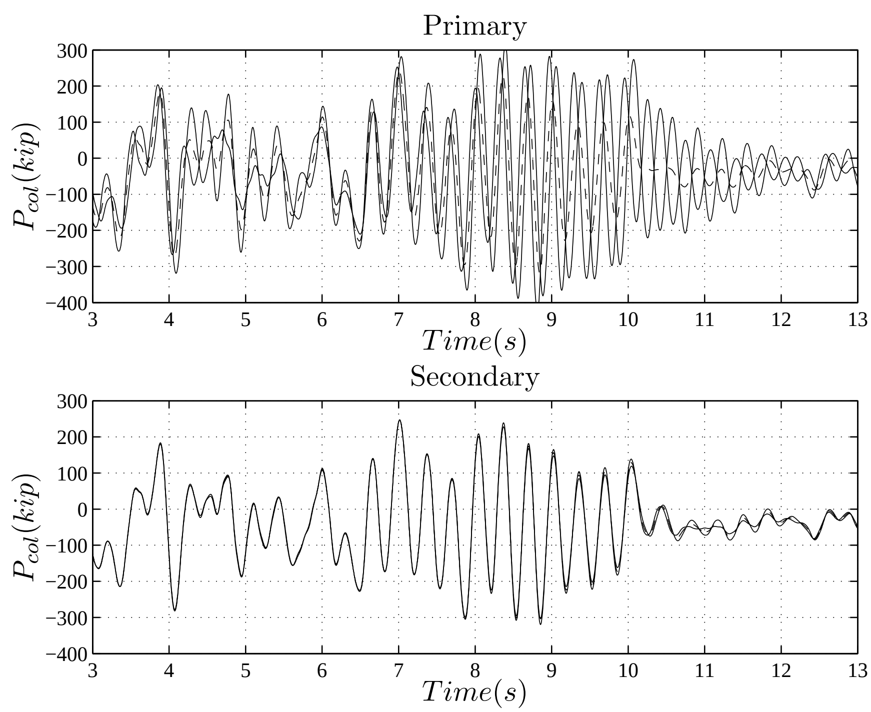

Figure 88: Column force response with sensitivity to building stiffness, Northridge - Sylmar Converter Station motion, founded on dense sand.

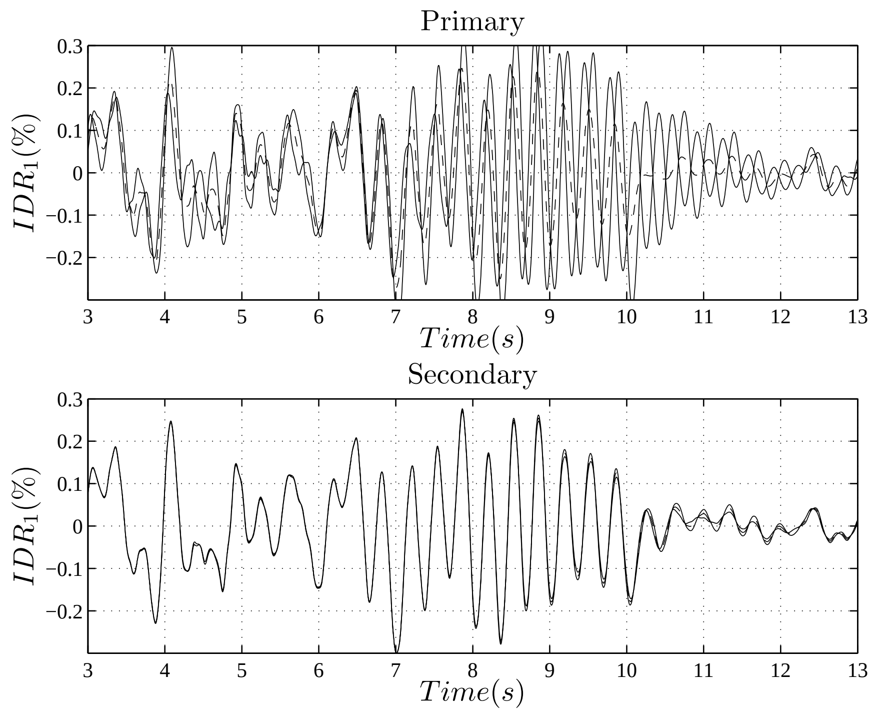

Figure 89: First-story IDR response with sensitivity to building stiffness, Northridge - Sylmar Converter Station motion, founded on dense sand.

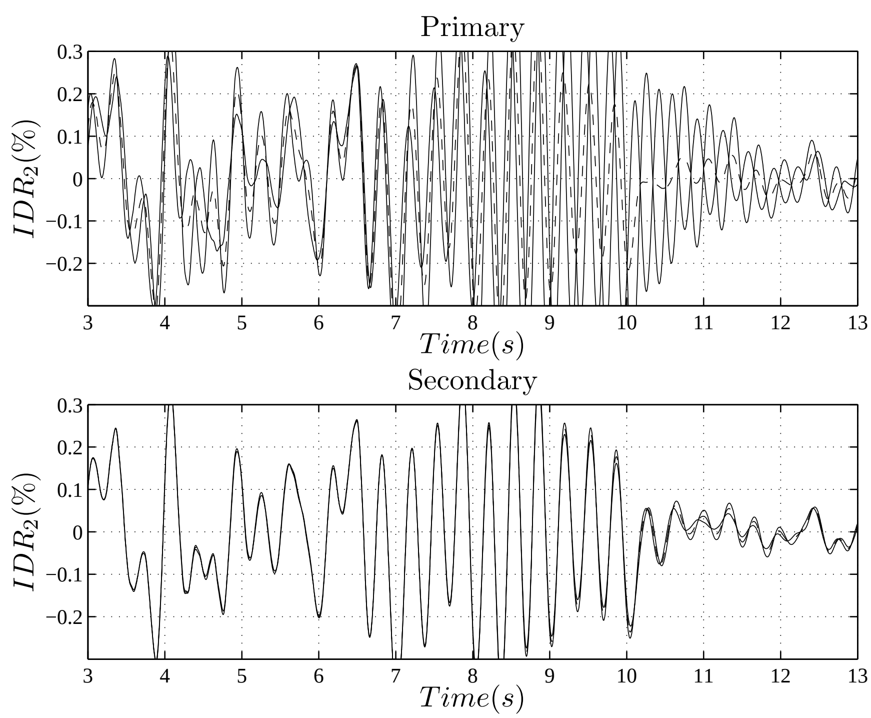

Figure 90: Second-story IDR response with sensitivity to building stiffness, Northridge - Sylmar Converter Station motion, founded on dense sand.

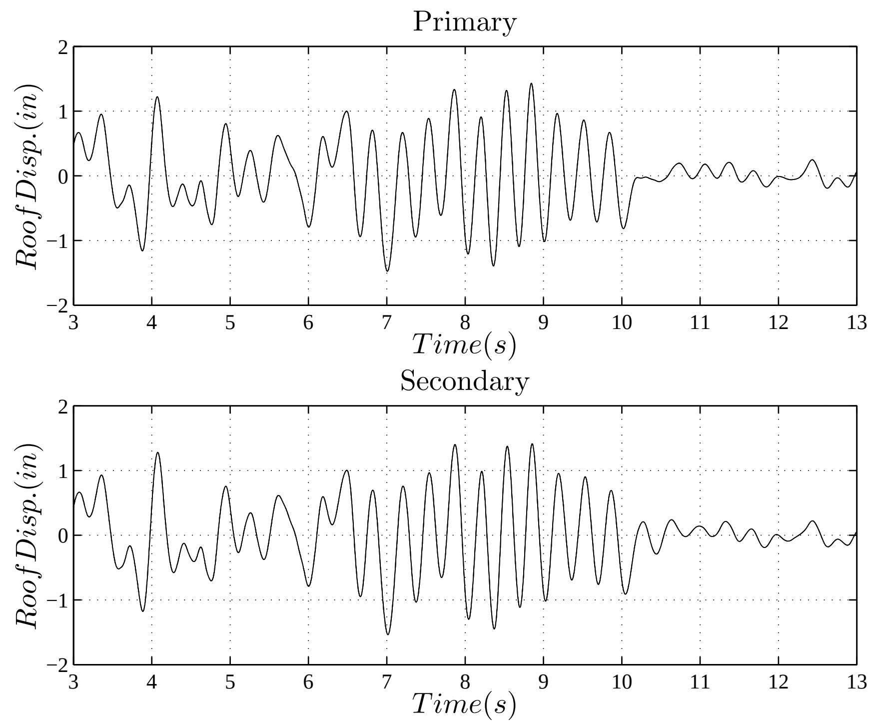

Figure 91: Roof displacement response with sensitivity to soil spring stiffness, Northridge - Sylmar Converter Station motion, founded on dense sand.

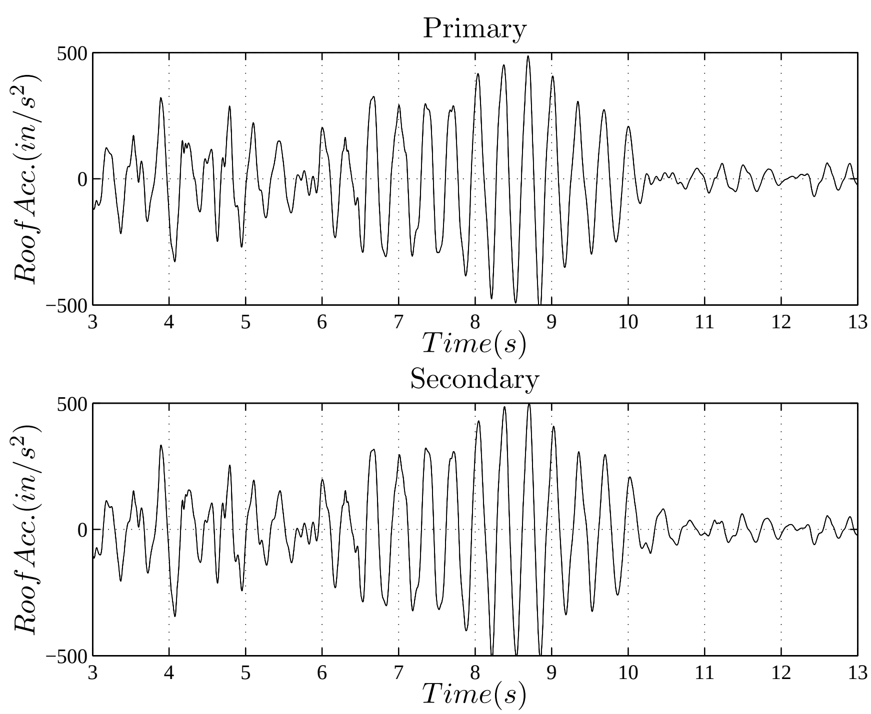

Figure 92: Roof acceleration response with sensitivity to soil spring stiffness, Northridge - Sylmar Converter Station motion, founded on dense sand.

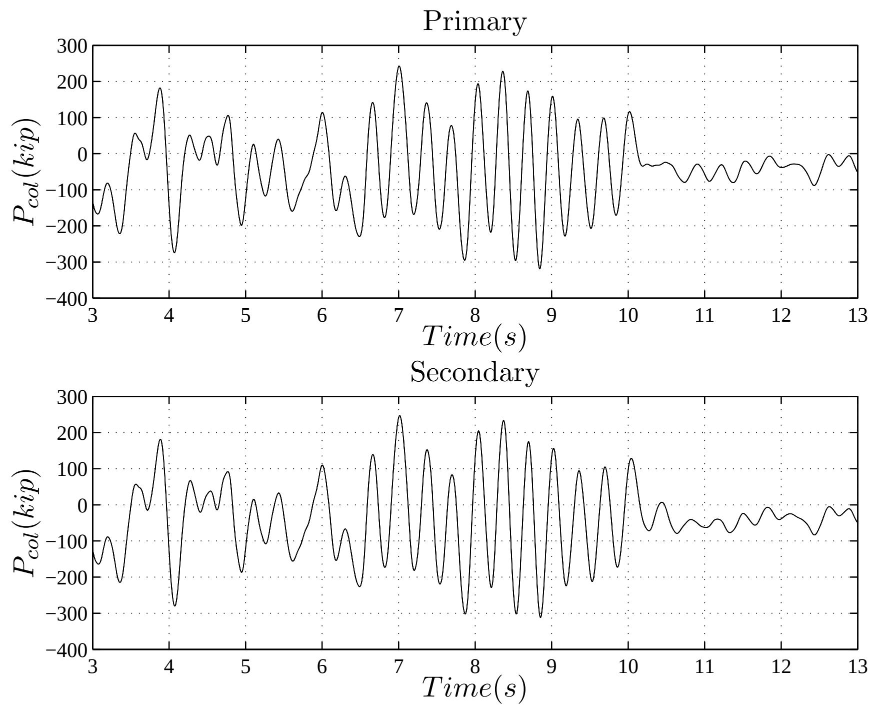

Figure 93: Column force response with sensitivity to soil spring stiffness, Northridge - Sylmar Converter Station motion, founded on dense sand.

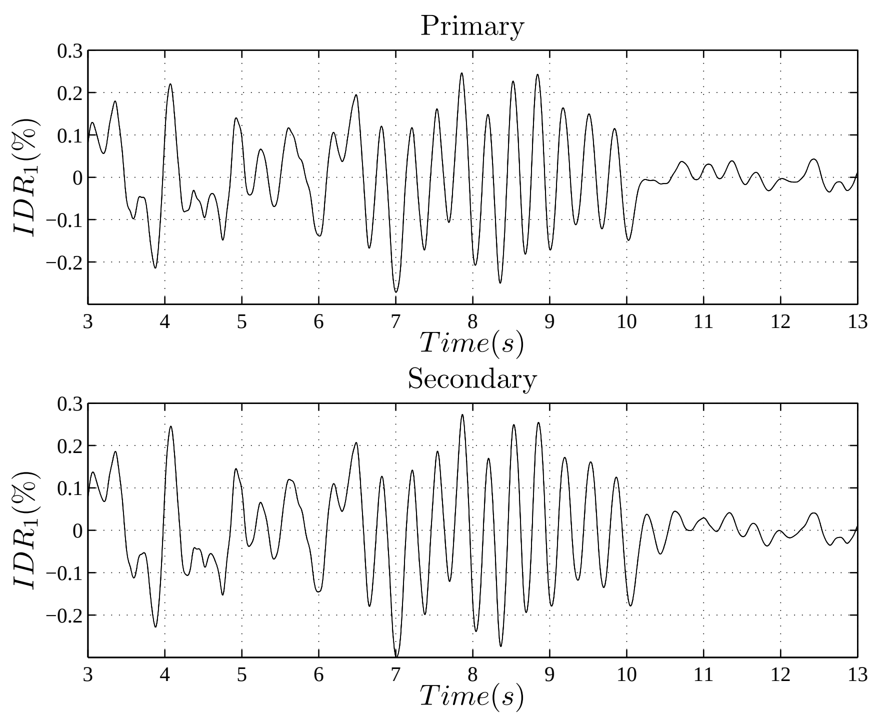

Figure 94: First-story IDR response with sensitivity to soil spring stiffness, Northridge - Sylmar Converter Station motion, founded on dense sand.

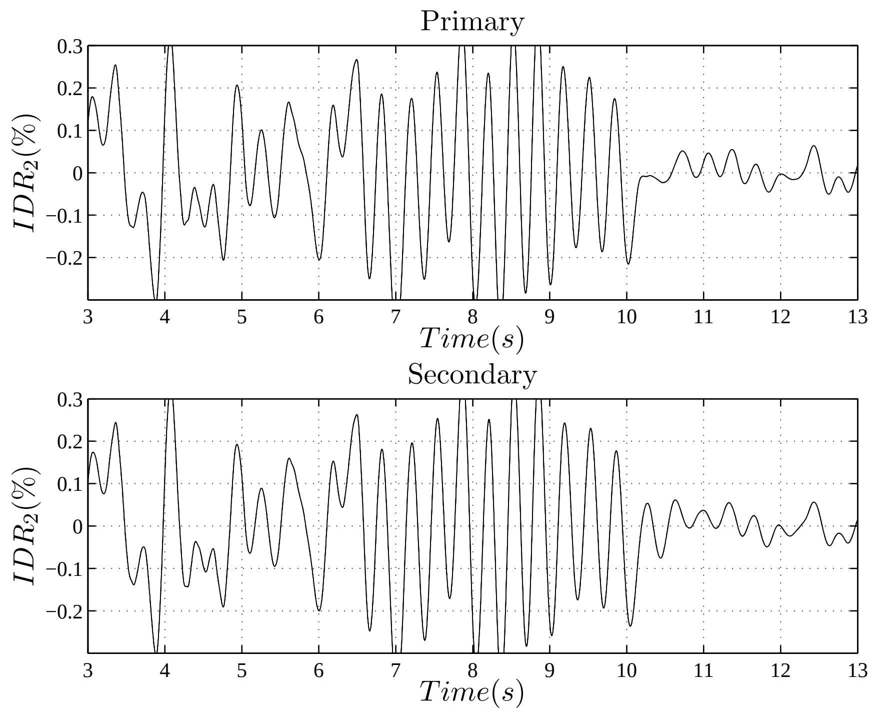

Figure 95: Second-story IDR response with sensitivity to soil spring stiffness, Northridge - Sylmar Converter Station motion, founded on dense sand.

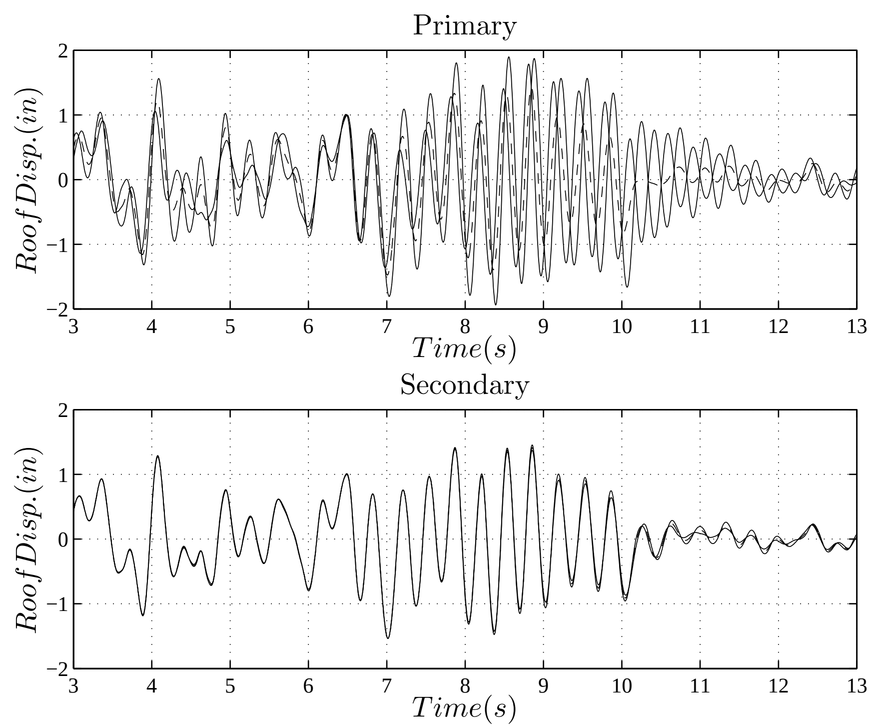

Figure 96: Roof displacement response with sensitivity to floor mass, Northridge - Sylmar Converter Station motion, founded on dense sand.

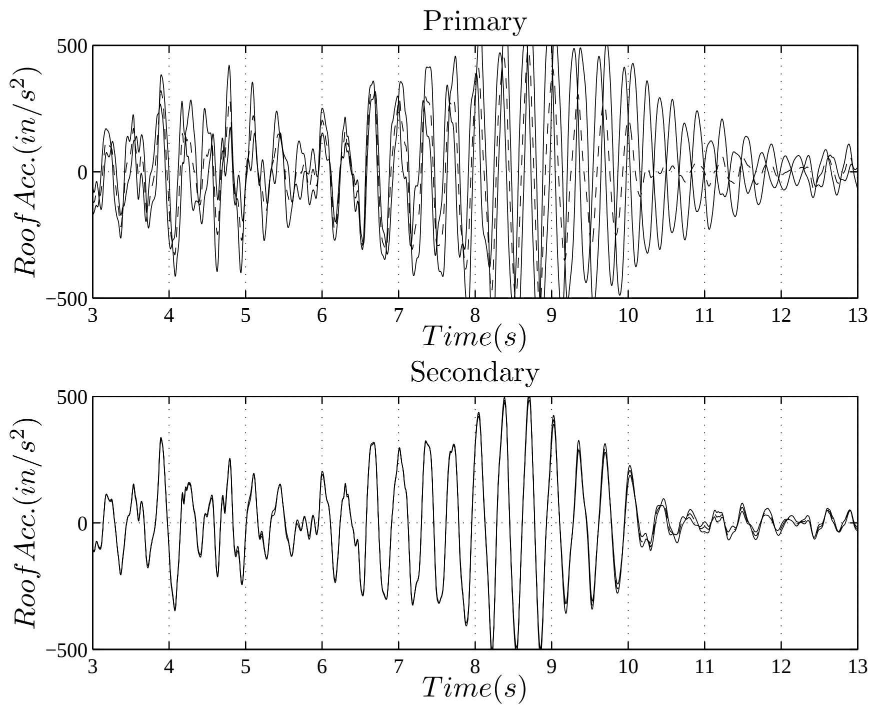

Figure 97: Roof acceleration response with sensitivity to floor mass, Northridge - Sylmar Converter Station motion, founded on dense sand.

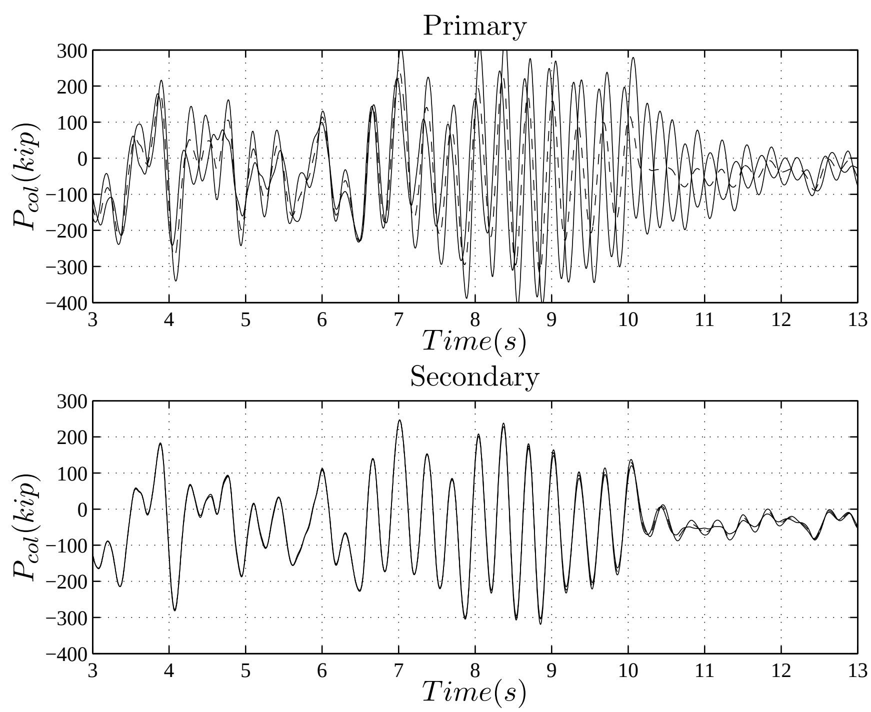

Figure 98: Column Force response with sensitivity to floor mass, Northridge - Sylmar Converter Station motion, founded on dense sand.

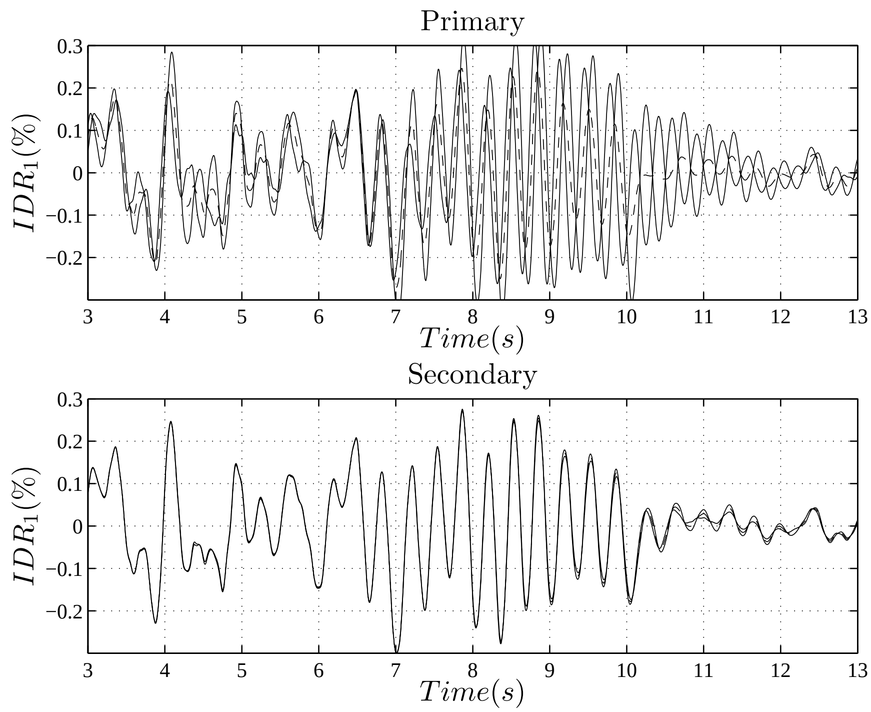

Figure 99: First-story IDR response with sensitivity to floor mass, Northridge - Sylmar Converter Station motion, founded on dense sand.

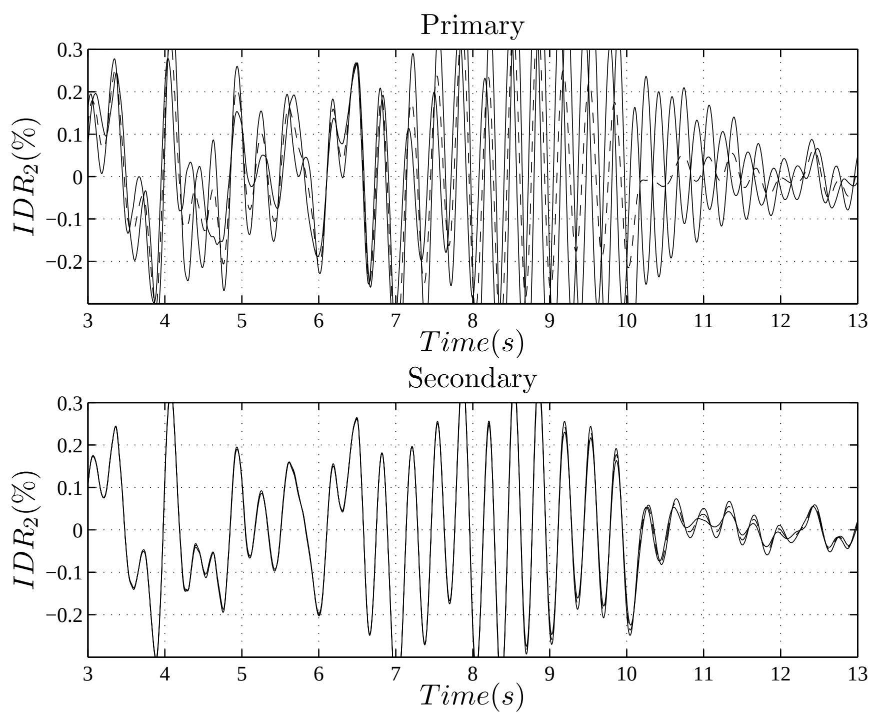

Figure 100: Second-story IDR response with sensitivity to floor mass, Northridge - Sylmar Converter Station motion, founded on dense sand.

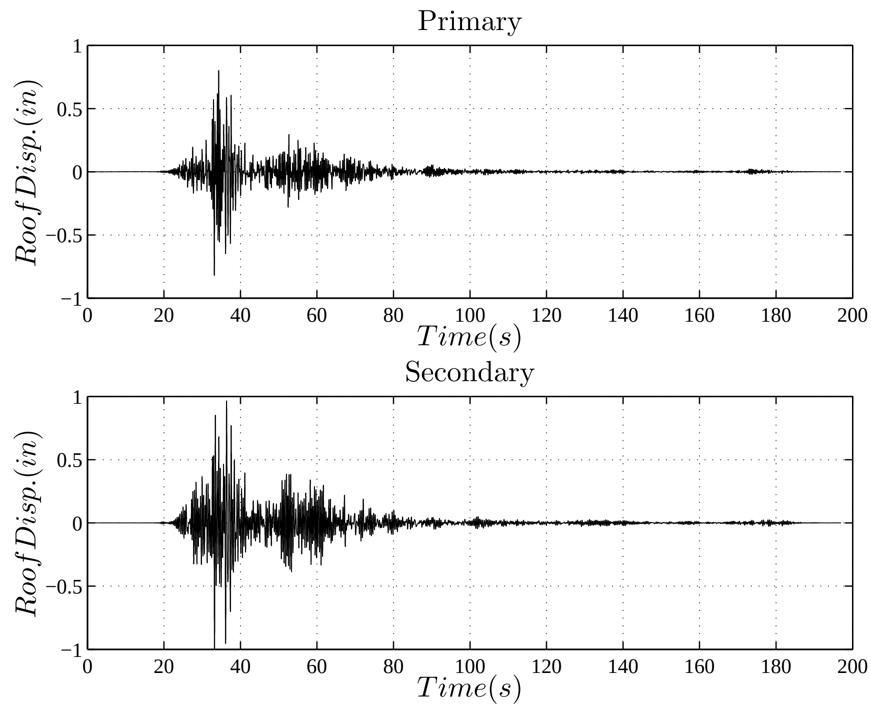

Figure 101: Mean roof displacement response, Chi Chi CHY034 motion, founded on soft clay.

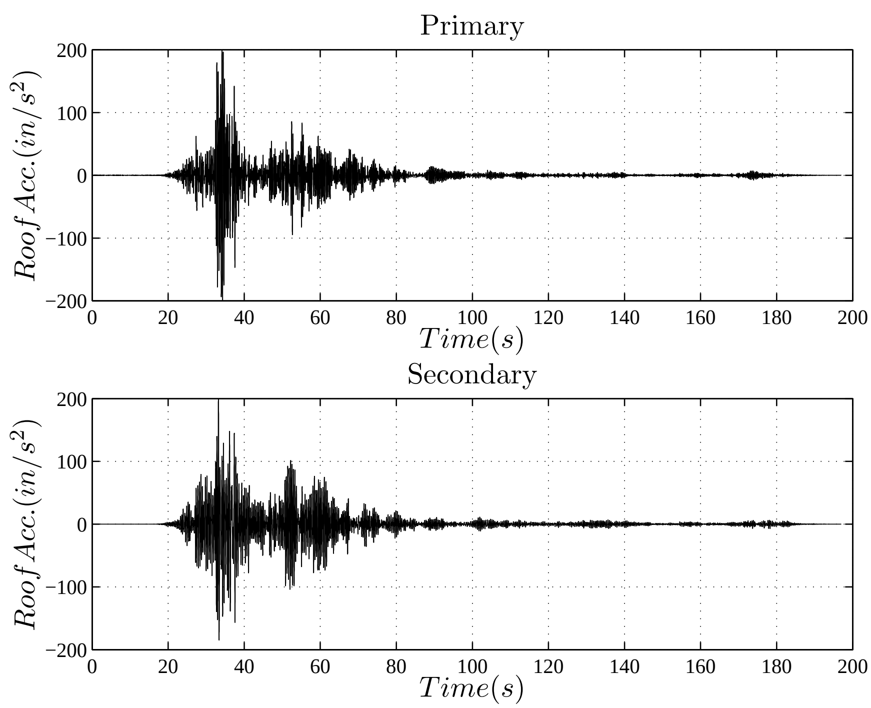

Figure 102: Mean roof acceleration response, Chi Chi CHY034 motion, founded on soft clay.

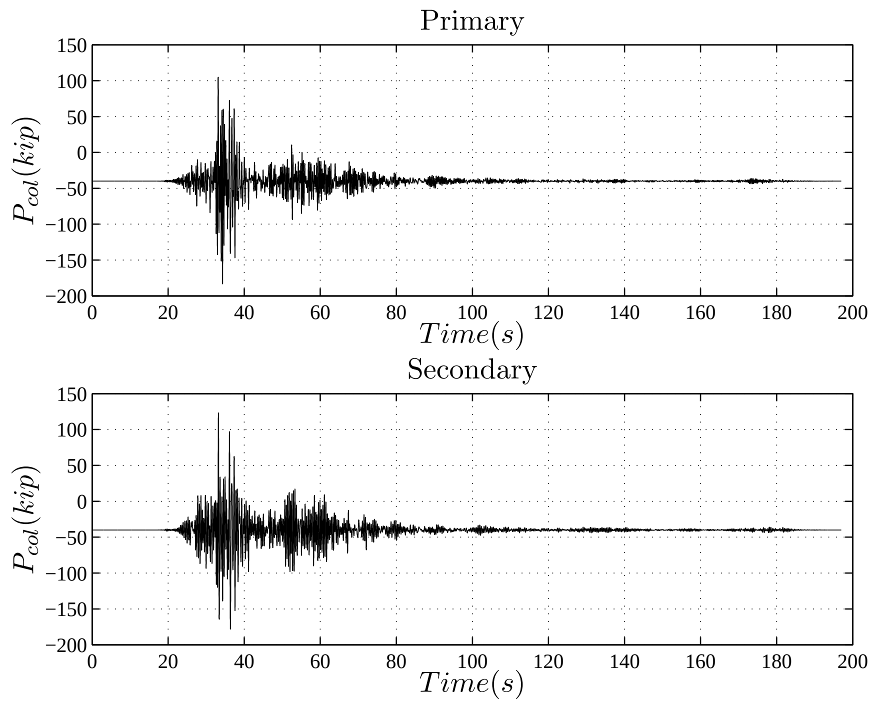

Figure 103: Mean column response, Chi Chi CHY034 motion, founded on soft clay.

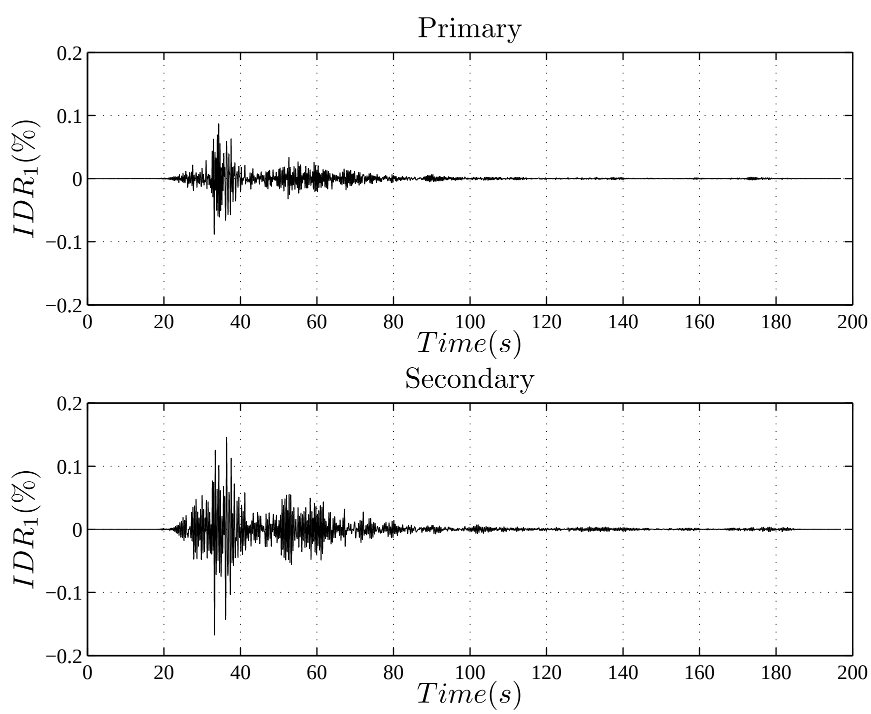

Figure 104: Mean first-story IDR response, Chi Chi CHY034 motion, founded on soft clay.

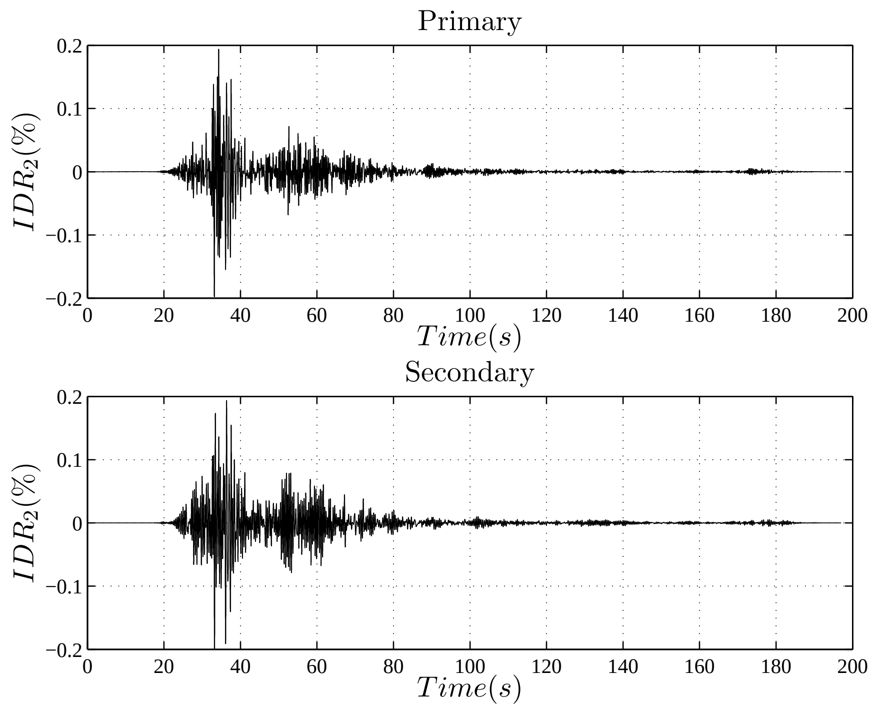

Figure 105: Mean roof displacement response, Chi Chi CHY034 motion, founded on soft clay.

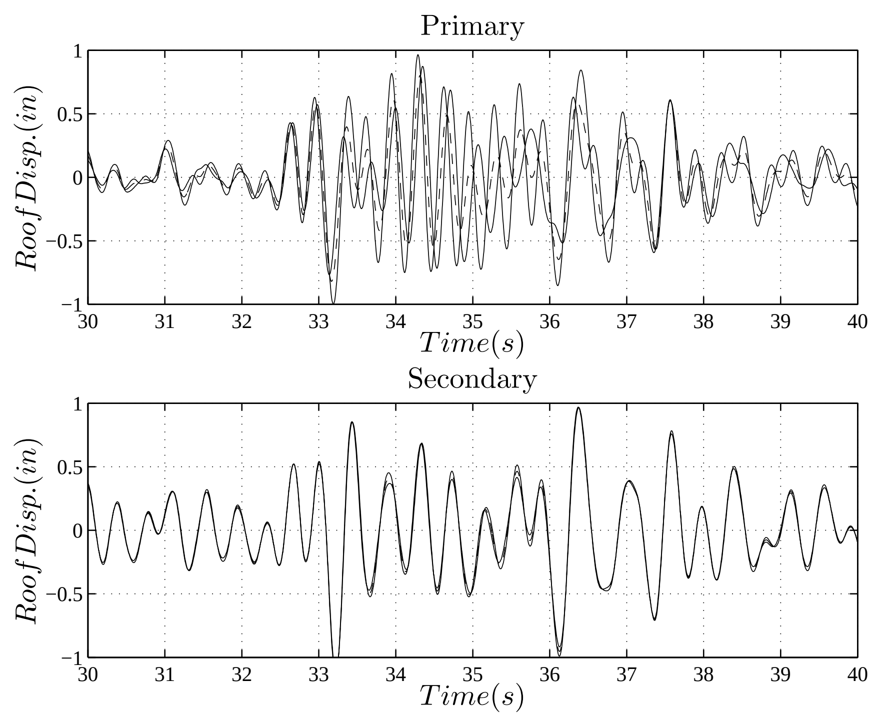

Figure 106: Roof displacement response with sensitivity to building stiffness, Chi Chi CHY034 motion, founded on soft clay.

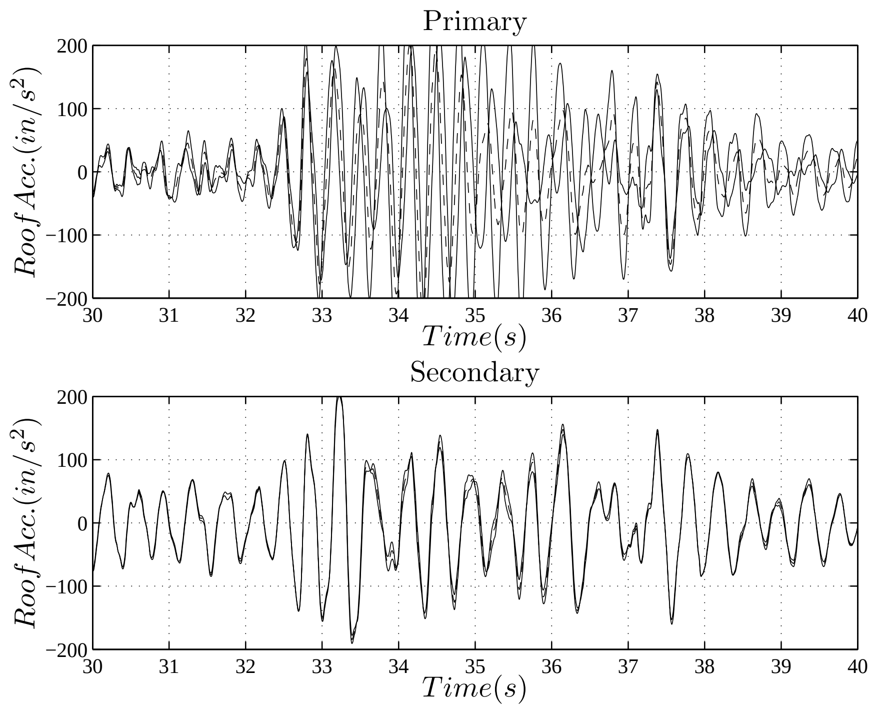

Figure 107: Roof acceleration response with sensitivity to building stiffness, Chi Chi CHY034 motion, founded on soft clay.

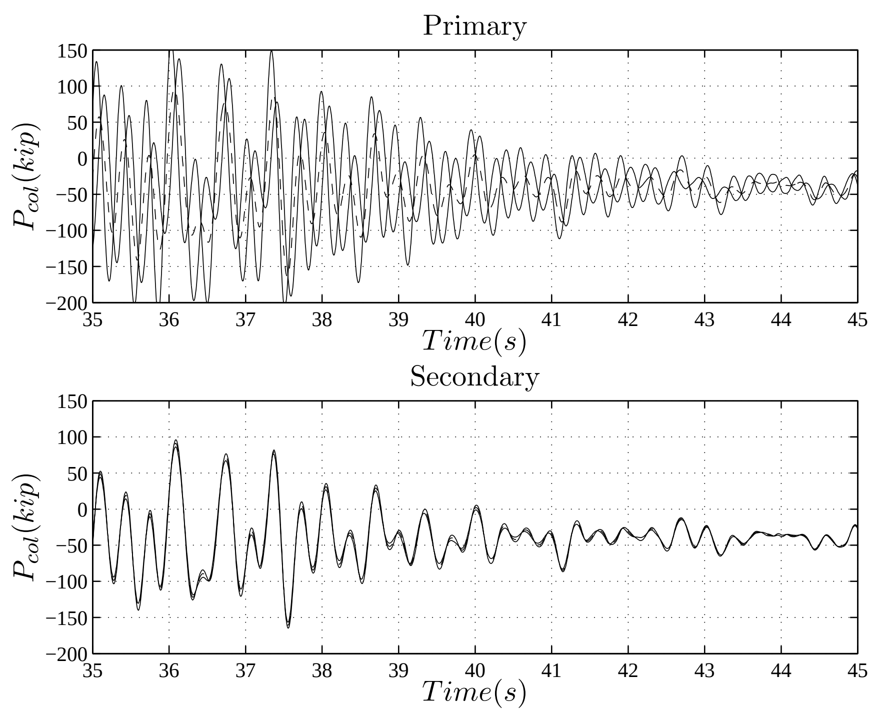

Figure 108: Column force response with sensitivity to building stiffness, Chi Chi CHY034 motion, founded on soft clay.

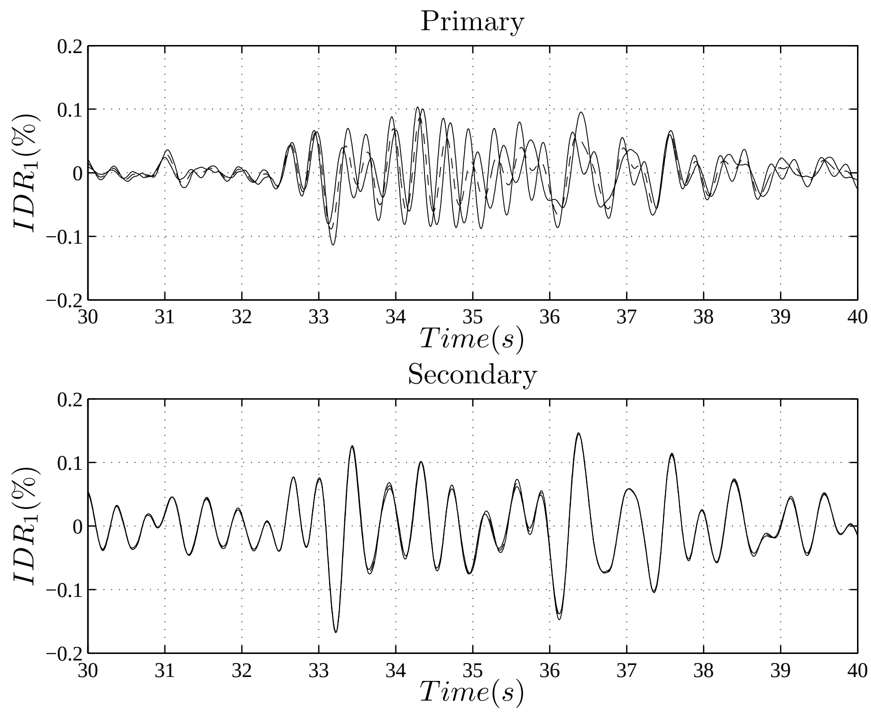

Figure 109: First-story IDR response with sensitivity to building stiffness, Chi Chi CHY034 motion, founded on soft clay.

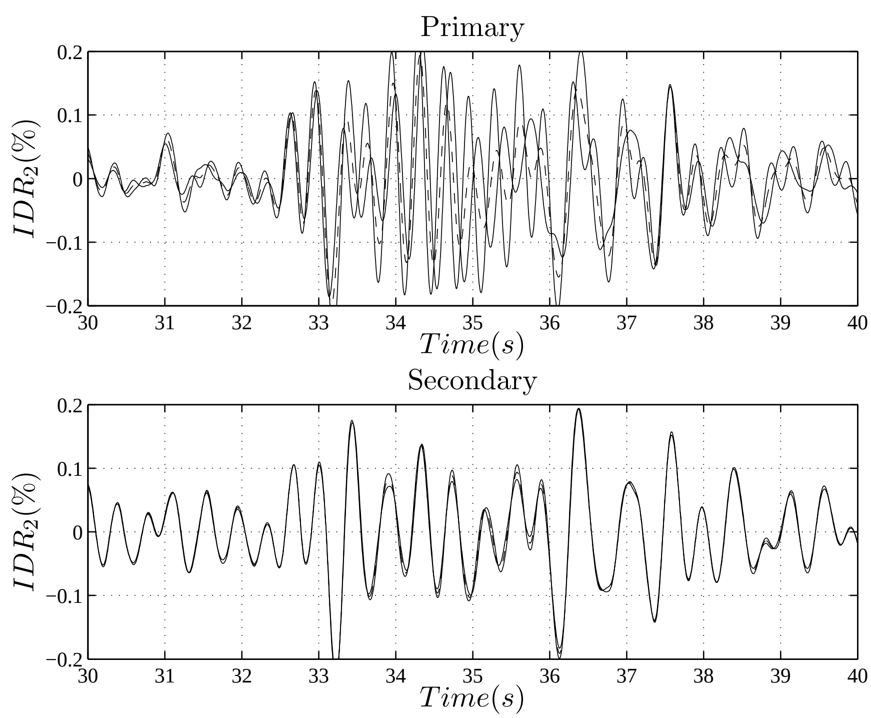

Figure 110: Second-story IDR response with sensitivity to building stiffness, Chi Chi CHY034 motion, founded on soft clay.

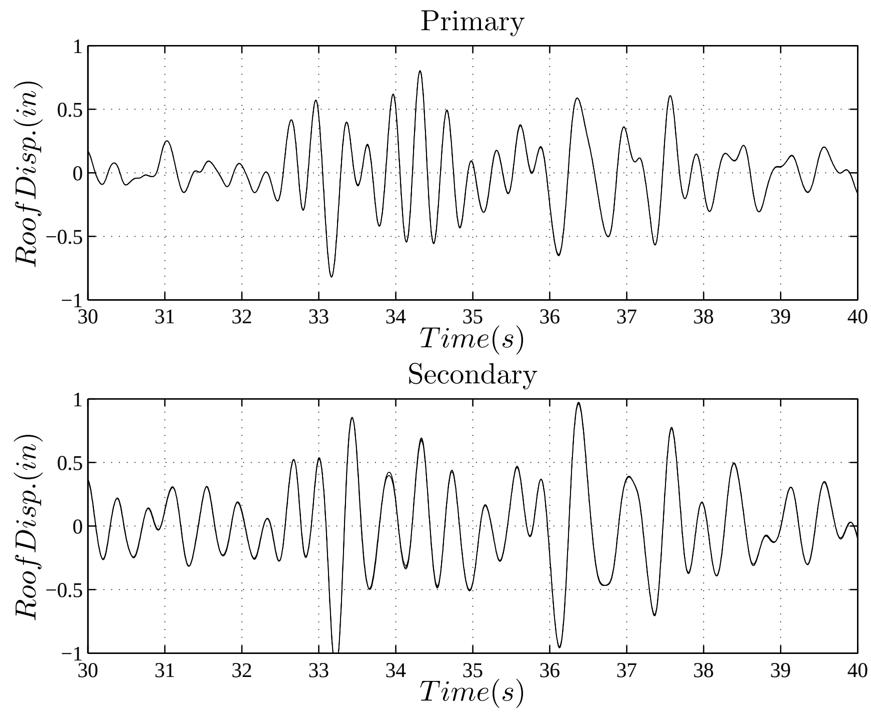

Figure 111: Roof displacement response with sensitivity to soil spring stiffness, Chi Chi CHY034 motion, founded on soft clay.

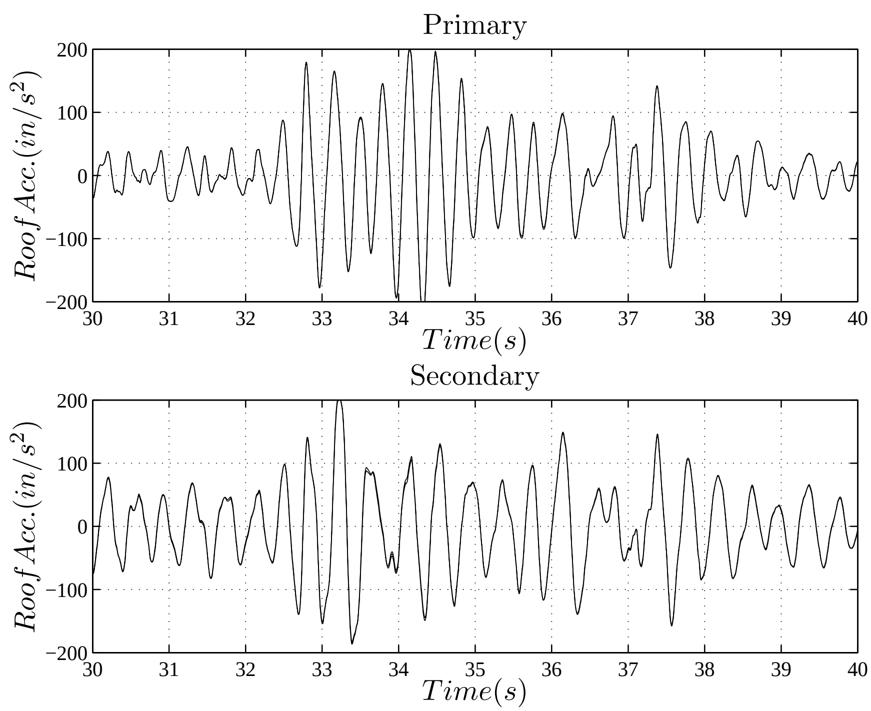

Figure 112: Roof acceleration response with sensitivity to soil spring stiffness, Chi Chi CHY034 motion, founded on soft clay.

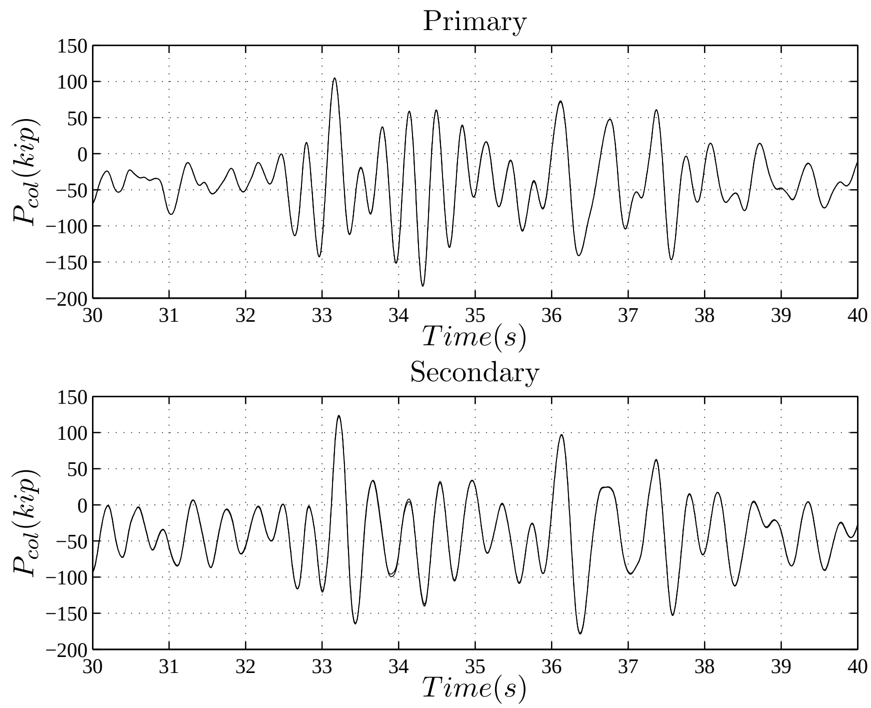

Figure 113: Column force response with sensitivity to soil spring stiffness, Chi Chi CHY034 motion, founded on soft clay.

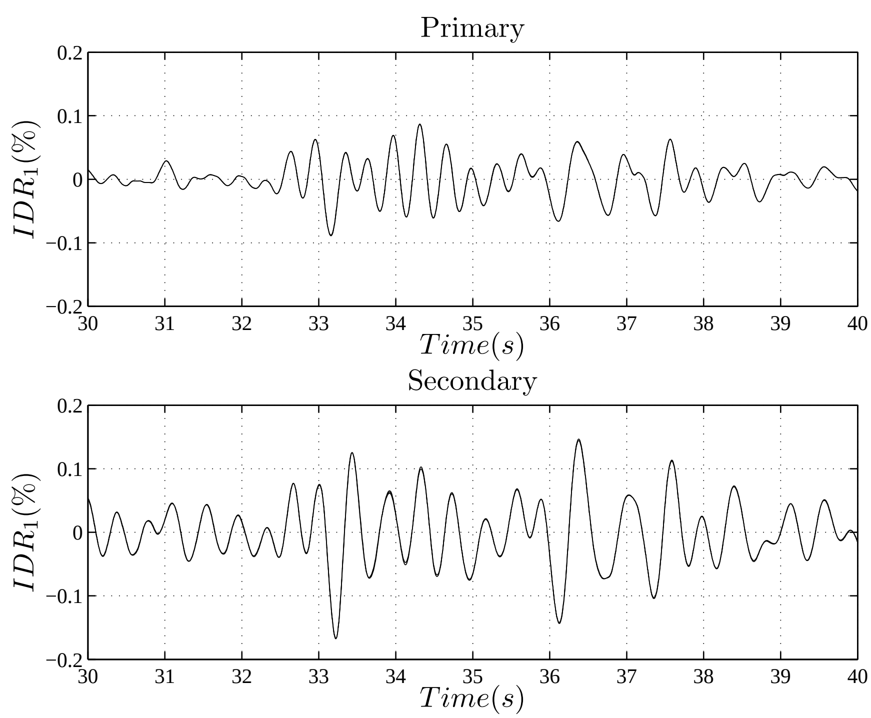

Figure 114: First-story IDR response with sensitivity to soil spring stiffness, Chi Chi CHY034 motion, founded on soft clay.

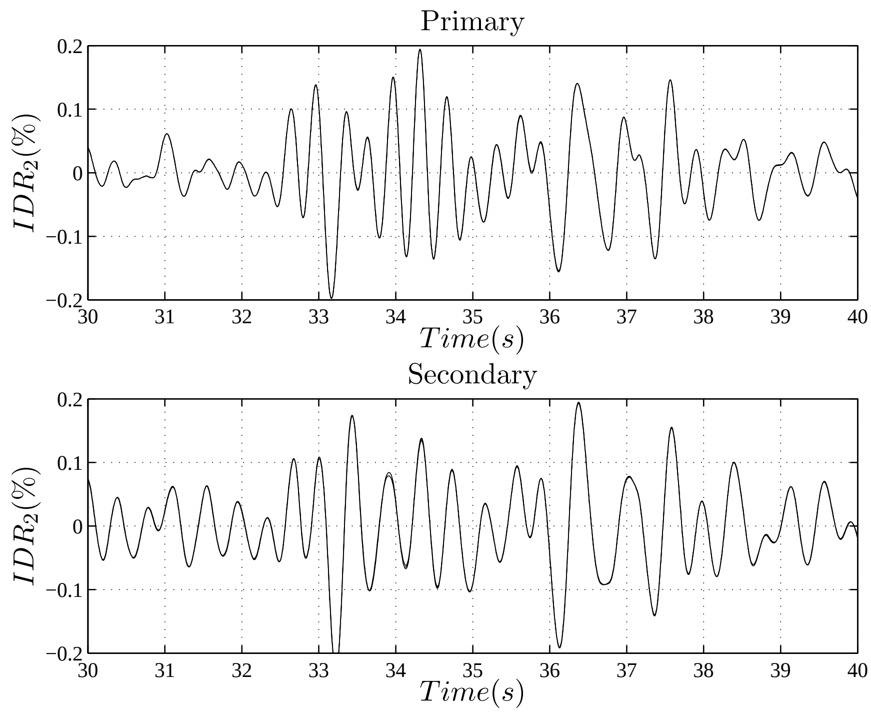

Figure 115: Second-story IDR response with sensitivity to soil spring stiffness, Chi Chi CHY034 motion, founded on soft clay.

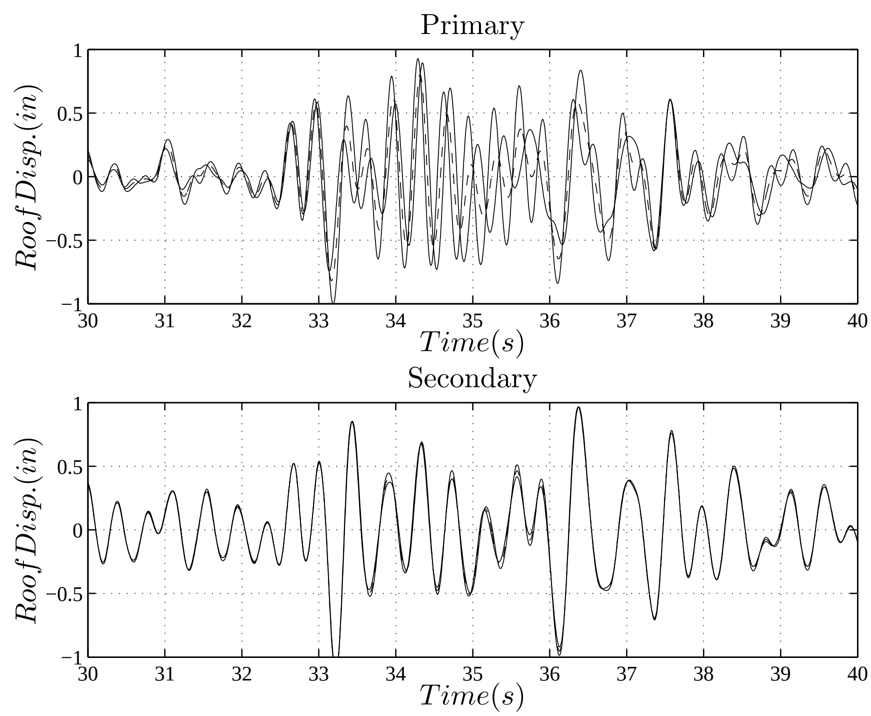

Figure 116: Roof displacement response with sensitivity to floor mass, Chi Chi CHY034 motion, founded on soft clay.

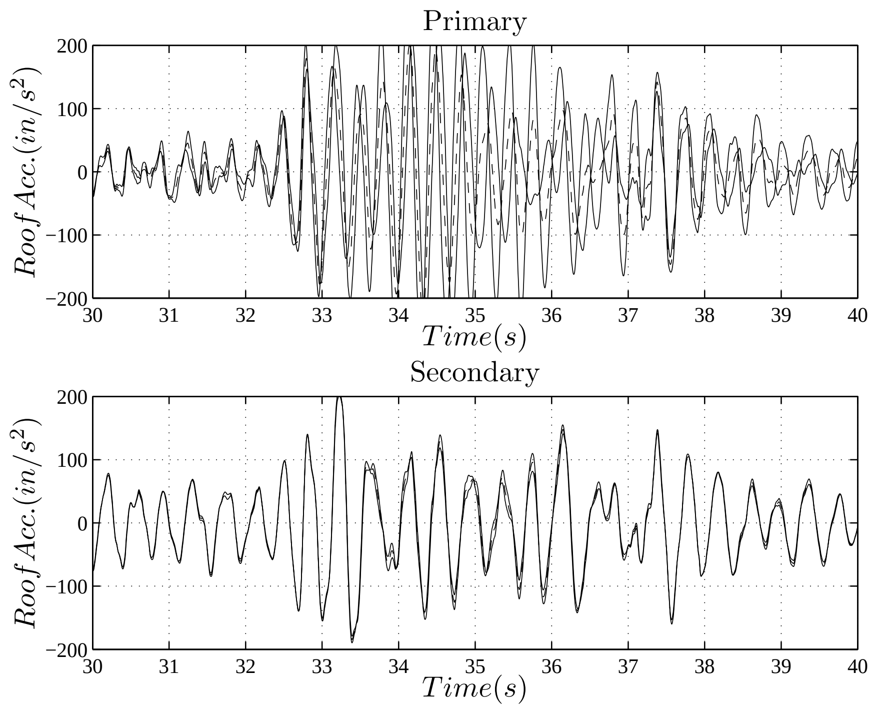

Figure 117: Roof acceleration response with sensitivity to floor mass, Chi Chi CHY034 motion, founded on soft clay.

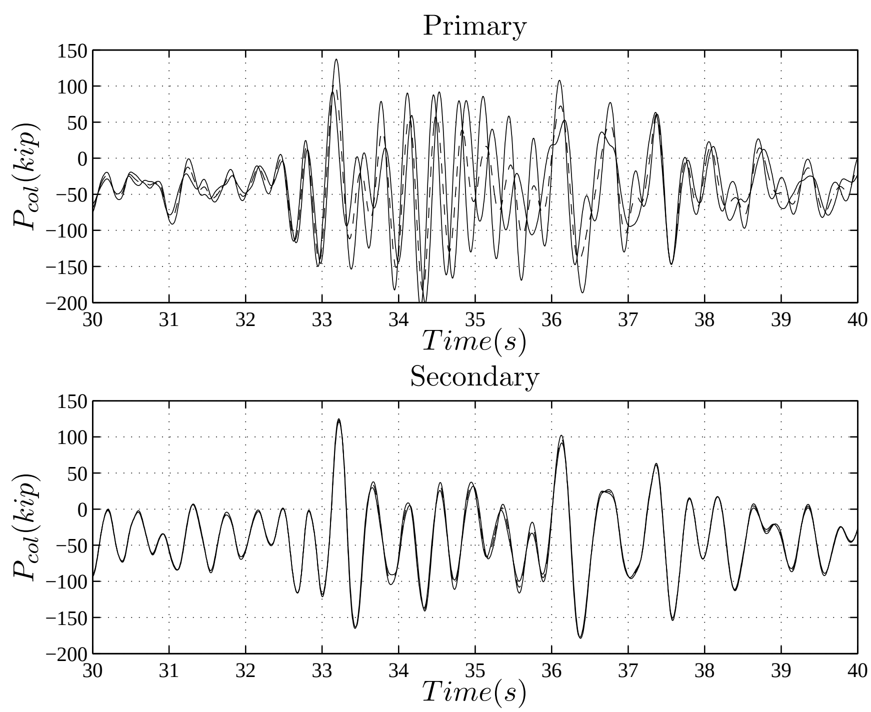

Figure 118: Column Force response with sensitivity to floor mass, Chi Chi CHY034 motion, founded on soft clay.

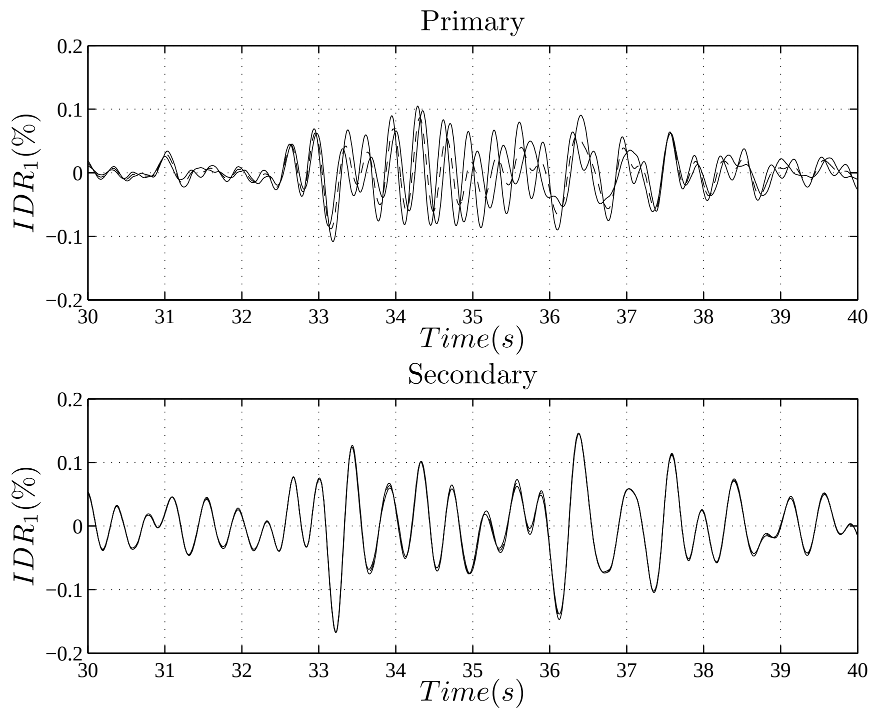

Figure 119: First-story IDR response with sensitivity to floor mass, Chi Chi CHY034 motion, founded on soft clay.

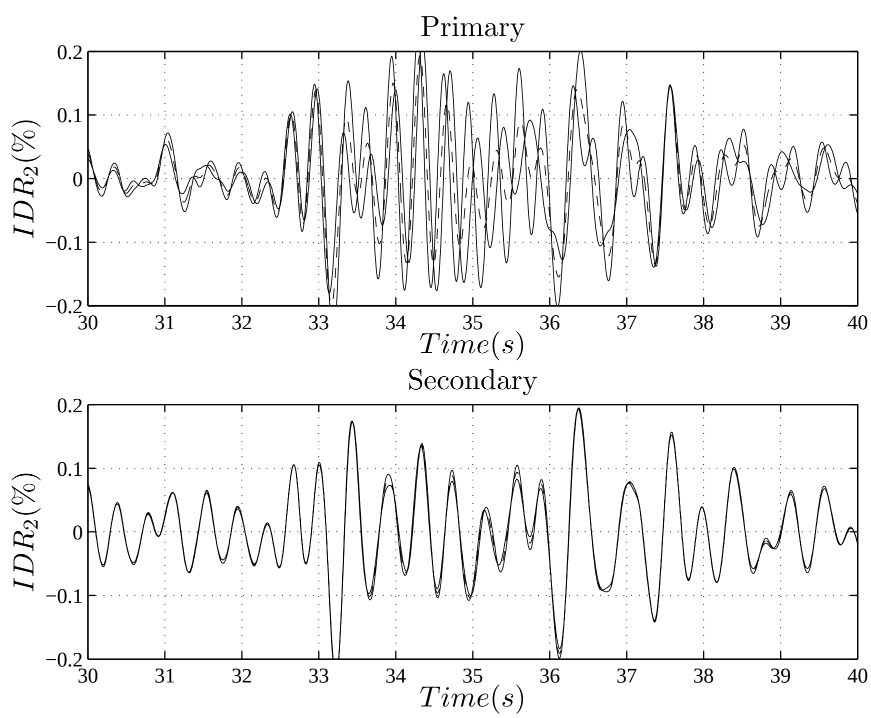

Figure 120: Second-story IDR response with sensitivity to floor mass, Chi Chi CHY034 motion, founded on soft clay.

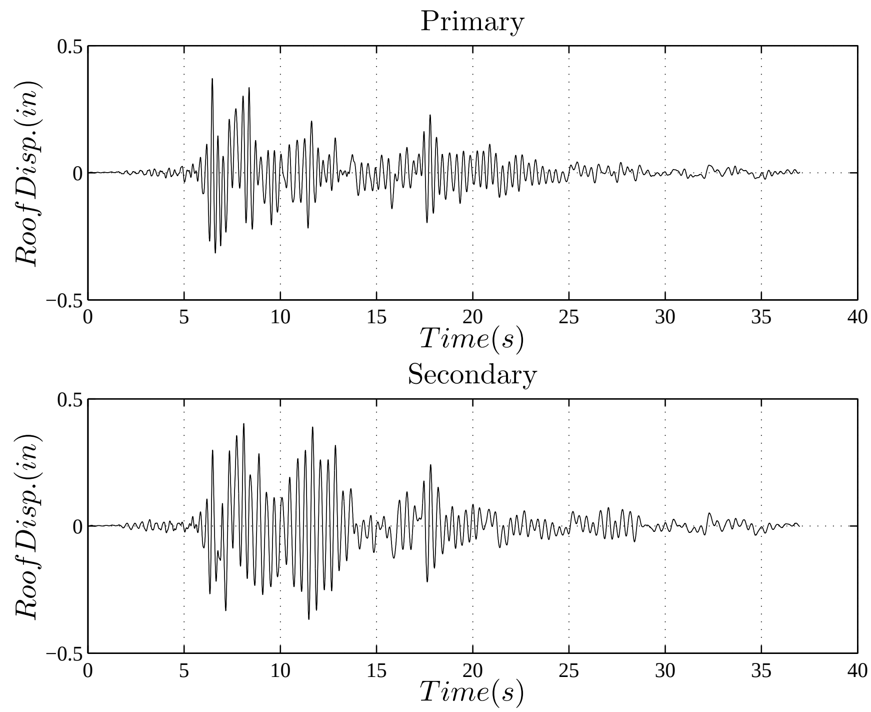

Figure 121: Mean roof displacement response, 1979 Imperial Valley - Brawley Airport motion, founded on soft clay.

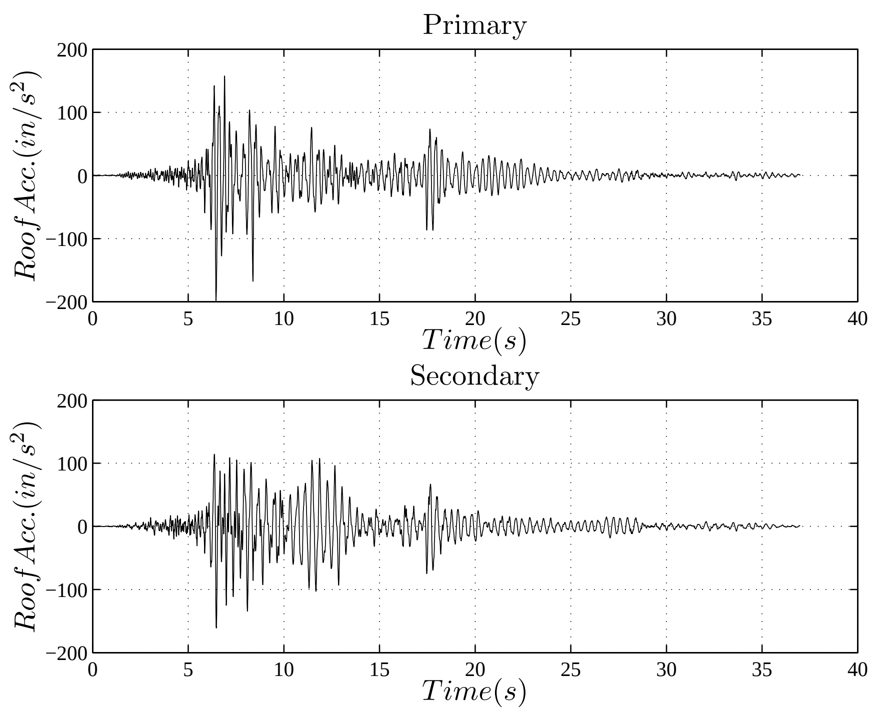

Figure 122: Mean roof acceleration response, 1979 Imperial Valley - Brawley Airport motion, founded on soft clay.

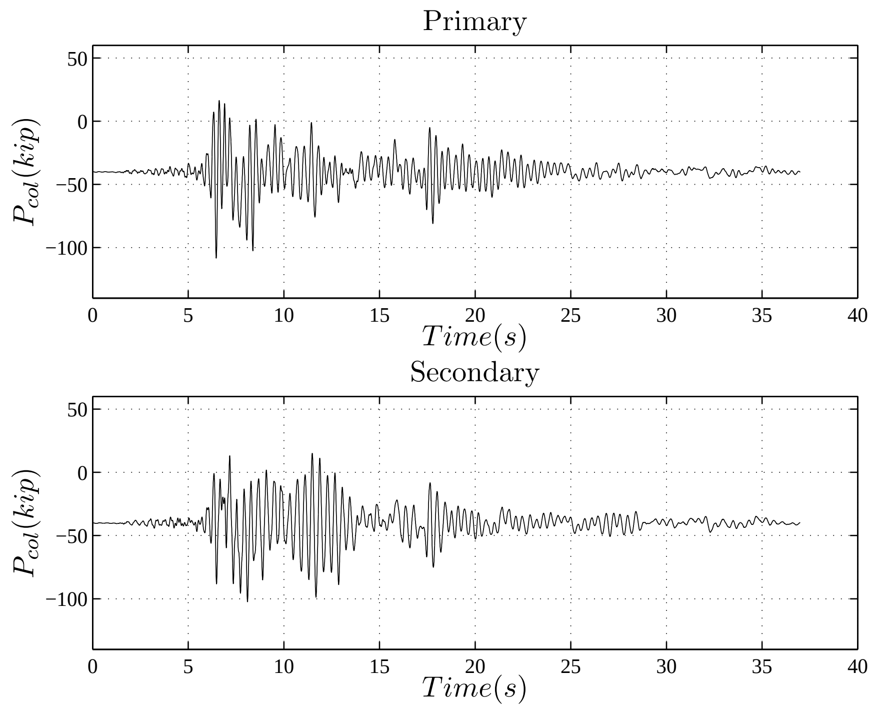

Figure 123: Mean column response, 1979 Imperial Valley - Brawley Airport motion, founded on soft clay.

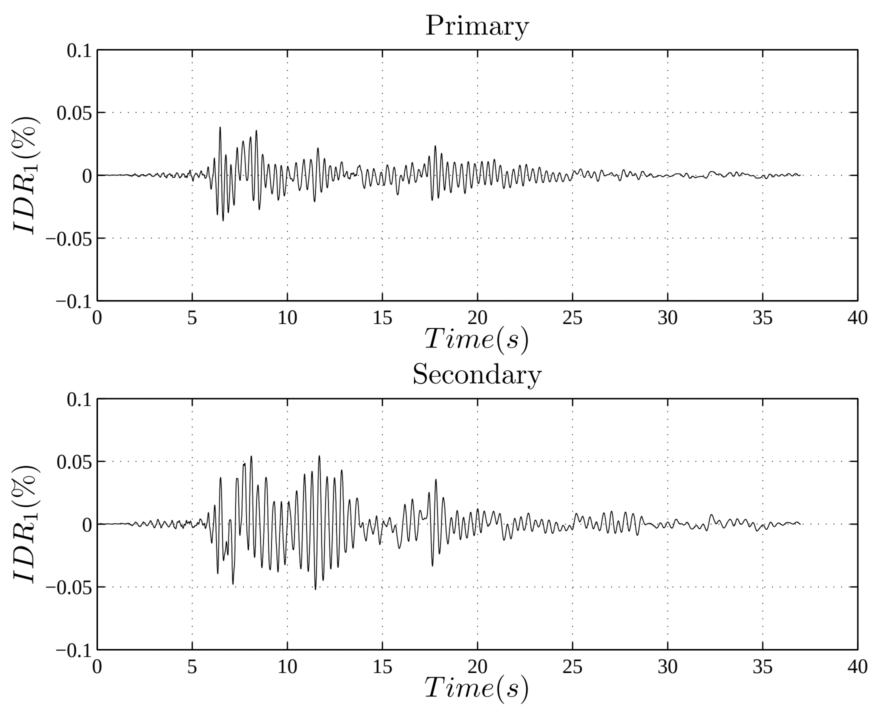

Figure 124: Mean first-story IDR response, 1979 Imperial Valley - Brawley Airport motion, founded on soft clay.

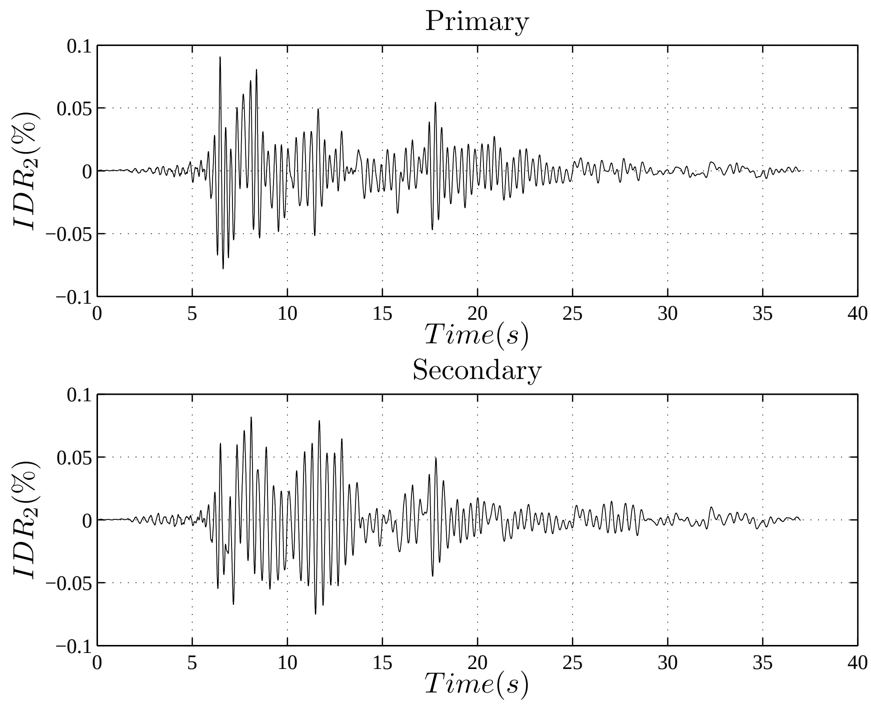

Figure 125: Mean roof displacement response, 1979 Imperial Valley - Brawley Airport motion, founded on soft clay.

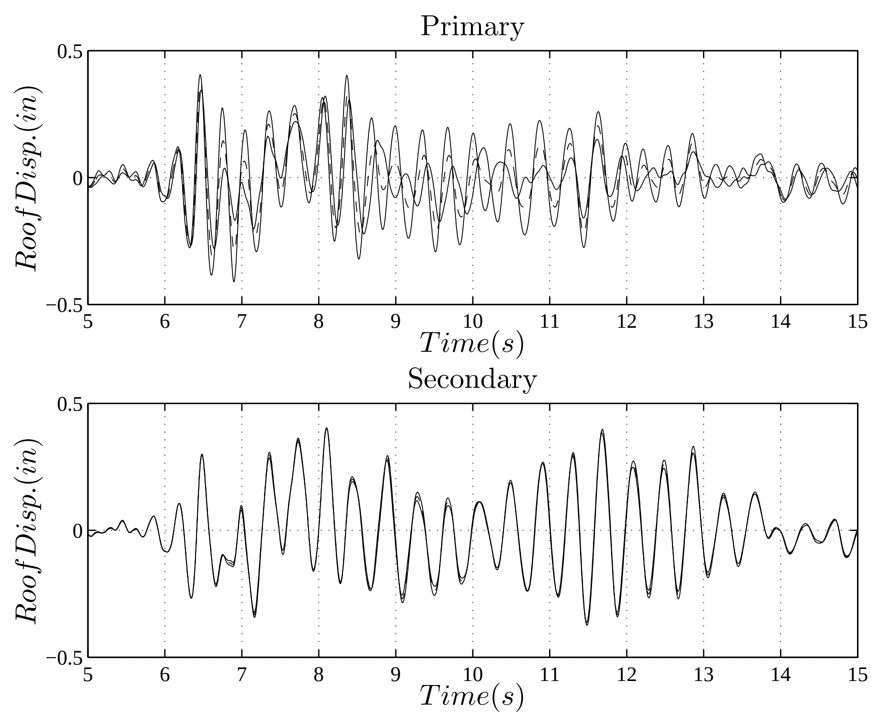

Figure 126: Roof displacement response with sensitivity to building stiffness, 1979 Imperial Valley - Brawley Airport motion, founded on soft clay.

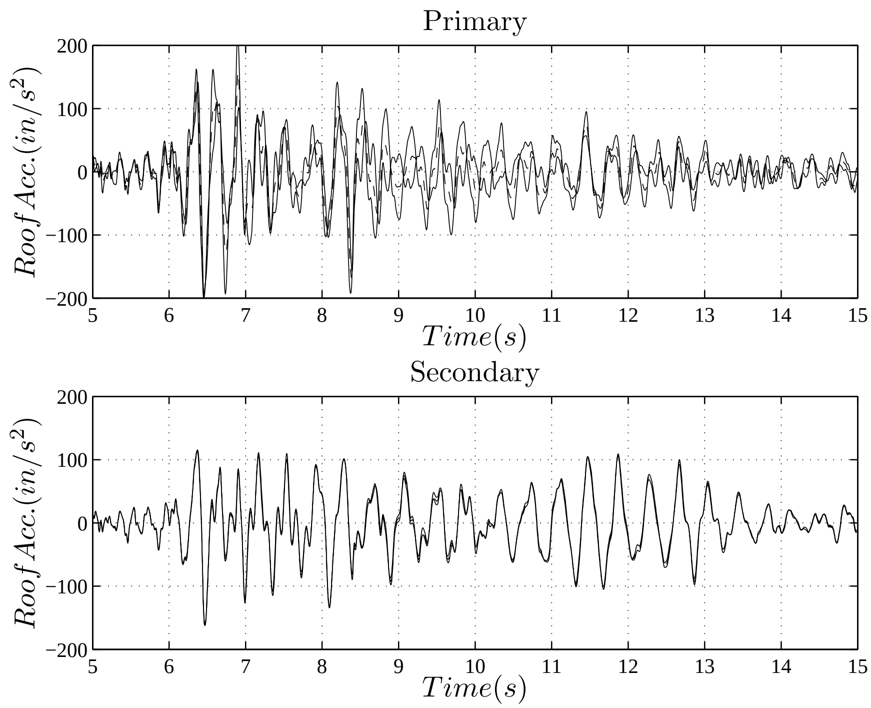

Figure 127: Roof acceleration response with sensitivity to building stiffness, 1979 Imperial Valley - Brawley Airport motion, founded on soft clay.

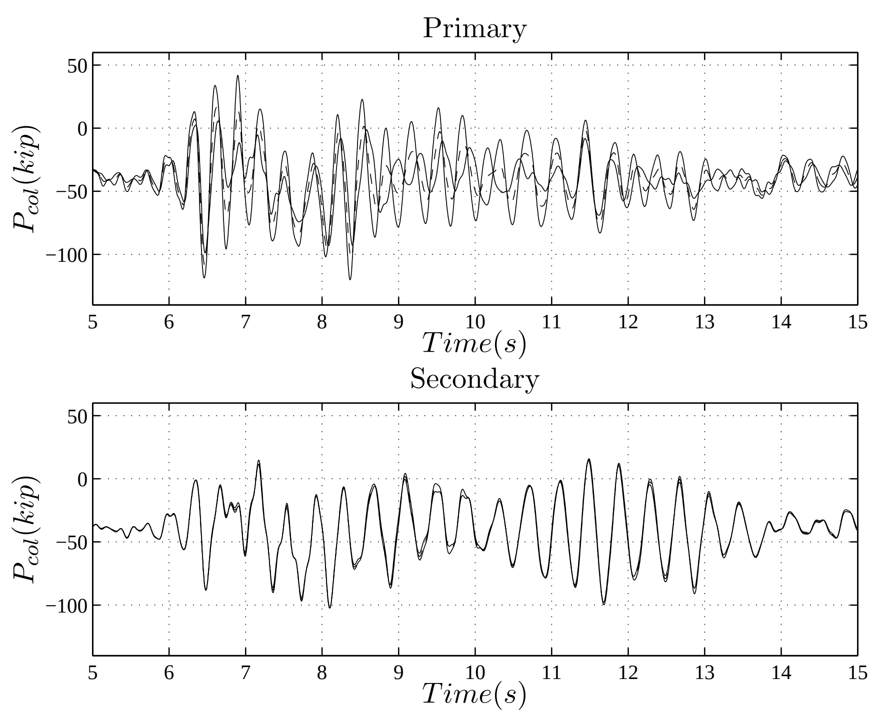

Figure 128: Column force response with sensitivity to building stiffness, 1979 Imperial Valley - Brawley Airport motion, founded on soft clay.

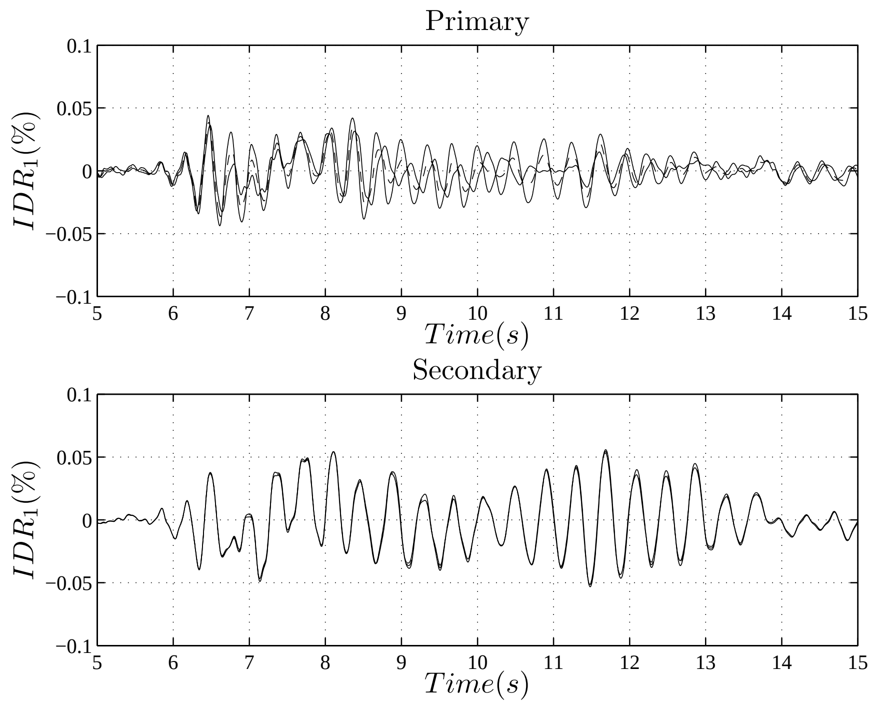

Figure 129: First-story IDR response with sensitivity to building stiffness,1979 Imperial Valley - Brawley Airport motion, founded on soft clay.

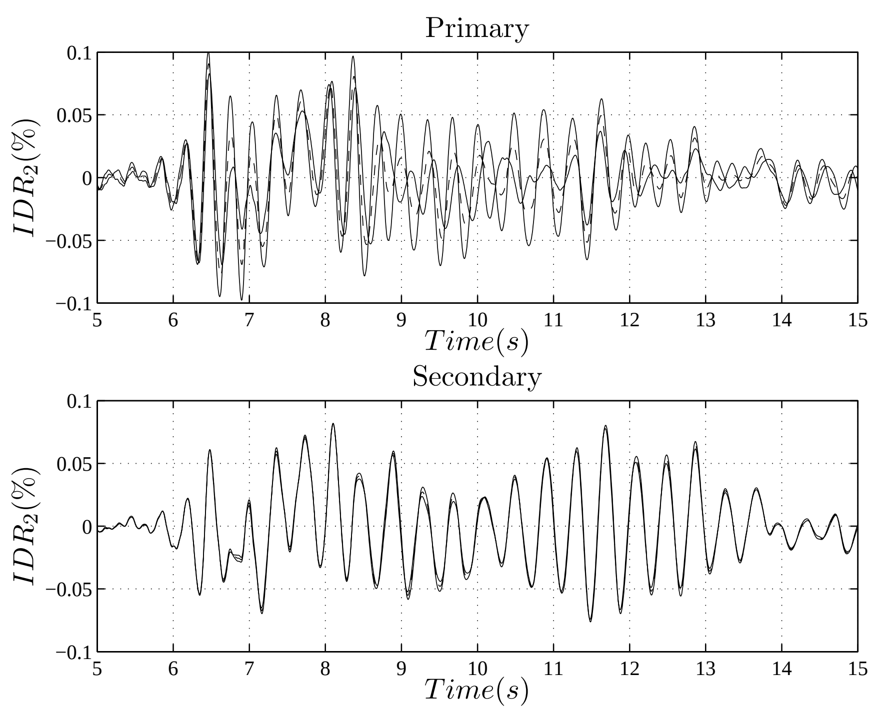

Figure 130: Second-story IDR response with sensitivity to building stiffness, 1979 Imperial Valley - Brawley Airport motion, founded on soft clay.

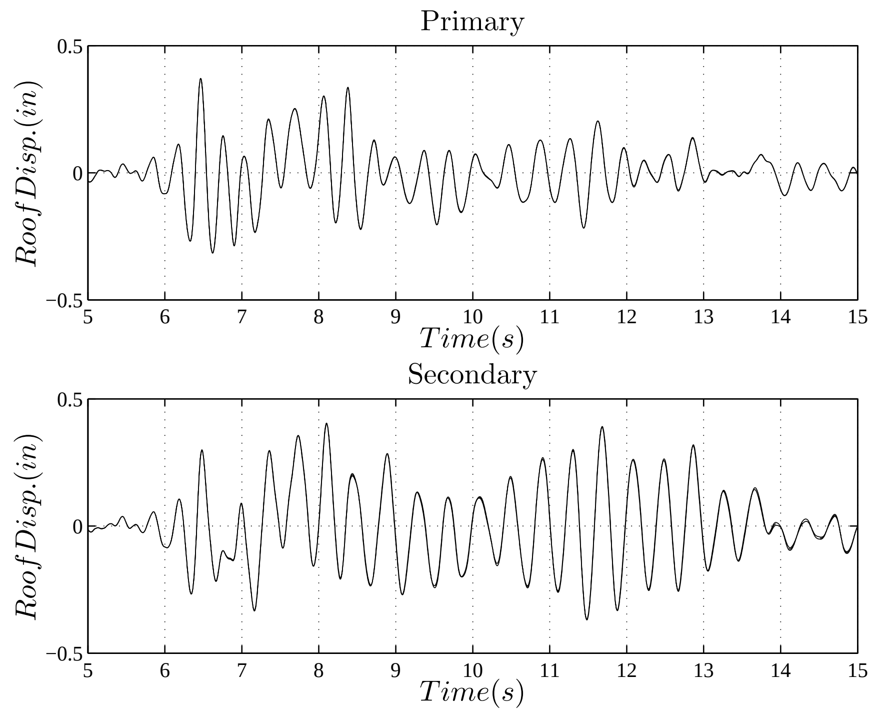

Figure 131: Roof displacement response with sensitivity to soil spring stiffness, 1979 Imperial Valley - Brawley Airport motion, founded on soft clay.

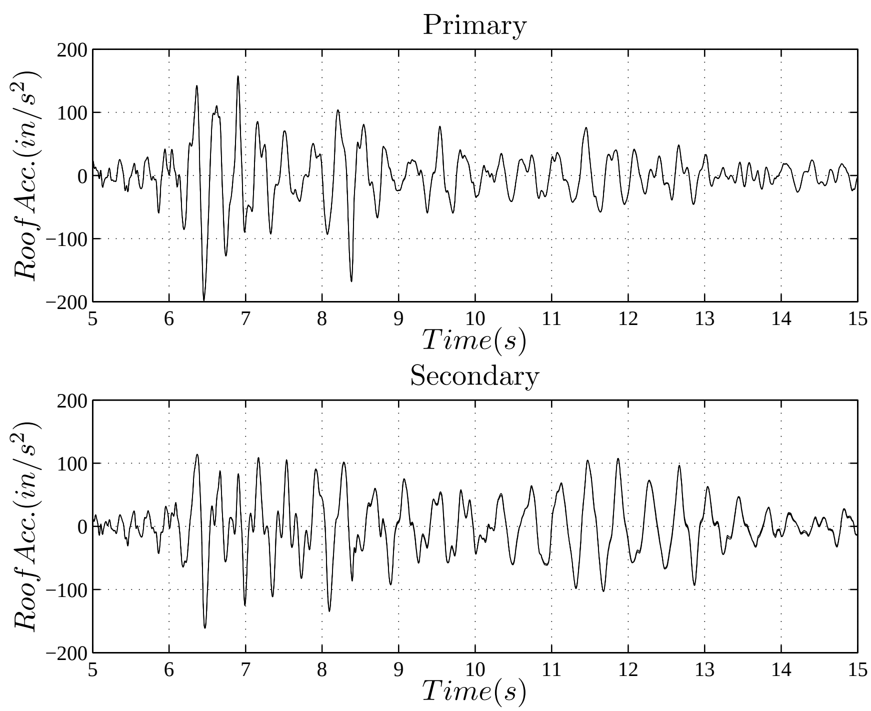

Figure 132: Roof acceleration response with sensitivity to soil spring stiffness, 1979 Imperial Valley - Brawley Airport motion, founded on soft clay.

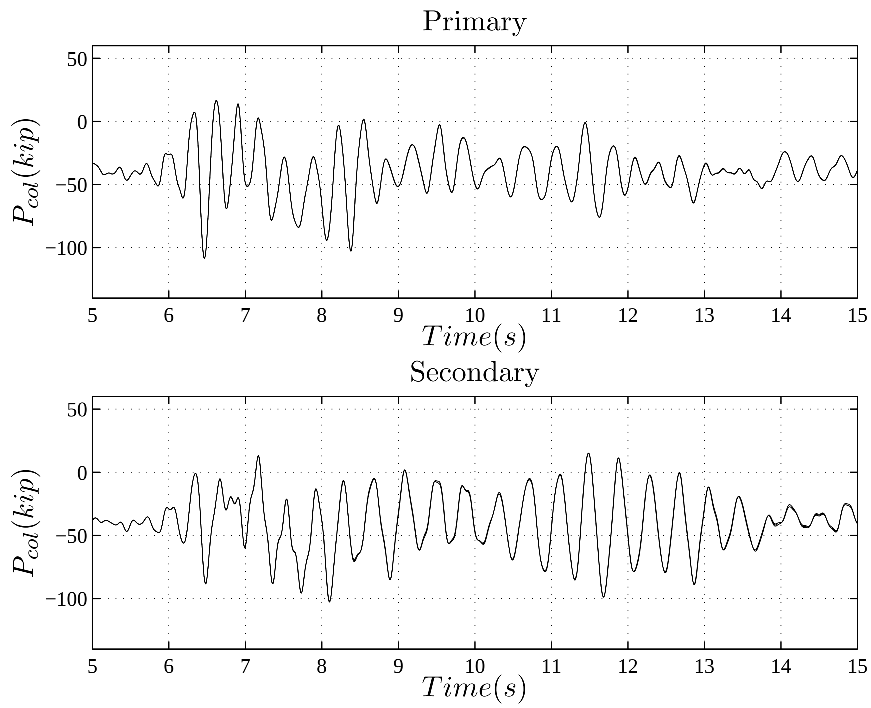

Figure 133: Column force response with sensitivity to soil spring stiffness, 1979 Imperial Valley - Brawley Airport motion, founded on soft clay.

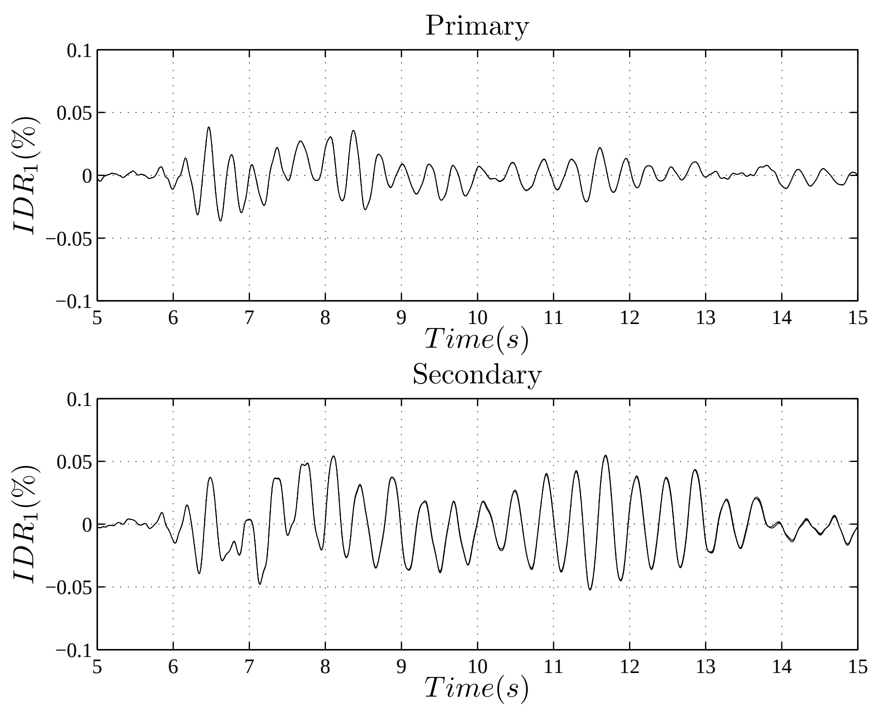

Figure 134: First-story IDR response with sensitivity to soil spring stiffness, 1979 Imperial Valley - Brawley Airport motion, founded on soft clay.

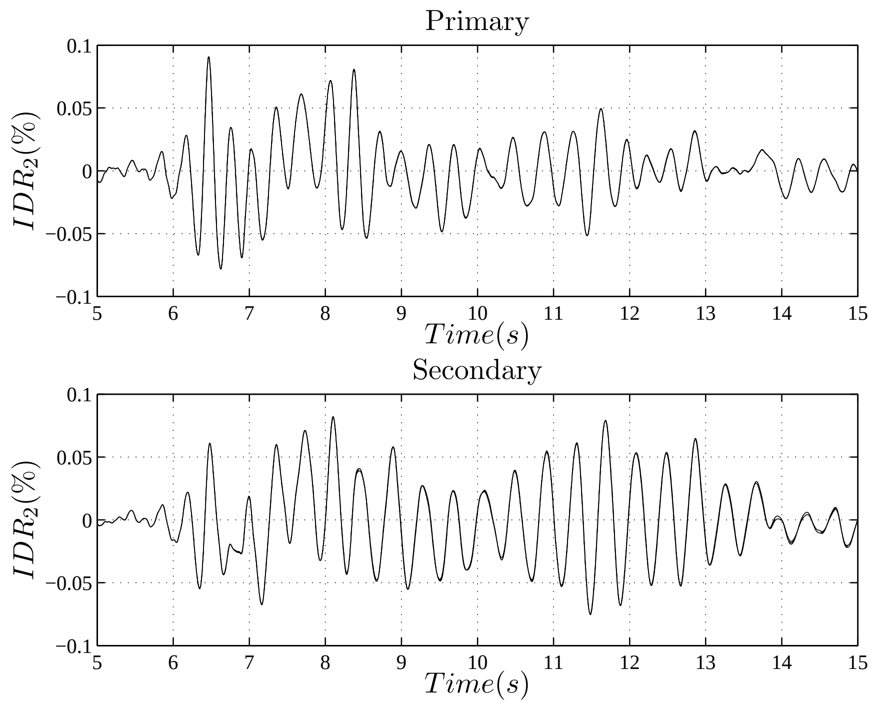

Figure 135: Second-story IDR response with sensitivity to soil spring stiffness, 1979 Imperial Valley - Brawley Airport motion, founded on soft clay.

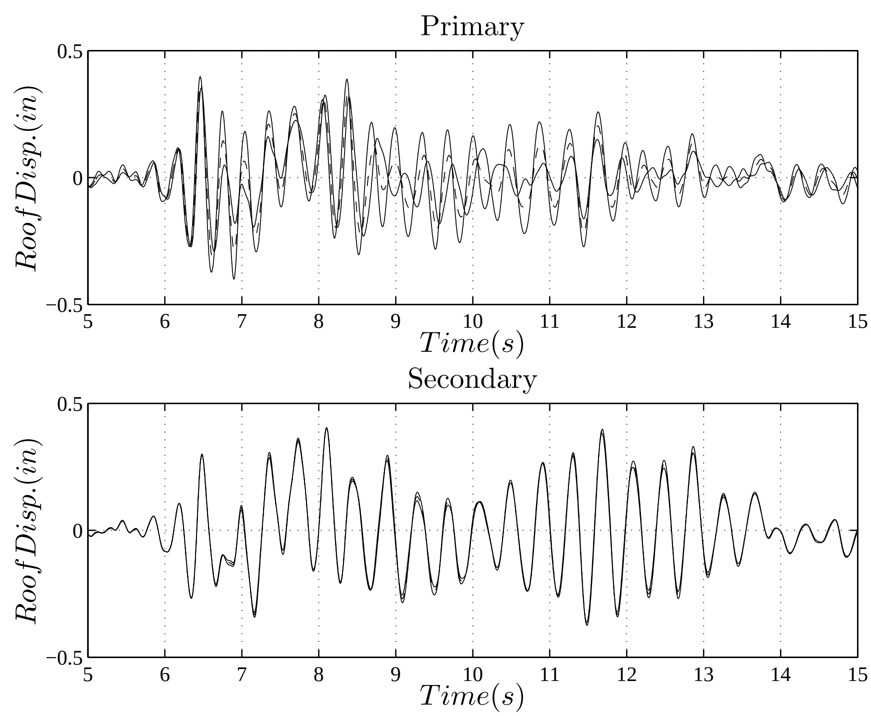

Figure 136: Roof displacement response with sensitivity to floor mass, 1979 Imperial Valley - Brawley Airport motion, founded on soft clay.

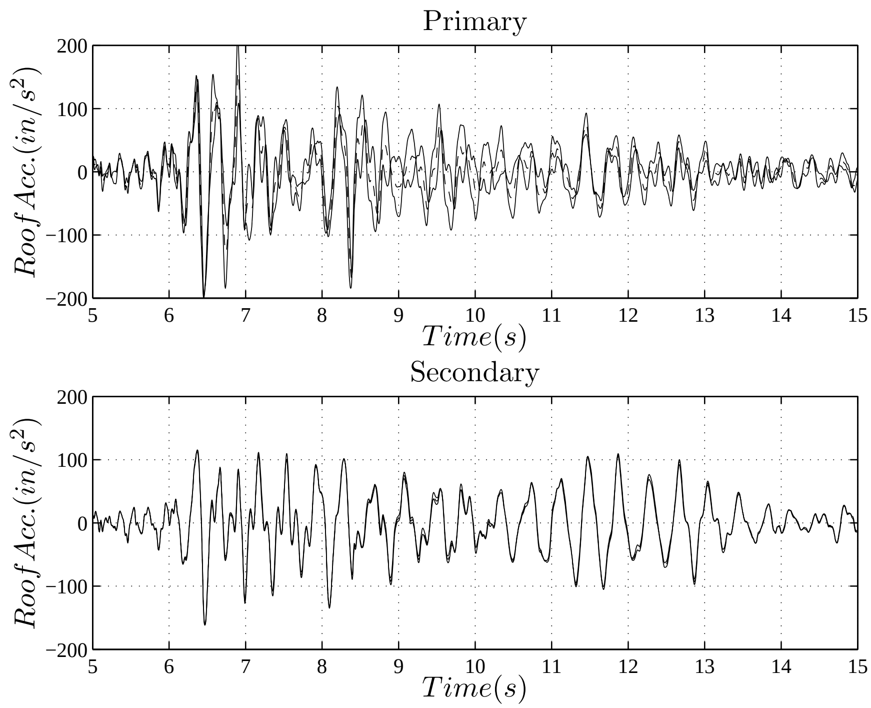

Figure 137: Roof acceleration response with sensitivity to floor mass, 1979 Imperial Valley - Brawley Airport motion, founded on soft clay.

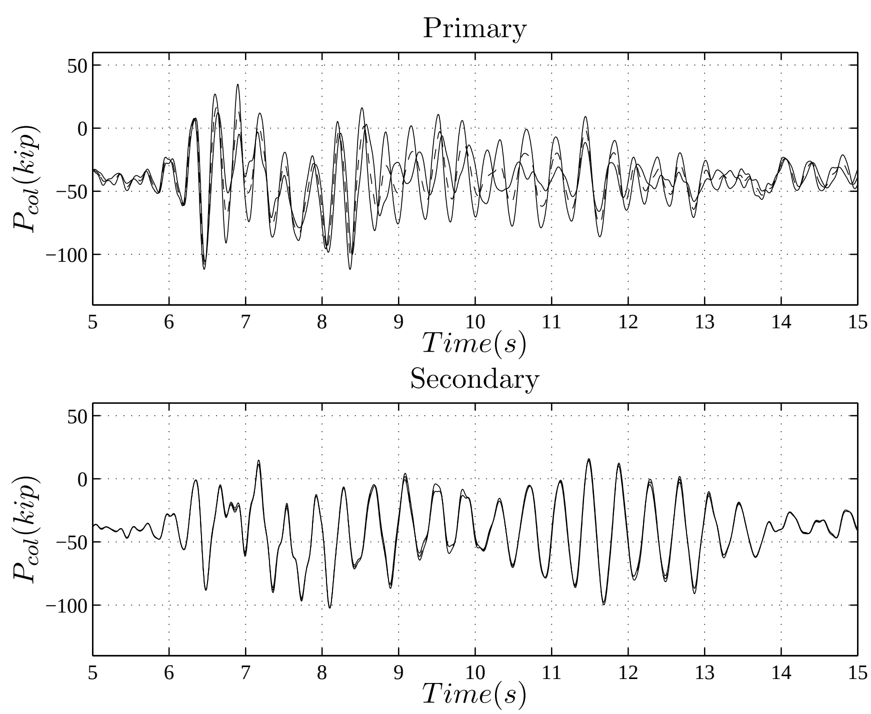

Figure 138: Column Force response with sensitivity to floor mass, 1979 Imperial Valley - Brawley Airport motion, founded on soft clay.

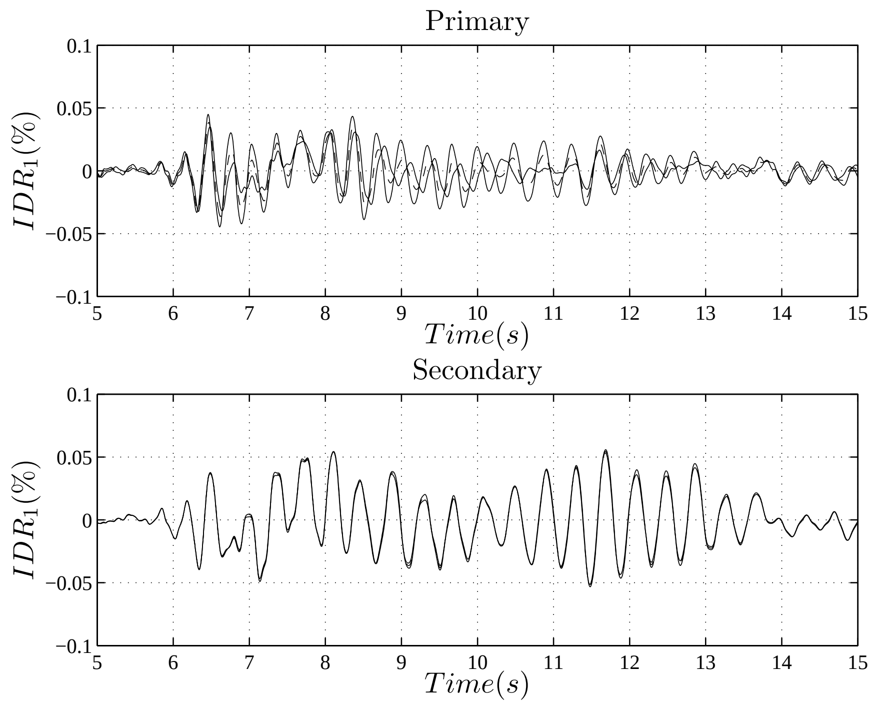

Figure 139: First-story IDR response with sensitivity to floor mass, 1979 Imperial Valley - Brawley Airport motion, founded on soft clay.

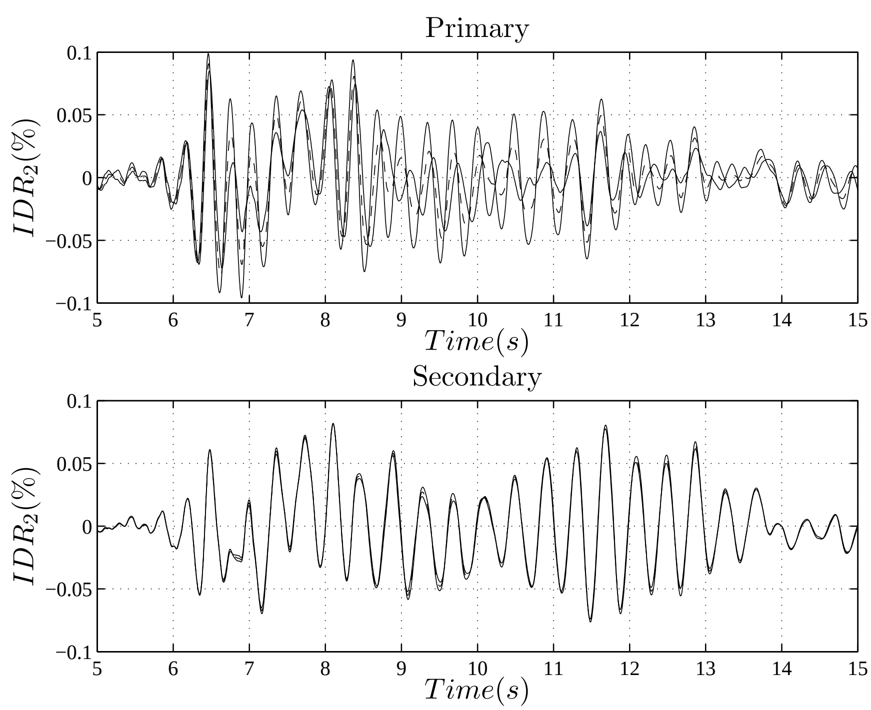

Figure 140: Second-story IDR response with sensitivity to floor mass, 1979 Imperial Valley - Brawley Airport motion, founded on soft clay.

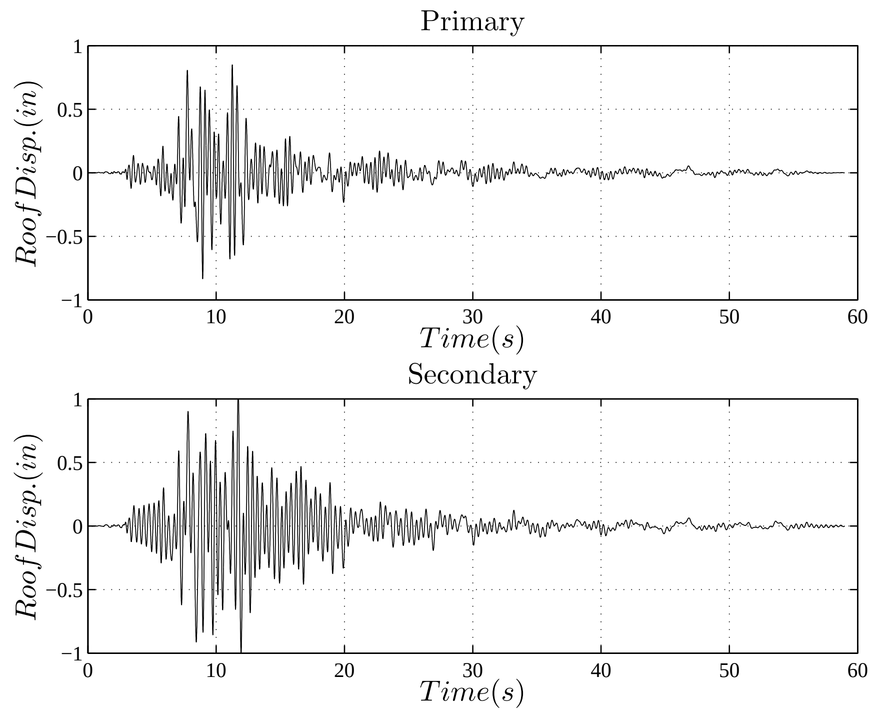

Figure 141: Mean roof displacement response, Loma Prieta Hollister - South & Pine motion, founded on soft clay.

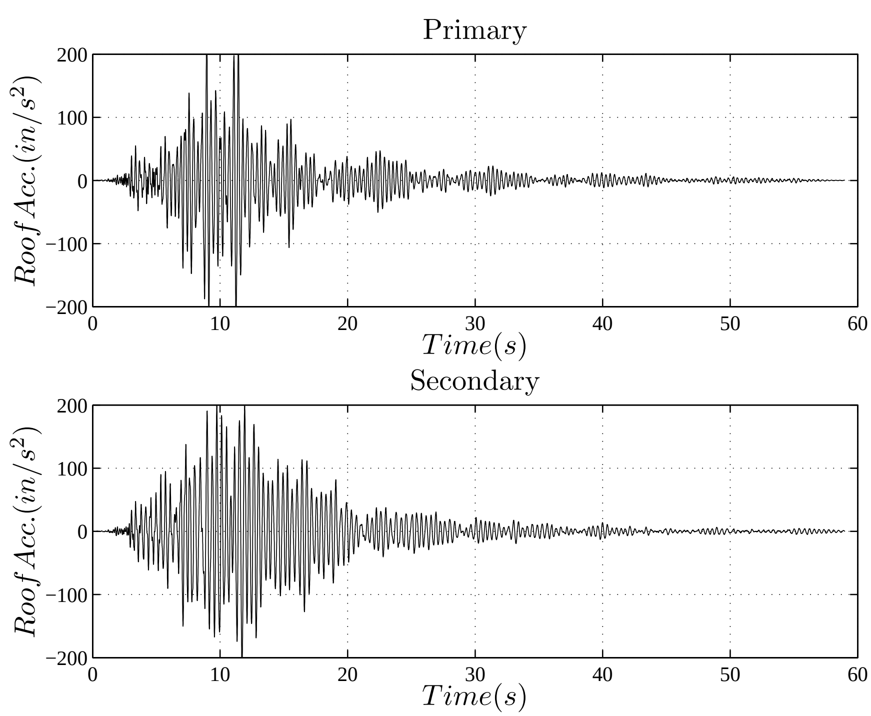

Figure 142: Mean roof acceleration response, Loma Prieta Hollister - South & Pine motion, founded on soft clay.

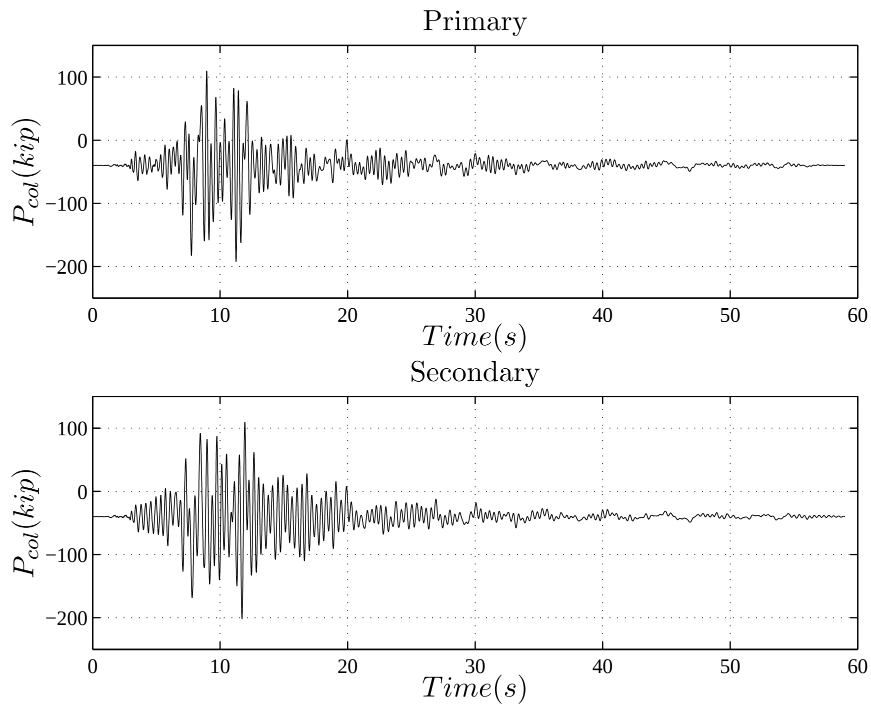

Figure 143: Mean column response, Loma Prieta Hollister - South & Pine motion, founded on soft clay.

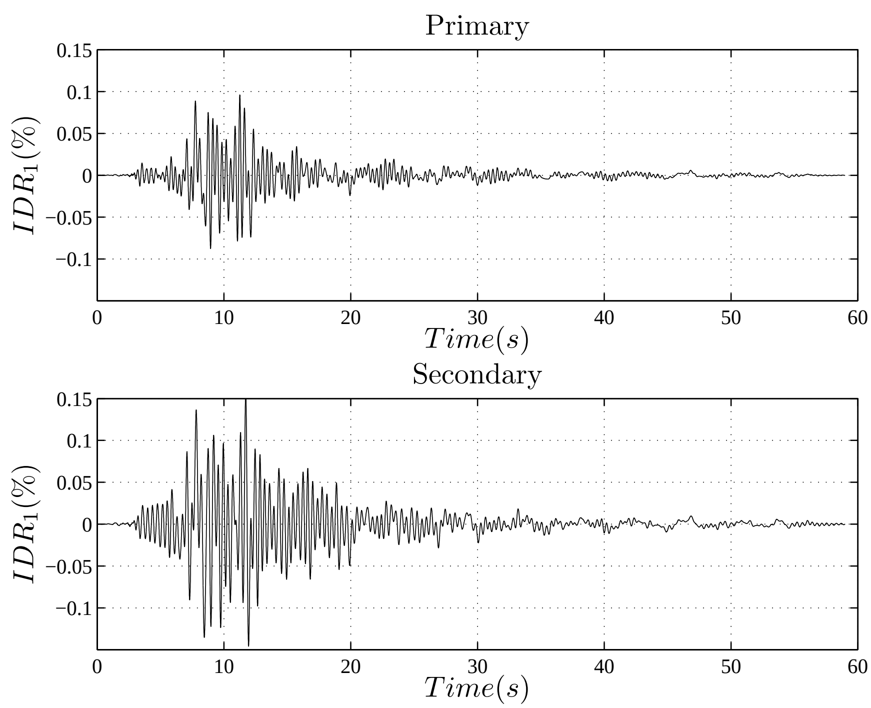

Figure 144: Mean first-story IDR response, Loma Prieta Hollister - South & Pine motion, founded on soft clay.

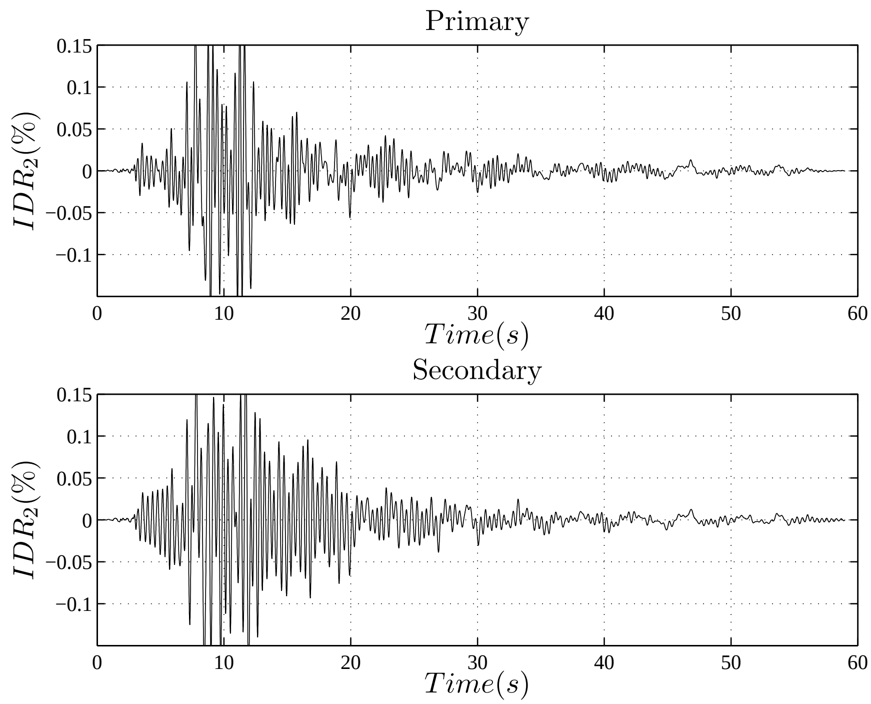

Figure 145: Mean roof displacement response, Loma Prieta Hollister - South & Pine motion, founded on soft clay.

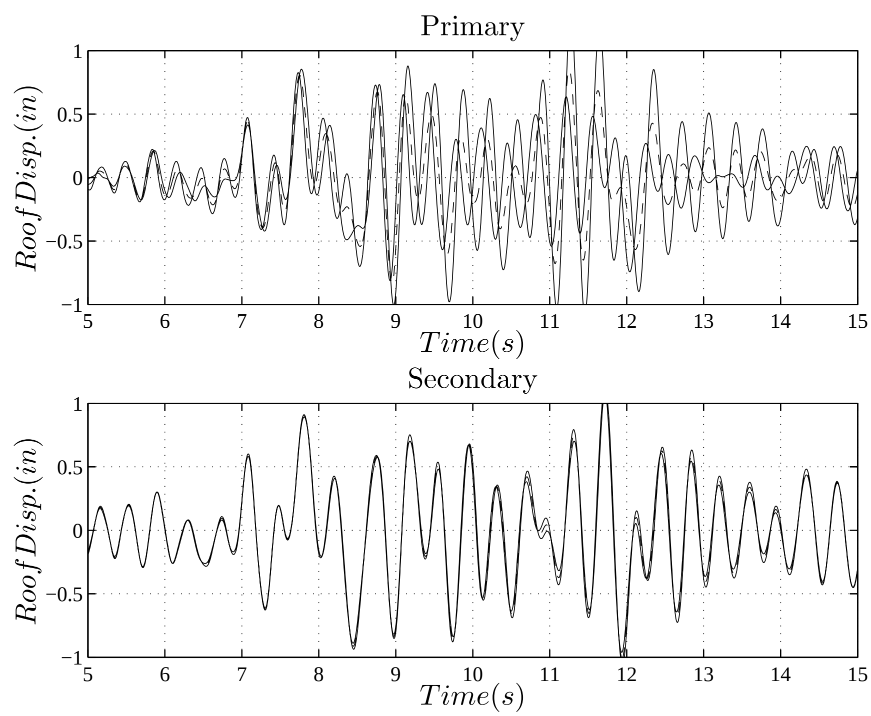

Figure 146: Roof displacement response with sensitivity to building stiffness, Loma Prieta Hollister - South & Pine motion, founded on soft clay.

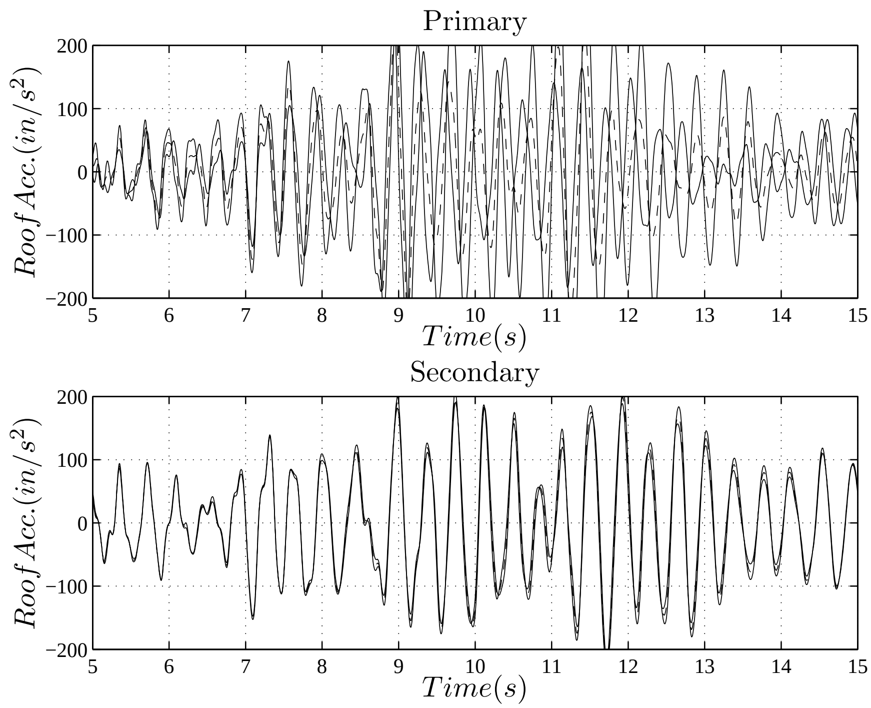

Figure 147: Roof acceleration response with sensitivity to building stiffness, Loma Prieta Hollister - South & Pine motion, founded on soft clay.

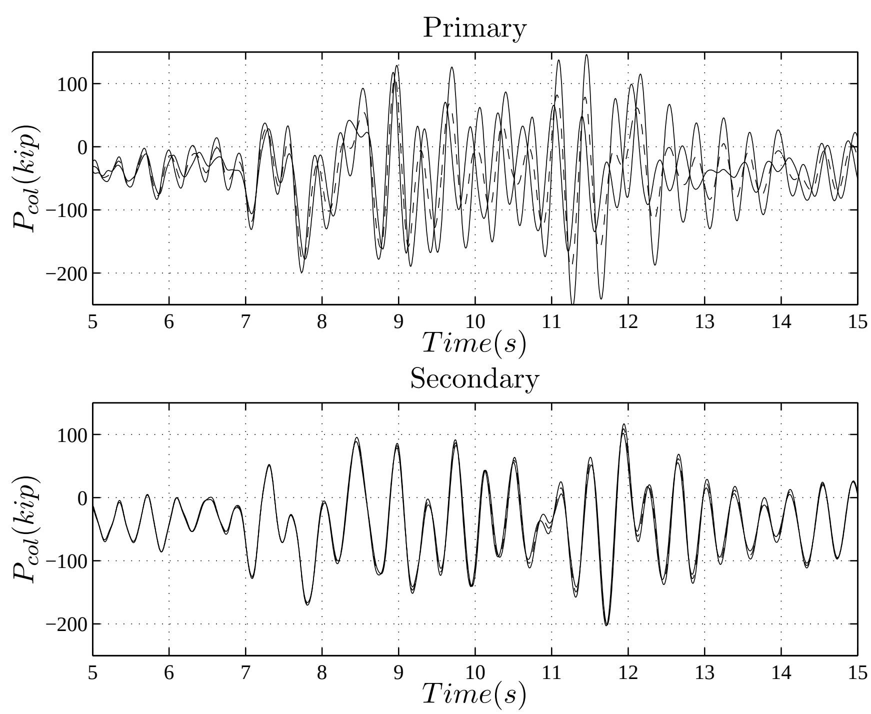

Figure 148: Column force response with sensitivity to building stiffness, Loma Prieta Hollister - South & Pine motion, founded on soft clay.

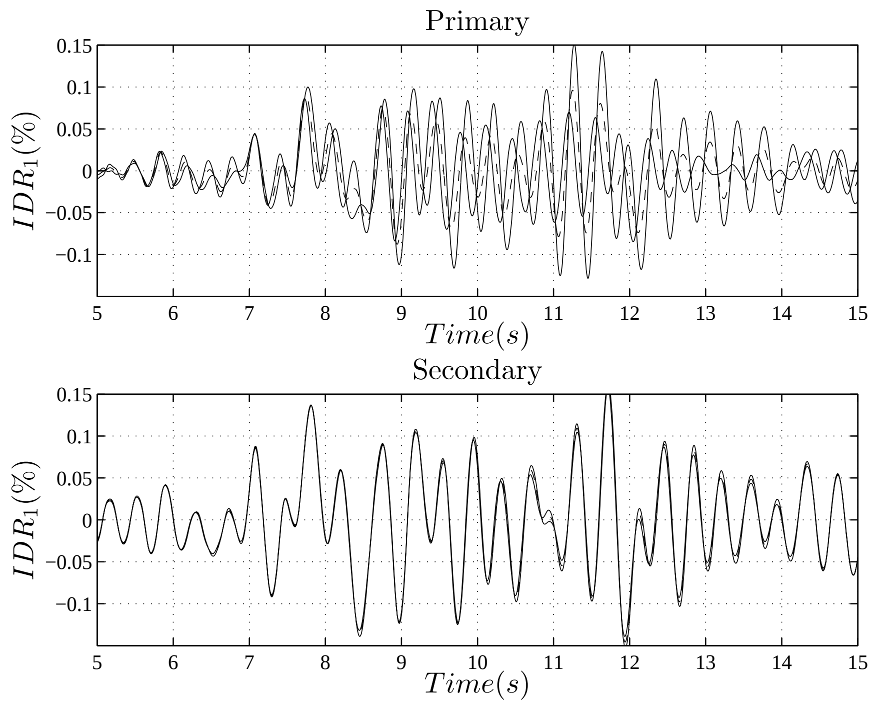

Figure 149: First-story IDR response with sensitivity to building stiffness, Loma Prieta Hollister - South & Pine motion, founded on soft clay.

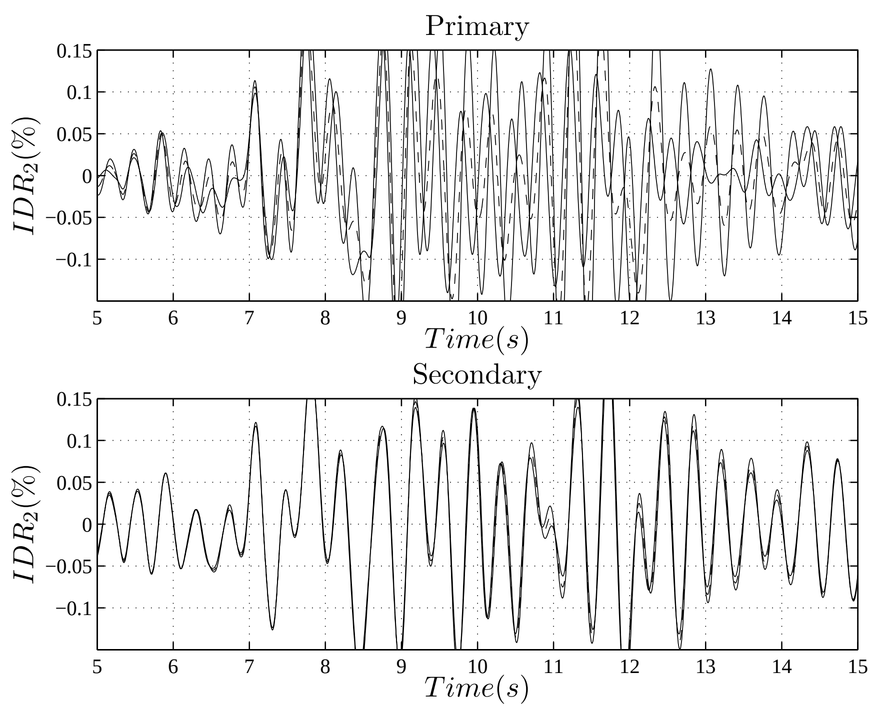

Figure 150: Second-story IDR response with sensitivity to building stiffness, Loma Prieta Hollister - South & Pine motion, founded on soft clay.

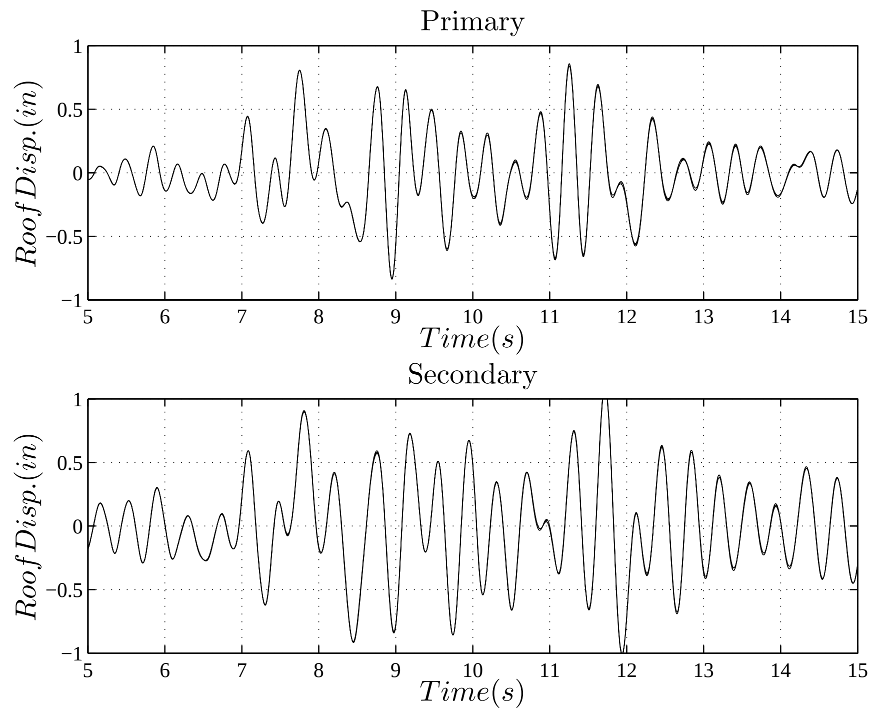

Figure 151: Roof displacement response with sensitivity to soil spring stiffness, Loma Prieta Hollister - South & Pine motion, founded on soft clay.

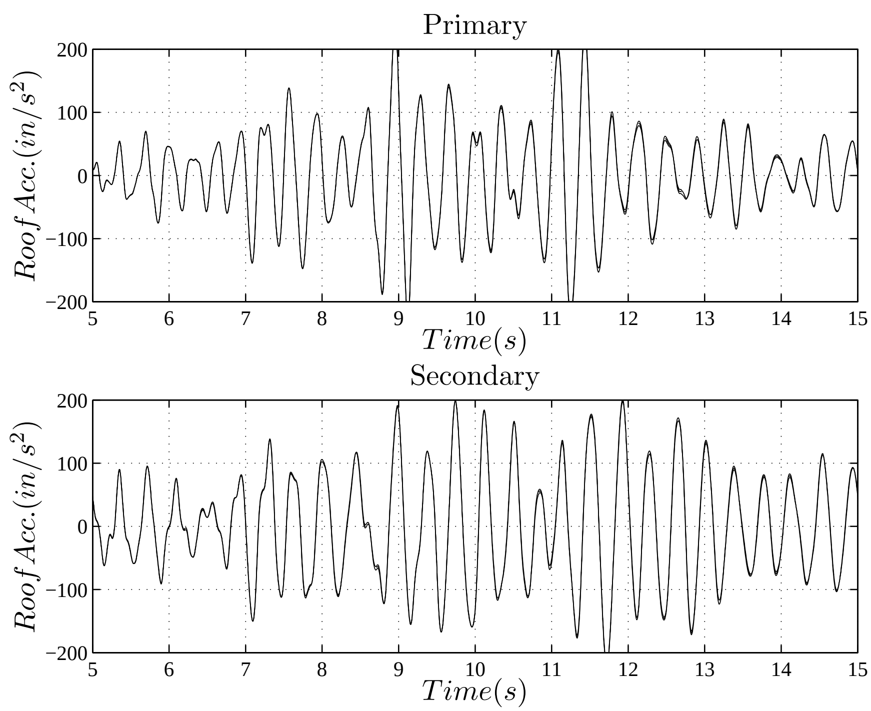

Figure 152: Roof acceleration response with sensitivity to soil spring stiffness, Loma Prieta Hollister - South & Pine motion, founded on soft clay.

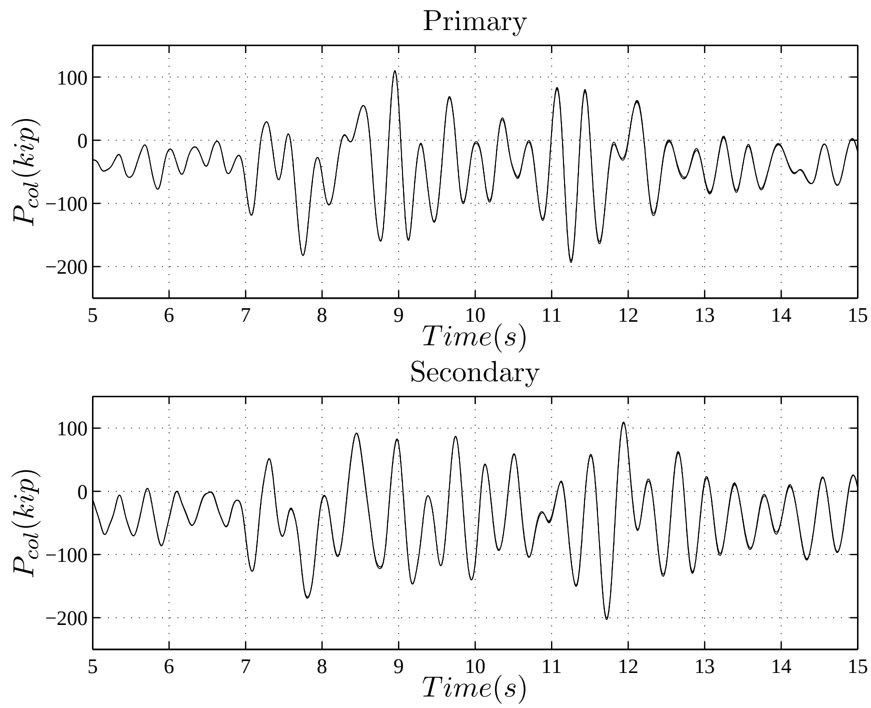

Figure 153: Column force response with sensitivity to soil spring stiffness, Loma Prieta Hollister - South & Pine motion, founded on soft clay.

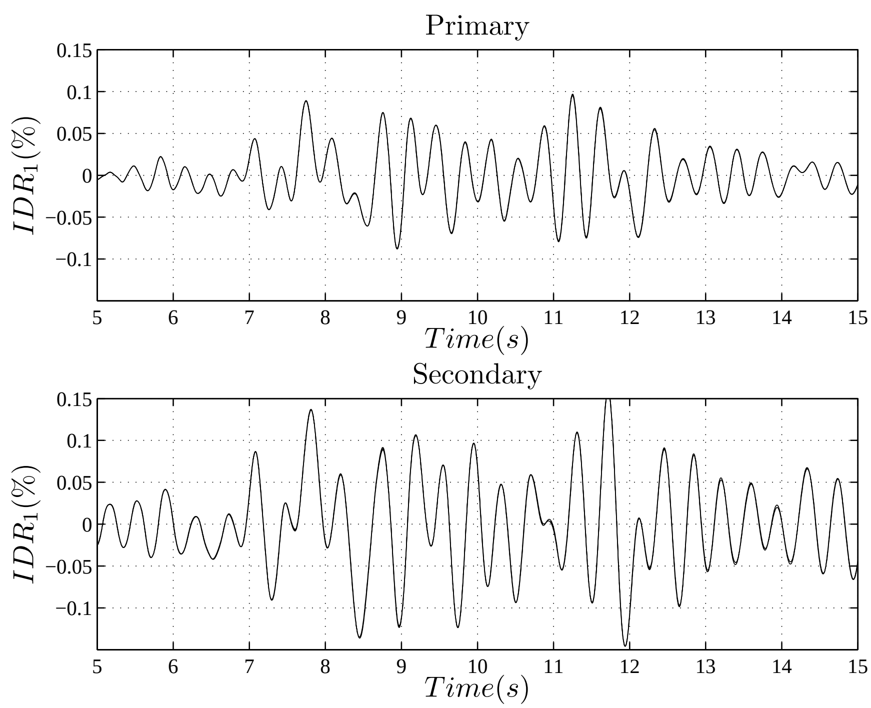

Figure 154: First-story IDR response with sensitivity to soil spring stiffness, Loma Prieta Hollister - South & Pine motion, founded on soft clay.

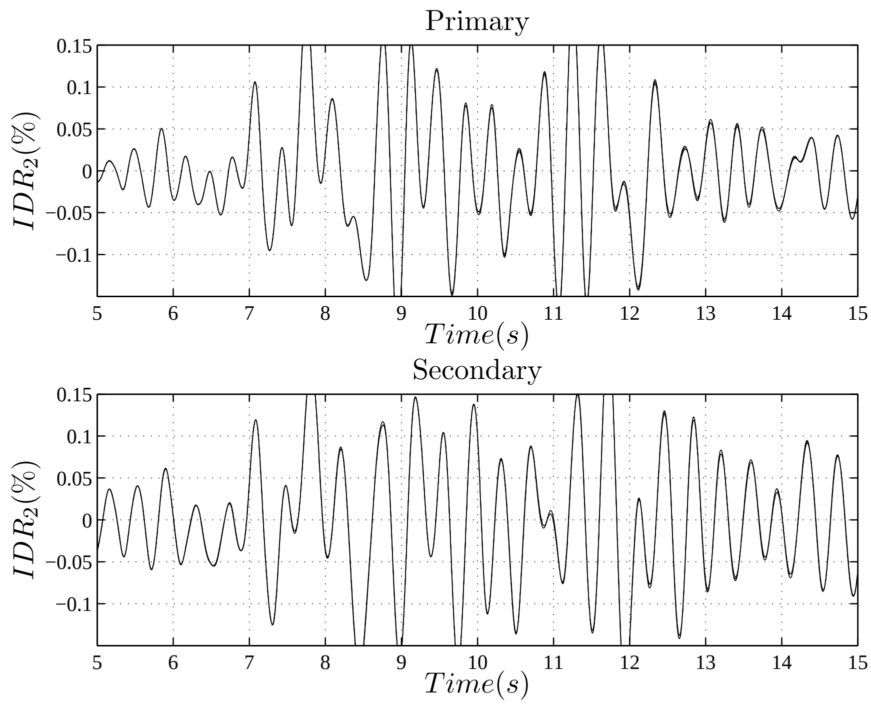

Figure 155: Second-story IDR response with sensitivity to soil spring stiffness, Loma Prieta Hollister - South & Pine motion, founded on soft clay.

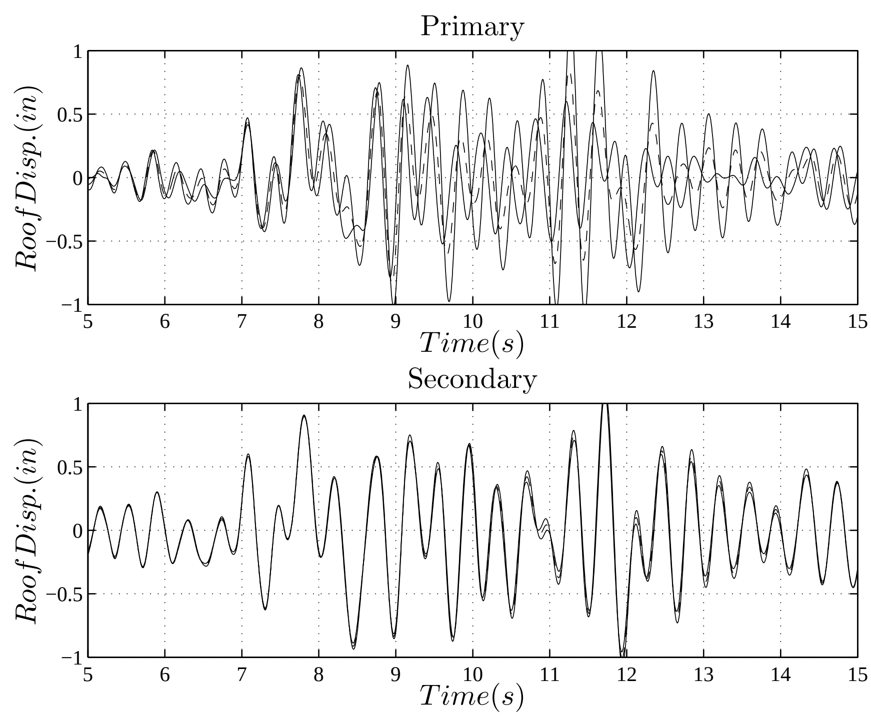

Figure 156: Roof displacement response with sensitivity to floor mass, Loma Prieta Hollister - South & Pine motion, founded on soft clay.

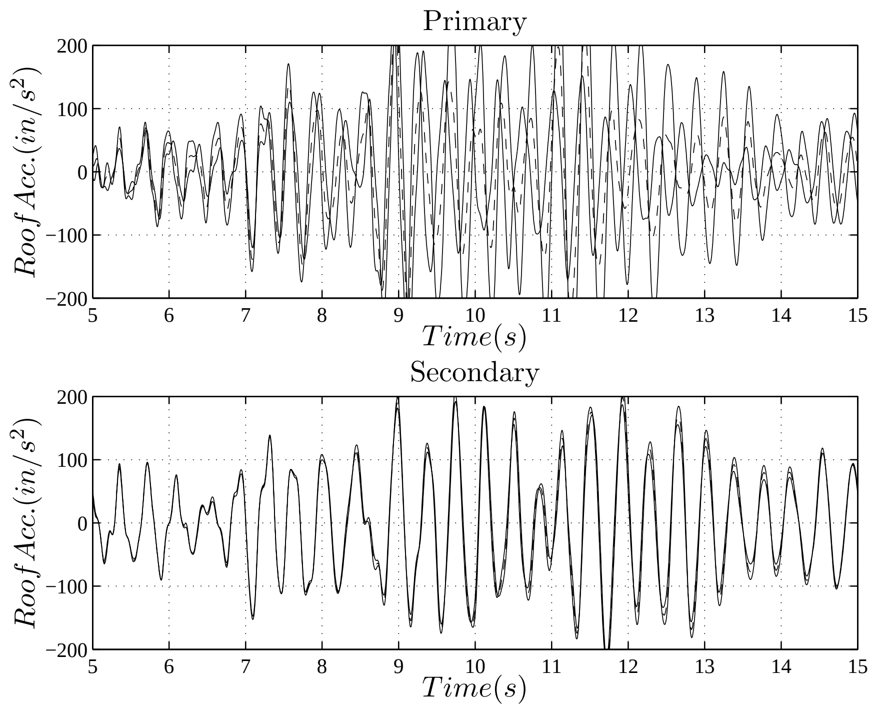

Figure 157: Roof acceleration response with sensitivity to floor mass, Loma Prieta Hollister - South & Pine motion, founded on soft clay.

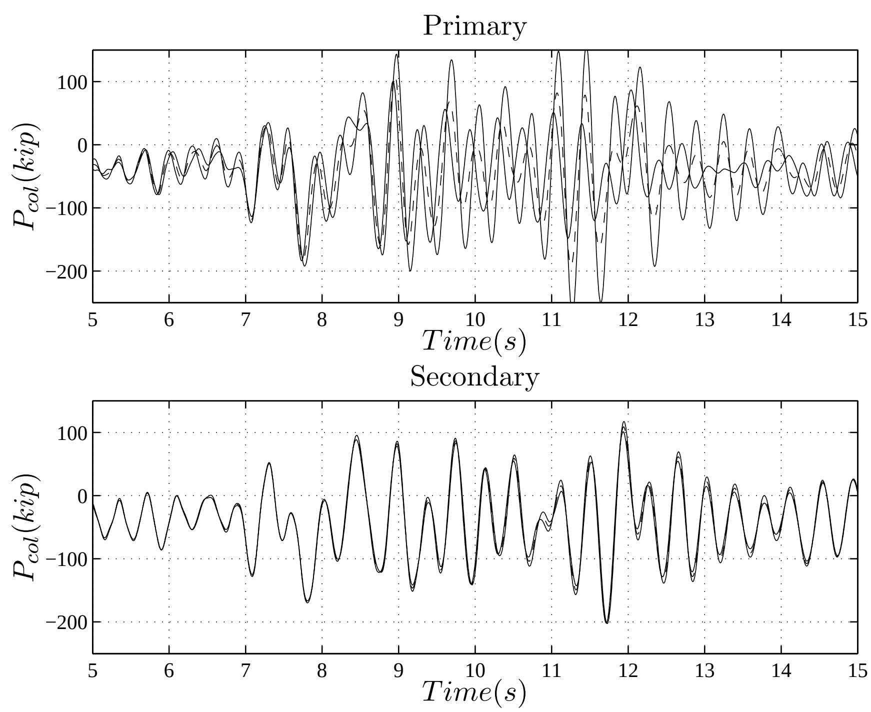

Figure 158: Column Force response with sensitivity to floor mass, Loma Prieta Hollister - South & Pine motion, founded on soft clay.

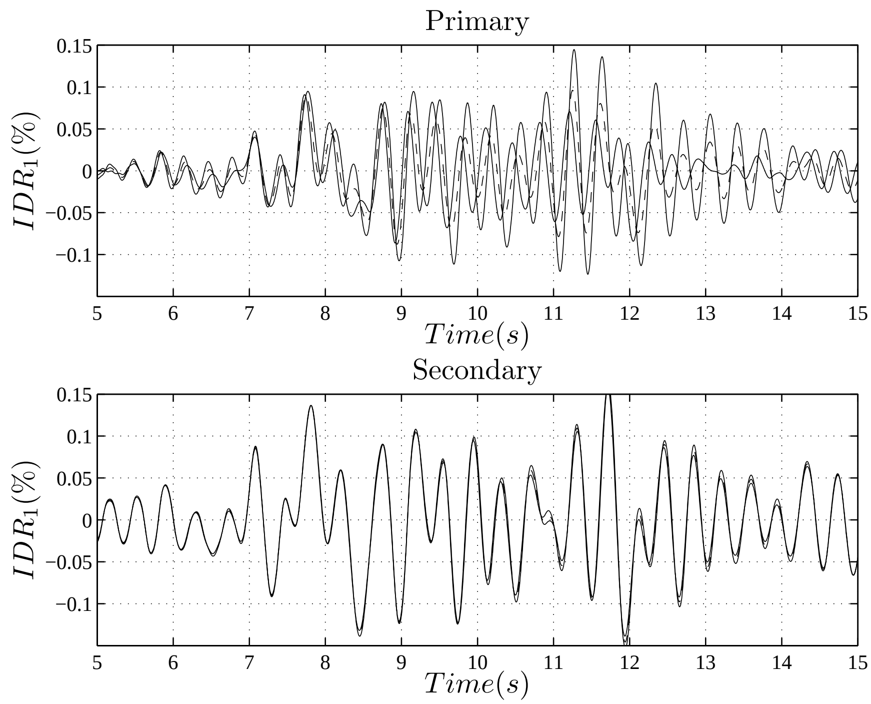

Figure 159: First-story IDR response with sensitivity to floor mass, Loma Prieta Hollister - South & Pine motion, founded on soft clay.

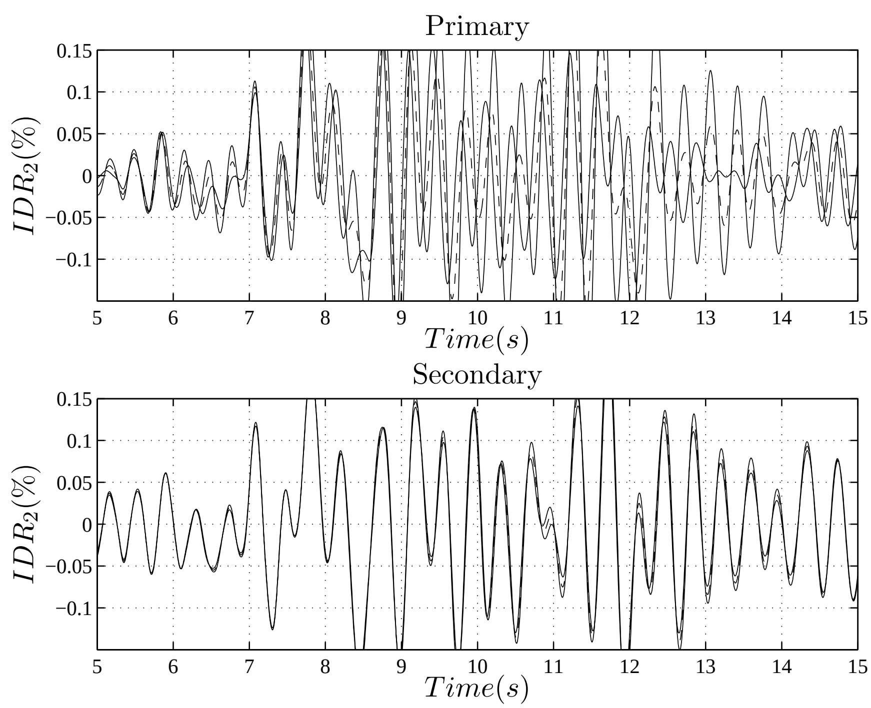

Figure 160: Second-story IDR response with sensitivity to floor mass, Loma Prieta Hollister - South & Pine motion, founded on soft clay.

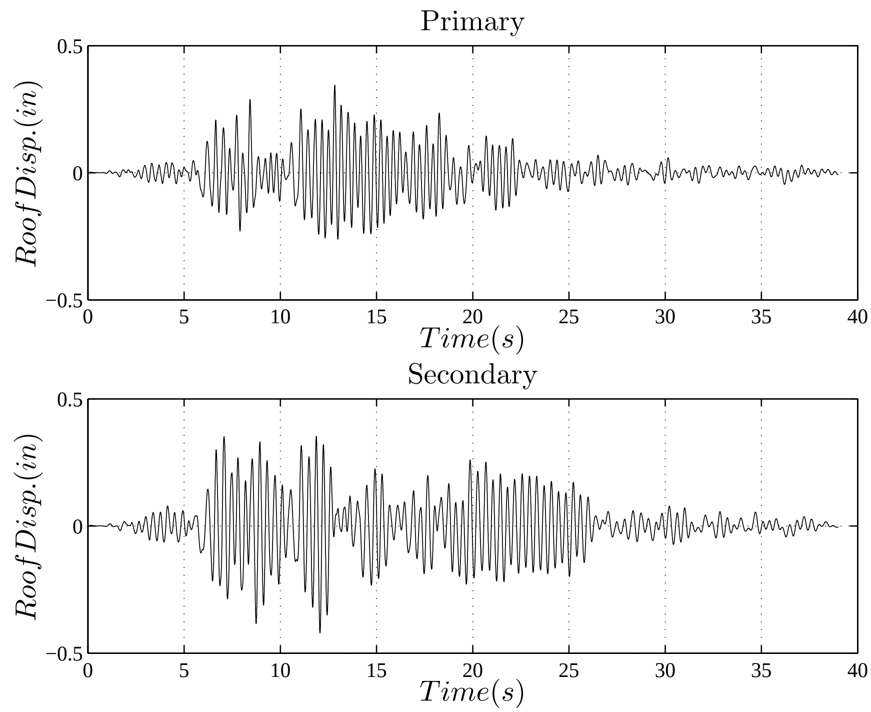

Figure 161: Mean roof displacement response, Loma Prieta Salinas - John & Work motion, founded on soft clay.

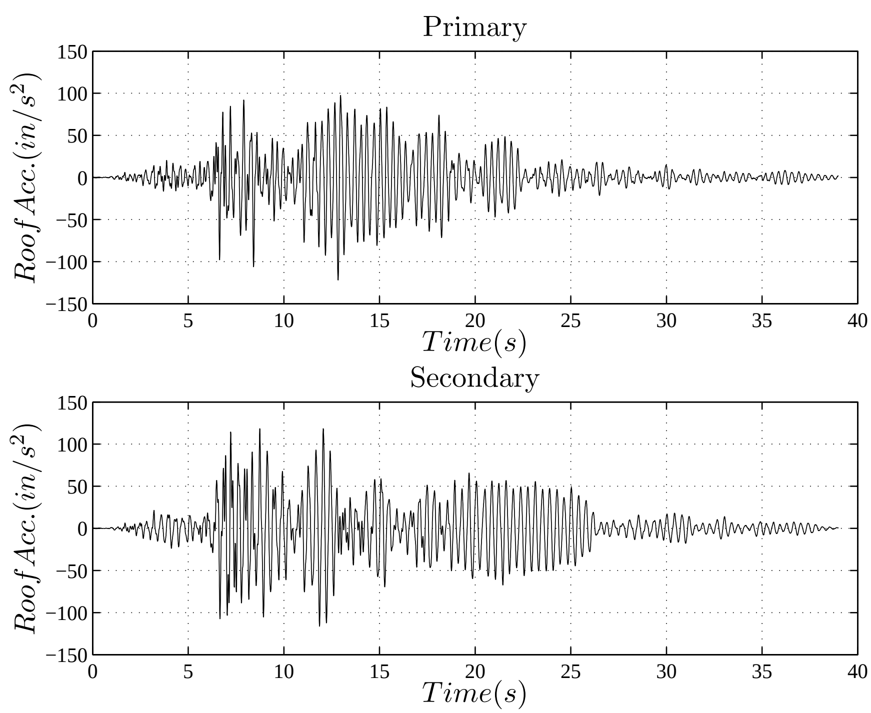

Figure 162: Mean roof acceleration response, Loma Prieta Salinas - John & Work motion, founded on soft clay.

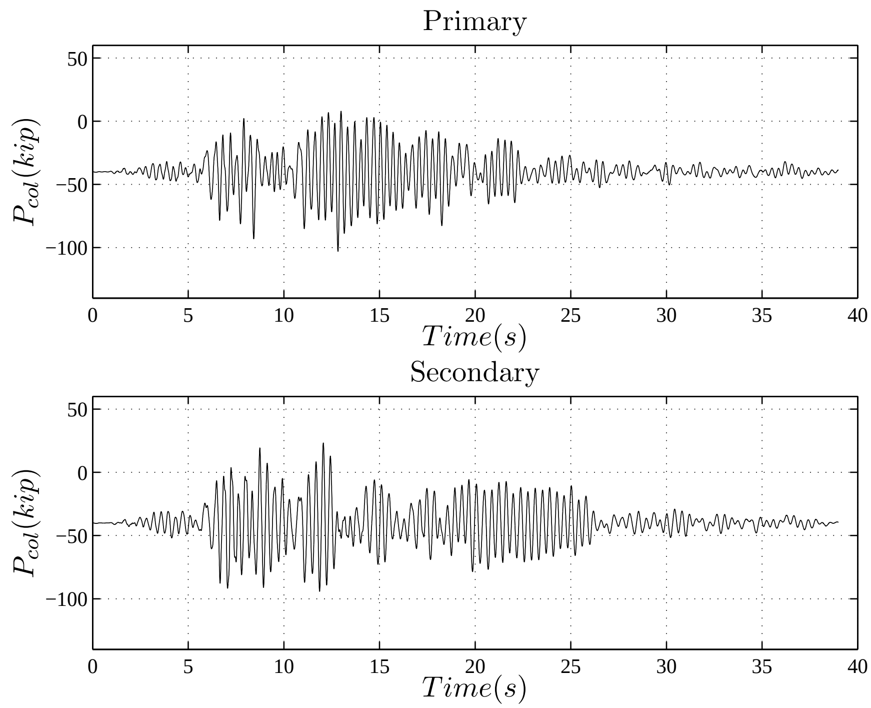

Figure 163: Mean column response, Loma Prieta Salinas - John & Work motion, founded on soft clay.

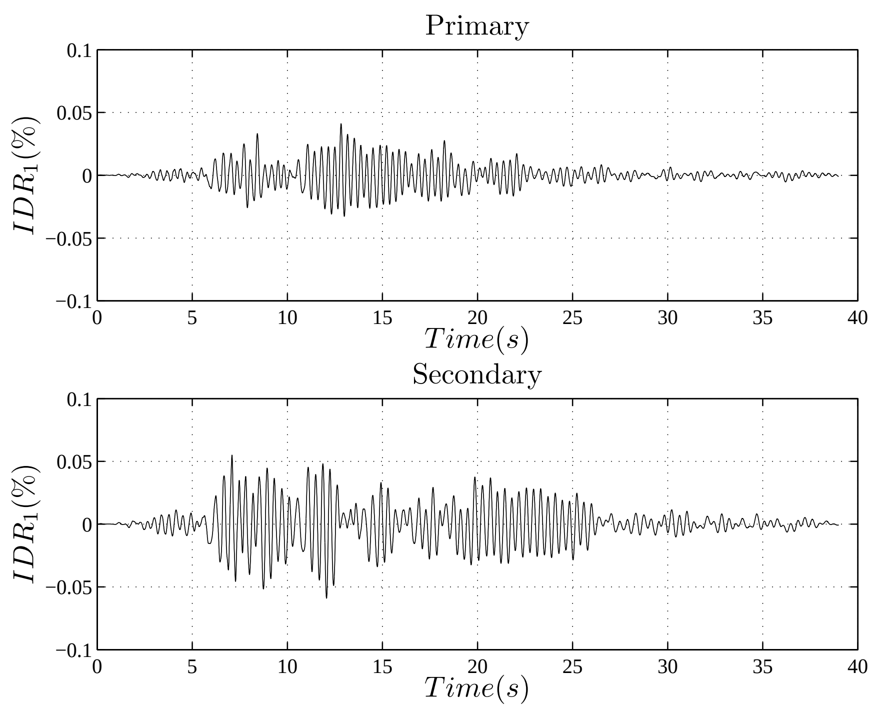

Figure 164: Mean first-story IDR response, Loma Prieta Salinas - John & Work motion, founded on soft clay.

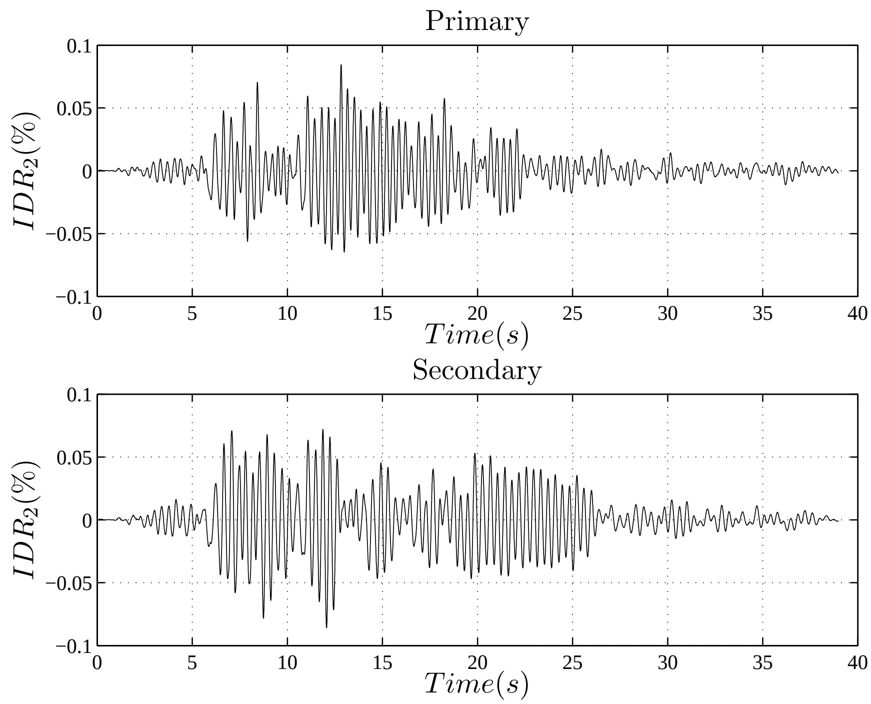

Figure 165: Mean roof displacement response, Loma Prieta Salinas - John & Work motion, founded on soft clay.

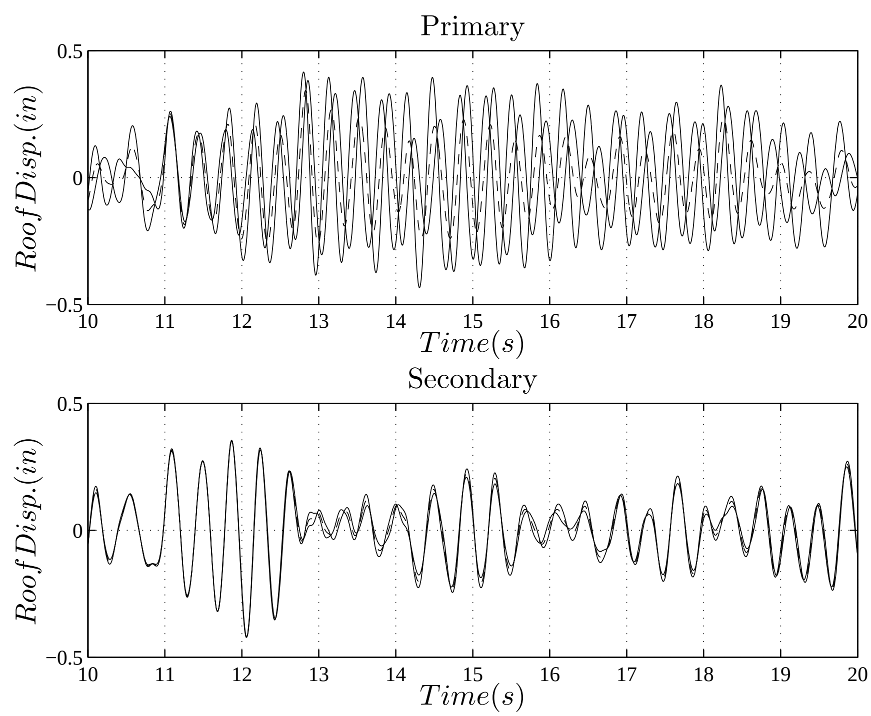

Figure 166: Roof displacement response with sensitivity to building stiffness, Loma Prieta Salinas - John & Work motion, founded on soft clay.

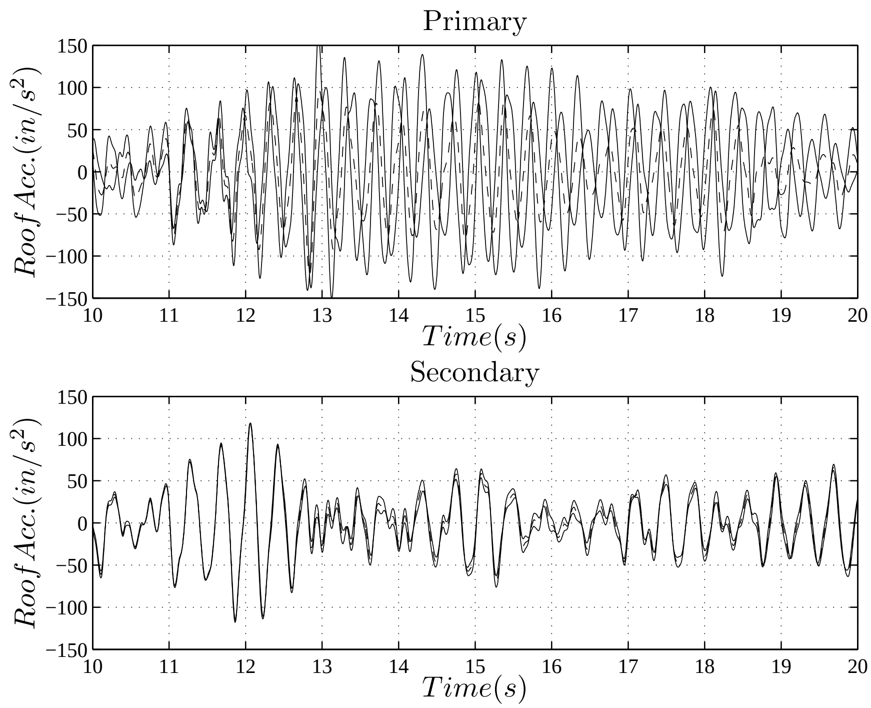

Figure 167: Roof acceleration response with sensitivity to building stiffness, Loma Prieta Salinas - John & Work motion, founded on soft clay.

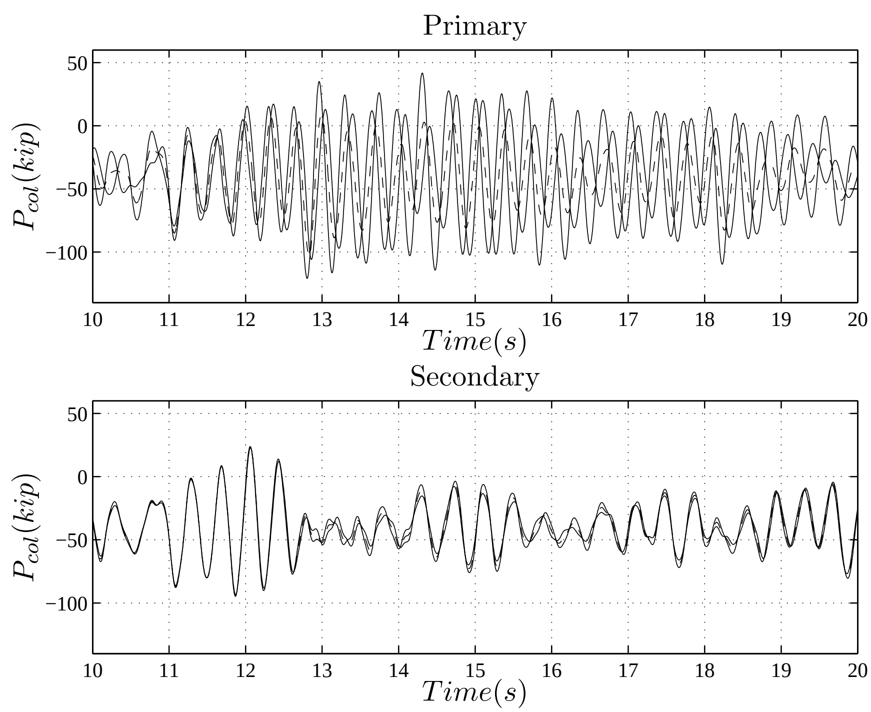

Figure 168: Column force response with sensitivity to building stiffness, Loma Prieta Salinas - John & Work motion, founded on soft clay.

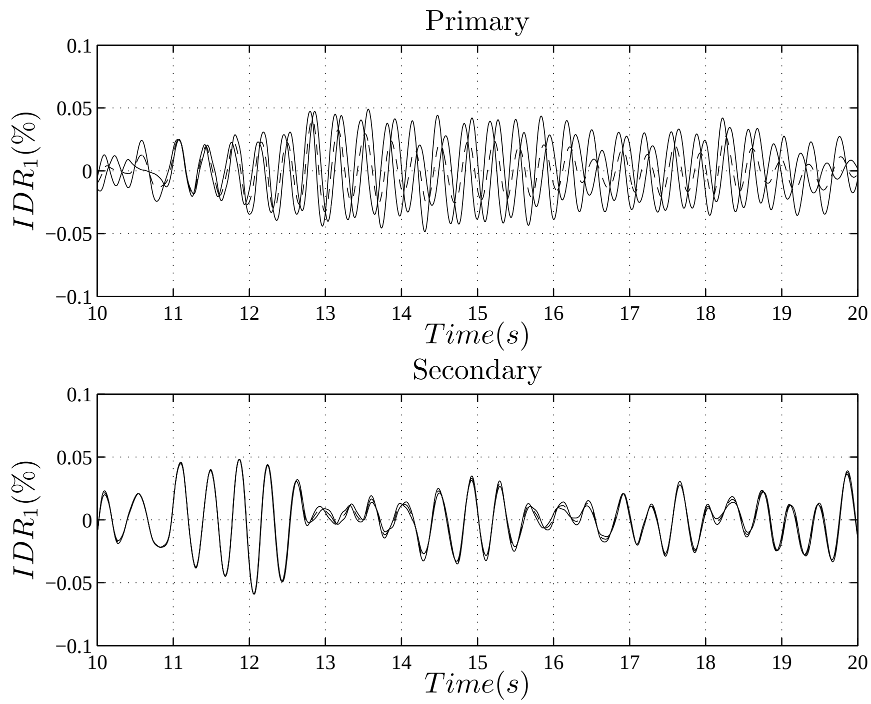

Figure 169: First-story IDR response with sensitivity to building stiffness, Loma Prieta Salinas - John & Work motion, founded on soft clay.

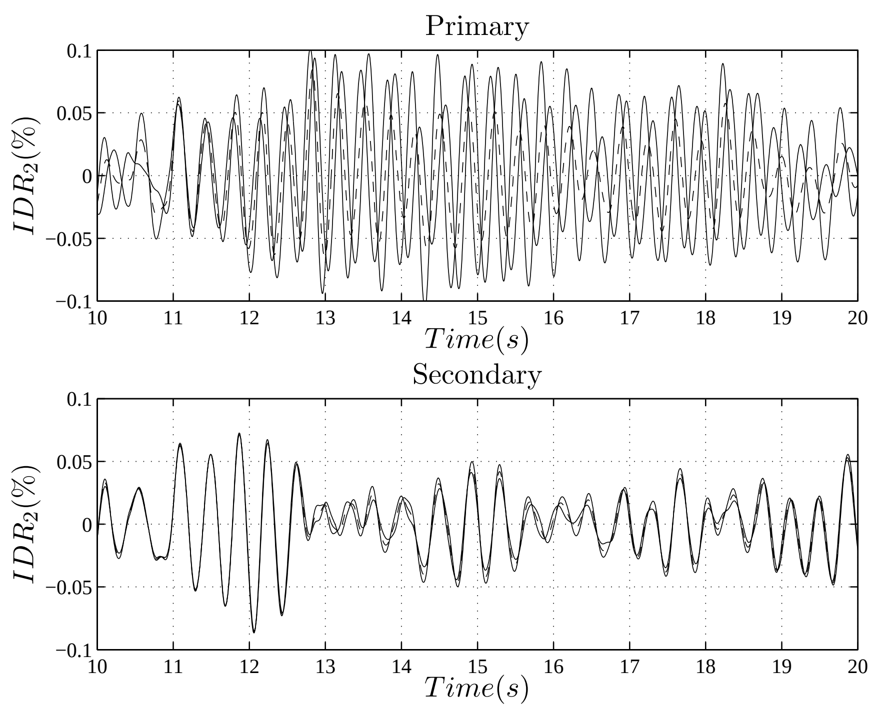

Figure 170: Second-story IDR response with sensitivity to building stiffness, Loma Prieta Salinas - John & Work motion, founded on soft clay.

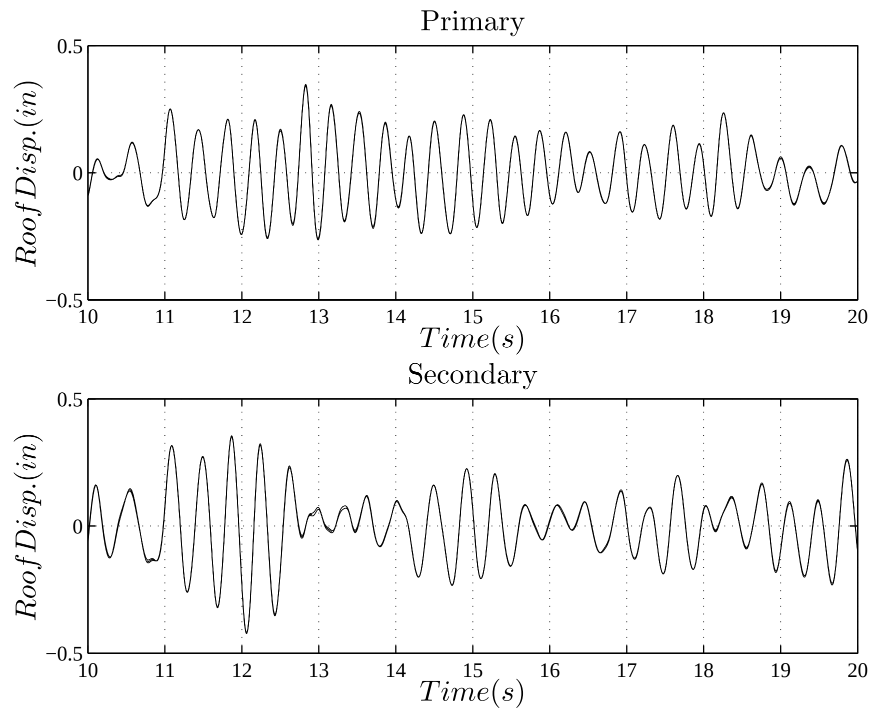

Figure 171: Roof displacement response with sensitivity to soil spring stiffness, Loma Prieta Salinas - John & Work motion, founded on soft clay.

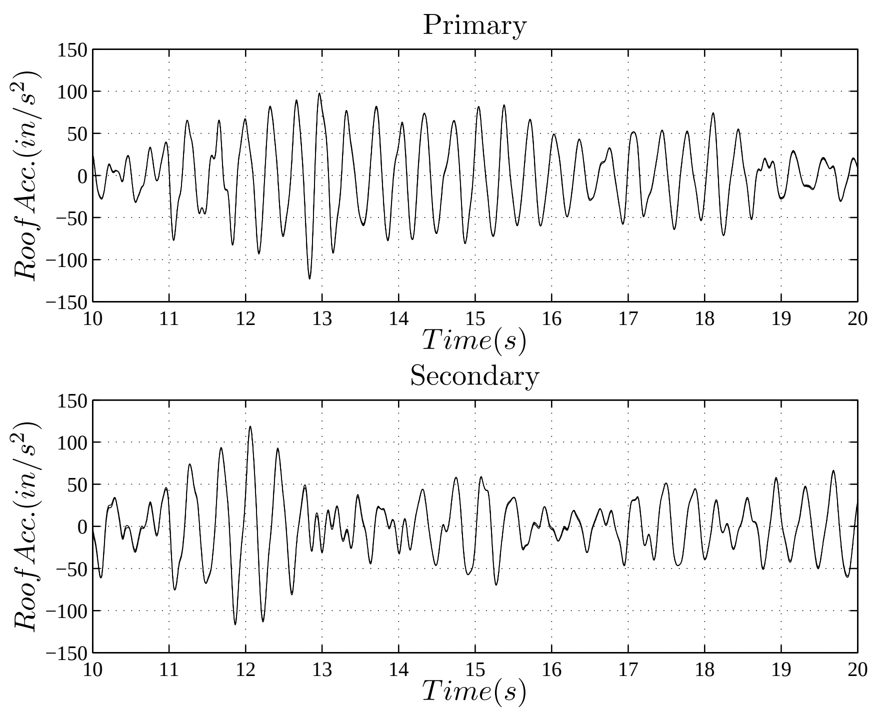

Figure 172: Roof acceleration response with sensitivity to soil spring stiffness, Loma Prieta Salinas - John & Work motion, founded on soft clay.

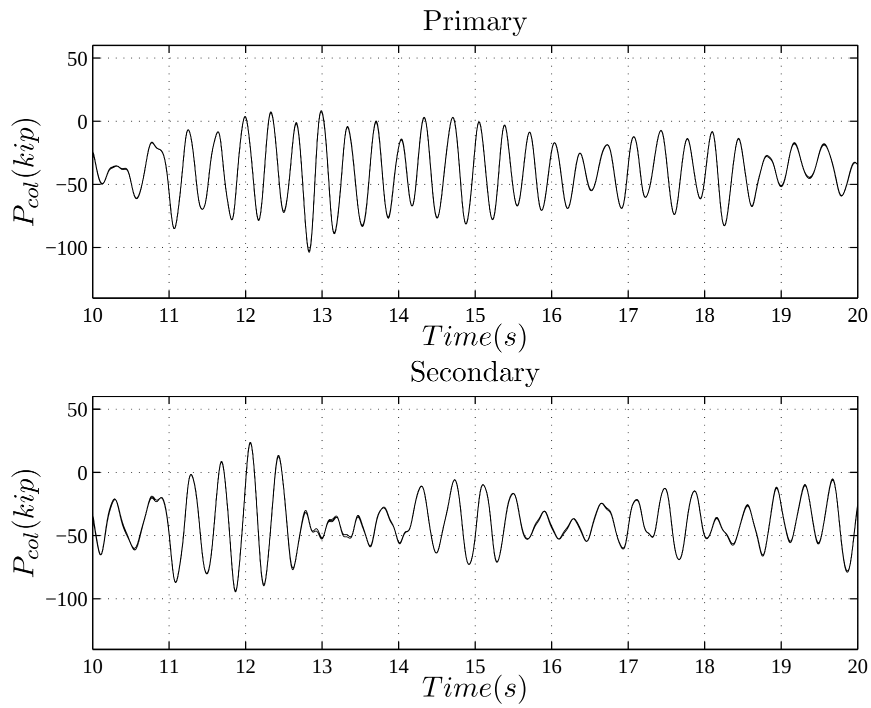

Figure 173: Column force response with sensitivity to soil spring stiffness, Loma Prieta Salinas - John & Work motion, founded on soft clay.

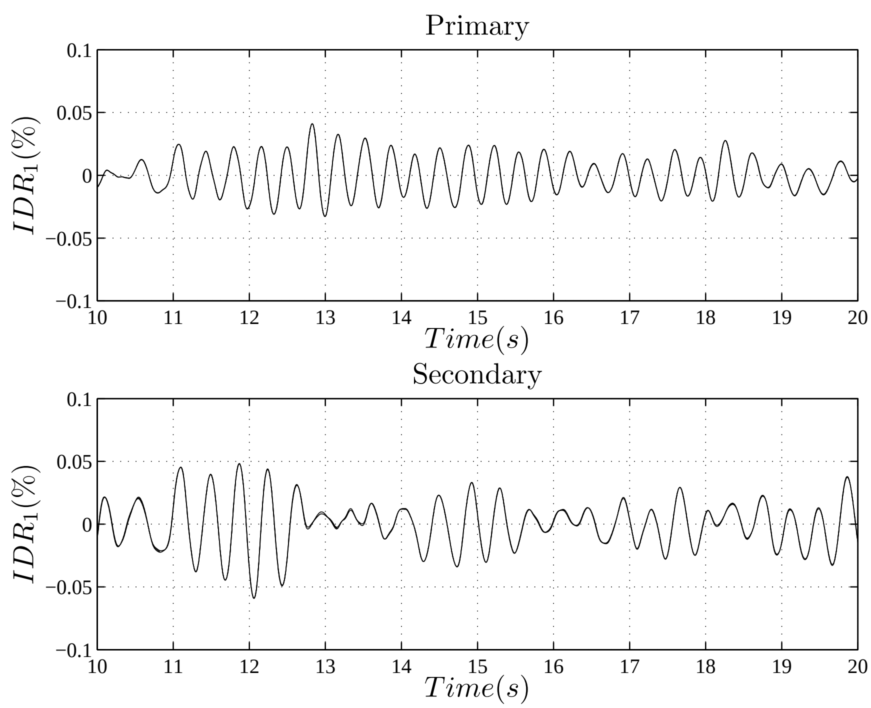

Figure 174: First-story IDR response with sensitivity to soil spring stiffness, Loma Prieta Salinas - John & Work motion, founded on soft clay.

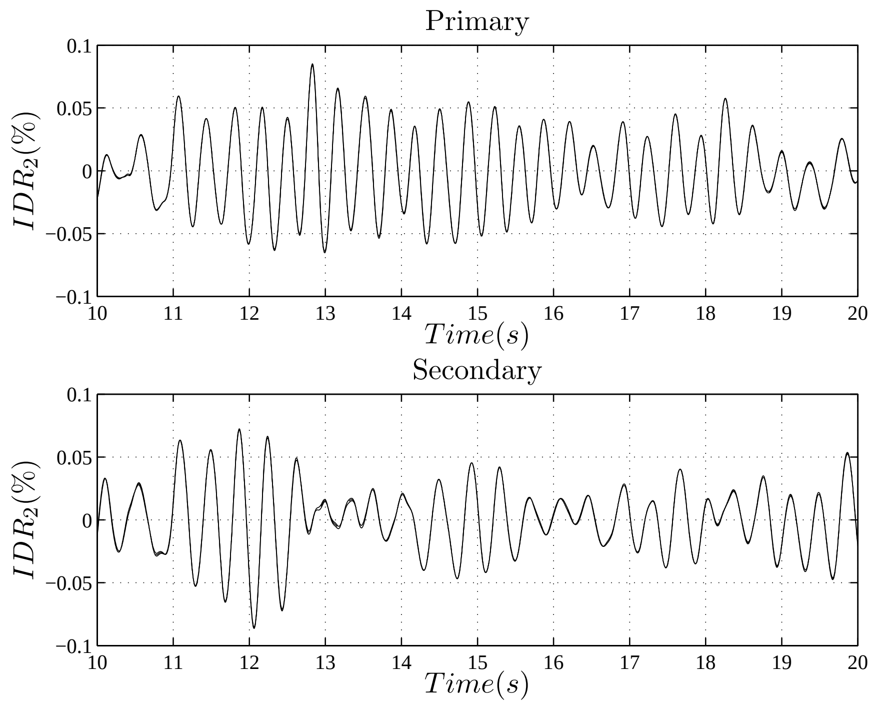

Figure 175: Second-story IDR response with sensitivity to soil spring stiffness, Loma Prieta Salinas - John & Work motion, founded on soft clay.

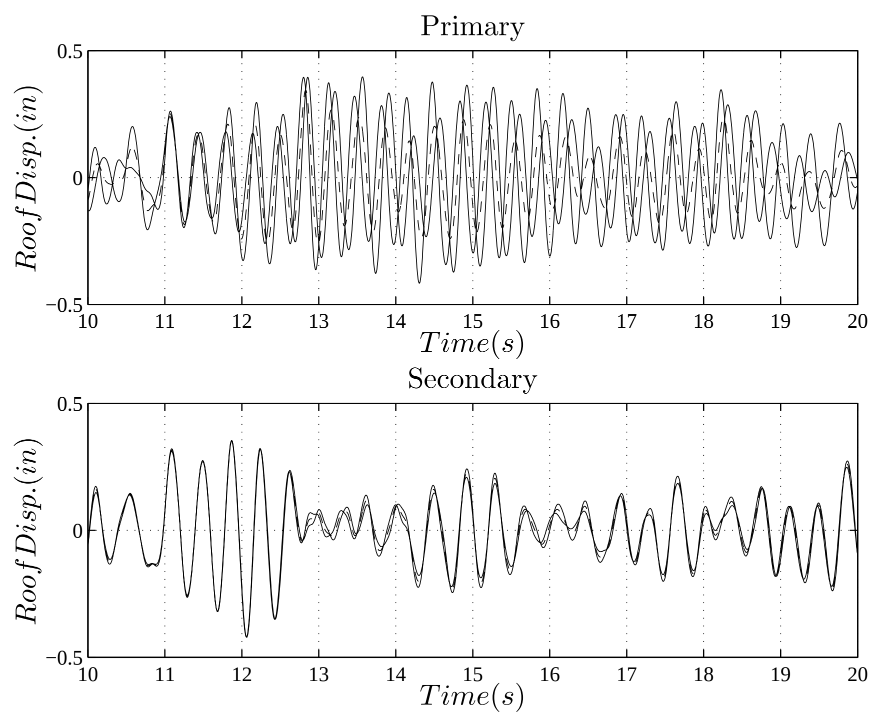

Figure 176: Roof displacement response with sensitivity to floor mass, Loma Prieta Salinas - John & Work motion, founded on soft clay.

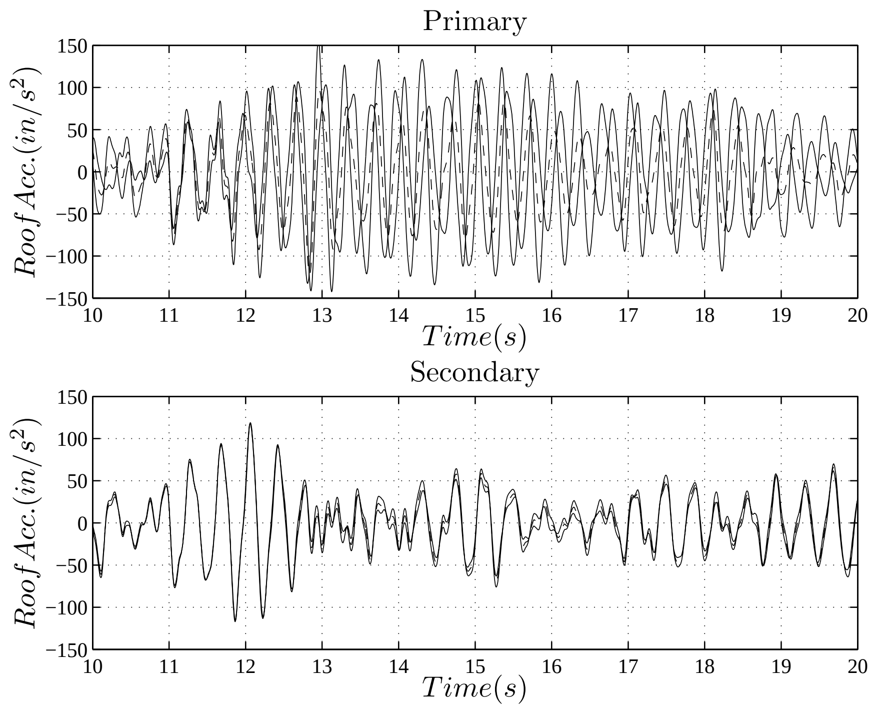

Figure 177: Roof acceleration response with sensitivity to floor mass, Loma Prieta Salinas - John & Work motion, founded on soft clay.

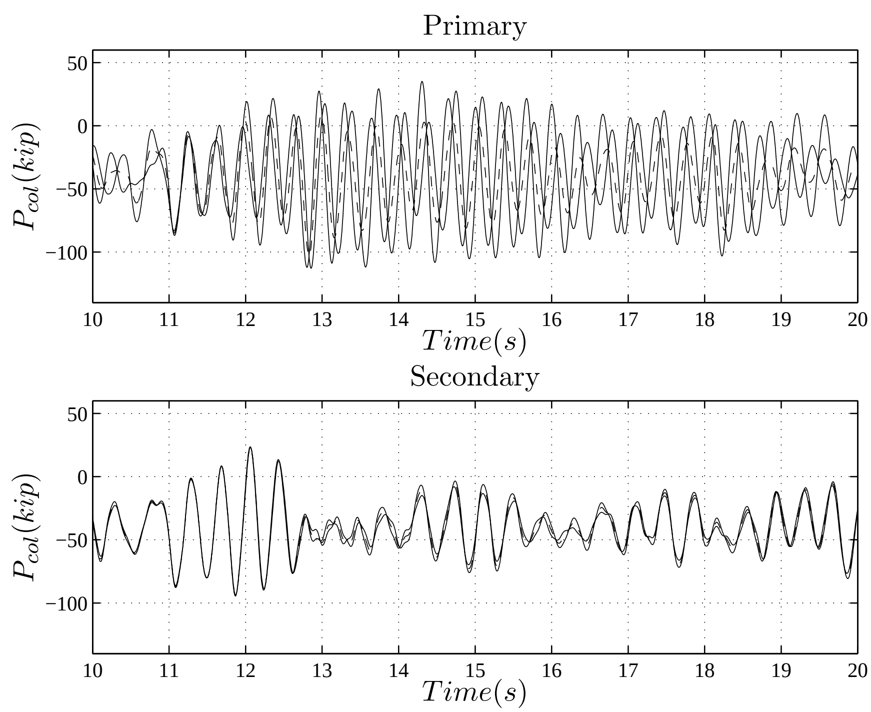

Figure 178: Column Force response with sensitivity to floor mass, Loma Prieta Salinas - John & Work motion, founded on soft clay.

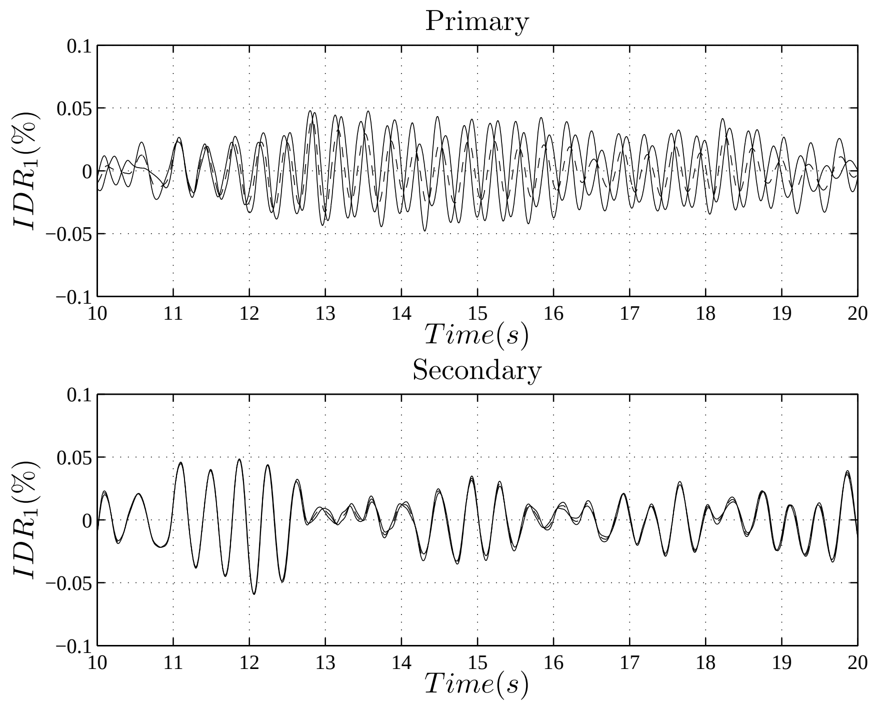

Figure 179: First-story IDR response with sensitivity to floor mass, Loma Prieta Salinas - John & Work motion, founded on soft clay.

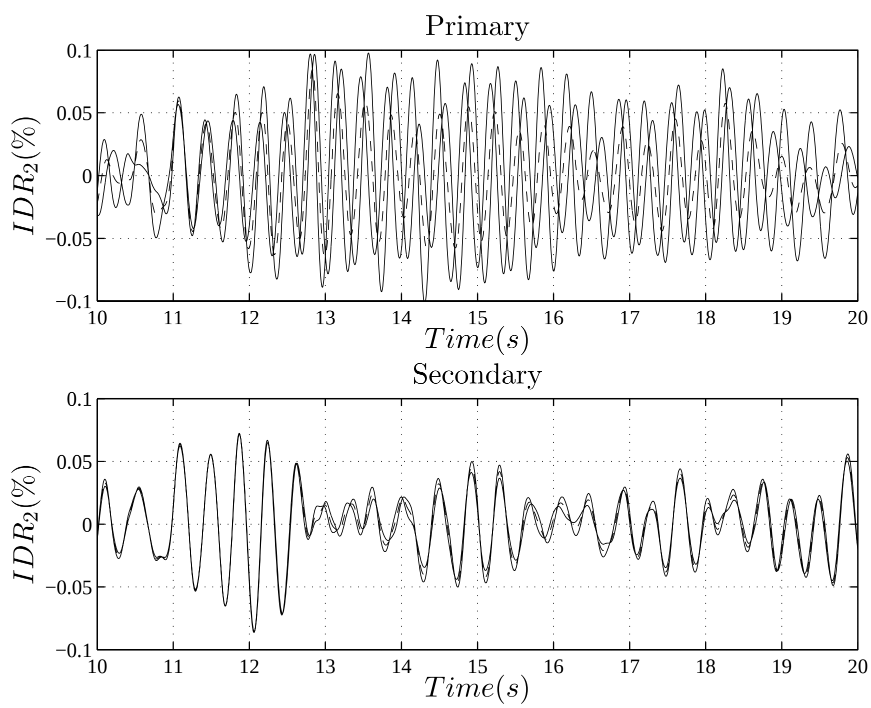

Figure 180: Second-story IDR response with sensitivity to floor mass, Loma Prieta Salinas - John & Work motion, founded on soft clay.

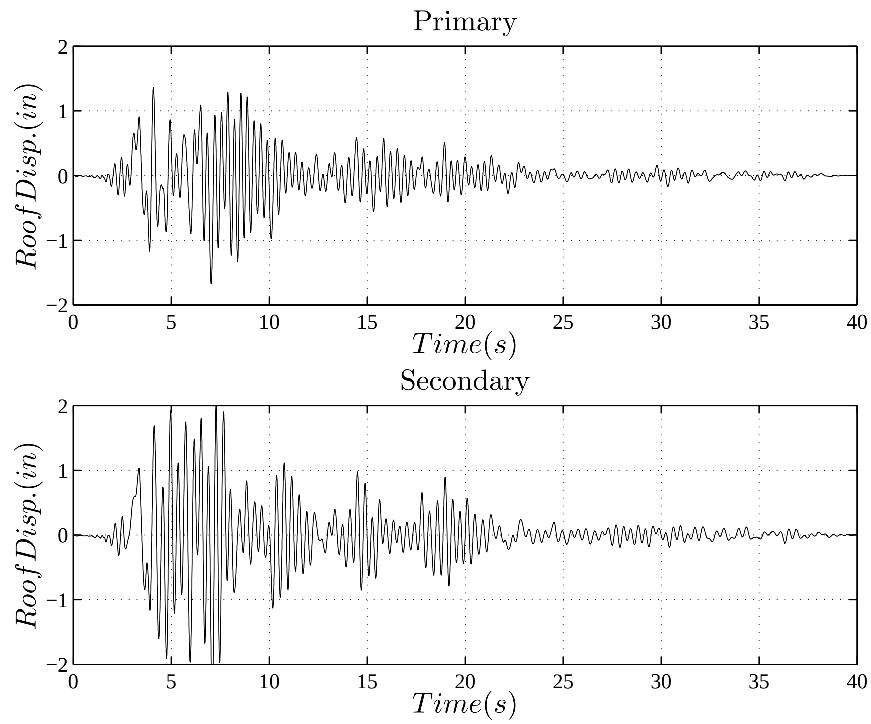

Figure 181: Mean roof displacement response, Northridge - Sylmar Converter Station motion, founded on soft clay.

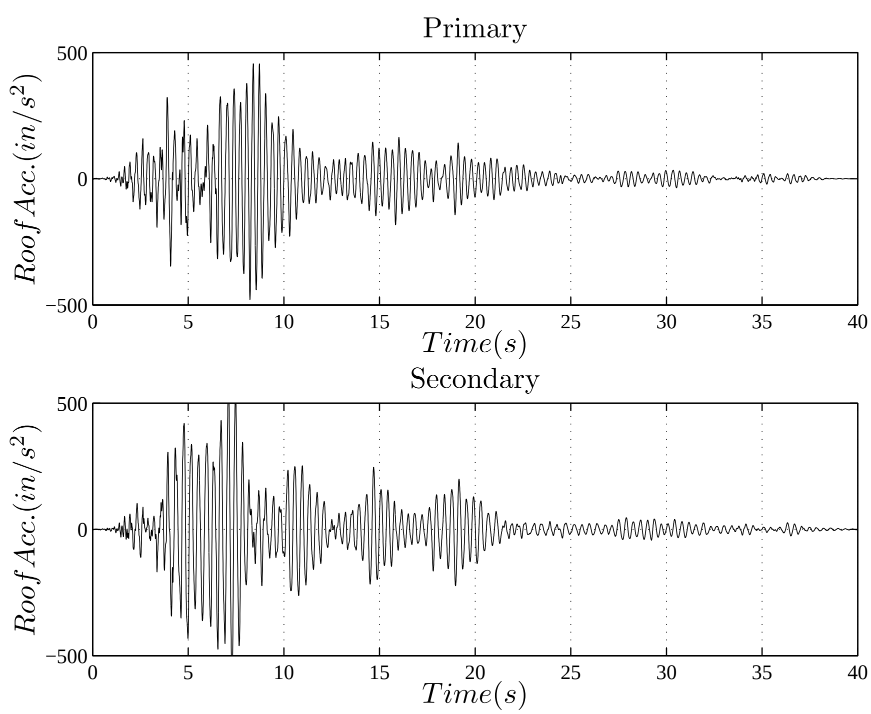

Figure 182: Mean roof acceleration response, Northridge - Sylmar Converter Station motion, founded on soft clay.

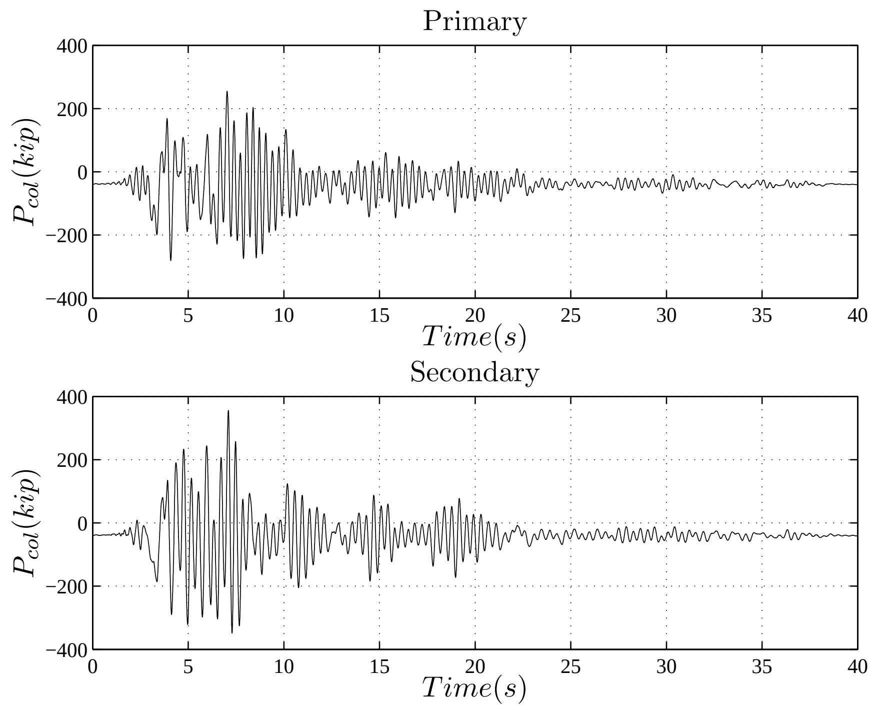

Figure 183: Mean column response, Northridge - Sylmar Converter Station motion, founded on soft clay.

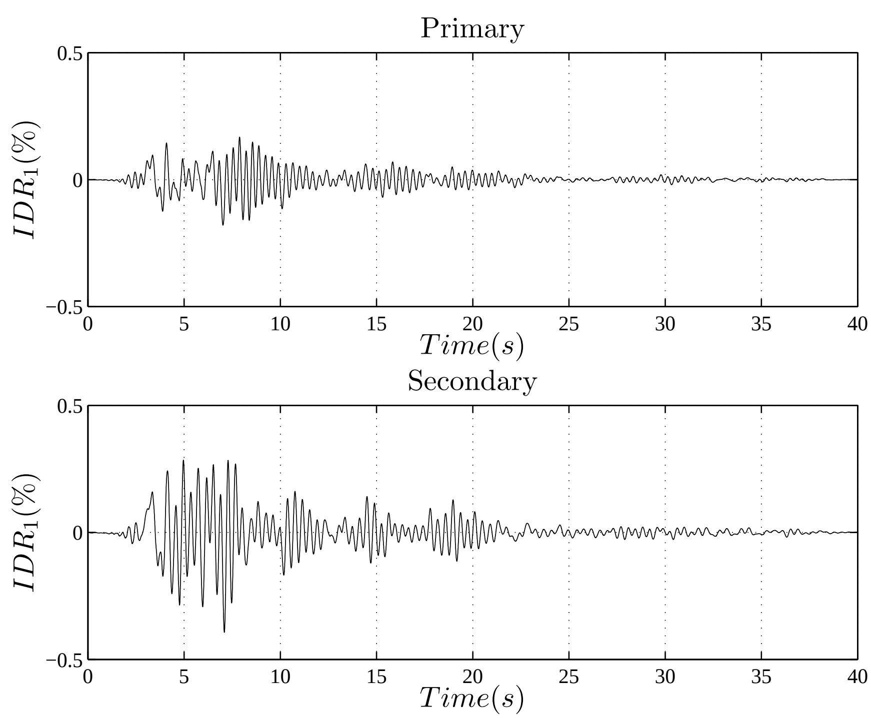

Figure 184: Mean first-story IDR response, Northridge - Sylmar Converter Station motion, founded on soft clay.

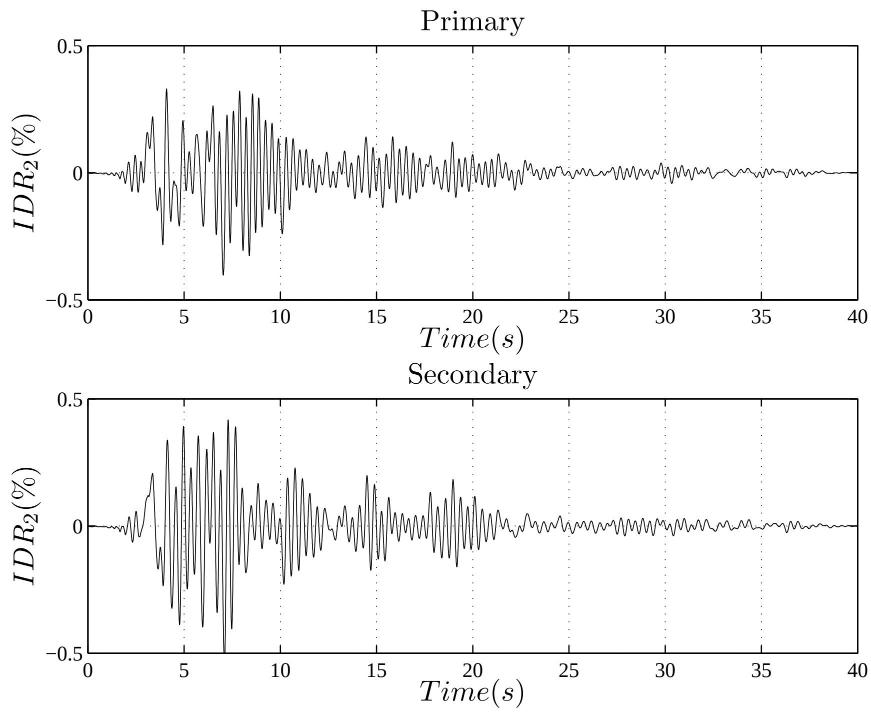

Figure 185: Mean roof displacement response, Northridge - Sylmar Converter Station motion, founded on soft clay.

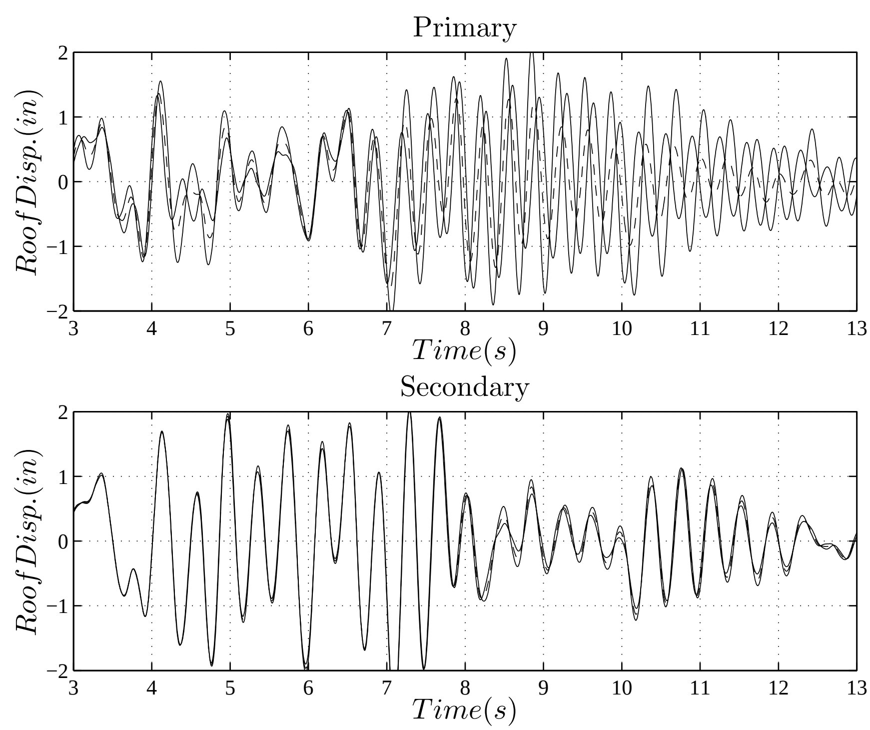

Figure 186: Roof displacement response with sensitivity to building stiffness, Northridge - Sylmar Converter Station motion, founded on soft clay.

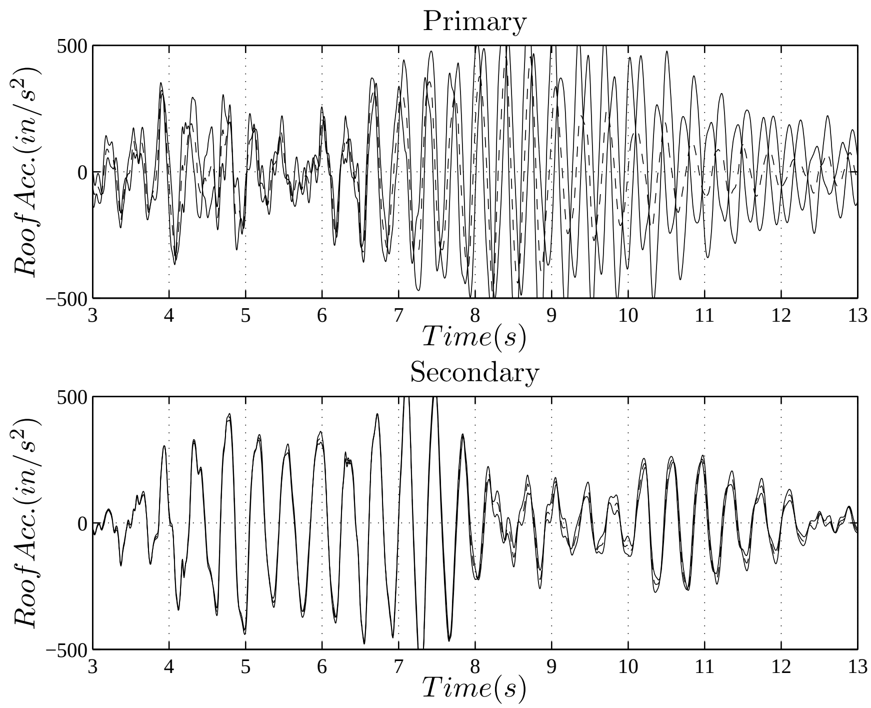

Figure 187: Roof acceleration response with sensitivity to building stiffness, Northridge - Sylmar Converter Station motion, founded on soft clay.

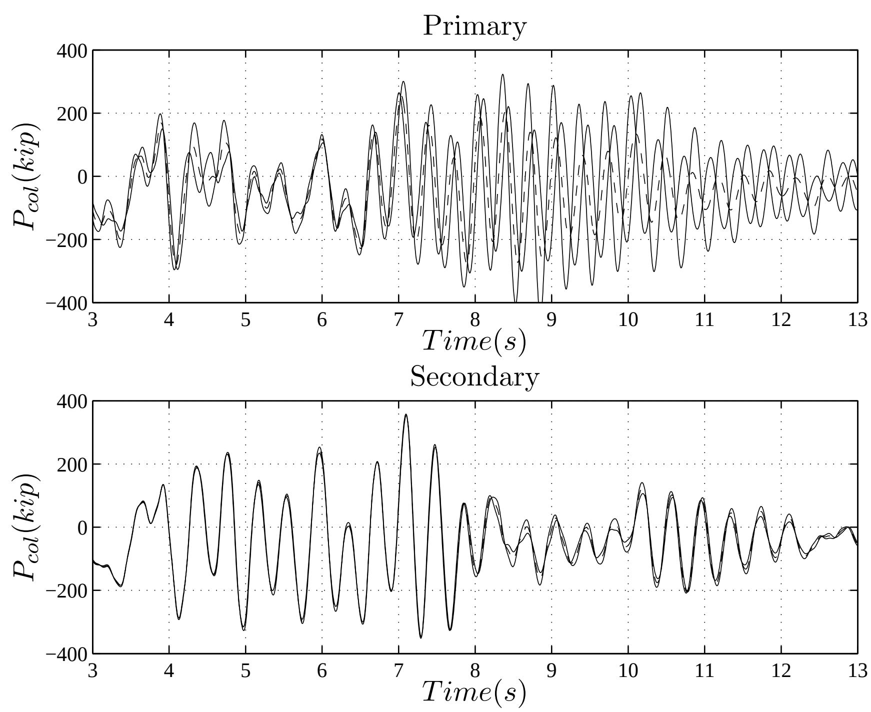

Figure 188: Column force response with sensitivity to building stiffness, Northridge - Sylmar Converter Station motion, founded on soft clay.

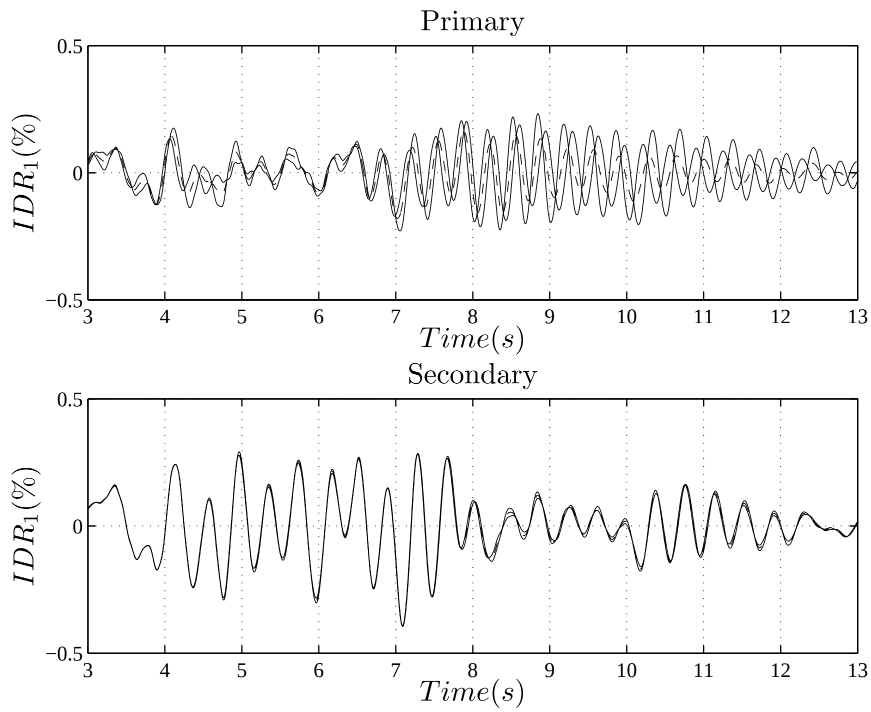

Figure 189: First-story IDR response with sensitivity to building stiffness, Northridge - Sylmar Converter Station motion, founded on soft clay.

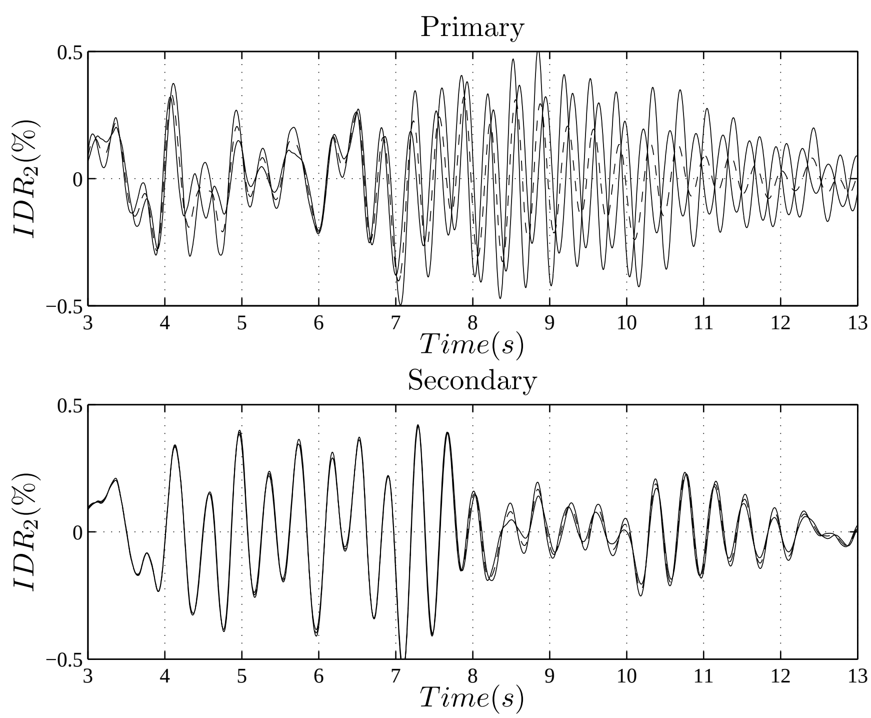

Figure 190: Second-story IDR response with sensitivity to building stiffness, Northridge - Sylmar Converter Station motion, founded on soft clay.

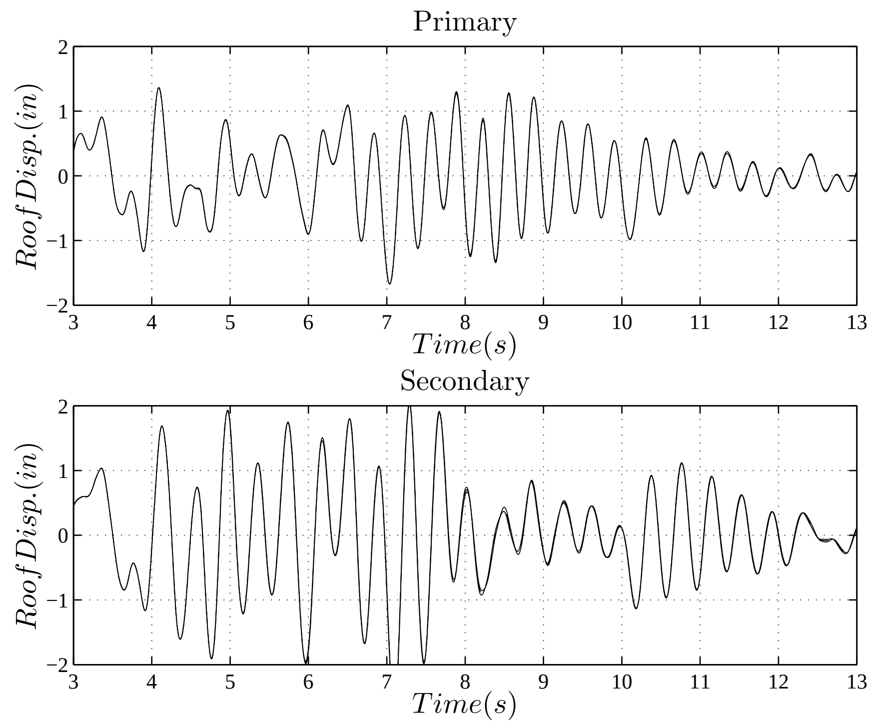

Figure 191: Roof displacement response with sensitivity to soil spring stiffness, Northridge - Sylmar Converter Station motion, founded on soft clay.

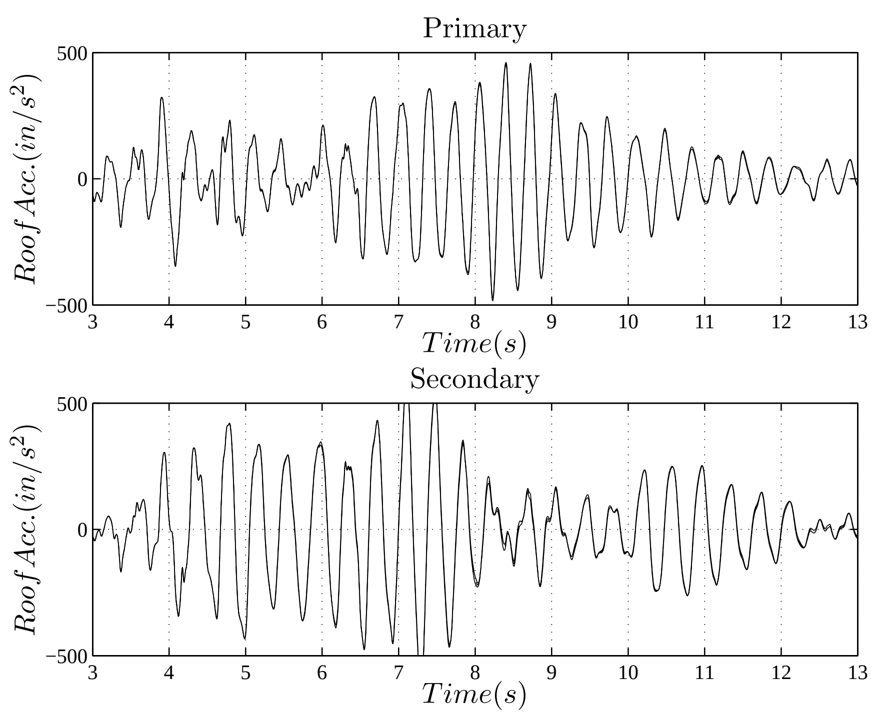

Figure 192: Roof acceleration response with sensitivity to soil spring stiffness, Northridge - Sylmar Converter Station motion, founded on soft clay.

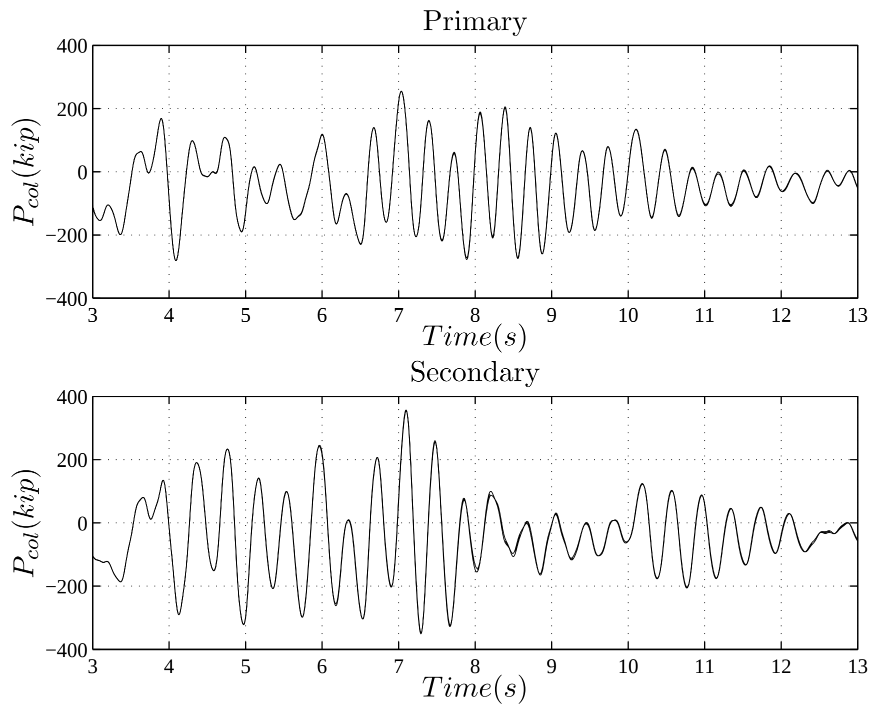

Figure 193: Column force response with sensitivity to soil spring stiffness, Northridge - Sylmar Converter Station motion, founded on soft clay.

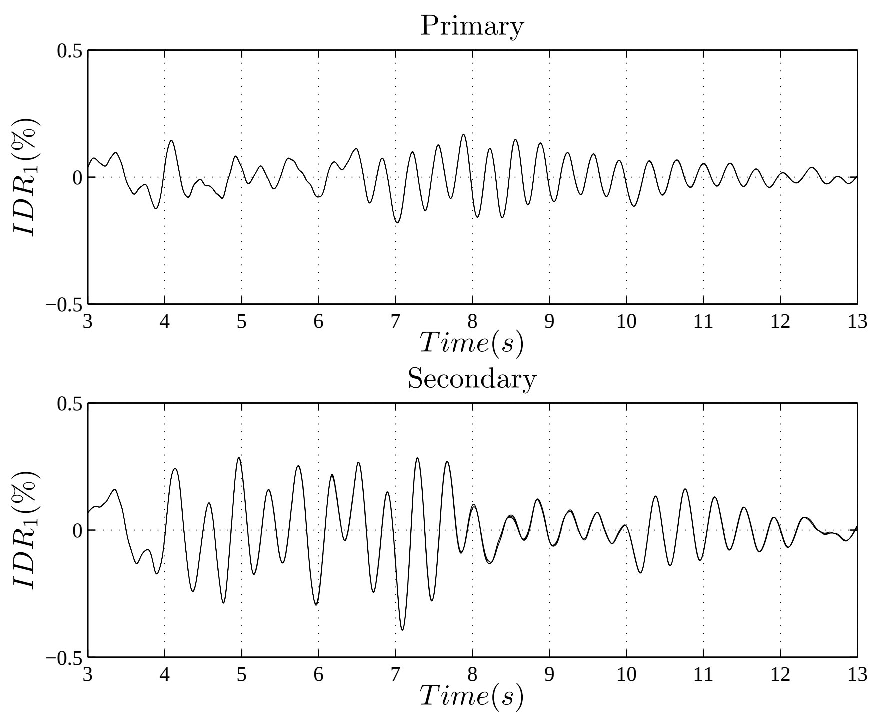

Figure 194: First-story IDR response with sensitivity to soil spring stiffness, Northridge - Sylmar Converter Station motion, founded on soft clay.

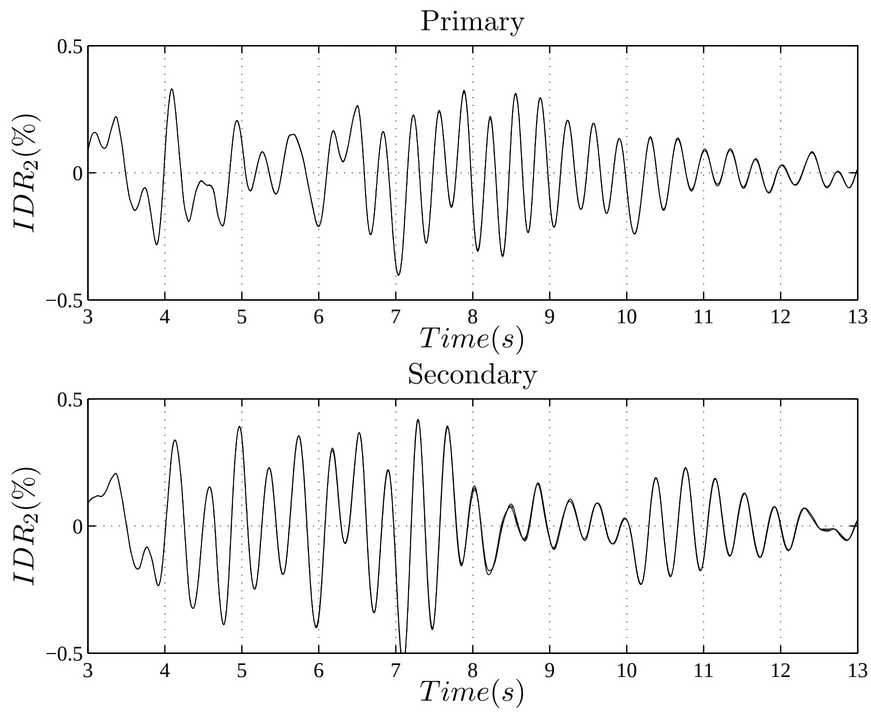

Figure 195: Second-story IDR response with sensitivity to soil spring stiffness, Northridge - Sylmar Converter Station motion, founded on soft clay.

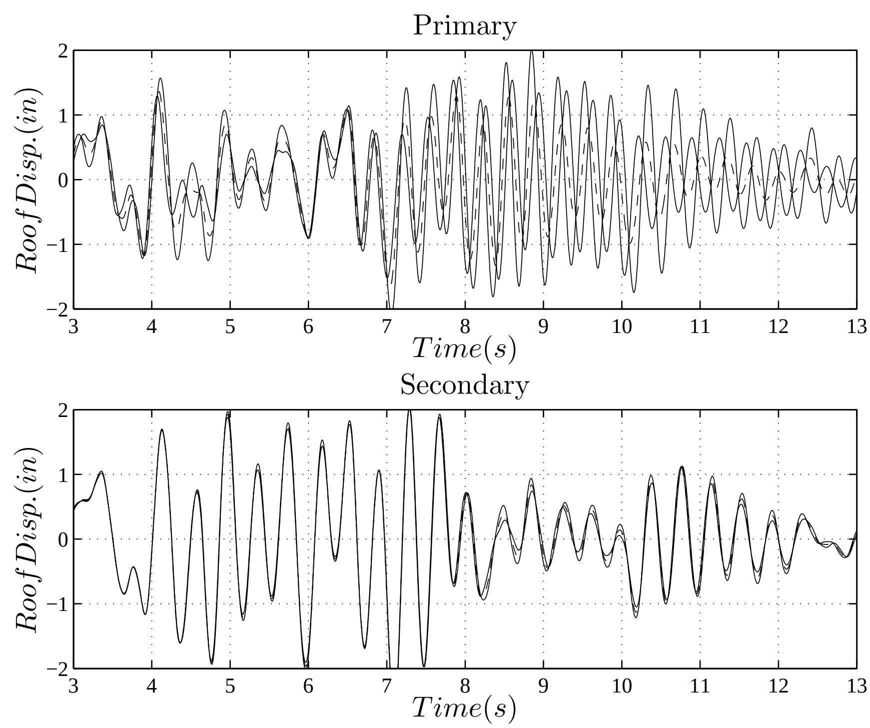

Figure 196: Roof displacement response with sensitivity to floor mass, Northridge - Sylmar Converter Station motion, founded on soft clay.

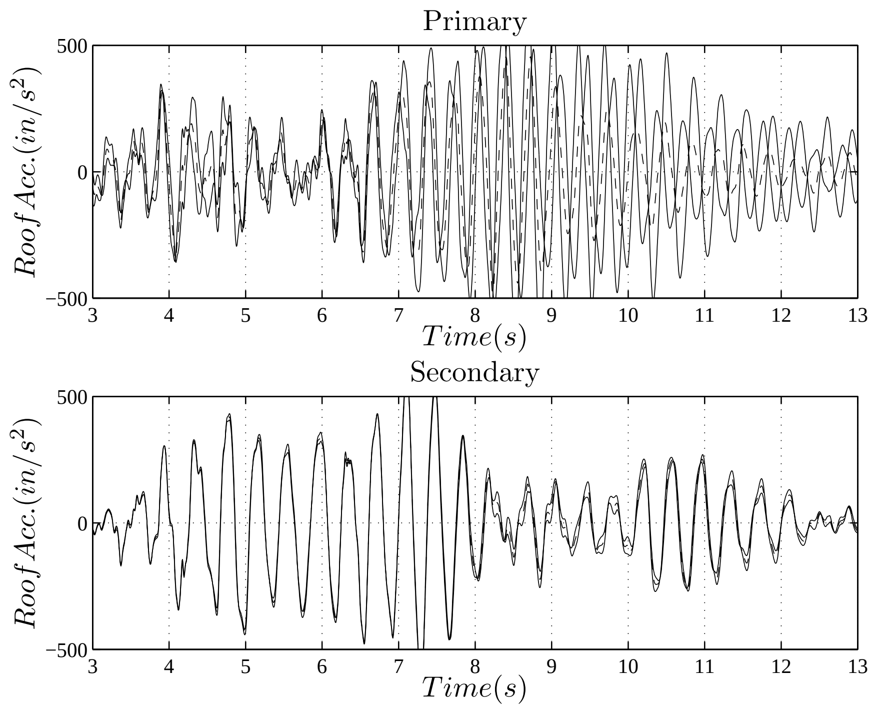

Figure 197: Roof acceleration response with sensitivity to floor mass, Northridge - Sylmar Converter Station motion, founded on soft clay.

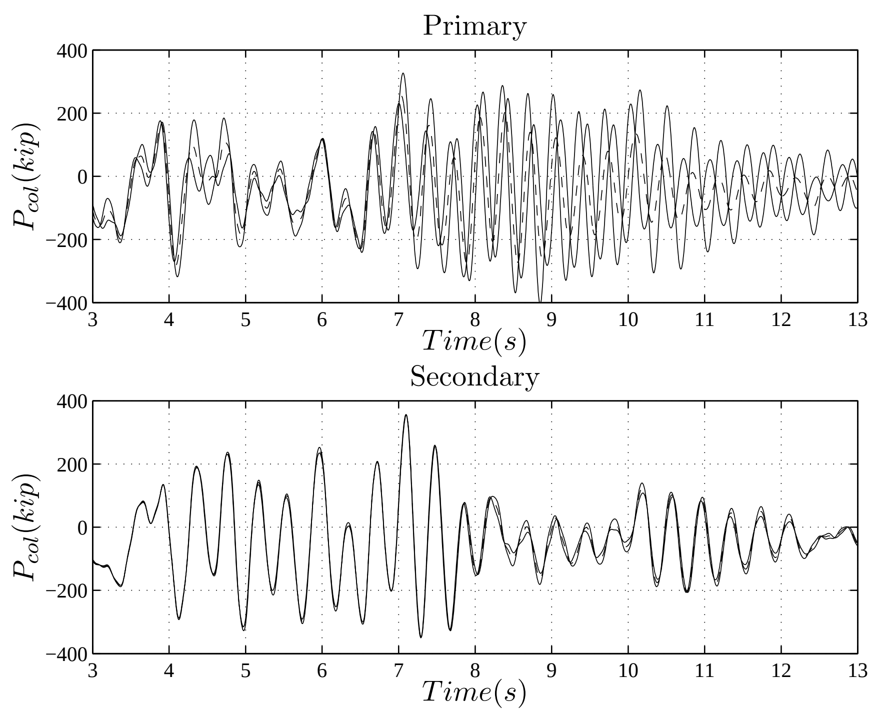

Figure 198: Column Force response with sensitivity to floor mass, Northridge - Sylmar Converter Station motion, founded on soft clay.

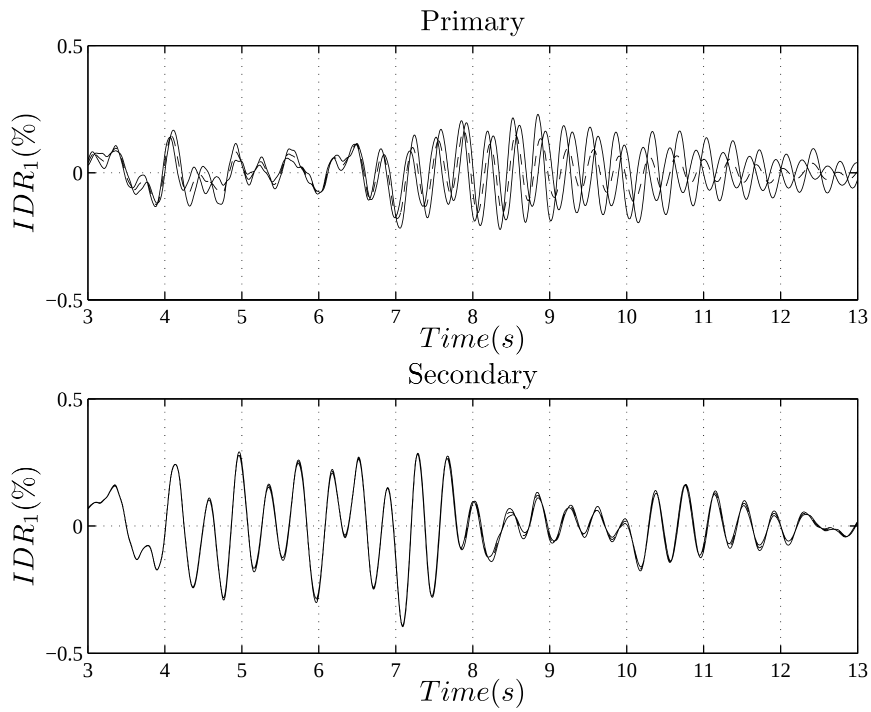

Figure 199: First-story IDR response with sensitivity to floor mass, Northridge - Sylmar Converter Station motion, founded on soft clay.

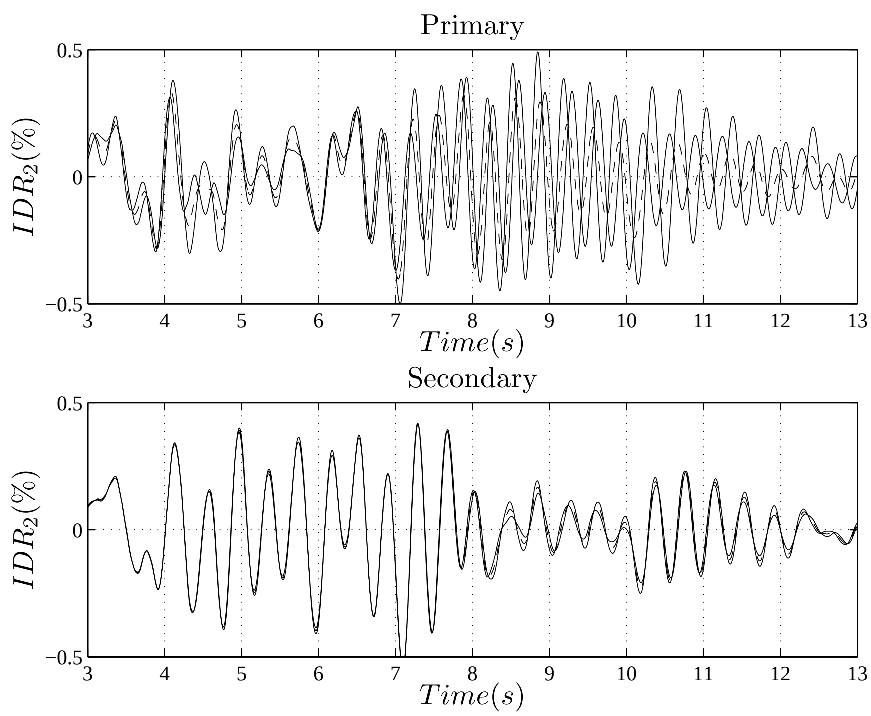

Figure 200: Second-story IDR response with sensitivity to floor mass, Northridge - Sylmar Converter Station motion, founded on soft clay.